SIMULATION AND EXPERIMENTAL VALIDATION OF TRACTOR OVERTURNING AND IMPACT BEHAVIOUR

By

CHRISTOPHER JOHN CHISHOLM, B.Sc., C.Eng., M.I.Mech.E.

A DOCTORAL THESIS

Submitted in partial fulfilment of the requirements for the award of

Doctor of Philosophy of the Loughborough University of Technology

May, 1978

Supervisors: Professor F.D. Hales
Dr. R. Ali
Department of
Transport Technology

SIMULATION AND EXPERIMENTAL VALIDATION OF TRACTOR OVERTURNING AND IMPACT BEHAVIOUR

by

CHRISTOPHER JOHN CHISHOLM, B.Sc., C.Eng., M.I.Mech.E.

SUMMARY

Roll over protective structures (ROPS - safety cabs or frames) are required by law on agricultural tractors in the U.K. and many other countries to prevent drivers being crushed in overturning accidents. The research reported was aimed to help in the development of ROPS design and strength test criteria through a better understanding of the dynamics of overturning and estimation of the energy absorbed in the ROPS.

A survey of overturning accidents showed the types likely to result in the greatest ROPS damage: (i) an overturn down a steep bank more than 2m high, and (ii) a multiple roll accident.

A mathematical model of sideways overturning was developed. Equations describing the relationships between the forces and deflections at each point of contact between the tractor and the ground allowed the same model to cover tyre behaviour during overturning, and ROPS, wheel and soil behaviour during impact. A computer program based on the model was able to simulate both bank and multiple roll overturns.

Thirty bank overturning experiments in different conditions were used to validate the model. An experimental ROPS with controllable structural characteristics was instrumented for the recording of force and deformation at impact, and the overturning motion was analysed from cine film.

The simulations showed good overall agreement with the experimental results, both in dynamic behaviour and in energy absorbed in the ROPS. The relationship between tyre friction forces and ride-mode oscillation was found to have an important effect on the points at which tyre contact was lost and regained during overturning. This strongly influenced the roll angle and velocity at impact, and hence the way the energy was absorbed by the ROPS, the side of the rear wheel and the soil.

Running the simulations in a wide range of conditions established which parameters had the greatest effects during overturning and impact. Normally, the ROPS absorbs most of the energy due to impact roll velocity but only a small proportion of the major energy component, that due to vertical velocity. In an overturn down a very high bank, however, or in some types of multiple roll accident, the tractor is more nearly upside down at impact and needs a high vertical strength to prevent collapse.

PREFACE

The work reported in this thesis was carried out at the National Institute of Agricultural Engineering (NIAE), Silsoe, Bedford, under project 02006 (originally 1425), "Design and Test Criteria for Tractor Safety Cabs".[22] It has also been described fully in a series of NIAE Departmental Notes[31, 61, 62, 70, 71, 79, 80, 93] to which references are made as appropriate; where minor non essential details are covered only in the DN's this fact is indicated in the thesis. An interim report of progress was presented at the NIAE Tractor Ergonomics Subject Day[102] and several papers are being submitted to the Journal of Agricultural Engineering Research for publication.

A parallel study, carried out under contract to the Commission of the European Communities[17, 21, 82], is not reported in this thesis but is relevant in the discussion of results.

Permission and financial support for Ph.D registration were provided by the Agricultural Research Council, through the Director and Governing Body of the NIAE, to whom I am duely grateful.

I would also like to thank sincerely the large number of people who have contributed to this work:
Professor F.D. Hales and Dr. R. Ali of Loughborough University, Dave Manby, John Matthews and, particularly, Richard Stayner, NIAE, for continued guidance, advice and encouragement;
John Praties, Dick Potter and Graham Aldridge, Design Department, NIAE, for translating the experimental safety frame concept into engineering drawings, and Arthur Radwell and the Workshop staff for turning these into hardware;
G.R. Chalmers, Sid Bevis and Pete Ferguson, Engineering Services Department, NIAE, for design and construction of the overturning platform;

Deere and Company, for providing the designs for load-cells and displacement transducers, and Doug Filby, Jeff Hall and the late Laurie Fearne, Instrumentation Department, NIAE, for interpreting these designs and strain-gauging the transducers;

Cecil Cove, Dave Cooper, Hugh Foster, Colin Houghton and other members of Instrumentation Department, NIAE, for design and construction of the instrumentation system, and for assistance in its operation and calibration;

Derek Millard, Pete Fishwick, Bill Streader, Allan Boldero, George Beston and, particularly, Joe Morris, Ergonomics Department, NIAE, for invaluable assistance in the overturning experiments and in the tedious digitisation of cine film data;

Ron Stanbrook, Paul Brown, Alan Elliot and other members of Engineering Services Department, NIAE, for assistance in the overturning experiments and for repair of the tractor and frame;

Brian Watt, Roger Cove, Mike Scutt and Mrs. Cathy Pepper, Photographic Section, NIAE, for still and cine filming and processing of figures;

Dave Randle, Instrumentation Department, NIAE, for digitisation of magnetic tape recordings;

John Ashburner, of the National College of Agricultural Engineering, Silsoe, for discussion of structural analysis techniques;

John Parker, sandwich course student, Loughborough University, for analysis of laboratory impact test results, and members of Tractor Test Section, NIAE, for carrying out the tests;

Bedfordshire County Council, Michelin Tyres Limited, and Martin McAllister, Tractor Department, NIAE, for measurements of tyre friction forces;

Dr. Martin Moore and the late Eric Coleman, Engineering Research Department, NIAE, for carrying out specimen tensile tests and advising on the results, and for assisting in load-cell calibration;

Richard Cope, now Cultivation Department, NIAE, and others already mentioned, for assistance in moment of inertia measurement and calculation of results;

John Stafford, Tractor Department, NIAE, for soil mechanics advice;
David Higgs, Mathematics Department, Don Bottoms and Dave O'Neill, Ergonomics Department, NIAE, for assistance with statistical tests and advice on the interpretation;
Brian Cottrell and Phillip Dilley, Ergonomics Department, NIAE, for tedious plotting of simulation results;
Bill Course, Librarian, NIAE, for obtaining published papers and assisting with a literature survey on tyre side forces;
Alan Dale, Ergonomics Department, NIAE, for providing the polynomial-fitting program and Pete Fishwick for writing part of the magnetic tape recording analysis program;
Justin Jackson of the Computer Department, Rothamsted Experimental Station, for advice on CSMP, and other members of the Department for operating advice and tolerance in the face of large quantities of jobs and output;
Des Smith, Tractor Department, NIAE, for much valuable help and advice on practical aspects of overturning and impact tests;
Mrs. Ann Dalley, Tractor and Cultivation Division, NIAE, for the most rapid and efficient typing of the thesis and some of the DN'S, and Miss. Pat Cook, Tractor and Cultivation Division, NIAE, who typed most of the others with equal expertise.
Staff in other NIAE service and administration departments who have not been named but whose help is much appreciated.
And finally, special thanks to my wife Anne, and children Neil and Ian for their support, sacrifice and encouragement.

The work presented is original except where otherwise stated and has not been submitted for a degree at any other university.

C.J.C.

May 1978

CONTENTS

Page

Page

APPENDICES (Continued)

NOTATION

a_0, a_1, a_2	Polynomial coefficients.
A	Constant for material exhibiting strain rate sensitivity.
$b, b_1 - b_6$	Dimensions of top frame and transducer, mounting points (Figs. 5.12 and 6.6).
c	$\cos \theta_z$.
c_1	$\text{Cos}\ (\alpha' + \theta)$.
C	Damping coefficient.
C_t	$C/\Delta t$.
CH1 - CH9	Transducer signal voltages in channels 1 - 9 (Fig.5.12).
d	Diameter of frame upright.
DZ	Tractor forward speed.
e	Dimension of frame (see Fig. 6.6).
e_Δ	Lack of fit of frame upright due to over-constraint.
E	Young's modulus.
E_W	Pendulum input energy.
$E_{x31}, E_{x32}, E_{z32}$	Energies absorbed due to frame impact forces Fx_{31}, Fx_{32}, Fz_{32} (Fig. 5.13).
F	Impact force.
F_c	Impact force at plastic collapse.
F_C, F_V, F_H	Compressive, vertical, horizontal forces on frame.
F_{x1}, F_{y1}, F_u, F_v	Forces in directions x_1, y_1, u, v (Fig.3.2)
$F_{x3L1}, F_{z3L1}, F_{x3L2}, F_{z3L2}$	Impact forces in lateral and longitudinal tractor co-ordinate directions on load cells at L1 and L2 (Fig. 5.13).

$F_{x_{31}}$, $F_{x_{32}}$, $F_{z_{32}}$	Replaced impact forces in lateral and longitudinal directions on load cells at L1 and L2 (Fig. 5.13).
g	Acceleration due to gravity
	As a suffix: relating to centre of mass.
G	Elastic modulus of rigidity.
h	Height of frame uprights.
h'	Effective height of uprights between hinges.
h_o	Height of displacement transducer upright between joints (when vertical).
I	Second moment of area.
I_{xx}, I_{yy}, I_{zz}	Moments of inertia of tractor about lateral, vertical and longitudinal axes through centre of mass.
J	Polar second moment of area.
k	Elastic stiffness of frame at point of application of force in direction of force (section 6).
k_x	Flexibility (deflection per unit force) } Section 3
k_{x1}, k_{y1}, k_v	Flexibility in direction x_1, y_1, v } Section 3
KE X, KE Y, KE Z	Kinetic energy due to velocity in lateral, vertical and longitudinal directions.
KE AX, KE AY, KE AZ	Kinetic energy due to pitch, yaw and roll angular velocities.
l	Lift height of pendulum above impact point.
m	Mass.
Mps	Static plastic moment.
Mp	Dynamic plastic moment.
P	Resistance force of upright in plastic bending.

PE	Potential energy (defined in relation to zero at rest after impact).
Q_s	Skew factor.
r_g	Radius of gyration.
s	sin θ_z.
s_1	Sin $(\alpha' + \theta)$.
SCALE	Reproduction scale for film measurements.
t	Time.
t_{impact}	Impact time.
t_x	$\tan \frac{1}{2} \theta_x$.
t_y	Time to yield.
T	Constant for material exhibiting strain rate sensitivity.
$\bar{T}_\theta$	Rotation transform matrix from fixed $(\bar{x}_0)$ to body $(\bar{x}_3)$ co-ordinates.
$\bar{T}_\theta^{-1}$	Rotation transform matrix from body $(\bar{x}_3)$ to fixed $(\bar{x}_0)$ co-ordinates - the inverse of $\bar{T}_\theta$.
u	Transverse ground co-ordinate (Fig.3.2).
u'	Mechanical input variable of transducer (Appendix 4.3).
U_1, U_2, U_3	Coefficients of fitted calibration curve (Appendix 4.3).
U_{XV}, U_{XH}	Coefficients of fitted cross sensitivity calibration defining the relationship between F_V and V_{XV}, F_H and V_{XH}.
v	Normal ground co-ordinate (Fig. 3.2).
v'	Transducer amplifier output voltage (Appendix 4.3).
v_p	Pendulum impact velocity.

v_C', v_V', v_H'	Output voltages in relevant channels due to F_C, F_V, F_H.
v_{CM}'	Measured output voltage in compressive channel (includes cross sensitivity components due to F_V, F_H).
v_O'	Output voltage offset due to calibration resistor.
v_{OC}', v_{OV}', v_{OH}'	V_0' For compressive, vertical and horizontal load channels.
v_{XV}', v_{XH}'	Voltage in compressive channel due to F_V, F_H.
w	Recorded variable at analysis. } Appendix 4.3
w_o	Value of w due to calibration offset } Appendix 4.3
x, y, z	Lateral, vertical, longitudinal co-ordinate directions (Figs. 3.1, 3.2, 5.2).
x, y	Lateral, longitudinal co-ordinates for frame deflection: section 6 only (Fig.6.6).
x, y, z (Fig. 3.2) / x_o, y_o, z_o (Fig. 5.2)	Fixed co-ordinates.
x_{oB}, y_{oB}, z_{oB}	Differences in fixed co-ordinates of points P and Q.
x_g, y_g, z_g / x_{og}, y_{og}, z_{og}	Fixed co-ordinates of centre of mass.
x_{oD}, y_{oD}, z_{oD}	Fixed co-ordinates of marker pole datum point (Fig. 5.11).
x_{oP}, y_{oP}, z_{oP}	Fixed co-ordinates of P. (Marker point on base frame - origin for tractor-based co-ordinates).
$\bar{x}_o$, $\bar{x}_3$	The column vectors $\begin{vmatrix} x_o \\ y_o \\ z_o \end{vmatrix}$, $\begin{vmatrix} x_3 \\ x_3 \\ z_3 \end{vmatrix}$

x_1, y_1, z_1 (Fig. 3.2) x_3, y_3, z_3 (Fig. 5.2)	Body Co-ordinates.
x_{3B}, y_{3B}, z_{3B}	Differences in body co-ordinates of points P and Q.
x_{3g}, y_{3g}, z_{3g}	Body co-ordinates of centre of mass.
$x_{3D1}, z_{3D1}, z_{3D2}$	Body co-ordinates of displacement transducer top mountings (Fig. 5.12).
x_{3o}, z_{3o}	Body co-ordinates of centre of top frame (Fig. 5.12).
x_4, z_4	Top frame co-ordinates (Fig. 5.12).
x_{1fo}, y_{1fo}, v_{fo}	Constants in piece-wise linear structural characteristics - value of deflection at zero force.
x_b	Suffix b indicates variable value at time-step before current one.
x_1, XL	Limiting deflection for a structural line to be valid (Fig. 3.7).
x_{Ef}, y_{Ef}	Measured co-ordinates of bank edge in film analysis.
x_{Pf}, y_{Pf}	Measured co-ordinates of P in film analysis.
y_{ogmax}	Maximum value of y_{og}.
$\dot{y}_{ogmin}$	Minimum value of $\dot{y}_{og}$, i.e. maximum downward (negative) vertical velocity of the centre of mass immediately before impact.
α	Angle of bank slope to vertical (Fig. 3.1).
α	Angle of impact force to frame (section 6 only: Fig. 6.6).
α'	Angle of surface slope (Fig. 3.2).
β	Angle of ground surface (Fig. 3.6).
β	Angle of deflection of corner of frame (section 6 only: Fig. 6.6).

γ		Angle of approach (yaw) of tractor to bank edge.
δ		Frame deflection.
δ_e	Elastic	Displacement of point of application of force in direction of force (Section 6)
δ_P	Plastic	
δ_M	Maximum	
δ_L	General	
δ_i	Linear displacement of top of upright i in direction of plastic deformation.	(Section 6)
δx_{3o}, δz_{3o}		Deflections of centre of top frame, O in tractor co-ordinate directions. (Appendix 5.3).
δx_{3L1}, δx_{3L2}, δz_{3L2}		Deflections of load cell points L1 and L2 in tractor co-ordinate directions. (Appendix 5.3).
δy_{og}		Change in height of centre of mass from y_{ogmax} to value shortly before impact.
δ_{yi}		Change in length of frame due to horizontal deflection (Appendix 4.1).
$\delta\theta_{3x}$, $\delta\theta_{3y}$, $\delta\theta_{3z}$		Incremental pitch, yaw and roll angles relative to body position at previous time increment.
Δt		Step time increment.
$\overline{\Delta T}$		Incremental rotation transform matrix from body co-ordinates at one position to those at the next time increment.
θ $(\equiv \theta_z)$		Roll angle (Figs. 3.1., 3.2).
θ, θ_i		Angle of rotation of plastic hinge in frame upright (section 6, Fig. 6.7; Appendix 4.3).
θ_t		Angle of rotation of displacement transducer (Appendix 4.3).
θ_x, θ_y, θ_z		Pitch, yaw and roll angles (Fig. 5.2).

θ_{xmin}, θ_{ymin}, θ_{xmax}, θ_{ymax}	Minimum and maximum pitch and yaw angles up to impact.
θ_{3y}	Rotation (yaw) of top frame relative to tractor (Fig. 5.12).
λ	Angle of friction, $\tan^{-1}$.
μ	Dynamic coefficient of friction.
μ_{max}	Limiting coefficient of friction.
μ_B	Coefficient of friction between tyres and bank.
μ_s	Coefficient of friction on soil.
σ Dynamic, σ_o Static	Yield stress.
ϕ	Angle of rotation of top frame (section 6 only: Fig. 6.6).
ϕ	Angle of top surface of bank (Fig. 3.1).
ψ	Slip angle.
ψ_n	Normalised slip angle.

Notes:

(a) The notation and co-ordinate systems are consistent within each section. They are also consistent throughout the thesis with the following exceptions:

(i) In the two-dimensional model (Section 3), θ is used for roll angle and x_1, y_1 for the body co-ordinates. In the three-dimensional kinematic analysis of cine film data (Section 5, Appendix 5.2), θ_z is used for roll angle and x_1, y_1, z_1 for the first rotational transformation; x_3, y_3, z_3 for the body co-ordinates. (See Figs. 3.1, 3.2, 5.2).

(ii) A different co-ordinate system is used in section 6, and the variables α, β and ϕ have different meanings. (See Figs. 6.6 and 6.7).

(b) The conventional 'dot' notation is used to symbolise differentiation with respect to time, e.g:

$$\dot{x} = \frac{dx}{dt}, \quad \ddot{x} = \frac{d^2x}{dt^2}$$

(c) To avoid the repeated use in the text of lengthy phrases or algebraic symbols, some variables and parameters are referred to in shortened forms which are not strictly correct but should convey the intended meaning.

Lateral velocity, Vertical velocity	Velocities of the centre of mass.
ROPS	Roll over protection structure.
ROPS energy, wheel energy etc	Energy absorbed in deformation (lateral unless otherwise stated) of the ROPS, wheel etc.
Maximum ROPS energy	Energy absorbed at maximum deformation of the ROPS (lateral unless otherwise stated).
Moment of inertia	Polar moment of inertia about the roll axis through the centre of mass.

1. INTRODUCTION

The distribution and total number of fatal accidents on farms in the U.K. remained substantially constant in the decade prior to the introduction of legislation requiring safety cabs or frames to be fitted to all new tractors (Table 1).[1,2]

TABLE 1

Fatal accidents on U.K. farms

		1960	1967	1968	1969	1970	Mean 67–70
Accidents with tractors	Sideways overturns	24	31	29	32	27	29.75
	Rearward overturns	5	10	10	5	3	7.00
	Total overturns	29	41	39	37	30	36.75
	Total accidents	53	50	54	46	49	49.75
All farm accidents		125	135	136	136	130	134.25

Statistics for non-fatal injury accidents are inevitably less consistent because of inadequacy in reporting and in the definition of an accident. Accident severity, however, may be indicated by the proportion of reported injury accidents that are fatal. In overturning accidents this is about one third, compared with one per cent for other farm accidents.

The following conclusions may be drawn from the figures of fatal accidents on U.K. farms before the widespread use of safety cabs:-

1. About 37% of all deaths are directly connected with tractors.
2. Of these accidents about 74% are due to overturning. The number of deaths resulting from tractor overturns is considerably higher than that from any other single cause.
3. Of the tractor overturning accidents, the distribution of sideways and rearwards overturns is about 4:1.

4. The annual number of deaths resulting from tractor overturns is about 37, or about 9 per 100,000 tractors.

It has been shown[3] that the distribution of farm accidents in the U.S.A. is similar in the above respects to that in the U.K., and that tractor overturn accidents similarly occur in all types of terrain.

1.1. <u>THE DEVELOPMENT OF SAFETY CAB STRENGTH CRITERIA</u>

Although a theoretical study of tractor overturning was included in a publication as early as 1927[4], the first studies aimed at driver protection were carried out between 1954 and 1959. Most of this work was devoted to developing simple laboratory strength test techniques that would reproduce the impact received in overturning accidents. The work was mainly experimental, with little or no theoretical analysis of the overturning behaviour.

Sweden introduced safety cab legislation in 1959 following a series of tests to correlate the effects of a simulated accident with the impact of a pendulum weight[5]. The simulation consisted of tipping a tractor sideways off a one metre high platform onto a rigid surface. The strength of the safety frame and the energy of the pendulum impact were adjusted to give acceptable and equivalent deformation in the two comparative tests, and this impact energy formed the basis of their test code.

To improve the realism of the accident simulation, and in particular to introduce horizontal fore and aft forces to the cab due to forward motion, a tractor fitted with an experimental frame was overturned in a number of different field conditions in Norway, shortly after the original Swedish work[6]. The experimental frame was fitted with stiffly sprung members supporting the top, forward joint on the side first contacting the ground. After an overturning test the maximum spring deflection, and hence the maximum force, in each of three mutually perpendicular directions could be determined from mechanical indicators fitted to the springs. It was found that the vertical and longitudinal impact forces were typically of the same order as the lateral forces, and the energies absorbed by the springs in all three direction were similar to the lateral energies measured in the Swedish experiments. The Norwegian test code took account of these results, and required a front impact blow of equal magnitude to the side blow and inclined downwards at 45 degrees.

The results of the Norwegian tests, although valuable as a guide to typical force levels, do not greatly advance the understanding of overturning behaviour for the following reasons:-

1. The overturning conditions were not particularly severe, or closely controlled, and the results show considerable variability.
2. Only one weight and type of tractor was used.
3. The energy-absorbing characteristics of the springs were fundamentally different from those of real cabs.
4. No theoretical analysis was included to aid understanding of the significance of the measurements made.

Overturning experiments were carried out at the N.I.A.E. between 1961 and 1964 to assess how the experience gained in Scandinavia could best be used in the formulation of a safety cab test code for the U.K. It was established that the final distortion of frame designs tested by the Swedish procedure and then by overturning a tractor rearward and sideways on a gradient of 1 in $2\frac{1}{2}$ to 1 in 3 are reasonably comparable[7]. The pendulum test was accordingly adopted in this country with the same relationship between blow energy and tractor weight as in the Swedish code, but with a number of detailed modifications. Longitudinal impact and crushing tests were applied at both the front and rear of the cab. The method of lashing the tractor to the ground had been investigated by measurement of the static and dynamic restraining forces, and improved standardisation in this and other aspects of the test was recommended.

The limit on the permanent deflection of a cab during an impact test which was used in Sweden as the criterion for approving a safety cab was felt to impose unnecessary restrictions on design, particularly of larger cabs. The criterion that the cab must not enter a zone of clearance fixed in relation to the tractor was proposed, to allow increased deformation in larger cabs while maintaining a uniform standard of driver protection[8].

The overturning tests in U.K. also showed the value of preventing continued rolling of a tractor after overturning on a steep hillside, and it was demonstrated that extensions fitted to the top of the cab could limit the roll to about 90 degrees.

A theoretical study of overturning dynamics and plastic deformation in frames was published in New Zealand in 1967[9], before the establishment of a test code. The dynamic analysis was restricted to two dimensions (i.e., excluding forward motion), but covered two idealised types of overturn. The results demonstrated that a considerable proportion of the available energy can be absorbed in impact of the rear wheel on the ground, if this occurs before the impact of the frame. The calculated impact energy values were generally higher than the Swedish measured values for heavier tractors, although no experimental results were given. A number of laboratory impact tests on model and full sized frames showed that the deformation could be predicted fairly reliably in simple designs, but the need for research into more complex behaviour was indicated. The test code developed in New Zealand applies the same impact energy as in the Swedish test, since the effects of the higher energies calculated were considered to be offset by the satisfactory safety record in use of frames tested to the Swedish formula.

Tractor overtuning tests have been carried out by Deere and Company in the U.S.A. on tractors fitted with two-post 'roll-bar' frames[10]. The impact forces and resulting frame deformation were measured by transducers designed and built by the company. Although a number of sideways overturning tests were made in different conditions, no detailed comparison of impact energy levels is reported; however, the maximum frame deformation occurring in the overturning tests is recorded as being 30% higher than the deformation produced in a pendulum impact test to the Swedish formula.

In overturning tests carried out by N.I.A.E. using facilities provided by Deere and Company the O.E.C.D. pendulum rear impact formula (equivalent to the Swedish code) is shown to give energy values significantly lower than those measured in rearward overturn tests for tractors heavier than 6000 lb[11]. In a simplified theoretical study it was proposed that the pendulum impact energy be related to the tractor's wheelbase and weight, by a formula which fitted the experimental data available.

Other studies on this subject have been published, and some will be referred to later, but there is a lack of detailed, theoretical investigation with supporting experimental data which may be applied to sideways overturns in a realistic range of accident conditions.

Safety cab regulations

The original test code, now superseded in Sweden by the O.E.C.D. and Nordic countries codes, required the tractor to be subjected to pendulum impacts from the rear of energy equal to 250 + 0.04 W kgfm and from the side of energy 250 + 0.30 W kgfm, where W is the unballasted tractor weight in kg. In addition a vertical crushing test was included up to a force of twice the tractor weight. The criteria for passing the test were that the maximum frame deformations should not exceed about 25 cm (side blow) or about 4 cm (rear blow).

The following test codes differ significantly from the original code only in the features indicated:-

1. O.E.C.D.[12] Crushing test at front and rear; front impact of equal magnitude to old rear impact; fixed zone of clearance

in relation to tractor instead of maximum deflection limits, plus limit on excess of total deflection above permanent set; rear blow energy based on new formula[11] (1974).

2. U.K. (BS.4063)[13] As O.E.C.D.

3. Nordic countries Because it was felt that the O.E.C.D. energy formula is unduly severe on both very heavy and very light tractors, a new code was developed in 1971 in which the side impact blow energy is equal to the O.E.C.D. value for tractors in the weight range 2000 kg to 4500 kg, but of reduced magnitude above and below this range.

4. New Zealand Maximum allowable deflection in rear blow increased to 10 cm.

5. U.S.A. (A.S.A.E.)[14] The pendulum impact test is similar to the O.E.C.D. code but with equal side and rear blow energies of 1810 + 0.70 W ft lb, where W is the tractor weight in lb (250 + 0.21 W kgfm, W in kg). Direct comparison is not possible, since the weight W referred to must not be less than 130 lb per maximum p.t.o. horsepower, but A.S.A.E. energy values calculated for two wheel drive tractors are generally within ±5% of the O.E.C.D. values for side blow. A static loading test may be used as an alternative.

A draft international standard[15] and an EEC Directive[16] have also been under development for some years. Both follow the O.E.C.D. procedure very closely and

Also under development are draft O.E.C.D., ISO and EEC static loading test procedures all of which are closely similar[17]. Although static test methods are slightly less realistic than pendulum tests in simulating accident conditions, they offer significant advantages of better control and repeatability, and provide more information for safety cab development. The European and International procedures have more in common with their pendulum test counterparts than with the A.S.A.E. static test method, or with an international standard for tests on earthmoving equipment cabs[18].

Experience with safety cabs

The number of tractors with safety cabs in Sweden increased from 16,000 in 1960 to 133,000 in 1969, out of a total of about 270,000 tractors[19], and the fatalities from overturning accidents have declined as a result. None of the eight deaths resulting from overturns when safety cabs were fitted in the ten years after the introduction of legislation were due to failure of the cab, although one fatality has occurred in Norway after a failure. The other deaths have been caused by partial or complete ejection of the driver.

In the U.K. reports have been prepared on all known accidents involving tractors with safety cabs since July 1968. More than 400 accidents have been reported and the only fatalities have occurred when drivers attempted to leave or were thrown from the cab. Approximately 14% of the occupants were ejected during the overturn, and a further 7% jumped clear. About half the drivers were able to hold onto the steering wheel, and the number ejected is roughly one third of those who did not retain hold.

The main object of a safety cab is to prevent the driver being crushed by the tractor during an overturn. Injury is still possible, however, from impact of the driver against parts of the tractor and cab structure, and two thirds of drivers remaining in cabs of overturning tractors in the U.K. received minor injuries, mainly cuts and bruising. Serious injuries are rare because of the low accelerations in overturning accidents compared for example, with those in road accidents.

The philosophy of driver protection

The most effective device to protect drivers in road accidents, the safety-belt, is estimated to reduce the likelihood of serious injury by one half.[20] The tractor safety cab, at a much greater cost per vehicle, has achieved a reduction of fatalities from overturning accidents of the order of 95%. A decision must be made on the 'desirable' degree of protection to be provided by safety cabs, assuming that 100% protection can never be achieved. The basis for such a decision must inevitably be the relationship between the degree of protection provided and its cost, but the information that could form this basis is not available. Research is required to evaluate the dynamics of tractor overturns more reliably than hitherto, in order to show whether existing test standards maintain adequate and equitable protection for the drivers of all types of tractors and cabs, and may demonstrate how to design safety cabs most efficiently to provide the optimum protection.

1.2. SCOPE AND AIMS OF THIS STUDY

Although the U.K. has had legislation since 1970 requiring new tractors to be fitted with safety cabs, and most other countries have similar laws, the strength tests are based on a rather simple background and are continually being revised. One way of assessing the overall adequacy of these tests is to consider the safety record of cabs in use. A recent study by the author under contract to the E.E.C.[21] showed that damage in accidents exceeded that in equivalent standard tests in only about 5% of cases; in one accident of the 160 analysed the cab had collapsed completely and the driver would probably have died had he not jumped clear. This information gives a good indication of the general adequacy of test criteria but fails to show which parts of the test are least satisfactory and does not help greatly in understanding the relationship between accident type and cab damage.

To do this it is necessary to study the dynamic behaviour, and since accidents cannot be observed they must be simulated, by mathematical models, by experiments or by both. This is the approach used in the investigation reported in this thesis, with the following main objectives.(22)

1. To obtain a better understanding of the dynamic and structural behaviour of tractors and safety cabs in overturning accidents.
2. To improve criteria for the structural design and testing of safety cabs and frames.
3. To establish design theory to assist manufacturers in translating the structural requirements into practical designs.

It was considered essential that the simulation be related as closely as possible to real accidents. Because of the high degree of protection expected from safety cabs, the relevant accident types were the most serious that are reasonably likely to occur in normal agricultural circumstances.

The study therefore began with a survey of overturning accidents. A mathematical model was then developed to simulate the most important types. The model was validated by a series of overturning experiments, which also provided useful results in their own right. Finally the model was used to predict the behaviour in a wide range of conditions, and recommendations concerning test criteria were based on these results.

2. A SURVEY OF SIDEWAYS OVERTURNING ACCIDENTS

Introduction

Several analyses of tractor overturning accidents have been published both in Europe and in the U.S.A.[7,23-30] but they have been directed mainly to establishing the causes of accidents rather than the dynamics of tractor behaviour during overturning. The main object of this survey[31], reported in section 1, was to develop a classification system that would enable all sideways overturning accidents to be represented by a small number of general types suitable for simulation, in preparation for the mathematical and experimental study. In this way it was hoped to separate the effects of gross differences in the dynamic behaviour, requiring different mathematical or physical models for simulation, from differences of degree that may be studied more simply by changing parameters.

Tractors overturn rearwards only about a quarter as frequently as they do sideways, and in a much less varied range of circumstances. Rearward overturning is not covered in this thesis.

The likelihood of occurence of the different types of accidents is assessed in 2.2 to enable the results of future research to be applied to legislation covering the structural properties of tractor safety cabs. If simulation is capable of predicting the behaviour of overturning tractors then this analysis will assist in determining which kind of simulation should be used as a guide to test standards, to ensure the greatest driver protection at the least cost.

An analysis of driver injury and behaviour in 38 overturning accidents involving tractors with safety cabs is presented in 2.3. This information will assist in the preparation of details of the criteria for the design and testing of safety cabs.

Sources of Data

The Safety Inspectorate of the Ministry of Agriculture, Fisheries and Food (M.A.F.F.)* prepares reports on all tractor overturning accidents of which it receives information. Accidents are classified into fatal, non-fatal and those involving tractors with safety cabs. The law requires that all accidents that are fatal or result in injury to an employee are notified to the Ministry. While all fatal accidents are reported, it is likely that many accidents are not recorded where no-one, or only a farmer or member of his family is injured.

Fatal sideways overturning accidents in England and Wales from 1969 to 1971 inclusive form the major part of the data for this survey. Fatal accidents in Scotland are reported by the Department of Agriculture and Fisheries for Scotland, and have not been included. In addition analysis is presented of 38 accidents in the U.K. (including Scotland) involving tractors with safety cabs that occurred or were reported in 1971. Sixty-four of these accidents had been reported to April 1972, and this survey covers those from M.A.F.F. Serial Numbers 25 to 64 inclusive, except for two that related to rearward overturns. These reports also form the basis of the driver injury and behaviour analysis.

By studying mainly fatal accidents this survey concentrates on those cases where a safety cab would have been most beneficial, at the expense of biasing the accident distribution towards greater severity. The effects of this are discussed in section 2.4.

2.1. CLASSIFICATION SYSTEM

The main parameter that influences the type of overturning is the terrain profile, and it is often the terrain that initiates the actual overturn although other effects may be important in the events leading up to the final instability. The classification system also describes the ground hardness, state of vehicle control, implements and other factors contributing to the overturn.

*Now the Agricultural Branch of the Health and Safety Executive

Terrain

A type of sideways overturn shown diagrammatically in Fig. 2.1 has been used in several research studies on overturning accidents and safety cab testing[5,9]. The tractor tips about its tyres, which remain on the edge of the bank until the cab impacts the ground. Since the whole of the impact force is received by the cab this type of overturn can result in considerable energy absorption by the cab. In an accident where the tractor overturns on flat ground much of the energy may be absorbed when the side of the rear wheel strikes the ground before the cab [9].

It was thought that accidents of the type in Fig.2.1 were not very likely, because overturning would have to be initiated at the edge of the bank without the wheels falling over the edge. The only case that could be envisaged was a ridge or low wall at the top of the bank.

This was confirmed by the survey and no accidents were reported that were analogous to Fig.2.1. Three mutually exclusive classes were chosen, however, representing terrain profiles that generate different modes of tractor behaviour. With enough evidence it is possible to assign a class to every accident.

The three types of terrain are shown in Figs.2.2A, B and C respectively.

Class A: Overturning on flat ground, either level or with a uniform slope

Class B: Overturning initiated by the tractor mounting a bank or large obstacle from flat ground.

Class C: Overturning initiated by the tractor wheels falling over the edge of a bank, or into a ditch.

Although the assignment of terrain class was subjective it could be done with some certainty in most cases. Doubt arose more from insufficient reported information than from imprecise type definition.

Ground hardness

When a safety cab impacts the ground some of the tractor's kinetic energy is absorbed by deformation of the cab and the ground. The proportion of the initial energy that is absorbed by the cab can vary from zero to more

Fig.2.1 & 2.2 Types of Overturning — Ground Profile

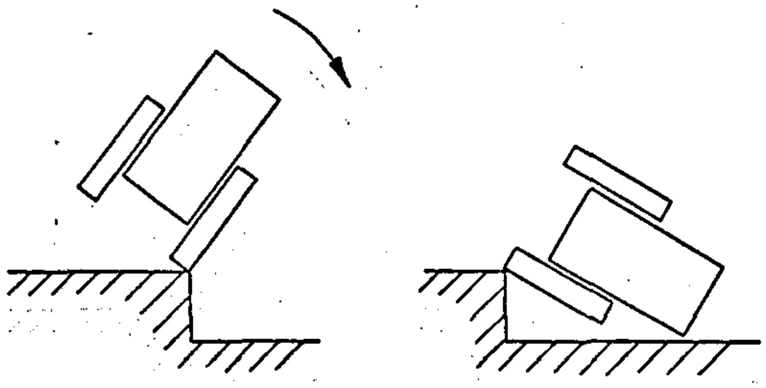

Fig.2.1
Tractor tips off bank, wheels remaining on edge

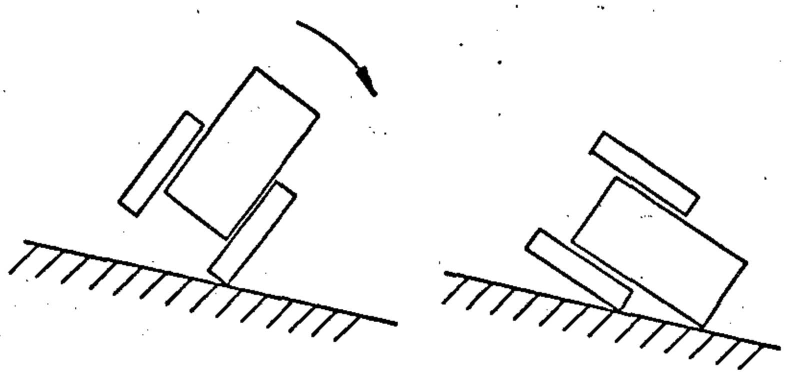

Fig. 2.2A
Overturning on flat ground, either level or with a uniform slope

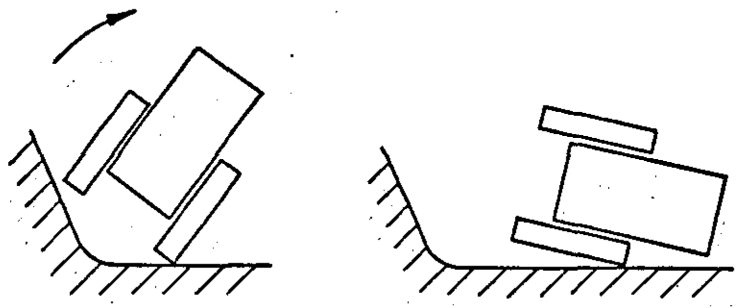

Fig.2.2B
Overturning initiated by tractor mounting bank or large obstacle

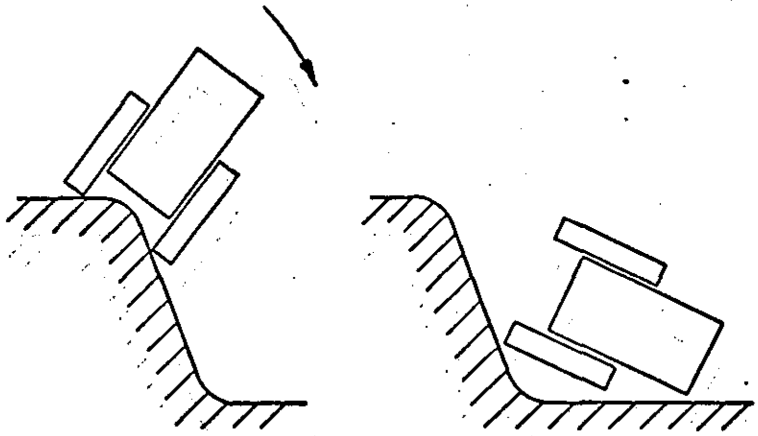

Fig2.2C
Overturning initiated by tractor falling over edge of bank or into ditch

than one, depending on the ground hardness and other factors. It is not possible to assess accurately from the accident reports the hardness of the ground onto which the tractors overturned, but in most cases a distinction can be made between surfaces such as concrete that probably would not deform visibly, and those where significant soil deformation would occur.

These two conditions are therefore designated respectively:-

H - hard ground;

S - soft ground.

This ground condition does not necessarily describe the type of surface the tractor was travelling on before it overturned. For example, several tractors travelling along roads overturned onto soft ground at the side, and in some cases the converse happened.

Vehicle control

Many accidents result from drivers losing control of their tractors, for instance on steep hills, because of inadequate brakes or overloaded trailers. One of two classes is assigned to each accident:-

L - Loss of control of the speed of the tractor before overturning

N - Normal operation (No loss of control).

Implements and trailers

The presence of an implement at the time of overturning is described by one of three classes:-

S - Solo tractor.

M - Mounted implement or equipment supported entirely or principally by the tractor.

T - Trailer or implement trailed from the drawbar.

The implement condition does not necessarily describe the arrangement before the start of the event culminating in the overturn; in some cases, for example, a trailer broke away during a long, out-of-control run downhill, and was not significant in the overturning incident. Such an accident would be classed as solo. The presence of an implement does not necessarily imply that it was a significant cause of overturning, although it would affect the dynamic behaviour.

Additional contributory factors

Where additional factors are considered important in the cause of overturning, although not necessarily in the events leading up to overturning, they are classified by a digit:-

1 - Side slope

2 - Sudden change of direction (steering)

3 - Surface with bumps or hollows

4 - Implement effect

5 - Other

Notation of classification

Each accident is described by a symbol-chain in the above order. For example:-

A - H - L - T - 1, 2 indicates a tractor and trailer overturning on uniform, hard ground after the driver had lost control, a side slope and change of direction contributing to the cause of overturning.

Where a classification is uncertain, either because of insufficient information or in a borderline case, the most likely class is given in parentheses.

2.2. RESULTS OF THE SURVEY - TYPE OF OVERTURNING

The classifications of the fatal overturning accidents in England and Wales, 1969 to 1971 are given in Appendix 2.1, and classifications and other data for the accidents involving tractors with safety cabs in Appendix 2.2.

These data are analysed in various ways below; in each case results are presented first for the 76 fatal accidents and then for the 38 accidents with cabs.

Distribution of type

The distribution by ground hardness, terrain and vehicle control of the fatal accidents is shown in Table 2.1 and for the accidents involving tractors with safety cabs in Table 2.2. None of the tractors involved in the fatal accidents was fitted with a safety cab. Uncertainties in the classification are included, but do not make a significant difference to the totals for each class, although they may affect individual entries.

Table 2.1

Distribution of fatal sideways overturning accidents in England and Wales, 1969-1971 by terrain, ground surface and vehicle control

Terrain Class	Year	Soft Surface			Hard Surface			Total		
		Control:		Total	Control:		Total	Control:		Total
		Loss	Normal		Loss	Normal		Loss	Normal	
A	1969	3	6	9	2	0	2	5	6	11
	1970	6	2	8	1	0	1	7	2	9
	1971	3	3	6	1	0	1	4	3	7
	Total	12	11	23	4	0	4	16	11	27
B	1969	1	0	1	2	4	6	3	4	7
	1970	1	0	1	3	1	4	4	1	5
	1971	1	0	1	3	3	6	4	3	7
	Total	3	0	3	8	8	16	11	8	19
C	1969	1	8	9	0	2	2	1	10	11
	1970	1	6	7	0	3	3	1	9	10
	1971	4	5	9	0	0	0	4	5	9
	Total	6	19	25	0	5	5	6	24	30
Total	1969	5	14	19	4	6	10	9	20	29
	1970	8	8	16	4	4	8	12	12	24
	1971	8	8	16	4	3	7	12	11	23
	Total	21	30	51	12	13	25	33	43	76

Table 2.2

Distribution of sideways overturning accidents in the U.K. involving tractors with safety cabs, 1971, by terrain, ground hardness and vehicle control

Terrain Class	Soft Surface			Hard Surface			Total		
	Control:		Total	Control:		Total	Control:		Total
	Loss	Normal		Loss	Normal		Loss	Normal	
A	3	12	15	0	3	3	3	15	18
B	2	1	3	1	2	3	3	3	6
C	2	11	13	0	1	1	2	12	14
Total	7	24	31	1	6	7	8	30	38

The distributions of the total number of accidents in each class expressed as percentages for both the fatal accidents and those involving tractors with safety cabs are given in Table 2.3, for terrain, ground hardness and vehicle control, and in Table 2.4 for implement condition and effect on overturning.

Table 2.3

Distribution of sideways overturning accidents by terrain, ground hardness and vehicle control - Percent of total number each year

Accidents		Terrain Class:			Surface:		Control:		Total Number
		A%	B%	C%	Soft%	Hard%	Loss%	Normal%	
Fatal	1969	38	24	38	66	34	31	69	29
	1970	37	21	42	67	33	50	50	24
	1971	30	30	39	70	30	52	48	23
	Total	36	25	39	67	33	43	57	76
Tractors with cabs		47	16	37	82	18	21	79	38

Table 2.4

Distribution of sideways overturning accidents by implement condition and implement effect on overturning - Percent of total numbers

Accidents	Implement condition:			Implement effect: on overturning			Total Number c Accident
	Solo tractor %	Mounted Implement %	Trailed %	Possible %	Probable %	Total %	
Fatal 1969-71	28	37	36	26	15	41	76
Tractors with cabs	18	29	53	11	39	50	38

Height and Slope of Bank in "C" - type accidents

In 35 out of the total of 44 "C"-type accidents the height of the bank is given in the accident report, but the steepness is described quantitatively in only 13 cases. These data are included in Appendices 2.1 and 2.2.

The distribution of bank height for the 35 "C"-type accidents is shown in Fig. 2.3; for each bank height the percentage of accidents occurring at greater height are plotted as ordinates.

The steepness of the banks varied from 1 in 3 to vertical.

Tractor speed and extent of overturning in accidents involving tractors with safety cabs

These data are tabulated in Appendix 2.2 and shown graphically in Figs.2.4 and 2.5. The distributions are plotted as the percentage of accidents in each doubling of the independent variable.

The tractor speeds recorded in the accident reports and referred to in this note unfortunately do not all relate to the instant of overturning, but in many cases to the speed before the events leading up to overturning. Sometimes, in loss-of-control accidents, the tractor would be travelling considerably faster at overturning than the speed reported, whereas in other instances braking or sliding could have reduced the speed significantly.

Deformation of safety cabs

The deformation recorded is normally the estimated linear distance out

Fig. 2.3 Cumulative Distribution of Bank Height in 'C'-Type Accidents

(Fatal accidents and those involving tractors with safety cabs — total number: 35)

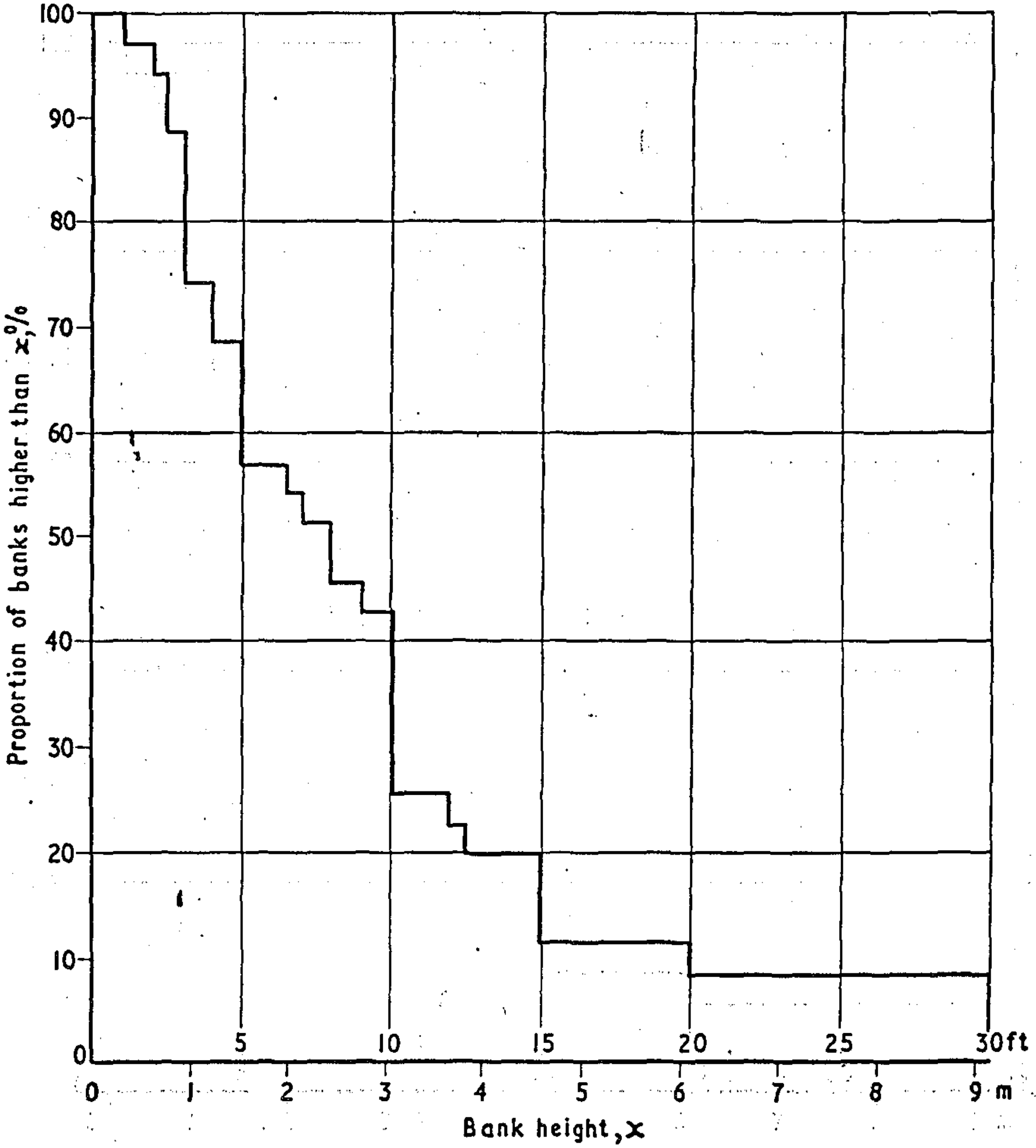

REF. TD 36602

Fig. 2.4 Distribution of Tractor Rotation During Overturning

(38 Accidents involving tractors with safety cabs)

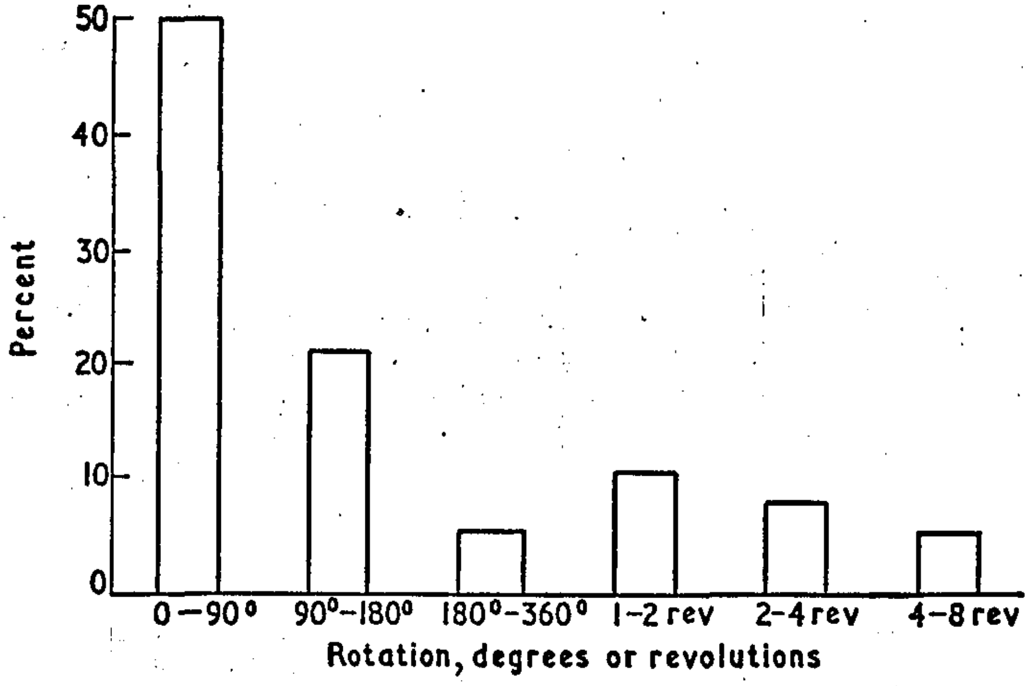

Fig. 2.5 Distribution of Tractor Speed Before Overturning

(34 Accidents involving tractors with safety cabs)

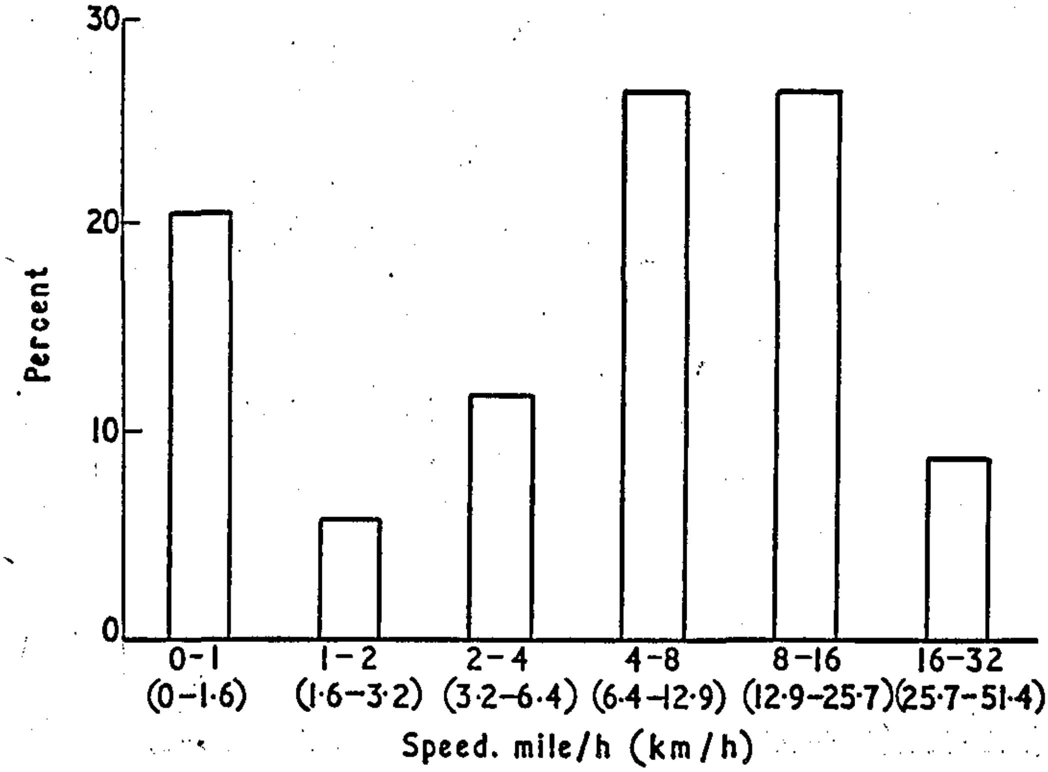

of true of the top cab member although in one case the angular displacement of the cab uprights is given.

Of the 38 accidents, no measurable deformation was reported in 17 and only "slight" in a further 6. The remaining 15 are tabulated below:-

Deformation:		Number reported:
0 to 1 inch	-	4
1 to 2 inch	-	4
2 to 4 inch	-	2
10 degrees	-	1
"Several inches"	-	1
Fracture and severe distortion	-	1
Unspecified	-	2

Thus in all but 4 or 5 of these accidents the cab displacements were considerably less than the normal range of deflection after O.E.C.D. tests on safety cabs. The accident in which the frame was fractured followed a downhill run of 300 yards by a driverless tractor at an estimated final speed of 25-30 mile/h.

2.3. OCCUPANT BEHAVIOUR AND INJURIES IN ACCIDENTS INVOLVING TRACTORS WITH SAFETY CABS

Occupant position after overturning

	Number of Drivers	Number of Passengers
Remained in cab throughout	28	0
Ejected during overturning	3	1
Jumped out intentionally	2	0
Unspecified	1	0
Total	34	1
Tractors that ran away driverless	4	
Total accidents	38	

The following analysis covers the 34 drivers who were in their cabs at the beginning of overturning.

Ability to hold onto steering wheel

Not enough is known at present about the forces on the driver during overturning accidents, or about the maximum forces that can be exerted by the hands and arms to assess the likelihood of drivers being able to retain hold of the steering wheel, although research in this area is planned. A driver is less likely to be injured in an overturning accident in a tractor with a safety cab if he is able to hold onto the wheel throughout, as the chance is reduced of being thrown against the cab or the ground.

Table 2.5 shows the number of drivers who retained hold of the steering wheel in these accidents. The proportion of drivers who did retain hold does not directly indicate the probability of being able to do so, since several drivers did not attempt to hold on.

Table 2.5

Drivers who retained hold of steering wheel throughout overturning accidents involving tractors with safety cabs

	Number who retained hold	Number who did not retain hold	Not known
Definitely	10	12	
Probably	5	3	
Total	15	15	4
% (of 34)	44	44	12

Drivers remaining in their seats during overturning

The O.E.C.D. test of tractor safety cabs[12] and a number of similar national tests use a criterion of approval that after impact tests the cab must not intrude on a fixed zone of clearance. The size of this zone is such that a driver should be protected from being crushed in an overturning accident, but the definition of the zone in relation to the tractor depends on the extent to which drivers are thrown around inside cabs during overturning.

Table 2.6 shows the number and proportion of drivers who remained in contact with the seat cushion throughout the accidents.

Table 2.6

Drivers remaining seated throughout overturning accidents involving tractors with safety cabs

	Stayed in seat	Thrown out of seat	Not known
Definitely	5	18	
Probably	3	2	
Total	8	20	6
% (of 34)	24	59	18

Injuries

Fifteen drivers were not injured.

The distribution of injury location and assumed agent for the remaining 19 is shown in Table 2.7. Some drivers received more than one injury.

Table 2.7

Location and assumed agent of injuries to drivers of tractors with safety cabs in overturning accidents

Location of injury	Assumed agent of injury						Total
	Cab			Tractor		Not known	
	Top*	Wiper motor	Unknown part	Transmission housing	Controls		
Head	3	1	6				10
Body	1		5			1	7
Legs			3	2	2	1	8
Arms			1		1	1	3
Not stated		1				1	2
Total	4	2	15	2	3	4	30
Total	21			5			

*Cab top includes roof and top frame members

One driver received broken ribs and collar-bone, but apart from this case the injuries were bruising or lacerations.

2.4. DISCUSSION AND CONCLUSIONS

1. The distributions of fatal accidents are similar in each of the three years considered (Table 2.1), particularly in the class totals (Table 2.3) where the only significant variation is the relatively low proportion of accidents involving loss of control in 1969. It may therefore be assumed that these distributions are typical of fatal accidents in England and Wales.

   The distributions of accidents involving tractors with safety cabs (Table 2.2) however, are different in several respects from those of fatal accidents (Table 2.3). In particular, the proportions of fatal overturns onto hard surfaces (33%) and involving loss of control (43%) are both about twice those of accidents involving tractors with safety cabs (18% and 21% respectively). Although the records for non-fatal accidents are probably incomplete, they may be more representative of all overturning accidents than the fatal ones. As might be expected, the distribution of fatal accidents is biased towards greater severity.

2. The proportion of accidents in which tractors overturned onto hard surfaces - about one-fifth for the tractors with cabs and one-third for fatal ones indicates that these types of impact must be considered "normal" in research and testing of safety cabs.

3. Considering the dynamics of the motion after the initial instability type 'B' may be treated as a special case of type 'A', as may type 'C' accidents where the bank is long and shallow. In each of these cases the side of the tractor's rear wheel probably impacts the ground before the cab and absorbs a considerable amount of energy. The only accidents that are likely to result in the frame receiving most of the energy are 'C' types on banks steeper than about 45° and with heights between about 8 ft. and 12 ft. For greatest energy absorption in the cab the ground surface impacted must be hard.

   From Fig. 2.3, bank heights between 8 ft. and 12.5 ft. featured in about

30% of the 'C' type accidents where the height was recorded, and in about half of these cases the banks were probably steeper than 45°. Since the proportion of all accidents that are 'C' type is just under 40% the number of overturns that include this combination of circumstances is estimated to be about 5% of the total. Only one-fifth of the fatal and one in fourteen of the 'C' type accidents with cabs were on hard surfaces, so that maximum energy input to the cab is likely in less than 1% of all overturning accidents.

4. In most of the 'C' type accidents the tractors had been travelling parallel or at a small angle to the edges of the banks before overturning but in at least five cases the tractors were driven over the banks at large angles. The dynamics of this type of accident are somewhat different, in that both front wheels fall over the edge before either rear wheel, and the direction of overturning is predominantly forwards rather than sideways.

5. In 8 of the 30 fatal 'C' type accidents the tractors fell into rivers, ditches or ponds containing water. These accidents have been included in the soft surface class, but may represent a sufficiently large proportion to warrant separate study. The driver was drowned, rather than crushed in only about 2 of these cases, but drowning may represent a relatively more important hazard with safety cabs.

6. The total numbers of fatal accidents in each year are not identical to the figures published by M.A.F.F. This is due to slightly different definitions of sideways overturning and is explained in Appendix 2.3.

7. Although tractor overturning accidents occur in a wide range of circumstances and conditions it has been found possible to classify them according to the dynamics of the behaviour into a small number of distinct types. Limitations of the classification system occur in borderline cases, where the accident reports contain insufficient

information and in particularly complex dynamic situations. The system describes the overturning incident and not the cause of events leading up to overturning, which may be of equal interest in other investigations.

8. No examples were found of the type of overturning represented in Fig.2.1 that has been used in some previous research studies, and it is concluded that this is not a type of accident frequently occurring in the U.K. which it is realistic to simulate for tests.

9. Safety cab legislation is designed to protect drivers from being crushed in a very high proportion of accidents, probably approaching 100%, and test codes are therefore based on the most severe "reasonable" accidents in terms of potential safety cab damage. One of the principal objects of this survey was to highlight these severe types of accident so that they may be simulated in research. In looking for such extremes this limited survey can only hope to point out the important types of accident, without being too precise about their frequency of occurrence.

The energy absorbed by a cab in its first impact with the ground depends on:-

(a) the initial kinetic energy of the tractor, which is proportional to the square of its speed in the absence of significant rotation;

(b) the change in potential energy if the centre of mass of the tractor falls during overturning;

(c) energy dissipated in deforming the ground and parts of the tractor such as tyres and wheels, and in sliding friction;

(d) the kinetic energy remaining after the first cab impact, which will eventually be dissipated as in (c) above or in further cab impacts until the tractor comes to rest. Further change in potential energy may occur during this process, which increases the quantity to be dissipated.

Parts (a), (b) and (c) relate to individual characteristics of an accident that can be considered separately and estimated if enough data is known.

Part (d) can only be assessed by dynamic analysis. Attention in section 3 of the discussion has concentrated on part (c) as this is the most complicated and variable. It is possible fortwo accidents to be apparently similar and yet result in considerably different cab damage because of energy absorbed by tractor wheel impact. While it could not be shown that absence of wheel impact was certain in any of the accidents, its probability was estimated to be about 5%.

There was not sufficient data to enable a correlation to be established between these conditions and severe safety cab deformation. The accident which resulted in the greatest cab damage occurred at very high speed, 25 to 30 mile/h, and this is thought to be the main reason. In other cases the deformation was perhaps surprisingly small, suggesting that the conditions for absorption of the highest proportion of energy in the cab were not encountered. In a sample of 38 accidents it is reasonable that situations with a probability of only a few percent may not appear. On the basis of this survey it was therefore considered that research on sideways overturning accidents should be concentrated on two types or conditions:-

(i) a tractor falling over the edge of a bank between 8 ft. and 12.5 ft. high with a slope between 50° and 90° to the horizontal, and landing on hard or soft ground;

(ii) accidents at high speed involving multiple rolls.

10. In half of the accidents involving tractors with safety cabs the angle of rotation during overturning was only about 90°, but in about a quarter the tractors rolled more than one complete revolution up to a maximum of eight in two cases (Fig.2.4). When a tractor rolls more than 360° the cab receives further impacts and the probability of the driver being ejected and injured is greatly increased. The wider use of proven devices to prevent continued rolling should be promoted more actively.

11. Tractor speed before overturning (Fig.2.5) was higher than 8 mile/h in 35% of accidents involving tractors with safety cabs. In reference 23 it is reported that only 27% of the sideways overturning accidents analysed occurred at a speed higher than 5 mile/h, and only 15% at over 9 mile/h. As has been discussed in section 2.2, data relating to speed must be interpreted with caution; it is likely, however, that a significant number of tractors overturn at speeds above 15 mile/h, or even 20 mile/h.

12. The effects of implements and trailers on overturning are twofold - they will modify the dynamics of the motion and they may contribute to the cause of overturning. In addition a load may induce loss of control which results in overturning, but this is outside the scope of this thesis.

    Implements or trailers were coupled to 82% of the tractors with safety cabs and 72% of those in fatal accidents. The equivalent figures quoted in references 23, 25 and 26 are 71%, 50% and 87% respectively. The proportion of accidents in which the machines were partly responsible for overturning was in the range 15% to 50%.

13. Fourty-four percent of drivers in accidents involving tractors with safety cabs were able to hold onto the steering wheel throughout overturning, and if all drivers had tried to hold on the proportion would probably have been slightly higher. It is likely, however, that in the most severe accidents the driver is not able to retain hold and safety cab design and test criteria must take account of this.

    Only a quarter of drivers remained seated throughout overturning, and this may similarly be expected to represent the less severe accidents.

14. Injuries received in accidents involving tractors with safety cabs were generally minor - bruising and laceration - and about half the drivers were not injured.

3. MATHEMATICAL MODELS OF OVERTURNING AND IMPACT

3.1 PREVIOUS WORK

In discussing mathematical analyses of overturning it is useful to differentiate between studies concerned solely with stability and those that go on to treat the impacts with the ground. Not only are the approaches generally different in the two cases, but the objectives are also different.

The earliest investigations, by McKibben[4] in 1927 and Worthington[32] in 1949, were directed towards finding criteria to prevent the instabilities that lead to overturning, and many more recent studies have pursued this approach. The value of this in demonstrating to designers and operators the conditions most likely to lead to accidents is not doubted, but despite more stable equipment and better education, tractors will continue to overturn.

Automatic devices sensing, for example, roll angle and velocity, have been suggested frequently but, apart from practical problems of cost and reliability, the stability thresholds would have to be very high for corrective action to be able to prevent the majority of overturns.

This was recognised in the experimental work by Moberg[5] which led to the introduction in Sweden of the first law requiring ROPS to be fitted to tractors. National and international legislation followed rapidly in many countries, and the prime need in overturning studies became the determination of the amount of impact energy absorbed in the ROPS. Studies of this kind remained in the minority, however, and work on stability continued, particularly in eastern Europe and the U.S.A. The more important of these investigations will be mentioned briefly before summarising work on impact.

Rearward overturning initiated by high rear axle torque combined with a draught force applied too high on the rear of the tractor, is much less common than sideways overturning in Europe. The proportion of rearwards overturns in the U.K. was about 15-20% a few years ago and has declined to perhaps 5-10% due to better driver education. This type of accident is outside the scope of the N.I.A.E. simulation. In the U.S.A., however, the proportion is much higher, figures of 25-60% having been quoted. This, and the relatively simple dynamics of rearing, led to a number of mathematical analyses, some of considerable sophistication and some validated by experiments[33-36]. An Italian study has also been published[37], and in the U.K. Manby[11] developed a simple analysis to determine the energy immediately before impact, supported by experimental measurements.

Apart from the particular case of rearing, overturning generally arises from a combination of three factors: sloping ground, bumps that cause roll or pitch motions, and cornering forces generated in tight turns. Most of the stability studies have concentrated on one, or perhaps two, of these factors.

The determination of even the static stability of a tractor on a slope is not straightforward because of the different tipping axes resulting from the front axle rotation about its longitudinal pivot. Articulated tractors, which are used widely in forestry and are becoming more common in agriculture, present an additional complexity[38, 39]. Daskalov[40] is typical of the East European researchers[41-44] in taking static slope stability criteria for different tractor heading angles as the starting point for a dynamic analysis. His analysis includes the effect of turns of constant radius starting from any direction in relation to the slope. It can handle tractor-trailer combinations in addition to solo vehicles but does not take ground roughness or tyre flexibility into account.

In constrast, recent U.S. research, mainly at Purdue University, has concentrated on the development of models treating the tractor as a spring-mass system. From a relatively simple tipping-axis analysis[45], complex models were produced which incorporated tyre flexibilities in vertical, transverse and longitudinal directions, tyre/soil force relationships and the inertias of the front axle, wheels and tractor chassis[46]. Two simulations are described: (i) a simple steering manuevre, and (ii) a tractor mounting a sinusoidal bump of various heights at different speeds, on side slopes from 0-30^{o} [47]. The envelope of overturning instabilities was determined and reasonable agreement found with results from a number of experiments.

The most sophisticated stability model is probably that developed by Davis[48, 49] from the general models of three-dimensional vehicle motion produced at Cornell[50]. Apart from his adaption of many model details to tractor overturning conditions, Davis's main contribution lay in the replacement of the three Euler angles by four variables he termed Euler parameters. These are defined as non-linear combinations of elements of the transformation matrix of direction cosines, and their purpose is to avoid the instability in equations based on Euler angles when certain rotations pass through 90^{o}. This is of value when the most general motions are to be considered, but the simpler technique of choosing a suitable sequence of rotations for the transform is adequate when only one of them is likely to exceed 90°, as is normally the case (see section 5.2).

Another significant feature of Davis's work was his choice of a bank type of accident. This was found to be important in the N.I.A.E. study, as discussed in section 2.

A novel approach to stability was introduced by Zakharyan(51) and developed by Spencer(52). Although their basic models were extremely simple, the introduction of a statistical representation of ground roughness allowed the establishment of overall probabilities of overturning, rather than the treatment of isolated cases under specific conditions.

The first significant impact models were those of Watson(9). To underline the distinction between the two approaches, the starting point for his simulations was the unstable equilibrium where the stability analyses ended. Two types of overturn were considered, shown diagrammatically in Figs. 2.1 and 2.2a. His slope accident is the normal case but the bank accident modelled the situation used by Moberg in laboratory studies, where one wheel remains on the top of the bank. The impacts at the sides of the wheels and ROPS were treated in two dimensions as pure plastic impulses, allowing a simple mathematical analysis. The significance of this, and of the accident types, is discussed later. Watson found that the energy absorbed in the ROPS impulse was much higher in the bank accident than in the overturn on a uniform slope, because of the different amounts of energy absorbed in impacts at the side of the wheel. This difference had been suggested by other workers and highlighted the importance of the bank accident. The bank heights tested, 1-4 ft (0.3-1.2 m) were necessarily rather arbitrary but the results led Watson to suggest inconsistencies in the energy/tractor weight relationships used in the Swedish test codes.

Schwanghart developed a three dimensional model of overturning on a uniform slope using a similar impact analysis[53]. The main purpose was to provide the German authorities with a simulation to replace their test to establish whether a tractor would continue to roll after the first ROPS impact. Impact energy could, however, be estimated, and both Schwanghart[54] and Boyer[55] developed extended models to overcome some of the limitations of the impulse analysis by simple considerations of ROPS and soil deformation. The three dimensional treatment was an approximation restricted to the incorporation of non-parallel tipping axes, and the analysis of the impulses that instantaneously changed the directions of these axes was not clearly described.

Schwanghart ran his simulations with data from individual tractor and ROPS, and with mean values taken from regressions of the vehicle parameters against mass. The energy absorbed in the ROPS was found to increase with mass in a relationship that could be approximated by a low order polynomial[56]. The absolute values for a slope of 1:2.5 were generally lower than those in current EEC, ISO and OECD static test proposals for tractors of less than about 4000 kg, and higher for heavier tractors.

A further, two dimensional extension to Watsons uniform slope model was published recently by Cobb[57]. The same treatment using plastic impulses was applied to all impacts except those at the ROPS; it is probably a better approximation in the case studied of a crawler tractor, where the tracks are more rigid than wheels and tyres. An analysis of the forces and deflections at the ROPS impact allowed this to be handled more realistically, although only one direction of ROPS deformation was included and supporting forces at other contact points were ignored. Soil and ROPS strengths were found to influence significantly the amounts of energy absorbed in the ROPS, but the overall relationship with tractor mass was approximately linear over the range 0-50,000 kg.

3.2. MODELLING APPROACH

Mathematical models are, inevitably, an idealised abstraction of reality. The art of model building lies in deciding what to leave out - to fix the level of abstraction so that the performance is sufficiently realistic for the intended purpose without requiring excessive time and effort in development. The sophisticated model of Davis cited above(48) took a great deal of time to adapt from other models, which themselves had been developed over many years. It was very successful in meeting its purpose of studying the effects of driver behaviour and terrain on stability, although it has not been completely validated in full-scale experiments. At the other extreme, the simple models of Watson(9), while helping to indicate important trends, may not be realistic enough to allow the comparisons that are required.

At the outset of the present study it was considered that the largest gap lay in reliable representation of impact behaviour. Furthermore, because of the complexity of overturning accident dynamics it was felt that models must be based firmly on realistic cases and be throughly validated experimentally. This placing of simulation as part of a wider programme increased the need for economy in model development(61).

The predominant motions in a sideways roll over occur in two dimensions, in the plane perpendicular to the direction of forward motion of the tractor. Accordingly, the models were developed initially in this two dimensional plane, with the possibility of extending them to three dimensions should the need be indicated by comparisons with experimental results. The main effort was directed towards achieving adequate realism in the model details, for example of tyre behaviour and non-linear structural characteristics.

3.3. INITIAL DEVELOPMENT

At first two separate models were produced, one for the overturning part of the bank accident and the other treating the general impact case. The dynamics of the initial overturning part of a multiple roll on a uniform slope are relatively simple if initial conditions are assumed, and the impact model was designed to cover both accident types. The impact model formed the basis of the final complete simulation and will be described later.

The initial bank overturning model and the computer program UPSET derived from it were based on the diagram shown in Fig.3.1. Tyre deflection in the plane of the diagram was ignored but the relationship between side force and slip angle, described later, were developed as part of this model. The equations of motion were derived directly from Newtons laws; the presence of colomb friction and the need to quantify forces made a Langrangian solution inappropriate.

The model has a maximum of three degrees of freedom, conventionally represented as lateral and vertical linear displacement of the centre of mass and rotation in roll, x_g, y_g and θ respectively. Roll angle is defined as negative clockwise for all the two-dimensional models. The constraint introduced at each tyre when in contact with the surface reduces the number of degrees of freedom by one and provides a geometrical relationship in its place.

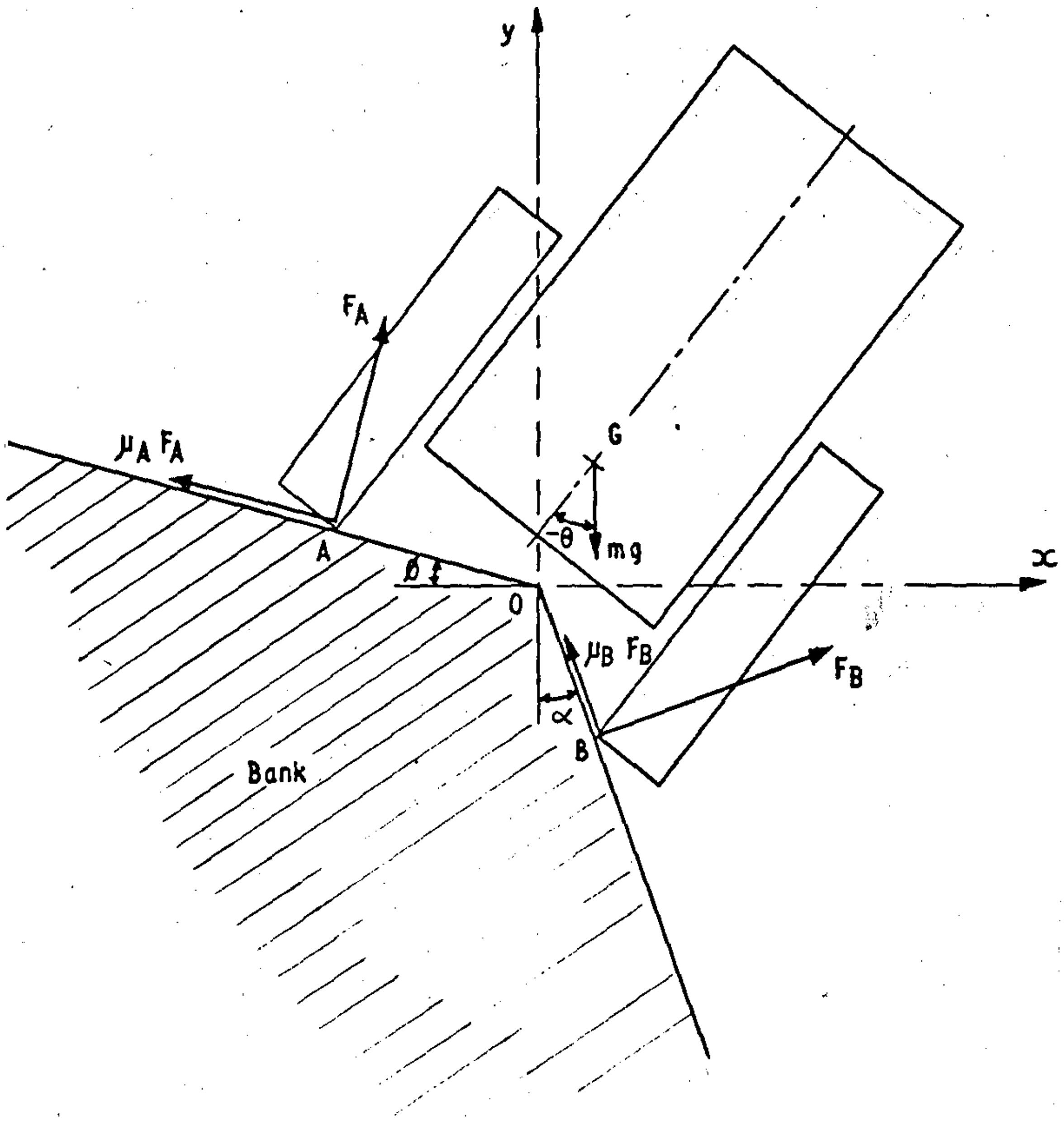

Fig. 3.1. Forces and coordinates for bank overturning model

Thus for most of the overturn, when both tyres are in contact, the model has a single degree of freedom and a single equation of motion. Although the development of this equation was reasonably straightforward, considerable algebraic manipulation was required and lengthy expressions resulted. As a further complexity the angle ϕ of the bank top surface was treated in this model as a variable, and its differential coefficients had to be included. The main purpose was to allow simulation of the behaviour when a helicoidal ramp was used to assist the overturn in the experiments, but the added generality would also have some value in relation to real accidents. The helicoidal ramp was not used, however, and ϕ was considered constant in the later models.

Comparisons with the experimental results were encouraging but the lack of tyre flexibility limited realism and resulted in several discrepencies in the simulation. In particular, it was not possible to include a representation of the chamfer at the edge of the experimental bank because of the invalid behaviour of rigid tyres at surface discontinuities. In addition, the exact point of loss of tyre contact was found to affect behaviour significantly, and this is influenced in real life by ride-mode vibration.

3.4. A GENERAL MODEL WITH VEHICLE AND GROUND FLEXIBILITIES AT CONTACT POINTS

Previous overturning models have treated each ground impact as a pure, plastic impulse. After impact the body was assumed to rotate about the impact point with a velocity determined from conservation of angular momentum. While this technique helps to give a broad indication of behavior and energy loss, it is strictly applicable only where impact forces are infinitely high compared with body weight and where the "coefficient of restitution" is zero. It also does not allow determination of the distribution of energy loss between the two impacting members.

The collapse force of ROPS are typically between one and 1.5 times tractor weight, with occasional higher and lower values; a significant proportion of the energy is absorbed elastically and recovered after impact. The real effects not represented in a plastic impulse analysis may be summarised as:

(i) Translational and rotational displacements during the finite impact period (which themselves change the body's energy state.

(ii) Geometrical changes due to finite deformation, which affect the moments of applied forces.

(iii) Velocities imparted after impact by elastic recovery.

(iv) The effects of forces at other body points in simultaneous contact with the ground.

A simple analysis under typical conditions indicated likely errors due to (i) alone of 15-40%.

The impact part of the present model therefore includes the force/deflection characteristics of both body and ground. The deterministic, time-domain simulation is based on the solution of four sets of equations:

(i) Relations of equilibrium between body and ground forces at each contact point;

(ii) Compatibility of body position and velocity vectors (x_g, y_g and θ), body contact-point deformation and ground deformation;

(iii) Structural relationships between force, deformations and deformation rate;

(iv) The equations of motion relating position vectors to applied forces.

The method as used involves two assumptions:

(a) All mass and inertia is concentrated in the "rigid" part of the body, which has three degrees of freedom;

(b) Each body contact point is directly connected to this "rigid" part by defined structural characteristics in two directions, which are independent of relative displacements of other points.

The method could doubtless be extended to include deforming members of finite mass. Ways round the second assumption for treating parallel structural elements are described later.

The method is effectively a generalisation of Cobbs[57] to include all possible contact points and directions of deformation, within the scope of a two dimensional model. Force-deflection characteristics have also been included in a single dimensional model by Emmerson, to study car body deformation on impact[58].

The general solution of the equations is made clearer by considering the effects of numerical integration. At each time step in a central integration method, the sets of equations (i) - (iii) above are solved to determine the current force matrix and hence the "rigid" body accelerations. Double integration of the accelerations generates new body position and velocity vectors which apply to the solution of (i) - (iii) in the next step. Thus, the various body points under simultaneous ground contact are coupled only through the integrations, and (i) - (iii) may be solved independently for each point. This solution is still not tractible in closed form in the general case, and further assumptions or iterative methods are required. This is described in the following section.

Although at first this method was developed to handle impact, the equations are equally suitable for describing tyre flexibility. When the limitations of UPSET became apparent, a new program ROVER (Roll over) was adapted from the IMPACT program to model the overturning phase of the bank accident. Assumptions of rigid ground and linear tyre stiffness in this phase allowed the use of simplified forms of the contact point equations and eased the development of velocity terms (damping) in the structural characteristics.

Finally, the two versions were incorporated into a single program TROLL (Tractor roll over) which covered the entire overturn and was suitable for multiple rolls as well as for the bank accident.

3.4.1. The contact-point equations

The forces and displacements at a contact point are shown in Fig.3.2 The tractor centre of mass position and roll angle are defined by coordinates x, y, θ relative to a fixed frame of reference. The position vectors of the contact point relative to the rigid body centre of mass are denoted by x_1, y_1, and the forces in these directions are those of the body acting on the ground. The local slope of the ground contact surface to the reference frame is α' and the ground coordinates u and v are transformations of x and y through α', with the same origin. The forces Fu and Fv are those of the ground on the body.

The three sets of equations may then be written as:

$$\text{(i)} \quad f1\,(Fx_1,\ Fy_1,\ Fv,\ \theta,\ \alpha') = 0 \qquad \text{-(3.1)}$$

$$f2\,(Fx_1,\ Fy_1,\ Fu,\ \theta,\ \alpha') = 0 \qquad \text{-(3.2)}$$

$$\text{(ii)} \quad f3\,(x_1,\ y_1,\ v,\ x_g,\ y_g,\ \theta,\ \alpha') = 0 \qquad \text{-(3.3)}$$

$$f4\,(x_1,\ y_1,\ u,\ x_g,\ y_g,\ \theta,\ \alpha') = 0 \qquad \text{-(3.4)}$$

$$\text{(iii)} \quad f5\,(Fx_1,\ x_1,\ \dot{x}_1) = 0 \qquad \text{-(3.5)}$$

$$f6\,(Fy_1,\ y_1,\ \dot{y}_1) = 0 \qquad \text{-(3.6)}$$

$$f7\,(Fv,\ v,\ \dot{v}) = 0 \qquad \text{-(3.7)}$$

$$f8\,(Fu,\ u,\ \dot{u}) = 0 \qquad \text{-(3.8)}$$

Knowing x_g, y_g, θ and α', this gives eight equations in eight unknowns. The relationship of (i) and (ii) are obtained directly by resolution and transformation, and may be rearranged in a number of ways to yield different combinations of variables. No amount of manipulation has been found, however, to permit a direct solution of the eight equations while (iii) remain in a general, non-linear form.

The first step towards a solution is to re-cast (3.8) as:

$$Fu = -\mu\, Fv \qquad \text{-(3.9)}$$

(the negative coefficient indicates that Fu is opposing the direction of movement, $\dot{u}$)

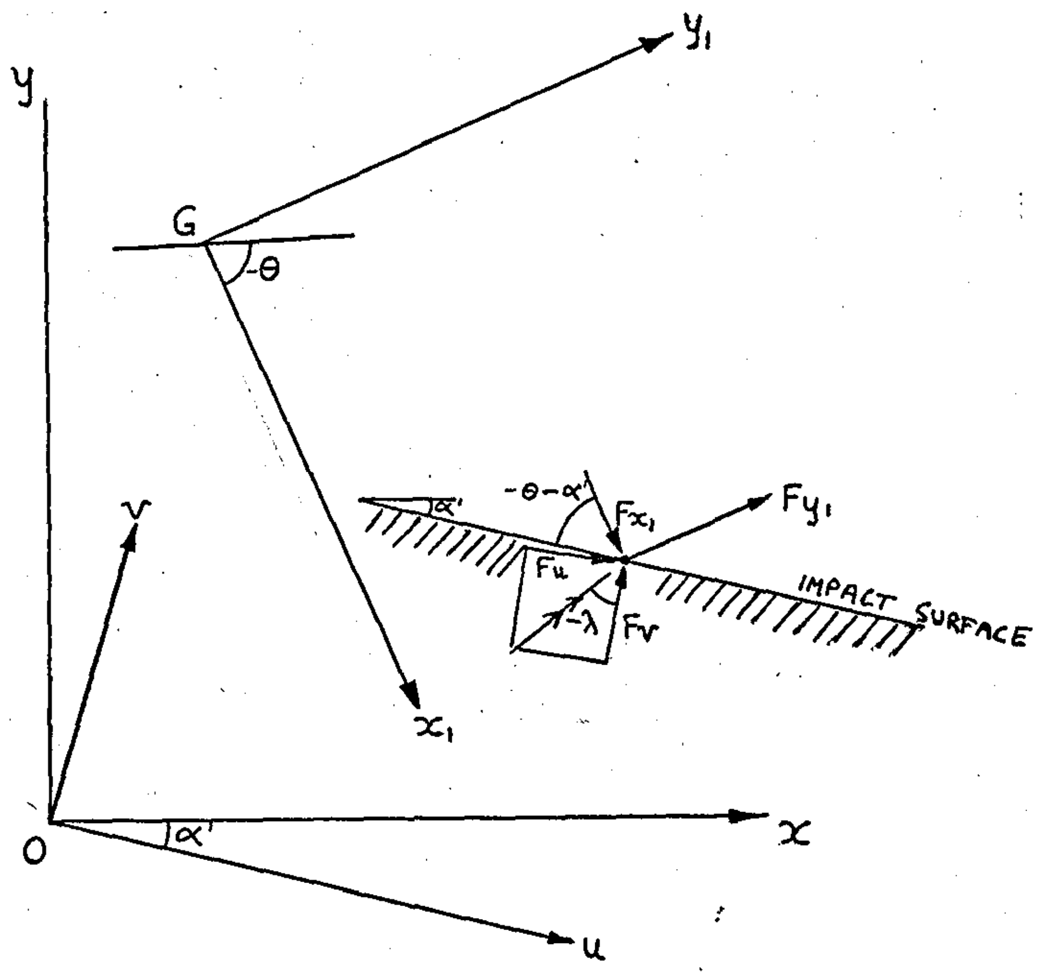

Fig. 3.2. Forces and coordinates at a contact point

The "coefficient of friction" μ may be considered not as a constant but as a continually varying function. It is assumed that μ varies relatively slowly in relation to the integration step-length, allowing it to be computed with sufficient accuracy from past values of forces, displacements and velocities. For a tyre or structure sliding on concrete or soil this is a reasonable assumption. If it were not, it would be necessary to perform an iteration on μ at each time step, a possible but lengthy operation.

If λ if defined by:

$$\mu = \tan\lambda \qquad -(3.10)$$

equations (1) and (2) are obtained in the most convenient form by resloving along and perpendicular to the resultant of Fv and Fu:

$$Fx_1 \sin(\alpha' - \lambda + \theta) + Fy_1 \cos(\alpha' - \lambda + \theta) + Fv \sec\lambda = 0 \qquad -(3.1a)$$

and $$Fx_1 \cos(\alpha' - \lambda + \theta) - Fy_1 \sin(\alpha' - \lambda + \theta) = 0 \qquad -(3.2a)$$

solving (1a) and (2a) for Fx_1 and Fy_1 in terms of Fv gives:-

$$Fx_1 = -Fv(\sin(\alpha' + \theta) - \cos(\alpha' + \theta)) \qquad -(3.11)$$

and $$Fy_1 = -Fv(\cos(\alpha' + \theta) + \sin(\alpha' + \theta)) \qquad -(3.12)$$

The geometrical transformations between u, v and x, y are:

$$u = x\cos\alpha' - y\sin\alpha'$$

and $$v = x\sin\alpha' + y\cos\alpha'$$

And the transformations between fixed and body coordinates are:

$$x = x_g = x_1 \cos\theta - y_1 \sin\theta$$

$$y = y_g + x_1 \sin\theta + Y_1 \cos\theta$$

These four equations together yield (3.3) and (3.4) most suitably as:

$$V = x_g \sin\alpha' + y_g \cos\alpha' + x_1 \sin(\alpha' + \theta) + y_1 \cos(\alpha' + \theta) \qquad -(3.3a)$$

and $$U = x_g \cos\alpha' - y_g \sin\alpha' + x_1 \cos(\alpha' + \theta) - y_1 \sin(\alpha' + \theta) \qquad -(3.4a)$$

The set of equations to be solved now consists of (3.3a), (3.11a) and (3.12), together with the structural relationships (3.5), (3.6) and (3.7). The velocity terms will be ignored temporarily and it will be shown later that they can be incorporated with the displacement terms in a numerical solution.

The most general solution, with (3.5), (3.6) and (3.7) in the form of arbitrary functions, would require iteration. If the force-displacement relationships can be represented by low order polynomials a direct solution may be possible in certain cases:

$$x_1 = a_0 + a_1 Fx_1 + a_2 Fx_1^2 + a_3 Fx_1^3 \ldots\ldots \qquad -(3.13)$$

and similarly for y_1 and V.

If: Fx_1 from (3.11) is substituted in (3.13), followed by the resulting expression for x_1 in (3.3a);

And similarly for Fy_1 from (3.12), then y_1 in (3.3a);

And finally for V from (3.13) in terms of F_V in (3.3a);

- the result is a polynomial of the same order as (3.13) in Fv.

The lowest order polynomial that could adequately represent elasto-plastic structural behaviour is a cubic. The effective transition from elastic to plastic phase would be very gradual, and the gradient in the plastic range too steep; performance in both aspects would be improved by a higher order curve.

A cubic with zero constant and quadratic coefficients could be solved, as could some higher order functions, but the resulting equations would be rather combersome. In view of the numerical solution used it is easier, more accurate and probably not much less efficient in computing time to use characteristics that are piece-wise linear.

These then become:

$$x_1 = x_{1fo} + k_{x1} \; Fx_1 \qquad -(3.5a)$$

$$y_1 = y_{1fo} + k_{y1} \; Fy_1 \qquad -(3.6a)$$

$$V = v_{fo} + k_v \; Fv \qquad -(3.7a)$$

where x_{1fo}, k_{x1} etc are constants for each straight line part of the approximation. In the computer program, the values of these constants are initially assumed at each step to be the same as for the previous step. If, after solution, the force (or deflection) is found to lie outside the bounds of that line the solution is recalculated with constants appropriate to the new range. The procedure is described more fully in section 3.5.

The parameter k in (3.5a)-(3.7a) represents flexibility, or inverse stiffness. This unconventional form is used not only to ease manipulation but to allow representation of rigid surfaces by finite values (i.e. k = o). Care is also needed in the form of the final equations for incorporation in the program to avoid sensitivity problems, the most extreme example being attempts to divide by zero. It is therefore most appropriate to solve first for the forces and then for the deflections.

The sequence of substitution is that suggested for the polynomial.

Put $s_1 = \sin(\alpha' + \theta)$

and $c_1 = \cos(\alpha' + \theta)$ —(3.14)

Then (3.5a) in (3.11) gives:

$$x_1 = x_{10} - k_x Fv (s_1 - \mu c_1) \qquad -(3.15)$$

and (3.6a) in (3.12) gives:

$$y_1 = y_{10} - k_y Fv (c_1 + \mu s_1) \qquad -(3.16)$$

(3.7a), (3.15) and (3.16) in (3.3a) give:

$$v_o + k_v Fv = x_g \sin\alpha' + y_g \cos\alpha' + (x_{10} - k_x Fv (s_1 - \mu c_1)).s_1 + (y_{10} - k_y Fv (c_1 + \mu s_1)).\ c_1$$

or
$$Fv = \frac{x_g \sin\alpha' + y_g \cos\alpha' + x_{10} s_1 + y_{10} c_1 - v_o}{k_v + s_1 k_x (s_1 - \mu c_1) + c_1 k_y (c_1 + \mu s_1)} \qquad -(3.17)$$

The denominator of (3.17) can be zero only if k_v is zero <u>and</u>:

<u>either</u> k_x is zero and $(\theta + \alpha') = \pm 90^\circ$

<u>or</u> k_y is zero and $(\theta + \alpha') = 0$

(excluding the trivial case when all three k are zero)

Any of these conditions amounts to a rigid body meeting a rigid surface, when the force would indeed be theoretically infinite. Equation (3.17) may therefore be accepted as appropriate for numerical solution.

F_{x1} and F_{y1} are determined from Fv in (3.11) and (3.12), whence x_1, y_1 and v from (3.5a), (3.6a) and (3.7a). Finally u is given by (3.4a) and Fu by (3.9). None of these equations is sensitive.

3.4.2. The contact points

Although the vehicle makes contact with the ground over finite areas, there are several points that may be considered as the effective centres of these areas, without likelihood of significant inaccuracy. The ten points selected around the periphery are shown in Fig. 3.3.

Points 4-7 are the tops and bottoms of the wheel rims. Points 9 and 10 are at the bottom of the tyres, either on the inside or on the outside edge according to the slope of the local ground surface. The choice of these six points and the manner of manipulating them are affected by the model constraint that each point must be independent of every other point. Had each of 9 and 10 been replaced by two points, one outside and one inside, the lateral deflections and forces of the two points on each tyre would be related to each other. Instead, the single point is "moved" when the tyre becomes perpendicular to the surface by changing the body-coordinate origin of the force-deflection curve in between integration steps. This is valid provided that the time derivative of this coordinate is preserved. During the greater part of the overturning phase the points are on the inside edges, as shown in Fig.3.1, and a single change for each tyre is made at the appropriate moment.

Contact at the wheel rims during impact raises another problem. Deformation of the wheel centre, or disc, is an important part of an overturning accident and contributes significantly to the energy dissipation. The simplest way of handling this deformation would have been to treat the tyre as the first, elastic stage of a single structural characteristic involving tyre and disc together. This would not have been entirely satisfactory for two reasons. Firstly, the limiting tyre force or deflection at which the rim makes contact depends on the angle of the wheel to the surface; the smaller this angle, the smaller the tyre deflection, up to the case where the wheel is parallel to the ground when the rim and tyre make nearly simultaneous impact. To incorporate this into the simulation

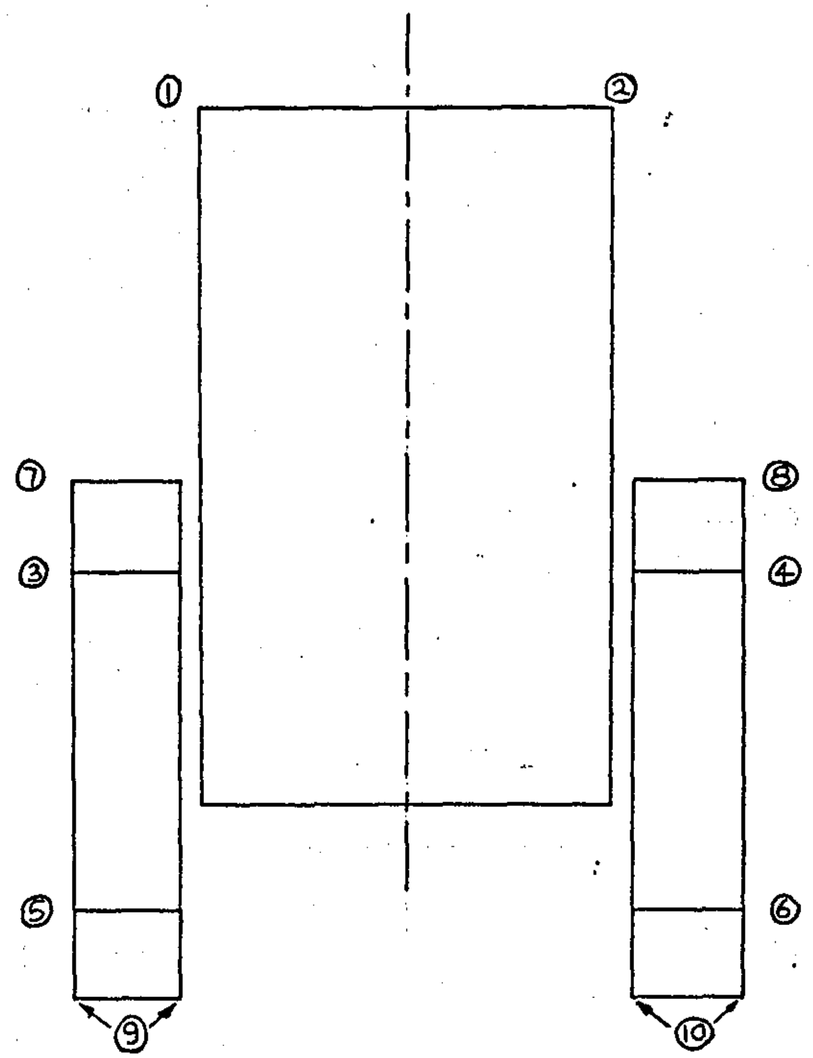

Fig. 3.3. The ten tractor contact points

would have required continuous updating of the structural characteristics. The other reason is that, when the rim is in direct contact, the effective point of application of the ground force to the vehicle is not at the tyre edge, point 9 or 10, but somewhere between this and the rim.

A complete modelling of this behaviour would have required moment-generating contact points, rather than those that simply apply forces to the body. This seemed an unnecessary complication. With separate contact points at tyre and rim the difficulties are largely overcome, but the base of the tyre must be made to move with the rim when this deflects. The same technique of shifting the origin of the tyre force-deflection curve was used, again with preservation of velocity.

Points 1 and 2 on the ROPS require similar treatment if they are both in contact with the ground together, when the tractor is inverted. The lateral deflections are not independent, since the points are normally connected by fairly strong members which are rigid in compression. In the simulation, the equations for point 2 are calculated first while the roll angle is less than 180° to the surface. The force origin of point 1 is then shifted appropriately. When the angle exceeds 180° this process is reversed, and the force origin of point 2 derived from the deflection of point 1. This is not strictly accurate because it allows the second point to deflect a small amount, probably in its elastic phase, in relation to the first. The lateral forces on both points are likely to be very small in the conditions when both are in contact, however, and the lack of realism is not significant.

3.4.3. The equations of motion

These follow directly from the forces at the n contact points given above. Ground forces or body forces could be used alternatively, the simplest forms being (Fig. 3.2):

$$\sum_1^n (Fv \sin\alpha' + Fu \cos\alpha') - m\ddot{x}_g = 0 \qquad -(3.18)$$

$$\sum_1^n (Fv \cos\alpha' - Fu \sin\alpha') - mg - m\ddot{y} = 0 \qquad -(3.19)$$

$$\sum_1^n (x_1 \cdot Fy_1 - y_1 \cdot Fx_1) + I_{zz}\ddot{\theta} = 0 \qquad -(3.20)$$

3.4.4. Damping

For contact-point characteristics including velocity dependent terms, the total force F is the sum of force F_x generated by the spring displacement and a force $F_{\dot{x}}$ proportional to the relative velocity of the contact point with respect to the rigid body or, in the case of the ground characteristics, to the fixed frame of reference.

Thus:

$$F_x = -\frac{1}{k_x} (x - x_{fxo}) \qquad -(3.21)$$

where $(^1/k_x)$ is the argument of the spring stiffness, the negative sign being necessary because Fx is defined as the force on the outside world; x_{fxo} is the constant defined by the value of x when f_x is zero.

And similarly:

$$F_{\dot{x}} = C\dot{x} \qquad -(3.22)$$

where C is the argument of the damping force coefficient. Since $\dot{x}$ is a relative value contributing to the contact point equations it cannot be calculated directly from the current rigid body velocities, any more than x can from the rigid body displacements alone. To a first approximation in a numerical solution, however, we may assume that

$$\dot{x} = (x - x_b) / \Delta t \qquad -(3.23)$$

where x_b is the value of x at the previous step and Δt the time increment.

Collecting these equations gives:

$$F = F_x + F_{\dot{x}} = -(\frac{1}{kx})\, x - (-\frac{1}{kx})\, x_{fxo} + (-C_t)\, x - (-C_t) x_b \qquad -(3.24)$$

where $C_t = C/\Delta t \qquad -(3.25)$

Rearranging (3.24) into the form of (3.5a), (3.6a), (3.7a) gives:

$$x = \frac{x_{fxo} + C_t\, k_x\, x_b}{1 + C_t\, k_x} + \frac{-k_x}{1 + C_t\, k_x} F \qquad -(3.26)$$

Applying (3.26) in the general variable x to the specific cases of x_1, y_1 and v allows the constants x_{1fo}, k_{x1} etc to be determined directly. Equation (3.26) applies to each linearised part of the non-linear spring characteristics with the appropriate values of x_{fxo} and k_x. The damping coefficient C will normally be constant but it also could be different for the different parts of the spring characteristic.

3.5. THE COMPUTER SIMULATION

3.5.1 Programming languages

The programs were all written initially in the IBM simulation language CSMP[59, 60]. This is intended to provide solutions to differential equations without requiring the user to pay detailed attention to the means of solution. Its main characteristics may be summarised as follows:

Advantages

(a) Several alternative integration routines provided with levels of sophistication from rectangular to fourth-order Runge-Kutta; very simple call statements.

(b) Automatic statement-order sorting, allowing parallel programming.

(c) A range of standard input functions provided.

(d) Simple control of parameter variation in multiple runs.

(e) Simple, pre-formatted output control, allowing rapid editting of variable names for printing.

(f) Simple-to-use plotting routines, with automatic scaling and labelling.

(g) Simple control of timing parameters (step length, output intervals, finish conditions, etc.).

Disadvantages

(a) Excessive storage requirements for program and intermediate files (requiring Private Volume disc in the RES implementation).

(b) Cumbersome translation and composition.

(c) Risks of the user treating the program as a 'black-box' and getting spurious results since he does not need to understand fully the solution algorithm.

(d) Inflexibility of input, output and plotting formats.

(e) Difficulty of handling arrays, sub-routines, double precision variables.

(f) Constraints on numbers of, e.g. integer variables, restricting in a large program.

The advantages listed as (a) and (d) - (g) proved valuable during program development, but eventually they became heavily outweighed by the disadvantages. The final progrram, TROLL, was therefore transcribed into FORTRAN IV, a relatively easy task since this possibility had been allowed for during the writing and development of the programs (CSMP translates the user's program into FORTRAN). Running the FORTRAN version led to a considerable improvement in program flexibility, running speed and efficiency. The author would advise against the use of CSMP except for simple programs where the user-provision of standard input functions and integration routines would cause disproportionate effort.

3.5.2 Integration methods

A Runge-Kutta method is generally considered to be the most efficient for simulations of this type. The existance of frequent discontinuities in the present model at changes in surface contact and structural characteristics, however, requires a relatively short step length. This limitation prevents a sophisticated integration routine from optimising the step length, and results in longer execution time than a simpler method, for the same overall accuracy. In addition, a routine which calls the model statements more than once each step would require special handling of the damping and friction equations that depend on variable values at the previous step.

Trials with the CSMP routines suggested that the second order Adams method was the best compromise. The CSMP version of this is:

$$x_{t+\Delta t} = x_t + (3\dot{x}_t - \dot{x}_{t-\Delta t})\,\Delta t/_2 \qquad -(3.30)$$

The second order contribution amounts to the estimate of the value of $\dot{x}_{t+\Delta t}$ as a linear extrapolation of $\dot{x}_{t-\Delta t}, \dot{x}_t$. By recasting the equation as

$$x_{t+\Delta t} = x_t + \dot{x}_t . \Delta t_t + (\dot{x}_t - \dot{x}_{t-\Delta t})\,\frac{\Delta t_t}{2} . \frac{\Delta t_t}{\Delta t_{t-1}} \qquad -(3.30a)$$

it is possible to change the step length during the simulation. This was done at impact, since the accelerations and frequency of discontinuities following impact are much higher than those before, and require a shorter step to acheive consistent accuracy.

3.5.3. Overall numerical accuracy

Numerical errors in this case arise from finite step length and finite word length, or rounding. The rounding errors are particularly significant because the contact-point equations contain both the large, rigid body displacements and dimensions, and the relatively small structural deflections. To meet the aim of obtaining reliable effects of parameter changes, the overall 'internal' accuracy of the simulation was constrained to the better than $\pm$ 1% in all cases. It was found that this could be met only by step lengths of no more than 0.001s and 0.0005s before and after impact respectively, and by using double precision variables. This resulted in a CPU time for a typical simulation of about 3 minutes.

Apart from numerical errors, the effect of punching errors in the coding, or even mathematical errors in the equations, may pass unnoticed in a complex simulation if they cause only small deviations from the expected behaviour. An energy balance check was installed in the program to aid debugging and to give an indication of numerical accuracy. The sum of potential energy change, kinetic energy change and work dissipated by relative displacements of the contact forces was calculated at each step. Although the deviation of this sum from zero is not an absolute or completely foolproof error indicator, it proved invaluable during program development. Once the presence of a mistake was established, however, considerable effort was often needed to find its source, particularly as a result of the extensive logical branching used in the program.

3.5.4. The program

An overall block diagram is given in Fig 3.4 and a flowchart of the contact point algorithm in Fig. 3.5. The tests for surface contact and change of structural lines are shown in Figs. 3.6 and 3.7 respectively. Certain details are discussed in Appendix 3.1.

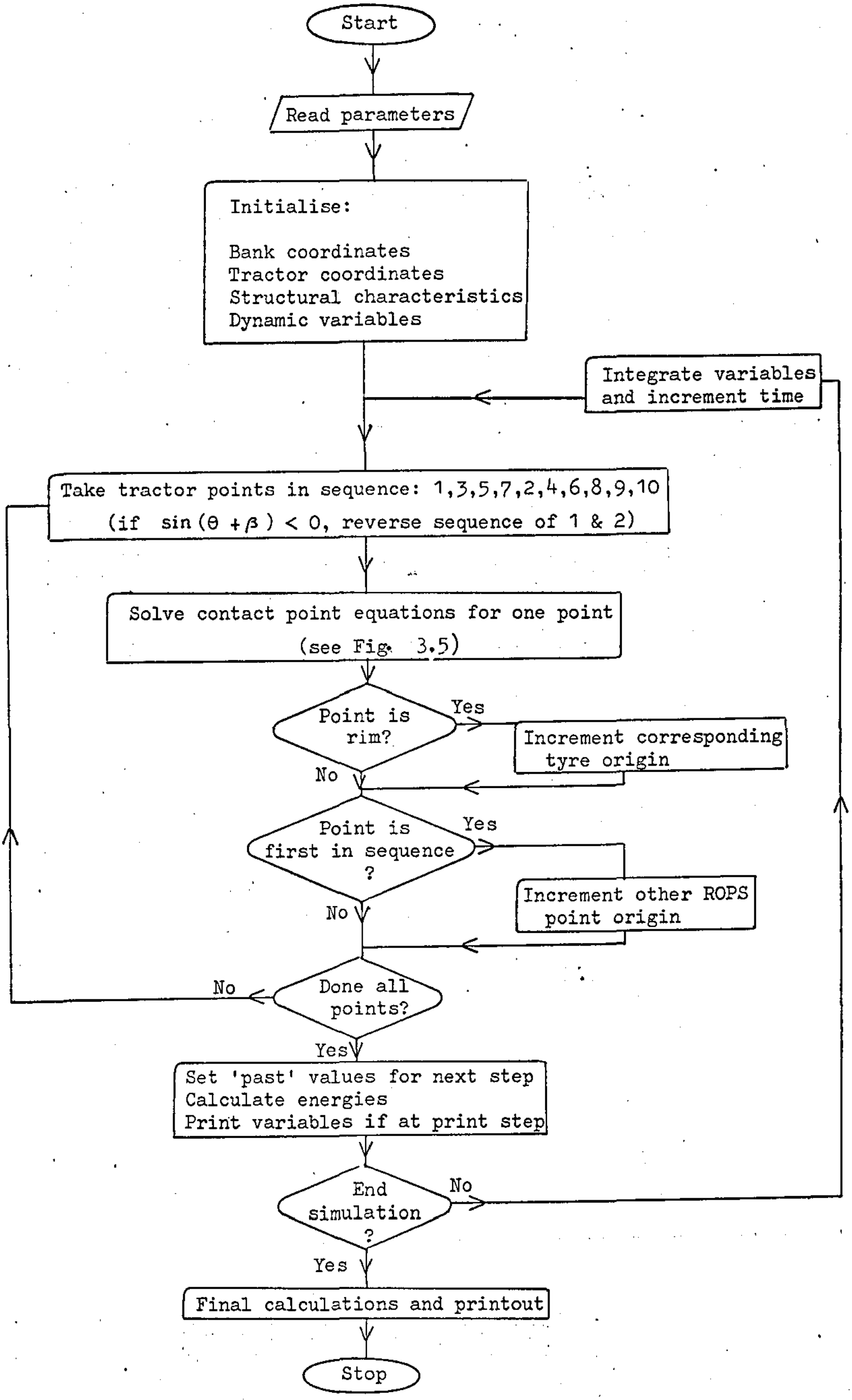

Fig.3.4. Block diagram of TROLL

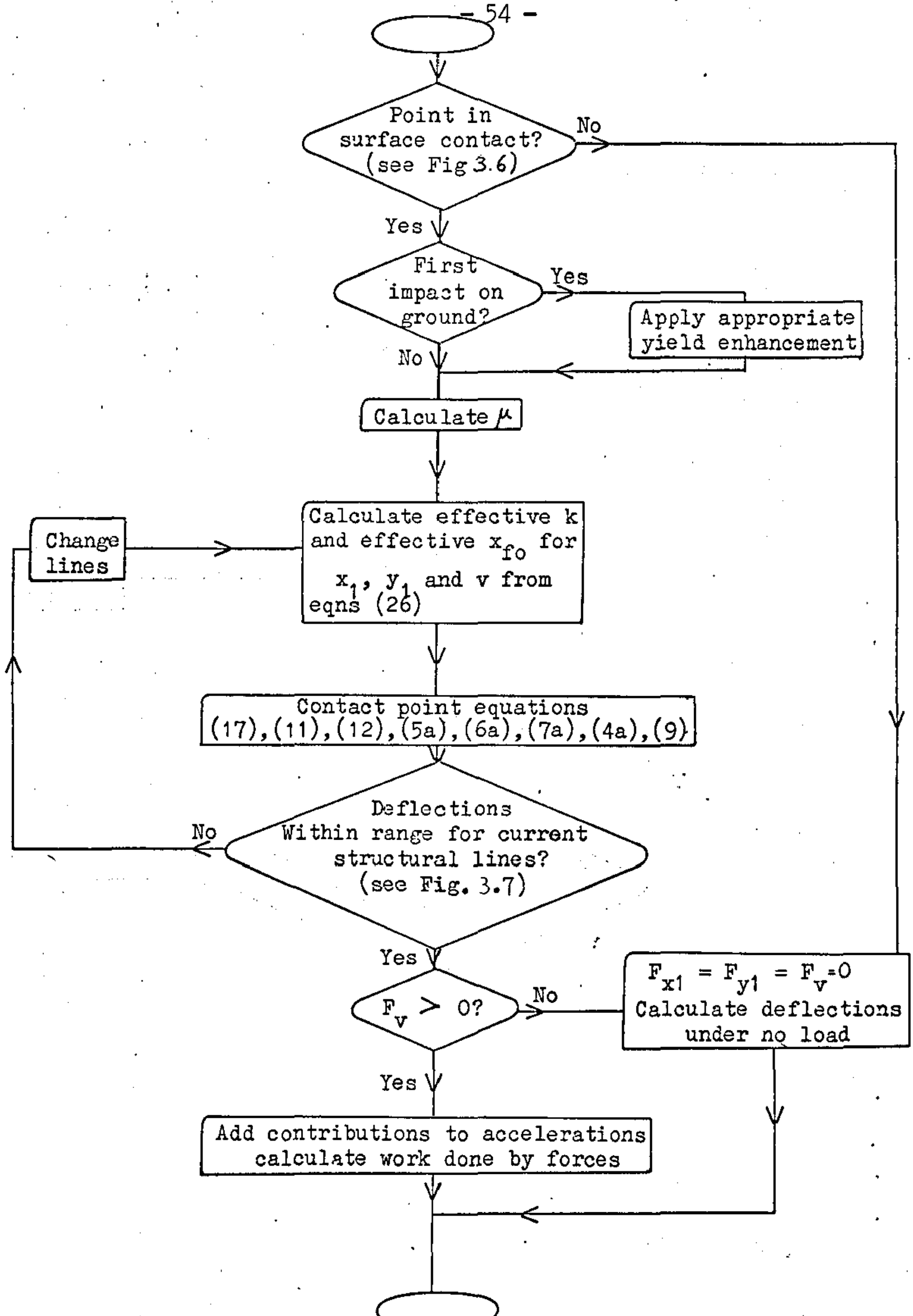

Fig.3.5 Operations on each contact point

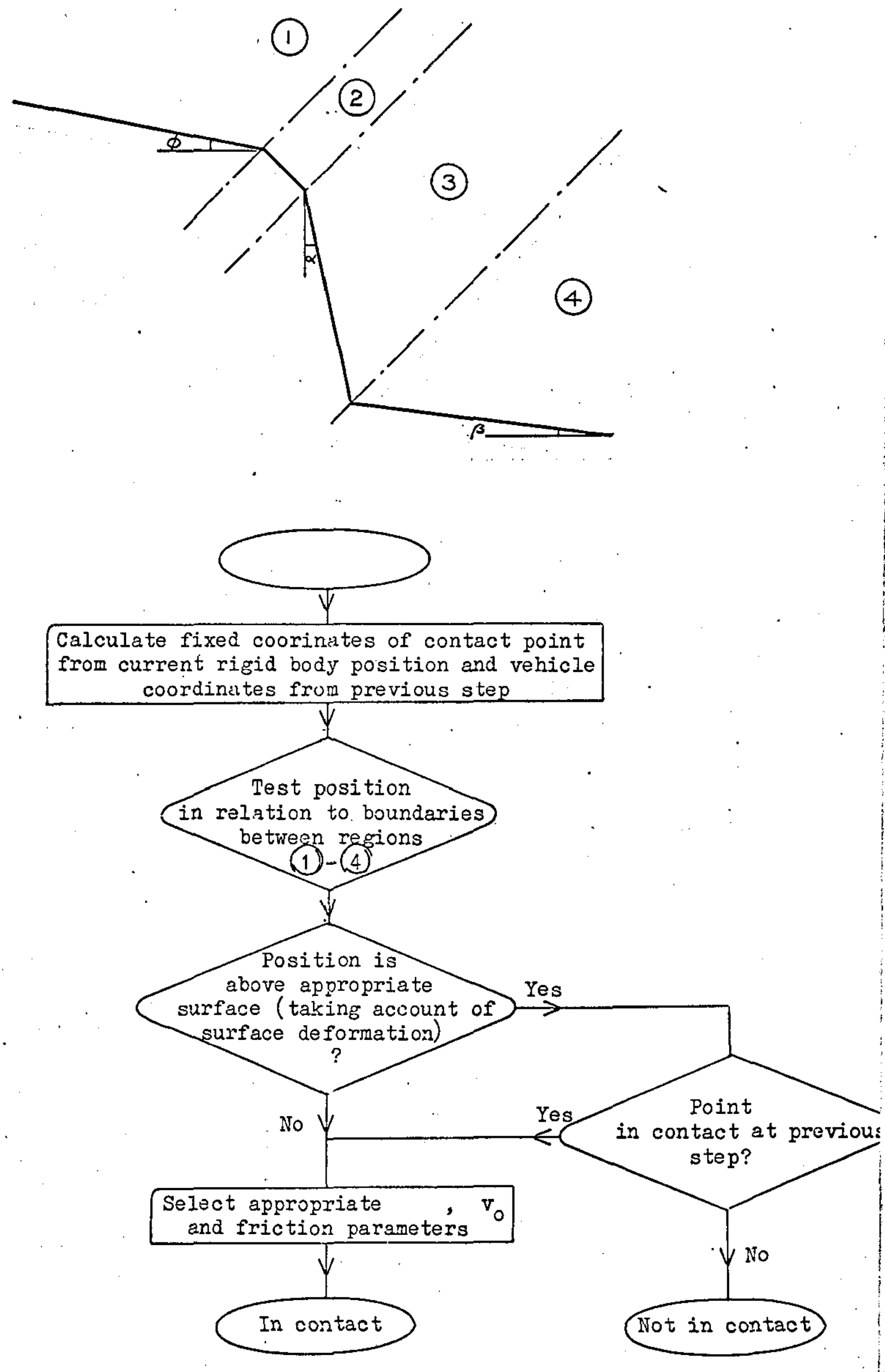

Fig.3.6 <u>Tests for surface contact</u>

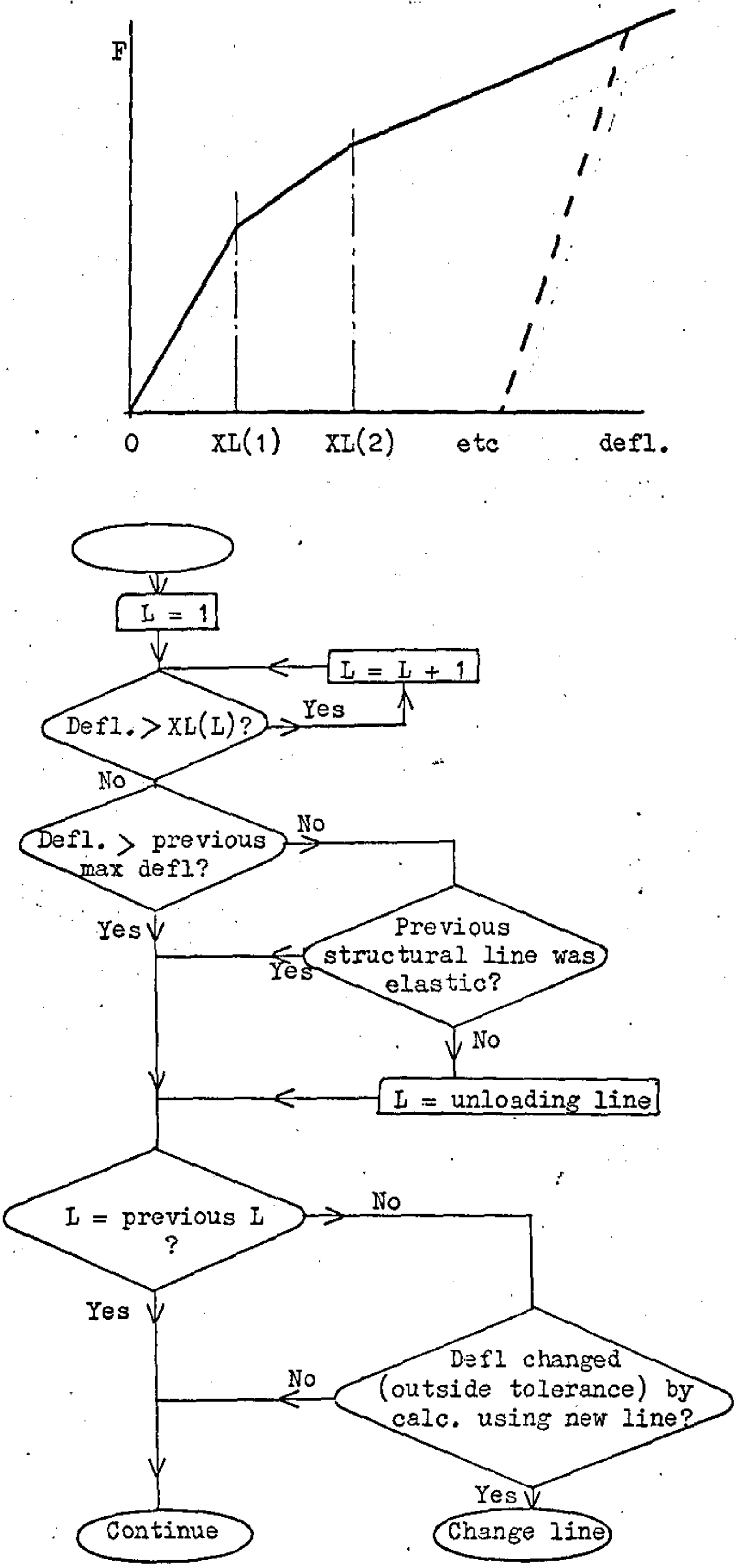

Fig.3.7 <u>Tests for structural line changes</u>

4. EXPERIMENTAL EQUIPMENT

The experimental validation of the mathematical models called for the measurement of tractor dynamic behaviour and frame forces and deformations. Variation of parameters such as tractor inertia and geometry, frame strength and ground profile was dictated by consideration of the mathematical models. Although overturning experiments had been carried out previously at the NIAE[7], the scope of the present work was such that an entirely new set of equipment and instrumentation was required.[62] About 30 overturns were planned. This called for a high dgree of robustness and reliability of the equipment and meant that a specially designed frame with minimum requirement for replacing deformed members was cheaper overall than using a new, commercially available frame for each test. It also justified significant capital expenditure on equipment and instrumentation, although some of this has wider application and would continue to be used after the completion of these tests.

4.1. TRACTOR AND EXPERIMENTAL SAFETY FRAME

The tractor used in the tests was a 30 kW (40 h.p.) Fordson Major. The basic tractor weight of 2330 kg. was increased to 3065 kg. by the frame and transducers described here. A rigid, braced safety frame had been fitted for previous overturning experiments and proved valuable for initial trials. For the main tests, however, a frame was required that would absorb energy in a similar way to a normal, commercial safety frame.

The main design objectives for the experimental safety frame and tractor base frame were as follows:

(1) Size, shape and structural behaviour to be generally similar to those to commercial safety frames, and capable of being easily varied from test to test within reasonable limits.

(2) Energy absorbing parts damaged after each test to be cheap and easy to replace, while maintaining known structural behaviour.

(3) Impact forces and energy-absorbing deflections to be capable of measurement using the transducers which were available at the time the frame was being designed.

(4) Some protection to be given to vulnerable parts of the tractor without significant effect on the likely overturning dynamics.

(5) Provision to be made for mounting ballast weights in different positions to alter the mass, the position of the centre of mass and the moments of inertia.

4.1.1. Design concept

Several potential solutions were considered. Since the load cells were designed to receive the impact forces directly from ground contact, some form of rigid top frame was required to transmit these forces to the energy-absorbing members. At first it seemed sensible to separate the duties of energy absorption and support for this top frame, as this would lend greatest flexibility to the design of the energy absorbers. Some safety frames for research have been made in this way, in one case using coil springs to absorb the energy[6] and in another, steel strip sheared by a cutting tool[63]. The deflection is entirely elastic in the first of these, entirely plastic in the second and neither behaves like a commercial frame. Two separate elements could be combined but when this is attempted in the several degrees of freedom (d-of-f) that the top frame needs - at least 3 - the solution becomes too complex and may be ruled out on both cost and space.

The design that was finally selected looked in general much like a commercial frame (Fig. 4.1). Absorbing the energy by elasto-plastic bending of steel bars is both realistic and simple. The immediate disadvantages are that the structural responses in the three d-of-f are not independent and the frame has redundancy and apparent over-constraint. The analysis of the behaviour is, however, fairly straightforward and can be verified by experiment (Section 6).

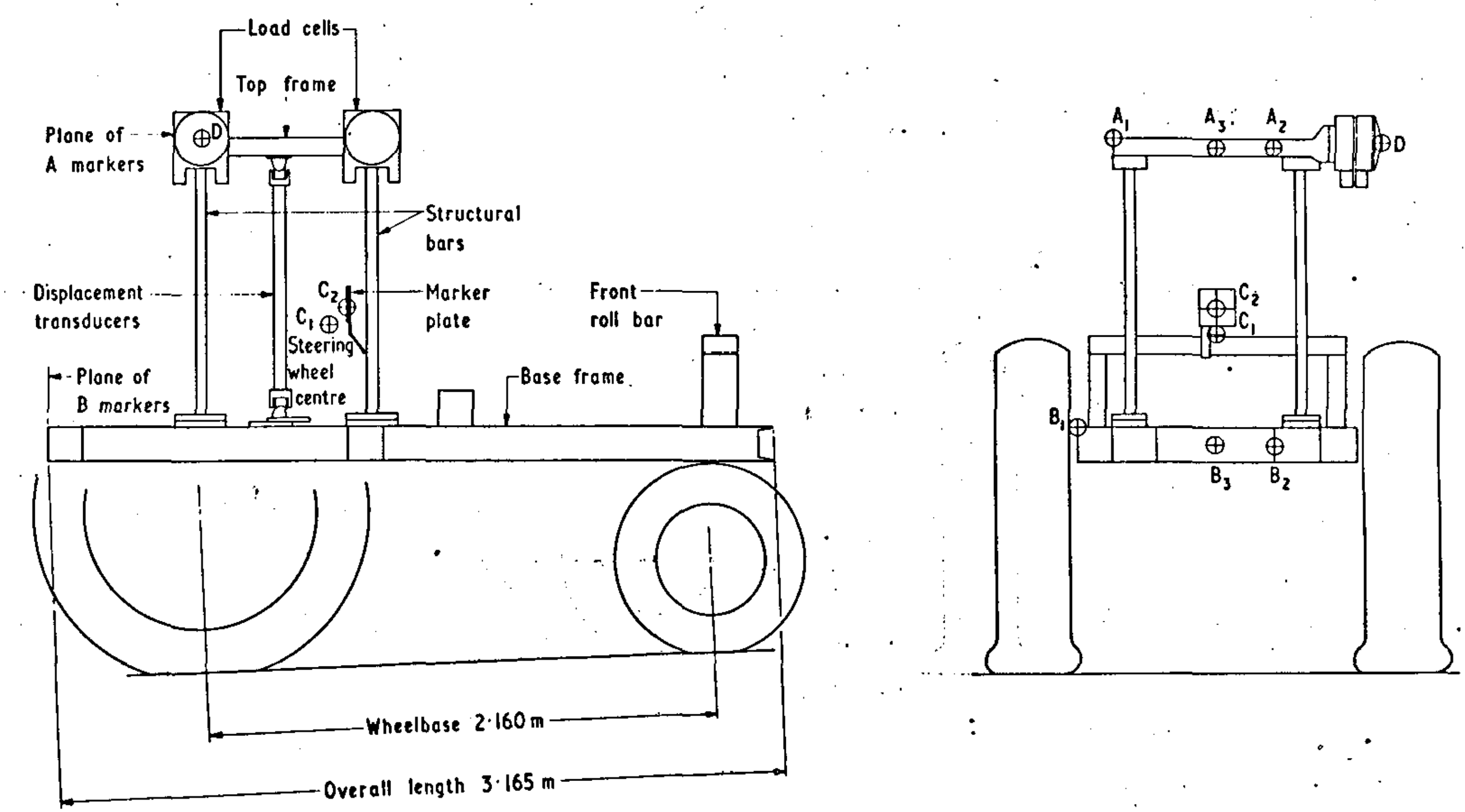

Fig.4.1. Experimental frame. A–D indicate film marker points.

The mode of failure after yield is for plastic hinges to form at each end of each of the four bars. The three d-of-f of the top frame may then be chosen as longitudinal translation, lateral translation and rotation about a vertical axis (yaw). For a commercial frame there are three further possible d-of-f: vertical translation and rotation about longitudinal (roll) and lateral (pitch) axis. Movement in these three modes requires deformation of some frame members vertically and, by their construction, frames are normally very stiff in this direction. Most frames are fixed to substantial parts of the tractor, such as the rear axle housing, either directly under the vertical frame members or through strong, rigid subframes. There are a few cases where, for example, the front support is provided by short lateral members fixed to the clutch housing; bending of these members would result in vertical deformation of the front of the cab under forces of the same magnitude as would cause horizontal deformation. A study of overturning accident reports shows these to be the exception, however, the deformations generally being restricted to "parallelogramming" of some or all of the four rectangles forming the vertical faces of the frame[21]. This is directly equivalent to the failure of the NIAE frame. The distribution of bending among the frame members will not necessarily be the same, however; plastic hinges may form in the top horizontal members of a commercial frame[64] whereas they will not do so in the NIAE frame. The overall structural behaviour is represented by effective external load-deflection characteristics for various directions of loading, however, and in this respect the NIAE frame is a good model of real life. The internal behaviour is not important for the structural dynamics and the frame may be considered as a "black box".

When the top frame suffers a general displacement, combining translation and rotation, it will not remain perfectly parallel to the base frame. This gives rise to slight lack-of-fit and overconstraint, which is discussed in Appendix 4.1. The lack-of-fit is compensated by small displacements of the plastic hinges and the overall effect on the structural behaviour is not significant.

4.1.2. Geometry

With the same basic top frame the overall height my be changed by choosing suitable upright lengths, and the width by fitting distance pieces between the frame and the load cells. It is not so simple to alter the length of the top frame but this was considered relatively unimportant.

The sizes of commercially available frames were considered before selecting the range of dimensions for the experimental frame. A few measurements made at NIAE are given in Table 4.1 and those for a much wider range of cases are reported by Schwanghart[53]. The object of variable geometry was to study the effect of changes on the overturning behaviour; it was not necessary for the experimental frame to have dimensions close to the average, provided they were representative.

Table 4.1 Dimensions(m) of some tractors and safety frames (1971)

Tractor/Frame	Rear Tyre dia.	Frame top dimensions			
		Height above rear axle	Width	Length	Longitudinal distance of rear corner behind rear axle
Ford 3000/Ford cab	1.22	1.47	1.07	1.14	0.20
Ford 4000/Ford cab	1.45	1.55	1.07	1.17	0.23
David Brown 1200/Stadri	1.50	1.60	1.17	1.25	0.30
Massey-Ferguson 165/Stadri	1.30	1.63	1.17	1.25	0.30
Leyland 344/Leyland	1.30	1.63	1.12	1.32	0.30
IHC 634	1.50	1.60	1.07	1.50	0.30
Fordson Major/NIAE experimental frame in "standard" condition	1.44	1.69	1.37*	0.96	0.12

*2 x the distance from tractor centre line to impact face to load cell with zero width extension.

The NIAE frame was wider than typical commercial frames, partly because of structural considerations in the design of the modified top frame (see 4.1.4 below). In addition, however, the size of the base frame imposed a limit of 1.54 m on th minimum track width, compared with a typical value of 1.32 m for a medium size tractor. Since it is the difference between frame width across the rear tyres that has most influence on impact dynamics, the minimum frame width of 1.37 m was representative.

The base frame was mounted so that it was was not quite parallel to the ground plane when the tractor was in its standard condition resting on its tyres but sloped downwards from rear to front at an angle of 2.1°. The uprights were perpendicular to both top and base frames. The slope had no significant effect on the dynamic behaviour but had to be considered, for example, when recording measurements that defined the dynamic attitude of the vehicle.[62]

4.1.3. <u>Structural characteristics</u>

Solid, round, mild steel bar was chosen as the upright material. Hollow sections are normally used for commercial frames but partial collapse of the section occurs under yield in bending. This makes the behaviour more difficult to analyse and would have been likely to result in failure of the end fixing clamps originally proposed. The circular section also simplified analysis since the bending response of each bar was uniform in all directions. Mild steel was the most appropriate material, its high ductility allowing large amounts of energy to be absorbed by plastic strain; it is universally used for commercial frames.

The horizontal load-deflection behaviour depends on the direction and point of application of the externally applied load; it is analysed in detail in section 6. An overall assessment may be obtained, however, by considering a representative response. The simplest case is equal deflection of the four uprights, which may result from either a sideways load at the mid-point of one side or a 45° load at a corner.

Assuming an idealised elasto-plastic response, the behaviour is chararacterised by two values: the collapse load and the elastic stiffness. Since the length of the bars is determined by the required overall height, the only parameter that may be varied to control structural behaviour is the bar diameter. If diameter is selected for a given collapse load then the elastic stiffness cannot be independently chosen.

To assess the realism of this predetermined load-stiffness relationship, values were derived from NIAE tests on a number of commercial frames. In figure 4.2 these collapse loads are plotted against elastic deflection to collapse, a more directly relevant measure of stiffness. Both measured and predicted data are only approximate. The measured loads are recorded maxima and the deflections the difference between recorded maximum and permanent. Asymmetry in the test loading probably gave slightly lower forces and larger deflections than in the symmetrical case used for the simple prediction.

In view of this the relationship for the experimental frame was considered to be reasonable. It was rather stiffer than a typical commercial frame at a given collapse load, but not unrealistically so.

The ratio of collapse force to tractor weight for the frames tested varied from 0.7 to 1.9 for rear impact and from 1.1 to 2.4 for side impact, with an overall mean of 1.44. In the symmetrical loading case the predicted ratios for the experiemntal tractor are given in Table 4.2.

Table 4.2 Predicted collapse force/weight ratios

Bar diameter, mm	Typical collapse force, kN	Tractor mass, kg, (and weight, kN)	
		Standard 3065 (30.06)	Ballasted 4015 (39.37)
36	30.5	1.01	0.77
42	48.4	1.61	1.23
48	72.2	2.40	1.83

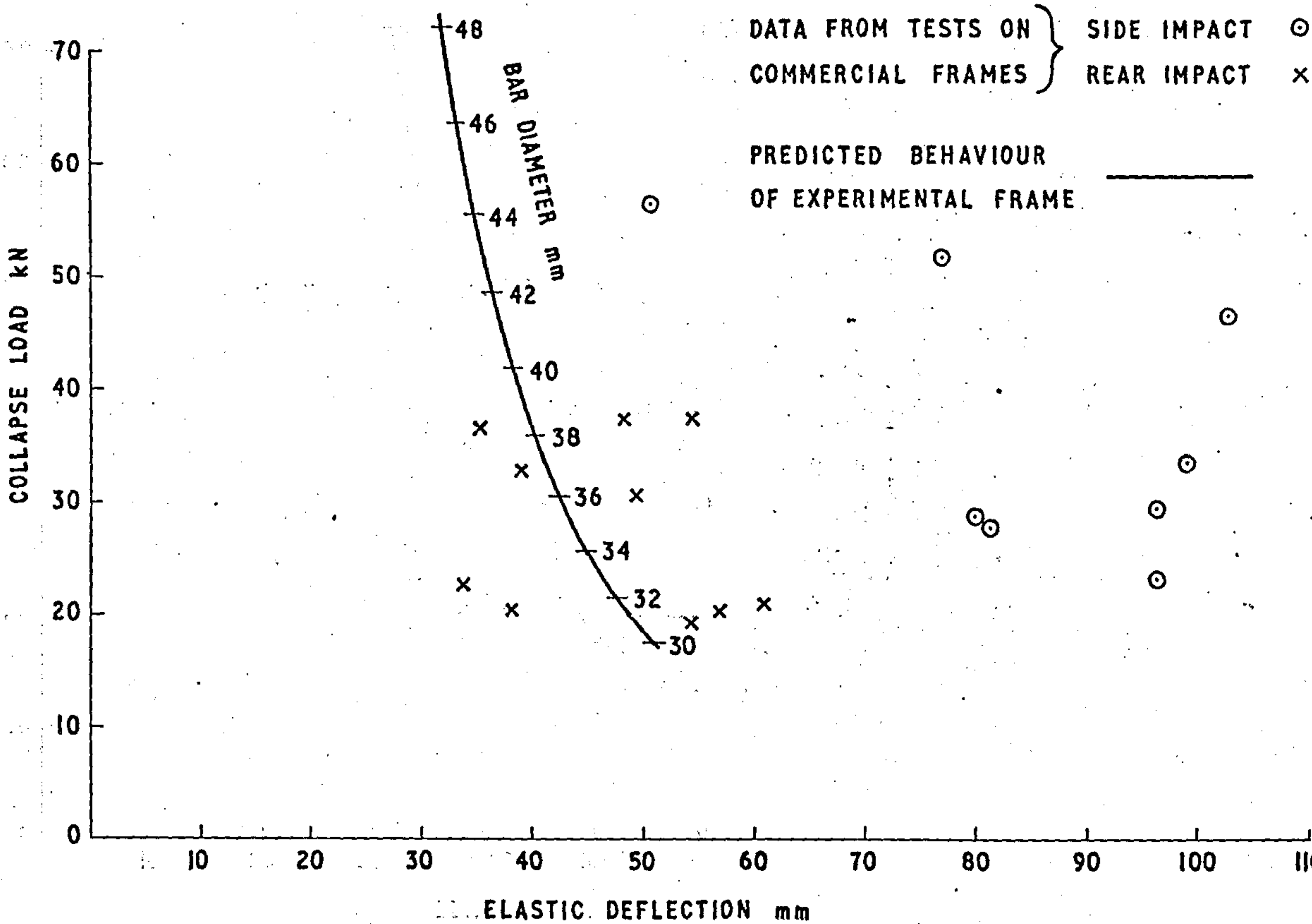

Fig. 4.2. The relationship between collapse load and elastic stiffness

4.1.4. Top frame and upright fixings

The initial design was based on the criteria that deflections in the top frame should have negligible effect on overall displacement and that replacement of the bars after a test should not involve fabrication. This resulted in a fairly massive construction with substantial clamps to hold each end of the parted-off bars (Fig. 4.3(a)).

When the complete frame, removed from the tractor, was subjected to pendulum impact tests the mass of the top frame resulted in a very high peak force at the moment of contact. The effect was inevitable because the only flexibility between the inertias of the frame and pendulum are those of local surface deformation and load-cell displacement. The same condition would arise when the tractor was overturned onto a concrete surface.

There are two main consequences of this behaviour: (i) the structural response may be affected, and (ii) the load cells may be damaged. It was concluded from the tests that the energy dissipated in deforming the bars was not significantly affected, i.e. the energy dissipated by local deformation was small. The time-history of loading may be modified slightly but this is of less importance. The load cells, on the other hand, were not capable of withstanding the peak force and some provision was needed to protect them.

Three parallel solutions were adopted: (i) for the pendulum tests a stiff cushioning pad was temporarily fixed to the impact face of the pendulum weight; (ii) as a more permanent measure the load cells were fitted with limit stops; and (iii) a lighter (Mark II) top frame was designed to improve the overall behaviour.

To reduce the mass the design criteria of the top frame had to be relaxed. Firstly, the requirement of insignificant deflection was replaced by one of adequate strength. As a result, elastic deflections could be expected to be typically 2.5 % higher than those calculated assuming a

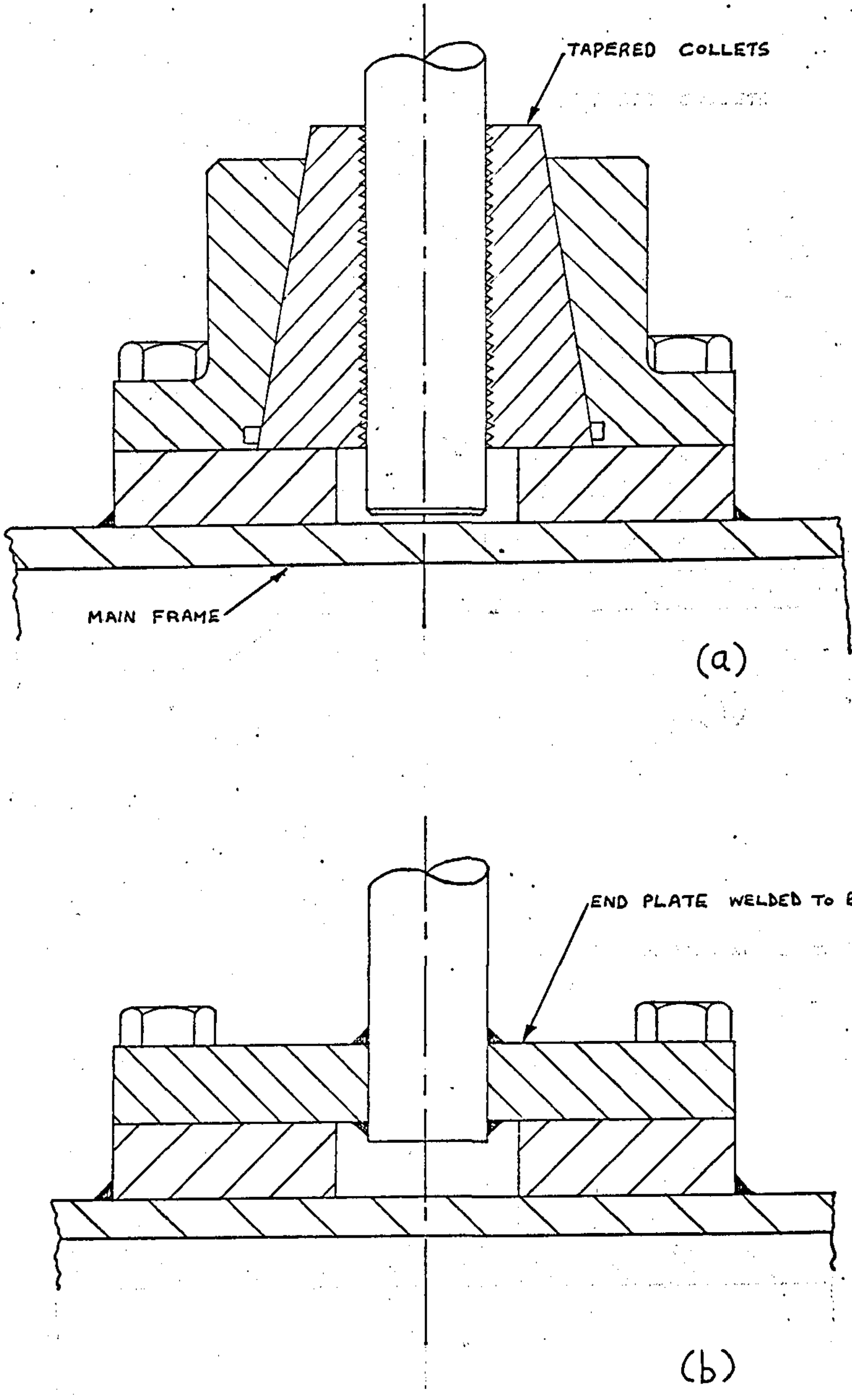

Fig. 4.3. Bar end fixing (a) Mk I design (b) Mk II design

rigid top, or nearly 5% in the worst case (see reference 62). This was considered to be acceptable since the elastic deflections were a relatively small part of the total; in any case, the measured deflections would still be correct, the error affecting only predicted behaviour.

Secondly, the bar end fixing method was changed to the arrangement shown in Fig. 4.3(b). Two runs of weld on each side of the plate were found necessary to resist the plastic bending moment of the bar.

The effective inertial mass of the Mark I top, including collars and one-third of the mass of the bars, was 286 kg, and for the Mark II, 124 kg. Load cells complete with cover plates and domes added a further 90 kg to these values.

The Mark II top was used for all the overturning tests but the Mark I was used for some of the laboratory impact tests, including those used as a basis for predicting the structural behaviour. This was confirmed with the Mark II top (section 6).

4.1.5. <u>Other details</u>

The base frame was made mainly from 6" x 6" x ½" (152.4 x 152.4 x 12.7 mm) rectangular hollow section mild steel. It was fixed to the tractor at three points: the rear axle housing, the top of the clutch housing and the front of the engine bearers.

Cylindrical steel ballast weights from the NIAE Single Wheel Tester[65] were used to increase the mass of the tractor by up to 60%. The six 250 kg and four 100 kg weights had spiggotted ends which were fixed to the base frame by clamp brackets. Details of the positions of the weights and the calculated inertial parameters for the combination used in the overturning tests are given in reference 62, and summarised in Table 5.3 (page 80).

<u>Rear wheel</u>

In many types of sideways overturn the tractor rear wheel transmits considerable impact force to the tractor. Since the wheel disc is weak it may deform plastically and absorb quite a large proportion of the total energy. A deformed disc is difficult to repair. The disc on the right-hand rear wheel, the overturning side, was therefore replaced by a system of 8 spokes fitted between the usual lugs on the rim and a ring fixed to the hub (see Fig. 4.4). The spokes were normally made of 80 x 12 mm mild steel strip and could be straightened easily in a press after overturn damage. The hole centre distance was chosen so that the spokes made an angle of about 75° with the rim to allow for deformation and torque transmission. The strength of the spoked wheel was comparable to that of the original disc wheel.

Remote control

A simple system allowed the tractor to be steered and the engine stopped from controls connected to it by a 50 m electric cable. These were the minimum requirements for safe operation; additional control of brakes and clutch would have been an advantage particularly for manoeuvring but the cost, complexity and effect on reliability were not considered to be worthwhile.

A double-acting hydraulic ram operated the steering arm. Oil from a fan-belt driven pump was metered to the ram by a two-way solenoid valve.

The 'driver' used a handset (Fig. 4.5) with two thumb-operated push switches, which caused the solenoid valve to admit oil to one or other side of the ram piston. There was no feedback or proportional control. The amount of movement of the steering depended on the length of time the push switch was kept depressed, and the response of the system was rapid. Driving by continued pressure on the switches led to instability because of human reaction delay. An oscillator was therefore incorporated that passed the switched current only on the positive part of each cycle. The driver used a potentiometer to alter the mark-space ratio and thus set the overall sensitivity to the highest value compatible with his own reaction time.

Even with this refinement the system was fairly crude and at higher speeds accuracy suffered if stability was maintained. With practice, however, a straight course could be followed satisfactorily at speeds up

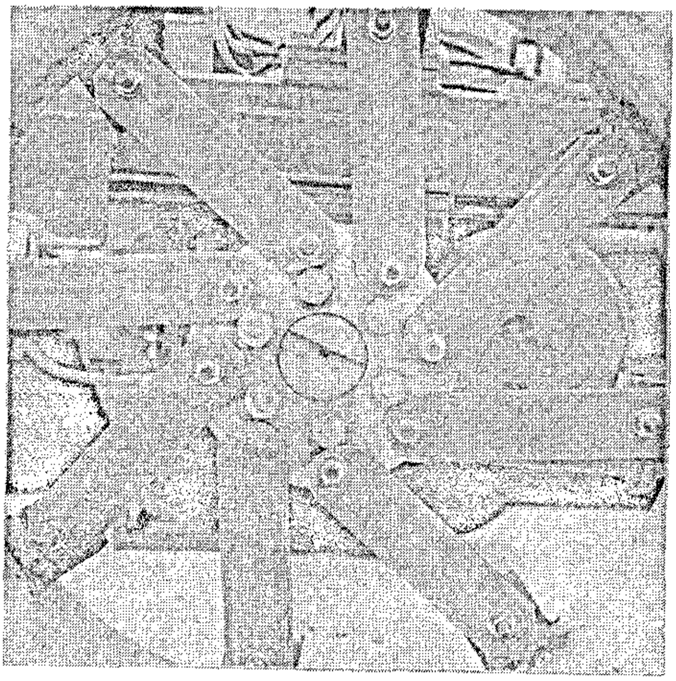

Fig. 4.4
Spoked rear wheel

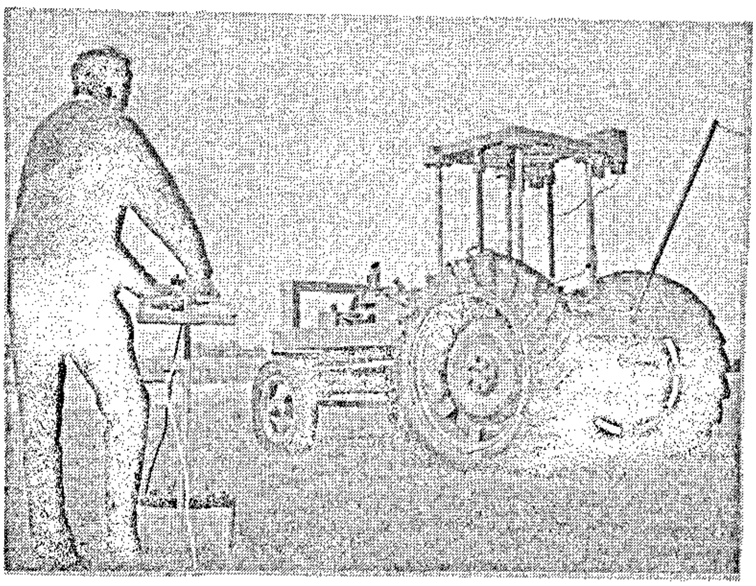

Fig. 4.5
Remote control

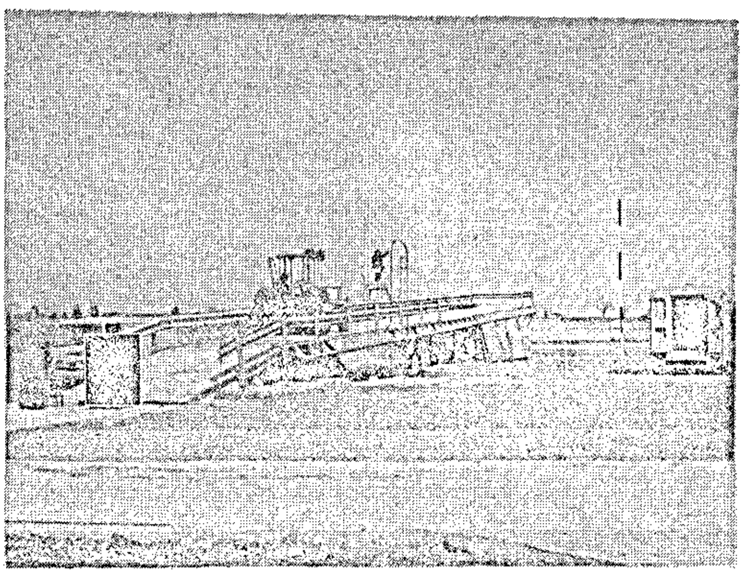

Fig. 4.6
Overturning platform.
Equipment positioned
for start of test

to about 4 m/s (9 mile/h). This was considered to be an adequate limit and most tests required a speed of only 1.5 m/s (3.4 mile/h). A more sophisticated system would have added considerably to the cost and time of construction.

A linkage to release the clutch and an extension on the gear lever allowed the tractor to be started by an assistant while the driver operated the handset. Chocks prevent the tractor rolling back when the clutch is disengaged; a mechanical interlock prevented accidental selection of reverse gear.

4.2. PLATFORM FOR OVERTURNING TESTS

The survey of overturning accidents indicated the type of site conditions required: a bank between 2.5 and 4 m high with a slope variable between 50° and 90° to the horizontal and provision for landing on hard or soft ground.

The most important criterion in choosing the maximum height was the extent of the roll angle reached by the tractor as it slid down the bank. For testing in the most severe realistic case this angle must be large enough to allow the frame to hit the ground before the side of the rear wheel - somewhere between 90° and 135° depending on the tractor/frame geometry.

The mathematical model was not available when the equipment was being designed. Evidence therefore had to be taken from two sources: accident reports and tests in similar conditions. The accident survey indicated only the likely range of bank heights, and since the slope is not always reliably reported it is not certain that the accidents involving the highest banks would be the most severe.

The only suitable test data that was available covered an NIAE overturn to the U.S. standard ASAE 306.2.[14] Although the bank height was only 1.27 m extrapolation of the analysed behaviour indicated that a height of just over 2 m would result in the required roll angle. Taking this value directly was not appropriate because the ASAE test includes a ramp to lift the up-slope wheels, thereby increasing the roll velocity; in addition, the affect of slope was not known, that of the ASAE test being 50°. Combining this evidence with practical considerations resulted in a choice of 2.5 m as the maximum height.

A search for a natural local site was unrewarding and the most suitable way of achieving the objective was the construction of a special platform (Fig. 4.6). The overall layout is shown in Fig.4.7. The height rises from 1.04 m to 2.74 m with a slope of 1 in 20.

The slope for the tractor to slide down was provided by strengthened steel plates each one bay (2.45 m) long, hinged at the top edge. The angle could be simply adjusted in $7\frac{1}{2}^{\circ}$ steps using the pinned struts at the bottom. Four plates are fitted at the high end and two at the low end. Their positions could be moved together along the platform by up to two bays without a serious gap appearing at the bottom.

A 250 m x 45° chamfer to the overturning edge was necessary to prevent it being fouled by the underside of the tractor at the steeper plate angles. This was also probably more realistic than a sharp edge for many accident conditions.

Two reinforced concrete pads each the width of two bays provided hard landing surfaces; the remainder of the ground was prepared top-soil to give the soft surface.

4.3. RECORDING THE DYNAMIC BEHAVIOUR

Two systems were used: (i) cine cameras to record the kinematics of overturning and impact, and (ii) strain-gauge force and displacement transducers to record on magnetic tape the impact response of the frame.

Details of the equipment are given in Appendix 4.2 and in reference[62].

Cine film recording

The most important tractor movement was in the vertical plane perpendicular to the edge of the bank. The main camera was therefore positioned with its optical axis aligned with this edge (Fig. 4.7). A long

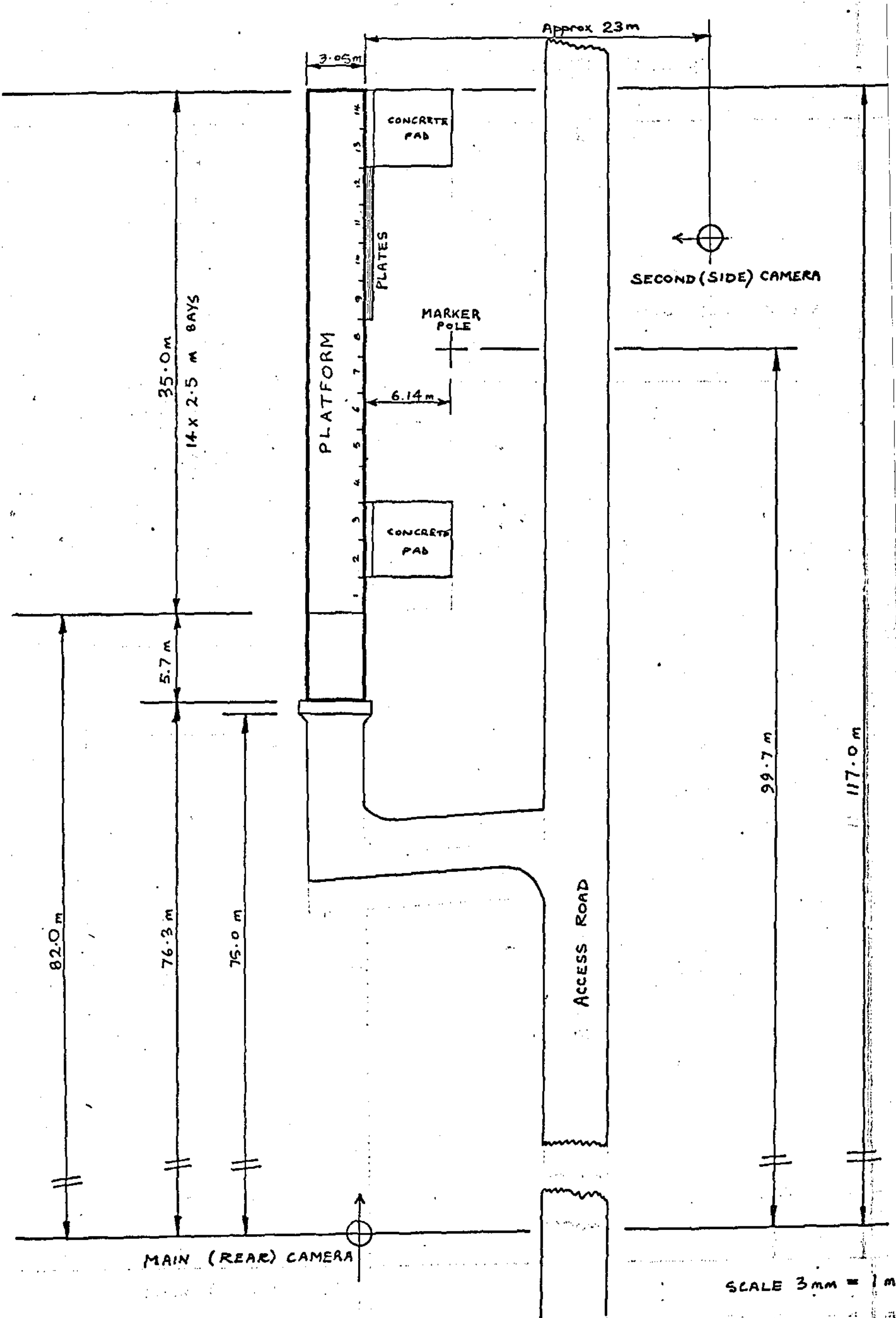

Fig. 4.7. Layout of overturning platform. Steel plates on bays 9-12 and side camera positioned for overturn onto soil

focus lens allowed a distant position which reduced the effect of parallax.

A second camera viewed the overturn from the side, mainly as a check on the forward motion of the tractor.

Timing equipment

Three forms of timing were needed: (i) a time-base for the cine film recording; (ii) a means of relating this time-base to that of the magnetic tape recording, and (iii) a method of determing the forward speed of the tractor. The time-base for the tape-recording was derived from the capstan-speed.

A large clock in the field of view of the rear camera provided the time-base. A one metre diameter face positioned at the start of the platform gave adequate resolution (Fig. 4.6). A single hand was given by a mains-powered synchronous motor at one revolution per second, giving a reading accuracy of better than 0.01s. Mains frequency was monitored during tests. On analysis, whole seconds are counted from an arbitrary datum.

The time scales of the two cameras and tape recorder were related to each other by firing two photographic flash guns, the firing being recorded on tape.

Tractor speed was measured by the interruption of a modulated light beam across the platform before overturning. The period during which the light beam was broken by the tractor was recorded by a timer-counter.

Another method of measuring speed was used in early tests before the light beam system was available, and later as a check. On analysis of the rear film, the rotation speed of the rear tyres was used to calculate forward speed from the known rolling radius.

Impact force transducers

Load cells at the front and rear corners of the impact side of the top frame sensed forces in horizontal, vertical and longitudinal directions (Fig. 4.8). Each of the two units comprised a pair of cells mounted back-to-back, each cell giving one compressive and one shear force. One compressive channel of each pair was redundant. The design of the cells, originated by

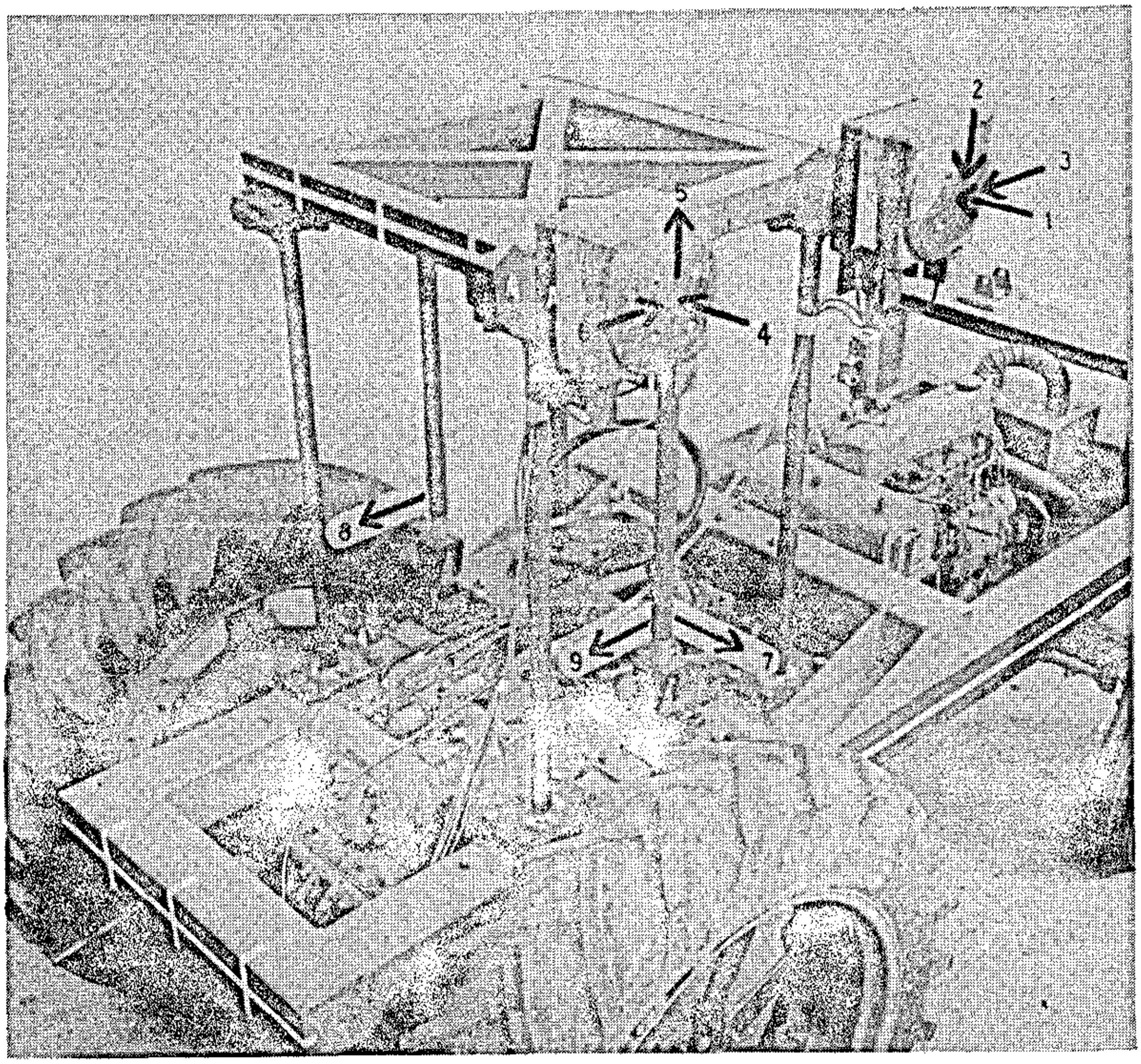

Fig.4.8 Transducer measurement directions. The arrow at each channel number indicates the sense of deflection of, or force on the top frame that results in positive amplifier output

Deere and Company[10], was a compromise between performance and size. Non-linearity and cross sensitivity was taken into account in analysis, and the overall accuracy, discussed in Appendix 4.3, was considered adequate for the purpose.

Maximum force capability was 225 kN. This was well above the highest likely frame collapse load of 70 kN but inadequate for transient inertial peaks caused by hard-surface impact. Mechanical limit stops were therefore fitted to prevent damage (Appendix 4.2).

The cells were protected from incidental damage by covers of 10 mm mild steel plate boxed in by 5 mm plate. The domed ground contact faces were not similar in shape to those of a normal cab or frame. The maximum contact area of 0.106 m^2 represented by the two 230 mm squares was, however, comparable to the 0.063 m^2 of a typical top frame member of 1.25 m long x 50 mm rectangular section.

An alternative solution (to more nearly approach convention) involved fitting a ground contact beam across the front and rear cells. Problems relating to the beam strength and overconstraint of the cells proved, however, to be insuperable.

Frame displacement transducers

These transducers were also adapted from Deere and Company designs.

Because of the height of the top frame above the base, conventional linear displacement transducers could not be used without a rigid super-structure inside the frame. This was avoided by using pin jointed vertical shafts to convert the linear movement to rotation of the pins, which was then measured by strain gauges. The shafts incorporated sliding joints to accommodate changes in length (Appendix 4.2).

Two units were used, each having hooke-joints to give two mutually perpendicular directions of rotation, both of which were fitted with sensors. The two units thus gave a total of four displacement measurements; one of these was redundant since the top frame had only three degrees of freedom (Fig. 4.8).

5. OVERTURNING EXPERIMENTS

5.1. EXPERIMENTAL CONDITIONS

A balanced experimental design was not appropriate in view of the prime requirement of validating the models and the high cost of tests - about £400 each test in staff time, including preparation. A total of about 30 tests was planned to allow at least some variation of each of the important parameters. The number carried out was 31; in one case (number 13) a steering failure invalidated the test, and in several others instrumentation or equipment faults made the results incomplete or difficult to analyse although partially useable. In view of the complexity of the equipment, however, the proportion of results recovered is high.

The parameters studied were chosen on the basis of the mathematical models. They are discussed below in approximate order of their expected influence on the dynamic behaviour. The values of the parameters for each test are given in Tables 5.1 and 5.2. One set of parameter values was chosen as a 'standard' condition (Table 5.1). In some cases a single parameter was varied from its standard value in each test but in other cases it was appropriate to vary two simultaneously, one affecting the overturning phase and one the impact phase. This further reduced the number of tests while still allowing comparison with the models.

Angle of bank slope to vertical (α)

Because of slight changes in geometry and fixing arrangements the true angles differed slightly from nominal. The difference was generally limited to about 1° except in the last four tests when the plates were repositioned for overturns onto the concrete surface, giving an intermediate α of 17.7° (Table 5.2).

Tests number 1 - 12 and 16 were used to study the effect of α(Table 5.1). From the initial results of these, two values of α, $7\frac{1}{2}^\circ$ and $22\frac{1}{2}^\circ$ were selected for investigating the other parameters in the remainder of the tests.

Table 5.1 Test numbers and summary of parameters

Condition	Axle stop	Nominal α (Bank angle to vertical), degrees: 0	$7\frac{1}{2}$	15	$22\frac{1}{2}$	30	$37\frac{1}{2}$
Standard A	No		2, 3	4 B	1	5	S 6
Standard A	Yes	16	10,11	8, 9 C	12	7	
Ballasted (mass = 4015 kg + change in centre of mass and moment of inertia)	No		27		24		
	Yes		26 D		25 D		
Low friction (μ = 0.1 – 0.15) + wide cab (1.67 m)	No				23		
	Yes		21		22		
On concrete	No			28 E			
On concrete + low friction	Yes			30 D,E			
	No			31 D,E			
Higher speed (3 ms^{-1})	No		15				
Larger approach angle (γ = 8°)	No		14				
Wide cab (1.67 m)	Yes		20		19		
Wide track (1.65 m)	Yes				17		
Wide cab + wide track (1.67 m) (1.65 m)	Yes				18		

NOTES

A. The conditions referred to as standard are:

Tractor mass: 3065 kg

Surface dry: (μ = 0.8–1.0)

Cab width: 1.37 m

Track width: 1.55 m

Bar diameter: 42 mm

Speed DZ: 1.5 ms^{-1}

Approach angle: 4° (γ)

Landing surface: soil

B. Front of tractor on concrete.

C. Partial failure of rear wheel.

D. 48 mm diameter bar.

E. α = 17.7° due to repositioning of plates.

Table 5.2. Details of parameters

Test number	Bank angle α, deg	Bank height at roll-off, m	Measured forward speed, DZ, m/S	Measured yaw θy at roll-off, deg	Cone penetration resistance, kN/m^2 at soil depths of:			
					0	3 in (76 mm)	6 in (152 mm)	9 in (229 mm)
1	22.9	2.15	N.R.	-6.3	N.R.			
2	7.8	2.16	N.R.	-4.5	N.R.			
3	7.7	2.25	N.R.	-8.1	N.R.			
4	15.1	2.27	1.44	-3.7	440	1080	1200	1150
5	29.3	2.10	1.47	-7.0	330	1360	1620	1760
6	37.9	1.98	1.50	-7.8	330	960	1260	1480
7	29.3	2.00	1.54	-5.2	560	970	1250	1290
8	15.1	2.04	1.50	-8.3	550	780	1150	1230
9	15.1	1.99	1.58	-6.3	630	740	1050	1210
10	9.2	1.95	1.53	-4.2	780	990	1120	1260
11	7.7	2.09	1.53	-7.2	780	990	1120	1260
12	22.9	2.08	1.57	-7.3	1230	1220	1200	1090
14	7.4	2.15	1.58	-15.0	540	950	1030	1070
15	7.4	2.24	3.16	-8.3	730	920	990	1320
16	1.0	2.11	1.55	-3.5	690	1150	1170	1050
17	21.4	2.23	1.61	-8.9	120	620	1250	1470
18	21.4	2.15	1.50	-6.0	450	800	1210	1230
19	21.4	2.13	1.51	-3.4	300	850	990	1140
20	7.4	2.13	1.67	-5.5	860	1250	900	980
21	7.4	2.02	1.61	-8.8	1140	1290	950	1080
22	21.4	2.00	1.62	-7.1	820	1310	950	1220
23	21.4	2.09	1.62	-4.5	280	2170	1940	1300
24	21.4	2.19	1.66	-4.0	850	1740	1330	1080
25	21.4	2.06	1.48	-6.3	610	1540	2120	1900
26	7.4	N.R.	N.R.	N.R.	710	1660	2180	1440
27	7.4	N.R.	N.R.	N.R.	800	1930	2120	1480
28	17.7	2.52	1.60	-6.9	Concrete			
29	17.7	N.R.	1.76	N.R.				
30	17.7	2.39	1.64	-7.4				
31	17.7	2.47	1.65	-4.7				

Height of bank

All the tests were carried out at the higher end of the platform but the true height at roll-off varied between 2.0 m and 2.5 m due to the slope. The variation is significant, particularly in comparing tests onto soil with those onto concrete (28 - 31) because of the change in nominal roll-off point. This is taken into account in the analysis.

Coefficient of friction between tyres and bank (μ_s)

The value of μ_s in the standard, dry conditions was 0.8 - 1.0. This was reduced to 0.1 - 0.15 in tests 21, 22, 23, 30 and 31 by covering the concrete with industrial plastic flooring and wetting this and the metal plates that form the bank slope with a detergent solution.

Soil characteristics

It was originally hoped to conduct many of the tests using the concrete impact surface, to avoid variation in soil hardness and to cover the most severe conditions. The effect of high peak forces on the measured structural behaviour and on the integrity of the vehicle were underestimated, however, and only four such tests were carried out (28 - 31), the last of which broke the main frame away from the tractor chassis.

For the remainder of the tests, the ground hardness was estimated from cone penetrometer readings at depths of 0, 3, 6 and 9 inches (0, 76, 152 and 229 mm) at ten positions covering the area where the tractor was expected to fall. Means of the ten values at each depth are given in Table 5.2. In tests 23 - 27 the ground was too hard at some of the ten stations to allow the penetrometer cone to be forced down by hand to the full depth. In a simple attempt to avoid bias by omitting these results they were estimated by the procedure given in Appendix 5.1.

Tractor inertial characteristics

The ballasting raised the centre of mass (cg) by 37 mm and increased the moments of inertia, thus influencing the overturning and impact behaviour; the mass increase affected mainly the impact. Details are given in Table 5.3. The ballasted condition was used in tests 24 - 27.

Table 5.3. Tractor inertial characteristics

Parameter		Unballasted	Ballasted	Increase
Mass, Weight, kN		3065 30.06	4015 39.37	} + 31%
*Centre of mass co-ordinates, m.	x_{3g} y_{3g} z_{3g}	0.016 -0.101 -1.422	0.019 -0.064 -1.454	+ 0.003 + 0.037 + 0.032
+Moment of Inertia, kg/m^2	I_{xx} I_{yy} I_{zz}	2795 2500 1255	3633 3425 1434	+ 30% + 37% + 14%

*Standard co-ordinate system relative to origin at centre of rear base frame - see Appendix II of reference (62).

+Moments of inertia about standard axes through centre of mass, assumed to be principal co-ordinates. I_{xx} and I_{zz} are measured; I_{yy} is estimated.

Tractor and frame geometry

There are two main effects of geometry on behaviour: (i) The relationship between track width and cg height influences the overturning behaviour, and (ii) the inclination of a plane touching the tops of the frame and rear wheel determines the roll angle at which the frame will just contact the ground first.

The minimum track width was limited to 1.55 m by interference of the base frame. A single variation of this parameter to 1.65 m was used in tests 17 and 18.

The standard frame width, defined as twice the distance from centreline to load cell faces, was 1.37 m. A single variation to to 1.67 m was used in tests 18 - 23, i.e. in combination with the wide track in 18, and with low friction in 21 - 23. Frame width was chosen in preference to height as the varied parameter so that the upright length, and hence structural charateristics would not be changed.

The geometrical parameters are compared in Fig. 5.1 with regression lines of dimensions against tractor mass fitted by Schwanghart (53) to data covering a wide range of tractors. The standard values are all appropriate for the mass of 3065 kg; the difference between overall width and track width reflects the rather narrow tyres used on the experimental tractor compared with modern practice, particularly outside the U.K.

Frame strength

Since the length of the structural upright bars was chosen to give a suitable overall height, bar diameter was the only parameter available to control structural characteristics. The diameter chosen as standard, 42 mm, gave a nominal collapse-force/unballasted tractor weight ratio of 1.6.

One other bar diameter was used: 48 mm, giving a nominal collapse force of 1.5 x standard. The tests concerned were two of the four ballasted tests, 25 and 26, and the two low friction tests onto the concrete landing surface, 30 and 31.

Tractor forward speed (DZ)

The experiments represented a type of accident which normally involves fairly low speed. In addition, it was not expected that speed would have much influence on the overturning dynamics or the sideways frame deflection on impact, although it could affect the longitudinal deflection. The nominal standard speed was 1.5 m/s (3.4 mile/h) and a single variation, 3 m/s (6.7 mile/h), was used in test 15.

Angle of approach of tractor to bank edge (Υ)

The aim of studying the most simple dynamic case would have been met by an insignificant small approach angle. In practice, however,

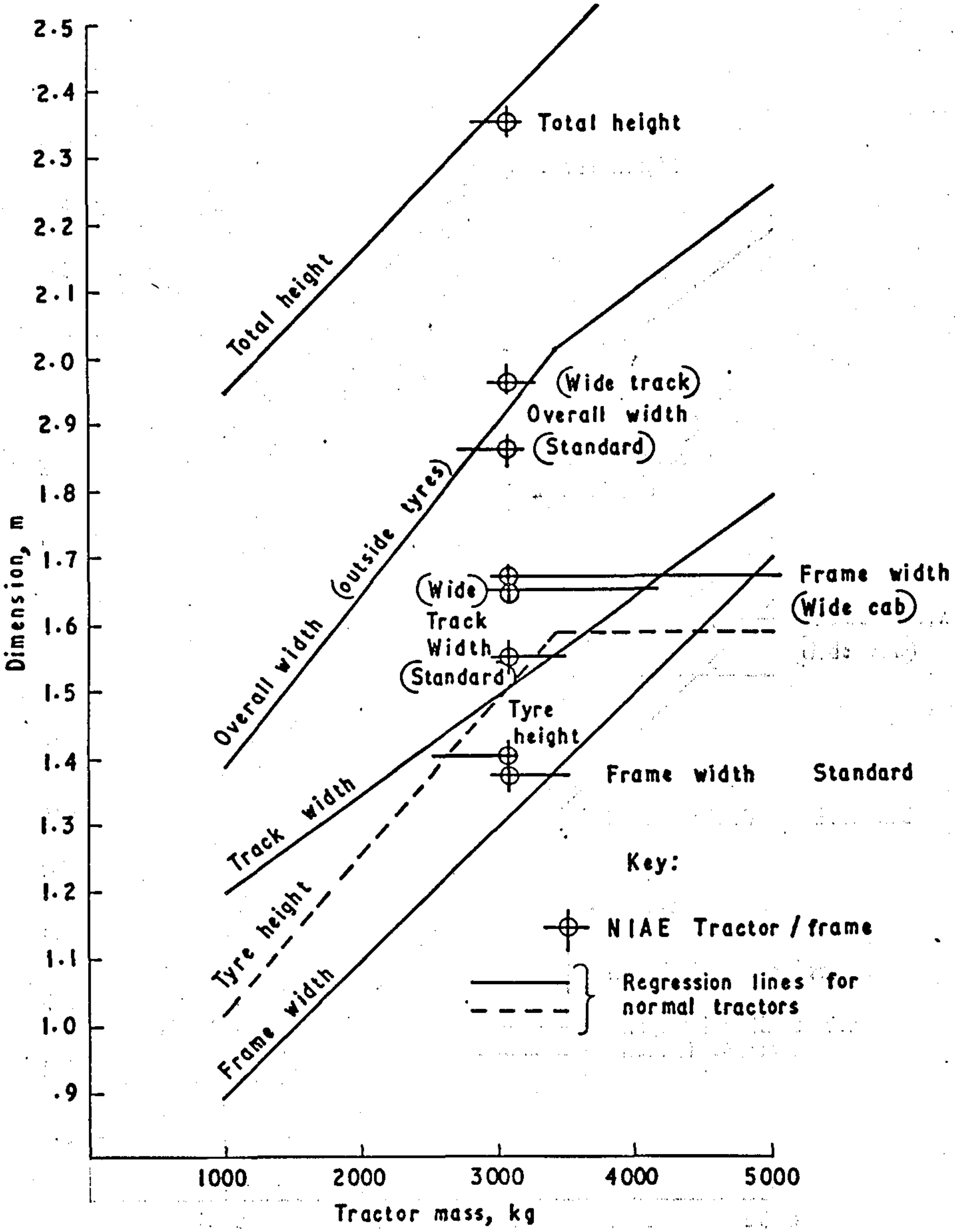

Fig. 5.1 Regressions of tractor dimensions against mass from Schwanghart (6) for comparison with values for the NIAE tractor and experimental frame.

this would have required a much longer platform to cope with the variable fall off point due to the limited accuracy of steering along the marker line. A nominal angle of 4^{o} was found to be a suitable compromise, and this was the standard value. A single variation to 8^{o} was used in test 14.

Values of yaw angle θ_y at roll-off are given in Table 5.2. These are generally greater than the nominal Υ, probably because the front wheels had just moved from the top surface of the platform and onto the chamfered edge. Following of the marker line was generally good and before roll-off the values of θ_y were closer to the nominal Υ.

Articulation of front axle about its longitudinal pivot

This last parameter is an artifact introduced after observation of the behaviour in the first few tests. The mathematical models in two dimensions could not predict rotations of the tractor in yaw and pitch, which were expected to be negligible during the overturning phase before impact. In the early tests significant yaw motions did, however, occur, roughly at the time when the rear axle was parallel to the sloping side of the bank, i.e. as the left-hand, upslope wheels reached the edge. Study of the cine films showed that the roll angle of the front axle was lagging that of the rear by the amount allowed by the front axle pivot stops. As the left-hand rear wheel reached the bank edge and began to slide down the slope, the front wheel was still on the top of the platform and became "hooked" momentrarily on the edge. The significance of this effect was checked for comparison with the models by fitting rigid stops in some tests to prevent the front axle from pivotting.

5.2. KINEMATICS OF THE OVERTURNING BEHAVIOUR

The films were analysed to determine the time-histories of displacements in the six co-ordinate directions, and hence velocities and energies. Analysis involved the frame-by-frame measurement of co-ordinates in the film plane of the tractor marker points. After scaling, this gave the vertical, lateral and roll motions directly, the longitudinal motion being estimated from tractor forward speed and impact position. Yaw and pitch angles, and hence co-ordinates of tractor points other than the markers, were found from the rotation transformation between fixed co-ordinates measured from the cine film and the known body co-ordinates of the marker points.

5.2.1. Analysis of cine films

The conventional co-ordinate system derived from aeronautical practice (Fig. 5.2) is appropriate for vehicle handling studies (66) where the predominant motions and large rotations take place in the horizontal, x-y plane. The principal overturning behaviour, however, occurs in the vertical plane perpendicular to the bank, and non-conventional co-ordinates (also shown in Fig 5.2) were chosen for this study for two reasons relating to the sequence of rotations from fixed to body co-ordinates:

(i) In the system used, the roll co-ordinate θ_z, the most important rotation, may be measured directly from the film since it is not distorted by the other rotations and maps directly. This led to a relatively simple mathematical treatment and increased accuracy.

(ii) Any system can handle indefinitely large rotations in one co-ordinate but rotations in the other two which pass through 90° create sensitivity problems and require additional sets of equations. The chosen sequence of rotations allowed large values of θ_z, the only rotation likely to exceed, say 45°.

The roll, pitch and yaw angles will be different in any particular tractor orientation from those defined according to another system. The differences will not be great, however, while two of the angles remain small; in any case it is possible to calculate rotations according to any system once the transformation matrix of direction cosines is known.

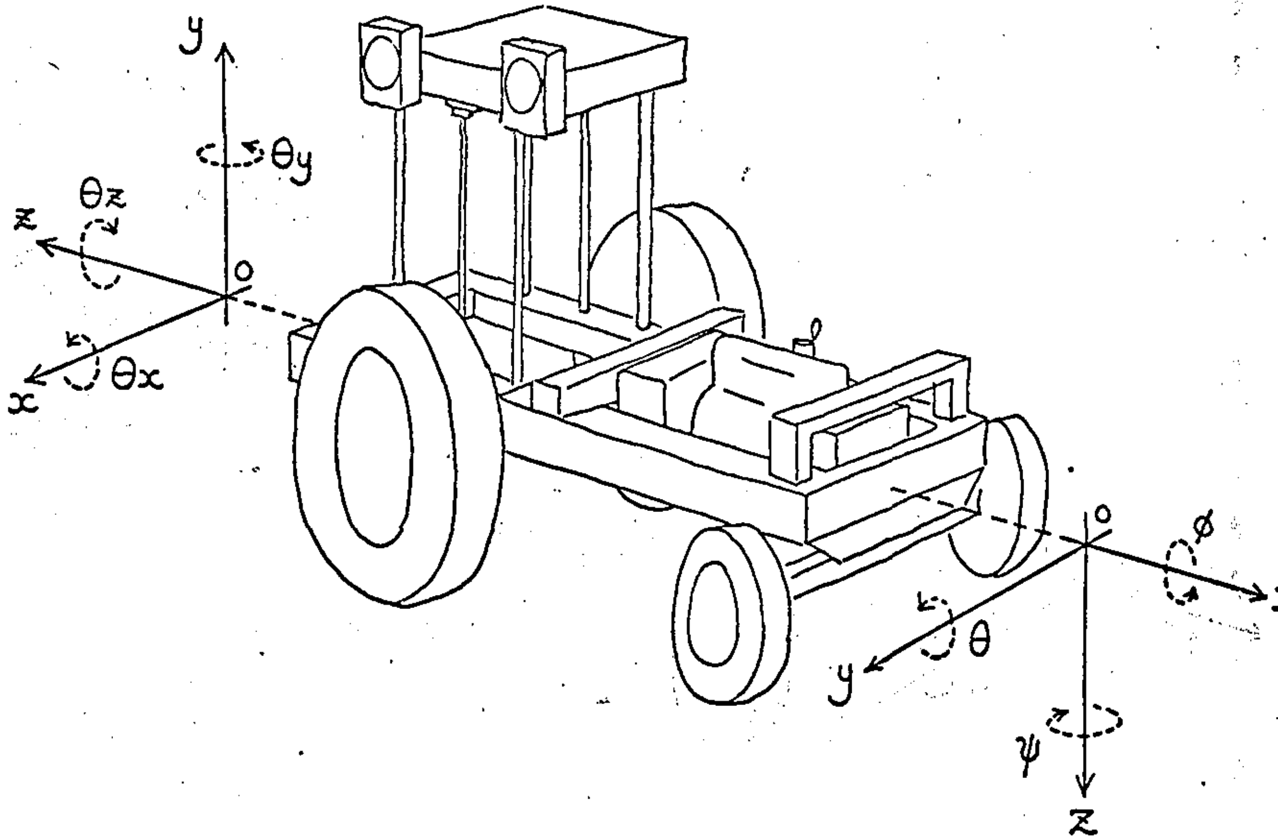

THIS SYSTEM		CONVENTIONAL SYSTEM
Lateral, +ve to right	x	Longitudinal, +ve to front
Vertical, +ve up	y	Lateral, +ve to right
Longitudinal, +ve rear	z	Vertical, +ve down

Sequence of rotation from fixed to body axes:-

(1) roll θ_z about Oz_0 to x_1, y_1, z_1	(1) yaw ψ about Oz_0 to x_1, y_1, z_1
(2) yaw θ_y about Oy_1 to x_2, y_2, z_2	(2) pitch θ about Oy_1 to x_2, y_2, z_2
(3) pitch θ_x about Ox_2 to x_3, y_3, z_3	(3) roll ϕ about Ox_2 to x_3, y_3, z_3

Fig. 5.2. Co-ordinate systems

The fixed co-ordinates x_o y_o z_o had as origin the point in the film plane which was a projection of the bank edge at roll-off. This point was chosen because it was relatively easy to define and overcame some of the problems due to the sloping surface of the platform. The origin for the body co-ordinates x_3 y_3 z_3 was the centre marker on the rear base frame of the tractor.

Method of analysis

The main analysis was based on the film from the rear camera, which was positioned over 100 m behind the overturning area with its optical axis aligned with the edge of the bank giving a view equivalent to Fig. 3.1. Techniques are available (67) for determing all six co-ordinates of general three-dimensional rigid-body motion from a single camera record. It is, however, difficult to overcome errors in the co-ordinate along the optical axis since the measurements depend on the separation of two points on the body in a plane only approximately parallel to the film plane. In addition, the mathematical development is more complex than the alternative procedure used for these experiments, described below. The other established technique using measurements from two cameras (68) is also more complex, more time consuming and suffers from synchronisation problems.

The mathemaical development of the analysis is described in Appendix 5.2. The rotation transform from fixed to body co-ordinates is first derived. Elements of this matrix are then used in conjunction with the measured co-ordinates to find the pitch and yaw angles θ_x and θ_y. The matrix is thus completely determined and may be used to find the co-ordinates of other points on the tractor, such as the centre of mass. Although the time derivates of the angular co-ordinates θ_x, θ_y and θ_z may be used to calculate energies this would require transformation of the inertia matrix. The alternative method described in Appendix 5.2 is to perform the calculation in the body co-ordinates by deriving a velocity transformation. This is more appropriate in giving angular velocities that may be identified directly with the tractor motion, although if pitch and yaw angles are both small the two methods give velocities with similar values.

The position of the tractor along the platform, the z_o co-ordinate, is required for a complete description of tractor position and for scaling the x_o and y_o co-ordinates from the film. The necessary absolute accuracy of z_o is not high, however, because of the large camera-tractor distance.

It would not have been possible to obtain z_o from analysis of the side view film but scaling assumptions would have been needed to take account of the movement of the tractor towards the film plane during overturning. This procedure was followed for a number of tests, from which it was concluded that z_o could be determined with sufficient accuracy using the assumption that the forward speed remains constant up to impact, after which it is zero. This is reasonable in view of the small components of force in the z_o direction during overturning and the small movements after impact. The scaling errors due to this assumption are less than 1%.

Finally, Appendix 5.2 covers the procedure for scaling the film measurements.

Recovery of information from film

Measurements were not required at every frame since the tractor movements between successive frames were small during approach and at the beginning of roll-off. The step interval was normally reduced from 25 frames during approach through 10, 5 and 2 to 1 frame near impact.

For the first fifteen tests the film was projected in the normal way onto a vertical screen. Measurement on the vertical surface was rather awkward, and for analysing the remainder of the tests, the projected beam was deflected by two surface silvered mirrors onto a horizontal table. A third technique was used for a repeat analysis of the first six tests, which was found necessary because of inaccuracies resulting from the different positions of the marker points used in the original analysis of these tests. The system used was a D-MAC digitiser at Cranfield Institute of Technology, adapted for use with a cine projector.

Computer implementation

A FORTRAN IV program KINEMA takes the digitised co-ordinates as input, together with a parameter list, and calculates the time histories which are then presented in tabular and graphical forms. The program was run on the ICL-4-70 computer at Rothamsted Experimental Station and used 30-60s of CPU time per run.

Velocity calculation

The clock time can be read to an accuracy of 0.01s, which is more than adequate as the time-base. In calculating velocities over a step of one or two frames, however, the small differences in clock time can lead to significant errors. Velocities for steps of less than 10 frames were therefore determined from the frame interval and the mean frame speed.

The individual velocity values also showed slight random errors due to limited resolution, and this was magnified by squaring in the energy determination. To reduce this fluctuation the velocities were smoothed by a simple triangular filter over 3 steps (weighting coefficients 0.25, 0.50, 0.25) or 5 steps (coefficients 0.1111, 0.2222, 0.3334, 0.2222, 0.1111).

Checks

Two checks on the measurements were provided. The first verified the z_o estimation and scaling procedure using the same technique as the z_o determination in the 6 degree-of-freedom method of analysis (67)

The second check used redundant measurement to verify the calculated position of a point on the top frame. Since this deformed under impact the check was invalid after this point but provided instead an estimate of frame deflection.

5.2.2. Time histories

Films were available for 27 of the 31 tests. The other four were:

Test No.13 – tractor steering failure caused premature, uncontrolled overturn.

Test No.26)
Test No.27) Films missing. No explanation could be found in spite of extensive searches.

Test No.29 Film cut short during outside processing.

The set of five time-history graphs and tabulated output from the 27 tests represents a considerable quanity of information. The time-histories were needed for comparison with the mathematical models but it was also necessary to summarise them in terms of values that could be used to compare the effect of parameter changes. This is done in section 5.2.3 below but first the results will be described in general terms using the sample plots for test 21 given in Figs. 5.3 to 5.6. The origin of the time scale is defined as the visually determined roll-off point. The arrow on the time scale indicates load-cell impact.

The gradual change in X_{og} and Y_{og} up to impact is shown in Fig. 5.3, together with some bouncing afterwards and eventually a steady resting position.

The roll angle θ_z (AZ) increases negatively from zero up to impact (Fig. 5.4) and then reduces to a resting value. The pitch θ_x (AX) and yaw θ_y (AY) angles start from values corresponding to the platform slope and edge approach angles respectively. Some fluctuation is present but in those tests where pitch and yaw depart significantly from zero, the change is typically fairly gradual, a single positive or negative peak being reached at, or shortly before impact.

Only the three most important velocities are shown in Fig. 5.5: $\dot{x}_{og}$ (XG), $\dot{Y}_{og}$ (YG) and roll $\dot{\theta}_z$ (AZ). In all tests the vertical velocity $\dot{y}_{og}$ continues to increase negatively up to impact; the peak may be reached slightly before the arrow due to impact of other parts of the tractor before the frame. In some tests the horizontal velocity $\dot{x}_g$

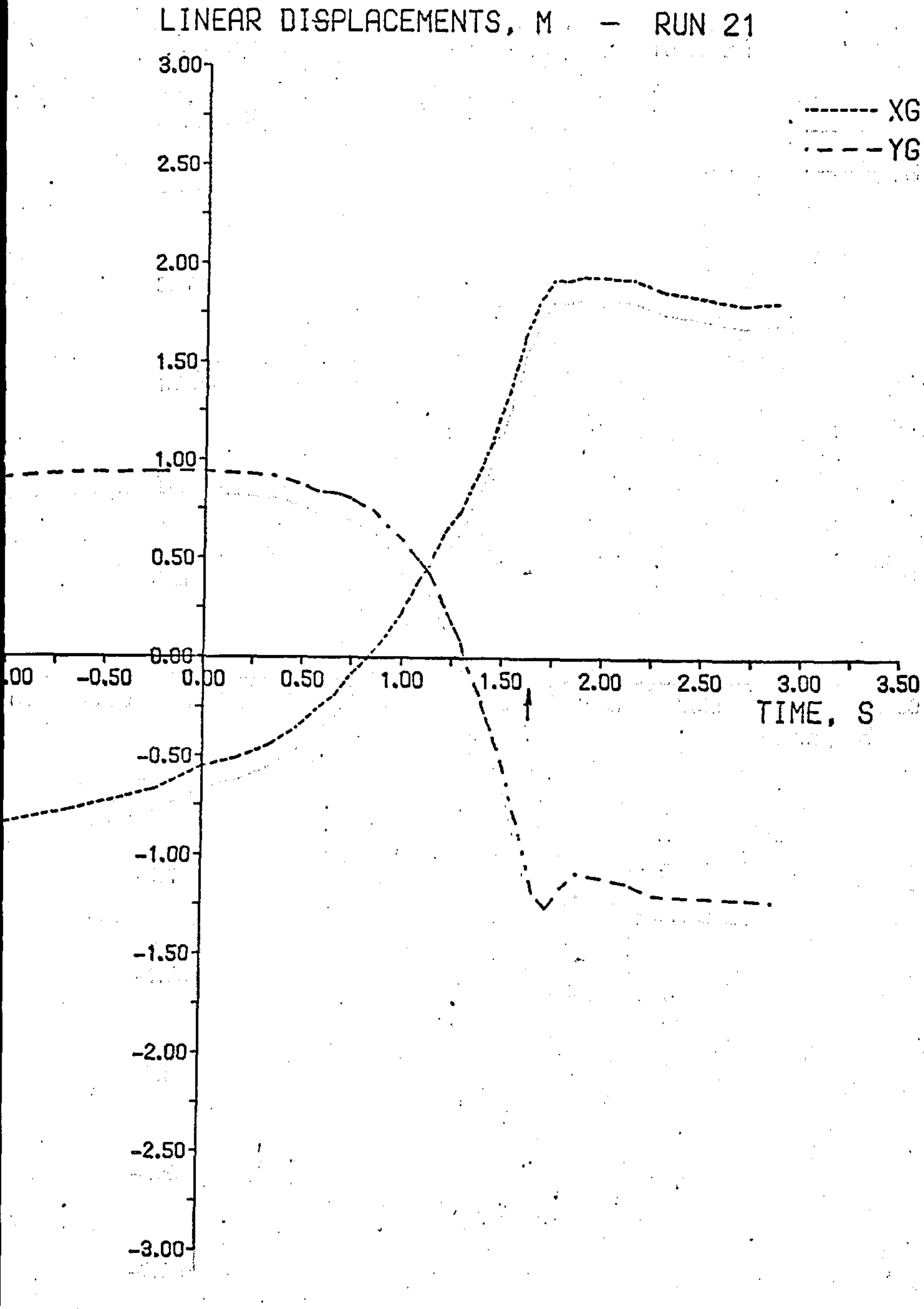

Fig.5.3. Sample plot of linear displacements from film analysis

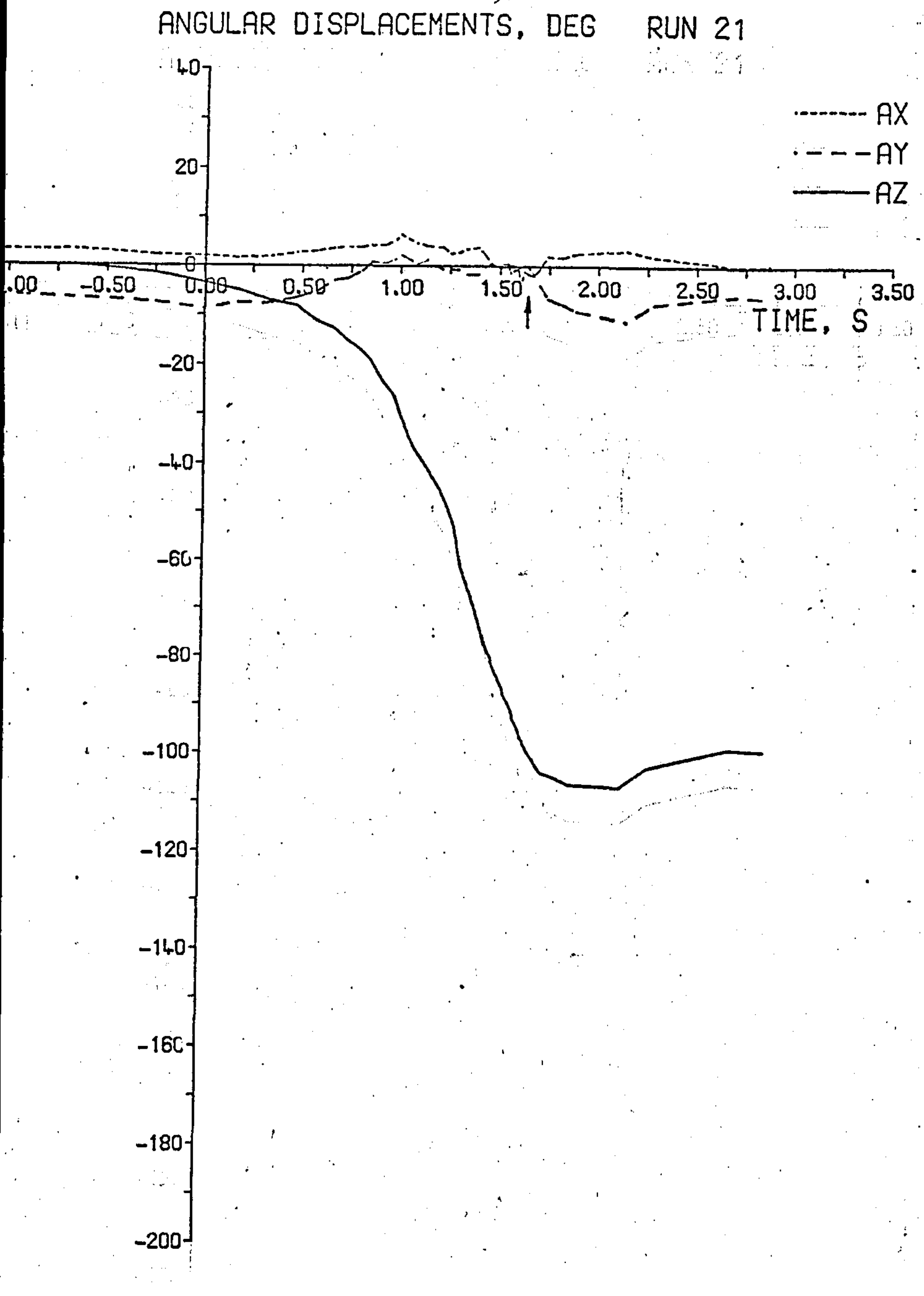

Fig.5.4. Sample plot of angular displacements from film analysis

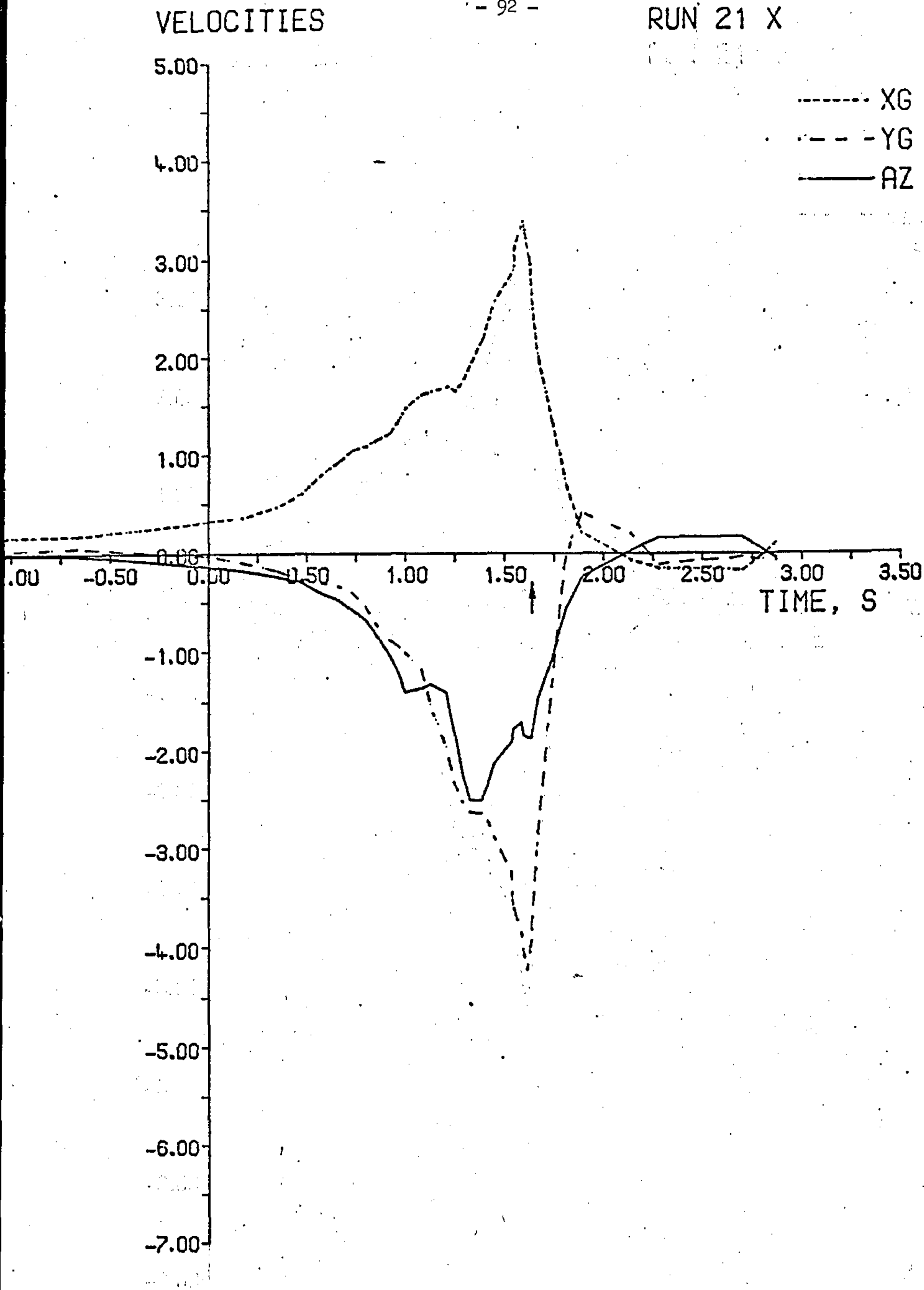

Fig.5.5. Sample plot of velocities from film analysis

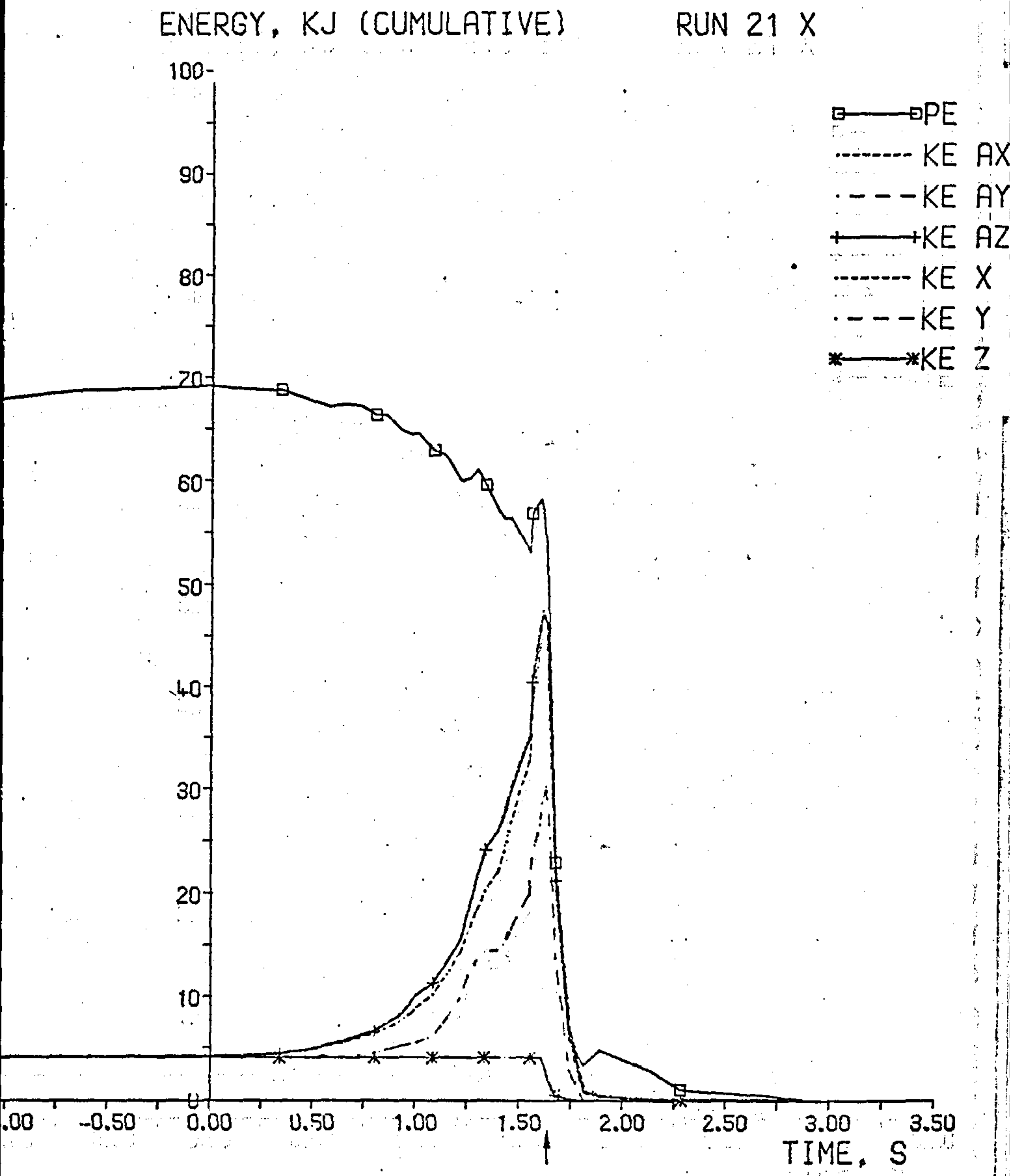

Fig. 5.6. Sample plot of energy from film analysis

behaves similarly but in others the rate of increase is lower and a peak is reached somewhat before impact. Roll velocity $\dot{\theta}_z$ also peaks before impact in many cases, the time of the peak being most clearly related to bank slope α and friction. At α of 0° or $7\frac{1}{2}^\circ$ (steepest slopes) the peak occurs significantly before impact, while at greater angles and high friction the roll couple provided by tyre forces remains important and $\dot{\theta}_z$ continues to increase up to impact. With low friction the roll couple is less and the peak $\dot{\theta}_z$ is reached early at all α .

The kinetic and potential energies are plotted cumulatively in Fig. 5.6 to allow transfer and dissipation to be readily visualised. In most cases the energies due to rotational velocities (KE AX, KE AY, KEAZ) are insignificant. Although roll velocity is a major component in the linear velocity of the tractor's extremities, its contribution to energy (KE AZ) is small because of the relatively low moment of inertia. The other two moments of inertia are greater but, except in one or two cases, the pitch and yaw velocities are very small.

The longitudinal velocities $\dot{z}_{og}$ are fairly similar in all tests except No. 15. (see section 2.8), so the energy plots may be effectively reduced to comparisons of kinetic energies (KE X, KE Y) due to lateral and vertical velocities $\dot{x}_{og}$ and $\dot{y}_{og}$, which are of the same order, potential energy (PE) and dissipation, which is given by the drop in total cumulative energy. The dissipation before impact is due mainly to friction losses at the tyres, and after impact to strain energy in the soil, frame tyres etc.

5.2.3. Instantaneous values

Since all the variables, including velocities and accelerations, change continuously with time throughout each test, they must be summarised either by overall values, such as means, or by representative single values. Means may not be very sensitive and may obscure important effects; if representive values are used they must be comparable for each test.

At first sight, the most appropriate points to select values appear to be either immediately before impact or at a constant time after roll-off. Values before impact are required for analysis of the impact behaviour and are presented later. They would also be suitable for the description of overturning behaviour but for the variation in height of fall due to the platform slope.

Taking values at a constant time after roll-off presents another difficulty. Values are changing slowly at the beginning of overturning and roll-off is poorly defined. Small variations in initial conditions such as yaw angle and velocity have significant effect on the behaviour of overturning but much less so later on.

Taking values after a specified fall of the centre of mass from its highest position was considered to be the best method for comparison. The fall chosen (δy_{og}) was 1.5 m, the greatest value that occured reliably before first impact in all tests. This gives a constant change of potential energy of 45.1 kJ for the majority of tests, when the tractor was unballasted, allowing direct comparison of kinetic energy changes. Since values are calculated at discrete steps a linear interpolation is used to estimate them at the specific y_{og}.

The results are presented in the same form as used in Table 5.1 to allow easy cross-referencing of parameters.

The kinetic energy gains for a centre of mass fall of 1.5 m are given in Table 5.4, as the sums of energies due to velocities in $x_o, y_o, \theta_x, \theta_y$ and θ_z co-ordinates at the selected δy_{og}; these energies are insignificant at roll-off, and the longitudinal velocity $\dot{z}_{og}$ was assumed to remain constant.

The lateral and vertical velocities $\dot{x}_{og}$ (DXG) and $\dot{y}_{og}$ (DYG) contributing most to the above energies are given in Tables 5.5 and 5.6. The roll velocity $\dot{\theta}_z$, while contributing relatively little to the energy, is also of interest and is given in Table 5.7.

Table 5.4. Kinetic energy gain, kJ for a centre-of-mass fall (δy_{og}) of 1.5 m

Condition	Axle stop	Nominal α (Bank angle to vertical), degrees: 0	$7\frac{1}{2}$	15	$22\frac{1}{2}$	30	$37\frac{1}{2}$
Standard A	No		33.0, 29.5	26.7 B	29.5	29.4	S 27.7
	Yes	28.4	24.2, 26.8	26.6, 25.2 C	24.6	22.7	
Ballasted (mass = 4015 kg + change in centre of mass and moment of inertia)	No				34.1		
	Yes		D		33.3 D		
Low friction (μ = 0.1 - 0.15) + wide cab (1.67 m)	No				33.1		
	Yes		30.1		36.6		
On concrete	No			25.0 E			
On concrete + low friction	Yes			32.9 D,E			
	No			33.7 D,E			
Higher speed (3 ms^{-1})	No		38.8				
Larger approach angle (γ = 8°)	No		25.6				
Wide cab (1.67 m)	Yes		28.1		21.5		
Wide track (1.65 m)	Yes				24.0		
Wide cab + (1.67 m) wide track (1.65 m)	Yes				21.4		

NOTES

A. The conditions referred to as standard are:

Tractor mass: 3065 kg
Surface dry: (μ = 0.8-1.0)
Cab width: 1.37 m
Track width: 1.55 m
Bar diameter: 42 mm
Speed DZ: 1.5 ms^{-1}
Approach angle: 4° (γ)
Landing surface: soil

B. Front of tractor on concrete.

C. Partial failure of rear wheel.

D. 48 mm diameter bar.

E. α = 17.7° due to repositioning of plates.

Table 5.5. Lateral velocity $\dot{x}_{og}$, m/s for a centre-of-mass fall (δy_{og}) of 1.5 m

Condition	Axle stop	Nominal α (Bank angle to vertical), degrees					
		0	$7\frac{1}{2}$	15	$22\frac{1}{2}$	30	$37\frac{1}{2}$
Standard A	No		2.41, 2.43	2.24 B	2.23	2.80	S 2.47
	Yes	2.11	2.83, 2.76	2.25, 2.56 C	2.28	2.50	
Ballasted (mass = 4015 kg + change in centre of mass and moment of inertia)	No				2.48		
	Yes		D		2.41 D		
Low friction (μ = 0.1 - 0.15) + wide cab (1.67 m)	No				2.77		
	Yes		2.82		3.23		
On concrete	No			1.90 E			
On concrete + low friction	Yes			2.81 D,E			
	No			2.48 D,E			
Higher speed (3 ms^{-1})	No		2.69				
Larger approach angle (γ = 8°)	No		2.65				
Wide cab (1.67 m)	Yes		2.65		1.96		
Wide track (1.65 m)	Yes				2.54		
Wide cab + (1.67 m) wide track (1.65 m)	Yes				2.02		

NOTES

A. The conditions referred to as standard are:

Tractor mass: 3065 kg

Surface dry: (μ = 0.8-1.0)

Cab width: 1.37 m

Track width: 1.55 m

Bar diameter: 42 mm

Speed DZ: 1.5 ms^{-1}

Approach angle: 4° (γ)

Landing surface: soil

B. Front of tractor on concrete.

C. Partial failure of rear wheel.

D. 48 mm diameter bar.

E. α = 17.7° due to repositioning of plates.

Table 5.6. Vertical velocity, m/s, for a centre-of-mass fall (δy_{og}) of 1.5 m

Condition	Axle stop	Nominal α (Bank angle to vertical), degrees: 0	$7\frac{1}{2}$	15	$22\frac{1}{2}$	30	$37\frac{1}{2}$
Standard A	No		-3.80, -3.88	-3.25 B	-3.69	-2.90	S -3.02
	Yes	-3.59	-2.53, -2.86	-3.33, -2.88 C	-3.07	-2.47	
Ballasted (mass = 4015 kg + change in centre of mass and moment of inertia)	No				-3.00		
	Yes		D		-3.15 D		
Low friction (μ = 0.1 - 0.15) + wide cab (1.67 m)	No				-3.52		
	Yes		-3.13		-3.43		
On concrete	No			-3.25 E			
On concrete + low friction	Yes			-3.44 D,E			
	No			-3.77 D,E			
Higher speed (3 ms^{-1})	No		-4.00				
Larger approach angle (γ = 8°)	No		-2.65				
Wide cab (1.67 m)	Yes		-3.12		-3.06		
Wide track (1.65 m)	Yes				-2.61		
Wide cab + (1.67 m) wide track (1.65 m)	Yes				-3.01		

NOTES

A. The conditions referred to as standard are:

- Tractor mass: 3065 kg
- Surface dry: (μ = 0.8-1.0)
- Cab width: 1.37 m
- Track width: 1.55 m
- Bar diameter: 42 mm
- Speed DZ: 1.5 ms^{-1}
- Approach angle: 4° (γ)
- Landing surface: soil

B. Front of tractor on concrete.

C. Partial failure of rear wheel.

D. 48 mm diameter bar.

E. α = 17.7° due to repositioning of plates.

Table 5.7 Roll velocity $\dot{\theta}_z$, rad/s, for a centre-of-mass fall (δy_{og}) of 1.5 m

Condition	Axle stop	Nominal α (Bank angle to vertical), degrees 0	$7\frac{1}{2}$	15	$22\frac{1}{2}$	30	$37\frac{1}{2}$
Standard (A)	No		-1.69, -1.97	-2.03 B	-0.97	-2.41	S -2.61
	Yes	-1.25	-1.72, -1.66	-1.51, -1.66 C	-1.56	-2.43	
Ballasted (mass = 4015 kg + change in centre of mass and moment of inertia)	No				-1.95		
	Yes		D		-1.47 D		
Low friction (μ = 0.1 - 0.15) + wide cab (1.67 m)	No				-1.84		
	Yes		-1.96		-1.97		
On concrete	No			-1.89 E			
On concrete + low friction	Yes			-1.88 D,E			
	No			-1.88 D,E			
Higher speed (3 ms^{-1})	No		-2.12				
Larger approach angle (γ = 8°)	No		-2.18				
Wide cab (1.67 m)	Yes		-1.47		-1.33		
Wide track (1.65 m)	Yes				-1.59		
Wide cab + (1.67 m) wide track (1.65 m)	Yes				-1.28		

NOTES

A. The conditions referred to as standard are:

Tractor mass: 3065 kg
Surface dry: (μ = 0.8-1.0)
Cab width: 1.37 m
Track width: 1.55 m
Bar diameter: 42 mm
Speed DZ: 1.5 ms^{-1}
Approach angle: 4° (γ)
Landing surface: soil

B. Front of tractor on concrete.
C. Partial failure of rear wheel.
D. 48 mm diameter bar.
E. α = 17.7° due to repositioning of plates.

The values of roll angle θ_z (AZ) for a y_{og} drop of 1.5 m are given in Table 5.8.

The main interest in pitch (θ_x) and yaw (θ_y) is the effect of the axle stop. It was considered that this would be revealed most clearly by the extreme values of these angles during overturning, rather than values at a y_{og} drop of 1.5 m as for the other variables. The minimum θ_x (i.e. maximum negative values) are given in Table 5.9 and maximum θ_y in Table 5.10. The two other extremes, maximum θ_x and minimum θ_y showed much less variation and are omitted.

Values immediately before impact are given in Tables 5.11 (energy) and 5.12 (roll angle). Although the load cell impact was clearly identifiable on the films, the first impact was often not, particularly where this occured at the front of the tractor. The impact values are therefore taken at the point when vertical velocity reached its maximum negative value, $\dot{y}_{ogmin}$. This was always on a sharp peak corresponding to the upward acceleration of first impact.

5.2.4. <u>Front axle articulation</u>

The effects of using axle stops to prevent articulation were subjected to statistical analysis.

The complete set of 27 tests was included; the axle stop was present in 15 of these and absent in the remaining 12. Considering only those parameters affecting overturning behaviour the majority of these tests may be paired; of those that are not paired it is reasonable to assume that the parameters are distributed in a way that allows bias to be ignored. The statistical test used was the Kruskal-Wallis one-way analysis of variance by ranks (69) which is equivalent in this case to the Mann-Whitney U test. The tests involved ranking the complete sets of 27 results and obtaining two sums of ranks, one associated with each of the axle stop conditions. The null hypothesis tested was that no significant difference in the variables existed between the two conditions.

Table 5.8 Roll angle θ_z, deg., for a centre-of-mass fall (δy_{og}) of 1.5 m

Condition	Axle stop	Nominal α (Bank angle to vertical), degrees					
		0	$7\frac{1}{2}$	15	$22\frac{1}{2}$	30	$37\frac{1}{2}$
Standard A	No		-92.8, -91.6	-93.4 B	-80.3	-106.0	S -105.0
Standard A	Yes	-89.1	-90.4, -84.6	-79.2, -84.6 C	-87.9	-93.7	
Ballasted (mass = 4015 kg + change in centre of mass and moment of inertia)	No				-95.5		
	Yes		D		-84.8 D		
Low friction (μ = 0.1 - 0.15) + wide cab (1.67 m)	No				-85.8		
	Yes		-84.0		-85.1		
On concrete	No			-92.3 E			
On concrete + low friction	Yes			-83.4 D,E			
	No			-83.8 D,E			
Higher speed (3 ms^{-1})	No		-95.7				
Larger approach angle (γ = 8°)	No		-95.5				
Wide cab (1.67 m)	Yes		-88.5		-81.1		
Wide track (1.65 m)	Yes				-83.7		
Wide cab + (1.67 m) wide track (1.65 m)	Yes				-80.4		

NOTES

A. The conditions referred to as standard are:

Tractor mass: 3065 kg
Surface dry: (μ = 0.8-1.0)
Cab width: 1.37 m
Track width: 1.55 m
Bar diameter: 42 mm
Speed DZ: 1.5 ms^{-1}
Approach angle: 4° (γ)
Landing surface: soil

B. Front of tractor on concrete.
C. Partial failure of rear wheel.
D. 48 mm diameter bar.
E. α = 17.7° due to repositioning of plates.

Table 5.9. Minimum pitch angle, θ_{xmin}, deg., up to impact

Condition	Axle stop	Nominal α (Bank angle to vertical), degrees					
		0	$7\frac{1}{2}$	15	$22\frac{1}{2}$	30	$37\frac{1}{2}$
Standard A	No		-10 -15	-13 B	-10	-20	S -24
	Yes	-2	-4 -2	-1 -1 C	-3	-2	
Ballasted (mass = 4015 kg + change in centre of mass and moment of inertia)	No				-13		
	Yes		D		-2 D		
Low friction (μ = 0.1 - 0.15) + wide cab (1.67 m)	No				-7		
	Yes		-4		+1		
On concrete	No			-20	E		
On concrete + low friction	Yes			-3	D,E		
	No			-4	D,E		
Higher speed (3 ms^{-1})	No		-8				
Larger approach angle (γ = 8°)	No		-9				
Wide cab (1.67 m)	Yes		0		-3		
Wide track (1.65 m)	Yes				+2		
Wide cab + (1.67 m) wide track (1.65 m)	Yes				0		

NOTES

A. The conditions referred to as standard are:

Tractor mass: 3065 kg
Surface dry:(μ = 0.8-1.0)
Cab width: 1.37 m
Track width: 1.55 m
Bar diameter: 42 mm
Speed DZ: 1.5 ms^{-1}
Approach angle: 4° (γ)
Landing surface: soil

B. Front of tractor on concrete.

C. Partial failure of rear wheel.

D. 48 mm diameter bar.

E. α = 17.7° due to repositioning of plates.

Table 5.10. Maximum yaw angle, θ_{ymax}, deg., up to impact

Condition	Axle stop	Nominal α (Bank angle to vertical), degrees 0	$7\frac{1}{2}$	15	$22\frac{1}{2}$	30	$37\frac{1}{2}$
Standard A	No		+7 +10	+10 B	+23	+20	S +25
	Yes	+6	+12 0	+2 +11 C	+2	+2	
Ballasted (mass = 4015 kg + change in centre of mass and moment of inertia)	No				+11		
	Yes		D		+6 D		
Low friction (μ = 0.1 - 0.15) + wide cab (1.67 m)	No				+5		
	Yes		+2		+5		
On concrete	No			+19	E		
On concrete + low friction	Yes			+8	D,E		
	No			+1	D,E		
Higher speed (3 ms^{-1})	No		+15				
Larger approach angle (γ = 8°)	No		+14				
Wide cab (1.67 m)	Yes		+3		+10		
Wide track (1.65 m)	Yes				+4		
Wide cab + (1.67 m) wide track (1.65 m)	Yes				+2		

NOTES

A. The conditions referred to as standard are:

Tractor mass: 3065 kg

Surface dry: (μ = 0.8-1.0)

Cab width: 1.37 m

Track width: 1.55 m

Bar diameter: 42 mm

Speed DZ: 1.5 ms^{-1}

Approach angle: 4° (γ)

Landing surface: soil

B. Front of tractor on concrete.

C. Partial failure of rear wheel.

D. 48 mm diameter bar.

E. α = 17.7° due to repositioning of plates.

Table 5.11. Total energy, kJ, at minimum vertical velocity, $\dot{y}_{ogmin}$ (energy at final rest defined as zero)

Condition	Axle stop	Nominal α (Bank angle to vertical), degrees 0	$7\frac{1}{2}$	15	$22\frac{1}{2}$	30	$37\frac{1}{2}$
Standard A	No		61.4, 60.4	53.9 B	58.3	52.6	S 44.8
	Yes	53.1	37.8, 52.7	37.2, 38.4 C	43.7	54.4	
Ballasted (mass = 4015 kg + change in centre of mass and moment of inertia)	No				66.9		
	Yes		D		64.5 D		
Low friction (μ = 0.1 - 0.15) + wide cab (1.67 m)	No				54.1		
	Yes		54.2		52.9		
On concrete	No			64.1 E			
On concrete + low friction	Yes			65.3 D,E			
	No			79.5 D,E			
Higher speed (3 ms^{-1})	No		77.6				
Larger approach angle (γ = 8°)	No		45.6				
Wide cab (1.67 m)	Yes		55.7		49.9		
Wide track (1.65 m)	Yes				55.5		
Wide cab + (1.67 m) wide track (1.65 m)	Yes				47.1		

NOTES

A. The conditions referred to as standard are:

Tractor mass:	3065 kg
Surface dry:	(μ = 0.8-1.0)
Cab width:	1.37 m
Track width:	1.55 m
Bar diameter:	42 mm
Speed DZ:	1.5 ms^{-1}
Approach angle:	4° (γ)
Landing surface:	soil

B. Front of tractor on concrete.

C. Partial failure of rear wheel.

D. 48 mm diameter bar.

E. α = 17.7° due to repositioning of plates.

Table 5.12. Roll angle θ_z, deg., at minimum vertical velocity, $\dot{y}_{ogmin}$

Condition	Axle stop	Nominal α (Bank angle to vertical), degrees: 0	$7\frac{1}{2}$	15	$22\frac{1}{2}$	30	$37\frac{1}{2}$
Standard A	No		-104, -105	-106 B	-84	-102	S -101
	Yes	-100	-93, -99	-87, -89 C	-94	-107	
Ballasted (mass = 4015 kg + change in centre of mass and moment of inertia)	No				-101		
	Yes		D		-95 D		
Low friction (μ = 0.1 - 0.15) + wide cab (1.67 m)	No				-96		
	Yes		-95		-96		
On concrete	No			-105 E			
On concrete + low friction	Yes			-100 D,E			
	No			-100 D,E			
Higher speed (3 ms^{-1})	No		-101				
Larger approach angle (γ = 8°)	No		-97				
Wide cab (1.67 m)	Yes		-98		-93		
Wide track (1.65 m)	Yes				-97		
Wide cab + (1.67 m) wide track (1.65 m)	Yes				-91		

NOTES

A. The conditions referred to as standard are:

- Tractor mass: 3065 kg
- Surface dry: (μ = 0.8-1.0)
- Cab width: 1.37 m
- Track width: 1.55 m
- Bar diameter: 42 mm
- Speed DZ: 1.5 ms^{-1}
- Approach angle: 4° (γ)
- Landing surface: soil

B. Front of tractor on concrete.

C. Partial failure of rear wheel.

D. 48 mm diameter bar.

E. α = 17.7° due to repositioning of plates.

The variable which first drew attention to the effect of the axle pivot was the yaw angle θ_y and this was expected to show a significant difference. In addition to its maximum value, θ_{ymax} given in Table 5.10, the minimum, θ_{ymin} was also tested. To assess the wider effects of the axle stop the test was applied to the maximum and minimum pitch angles (θ_{xmax}, θ_{xmin}), and to the variables at a δy_{og} of 1.5 m given in Tables 5.5 to 5.8. The significance levels associated with rejection of the null hypothesis in each case are given in Table 5.13. The rejection region is one-tailed in the case of θ_{ymax} since the direction of the expected effect is predictable; in all other cases it is two-tailed.

Table 5.13. Significant differences due to the axle stops

Variable		See Table	Level of significance	Direction of effect-values without stop are significantly:
Max and min yaw and pitch	θ_{ymax}	5.10	p 0.005	Higher
	θ_{ymin}		N.S.	–
	θ_{xmax}		p 0.02	Lower
	θ_{xmin}	5.9	p 0.001	Higher
Values at y_{og} drop of 1.5 m	x_{og}	5.5	N.S.	–
	y_{og}	5.6	N.S.	–
	θ_z	5.8	p 0.01	Higher
	θ_z	5.7	p 0.02	Higher

5.3. IMPACT BEHAVIOUR

The object of the analysis was to determine time histories of the forces acting on the frame, the resulting displacements and hence the energies absorbed.

5.3.1. Method of analysis

The top frame has three degrees of freedom of deformation if axial deformation of the members is ignored; hence three external forces and three deflections completely describe the behaviour. The vertical forces (channels 2 and 5) are of interest but they may impart energy only to the ground, not to the frame. The three degrees of freedom chosen for analysis were lateral (x_3) at each load cell and longitudinal (z_3) at the front load cell. The contact points were assumed to be in the centre of the load cell faces. The transformations of the impact forces and deflections are given in Appendix 5.3.

Digitising of recordings

The recordings were digitised on the Institute's PDP8e computer. Inspection of the recordings showed that the duration of the first impact was always less than 0.5s and that a digitising interval of about 0.001s would be adequate in relation to the impact force rise-time (typically 0.025s) and the resonant frequency of the top frame (about 10 Hz). Subsequent impacts after rebound were entirely elastic and all required information may therefore be obtained from the first. The resolution provided was approaching the minimum acceptable of about 1% of typical maximum signal excursion (0.2% of calibration offset level).

There were unfortunately a number of tests when faults in one or more channels of the tape recorder resulted in incomplete recordings. One of the purposes of simulataneous recordings on ultra-violet (UV) sensitive charts was to cover this eventuality and the relevant traces were therefore analysed by hand.

The gain and spacing of the traces on the 150 mm wide paper were a compromise between resolution and overlap. Readability and accuracy were therefore limited, and manual analysis data was used in the results only for the channel(s) missing from the tape recordings. Manual analysis of other channels was used as a check on the accuracy of this procedure, which was found to be satisfactory. The smallest digitising interval that could easily be differentiated was 0.005s. The resolution was approximately 0.5% of calibration offset level.

In five of the eight tests concerned (8 - 12), the only missing channel was number 8, the least important and generally smallest displacement. In the other three (14 - 16) all odd numbered channels were missing.

Computer implementation

Two FORTRAN IV programs were run in a Job Sequence on the ICL 4-70 computer to analyse the punched tape data. The first, CAL, determined the mean zero level and mean offset level of the calibration data for each channel and wrote them to a file for reading into the main program. The main program, AN14PL, calibrated the data, calculated the required forces, deflections and energies and produced graphical and printed output.

For runs in which signals were missing from the tape recording, the manually analysed data had to be merged with the other channels. Since the time increments were different, direct substitution was not possible. The program proceded step by step through the PDP8e data searched for a time in the manual data either side of the time in the main data at each step. A new value was then found for each missing or duplicated channel by linear interpolation based on the time differences.

The data were smoothed to eliminate the effect of instrumentation noise. An 11-term quadratic-tapered sinc function (70) was used for its combination of attenuation at high frequencies and good performance below cut-off, with minimum overshoot on impact pulses. The weighting coefficients are shown in Table 5.14 and give a nominal cut-off frequency of 148 Hz at the time increment used.

Table 5.14. Weighting coefficients for smoothing AN14PL data

Step	n	n + 1 n - 1	n + 2 n - 2	n + 3 n - 3	n + 4 n - 4	n + 5 n - 5
Coefficient	0.332	0.267	0.122	0.0	-0.038	-0.017

After smoothing and calibration, the forces and deflections in the three chosen co-ordinate directions are calculated according to the equations of Appendix 5.3. These variables are plotted against time and the forces are also plotted against the relevant deflections as the most direct representation of structural behaviour. Rectangular integration of these functions gives the energy components, which are also plotted against time to allow permanent and maximum instantaneous values to be extracted.

5.3.2. Time histories

Tape recordings were available for 27 of the 31 tests. The other four were:

Test no. 3 - Tape recorder failed to start.

Test no. 5 - A trailing umbilical cable snagged, disconnecting all six load-cell channels at the break-away joint.

Test no. 13 - Tractor steering failure caused premature, uncontrolled overturn.

Test no. 31 - Severe damage to the tractor caused breakage of the connecting plug for channel 7, the most important displacement (lateral).

All four tests onto the concrete surface (nos. 28 - 31) gave high transient force peaks, and in some cases there were also spikes on the displacement channels. The analysis of tests no. 28 and 30 was considered to be acceptable but no. 29 was rejected because of several small defects and unreasonable force-deflection results.

Although the force and deflection time-histories are of interest, they are inevitably of similar form for all tests. Frame collapse forces depend mainly on frame strength, and although directions of loading are also important the overall behaviour may be summarised most suitably by energy values. Two values are relevant for each of the three chosen co-ordinated directions x_{3L1}, x_{3L2}, and z_{3L2}: the maximum instantaneous energy and the final energy corresponding to permanent deformation after elastic recovery. The maxima are the more relevant in relation to both energy absorbed and driver protection.

These summarised data are illustrated by sample time histories described below.

The four main plots from a typical test (again, no. 21) are shown in 5.7 to 5.10. In this case the longitudinal force F_{Z32} is small (Fig. 5.7) but both lateral forces rise rapidly to peaks, drop slightly to plateaux during plastic deformation, then fall to zero during elastic recovery. The same phases are evident in the deflection time-histories Fig. 5.8. The two are combined in the force deflection diagram, Fig. 5.9, where the three stages are quite close to the straight-line approximations of the idealised form described in section 6.

The elastic behaviour is clear during recovery, the apparent elastic stiffness of about 0.6 kN/mm agreeing well with that found in laboratory tests (section 6); a strict comparison would require laboratory reproduction of the loading directions, but there is no reason to suspect that the agreement would not be confirmed. During loading, the recorded elastic behaviour is not so satisfactory. The rate of change of force is much greater here, and the explanation probably lies in a slight phase difference between force and deflection signals. The effect on energy is not likely to be significant. The longitudinal force deflection curve does not loop because the deformation is nearly elastic and the force remains small.

The final plot, Fig. 5.10, is an integration of the force-deflection diagrams. The curves are shown as time-histories to allow maximum and final values to be read off.

5.3.3. <u>Energy absorbed in the frame</u>

The maximum instantaneous sideways energy - the sum of the integrated F_{x31}/x_{31} and F_{x32}/x_{32} curves up to maximum deflection - are given in

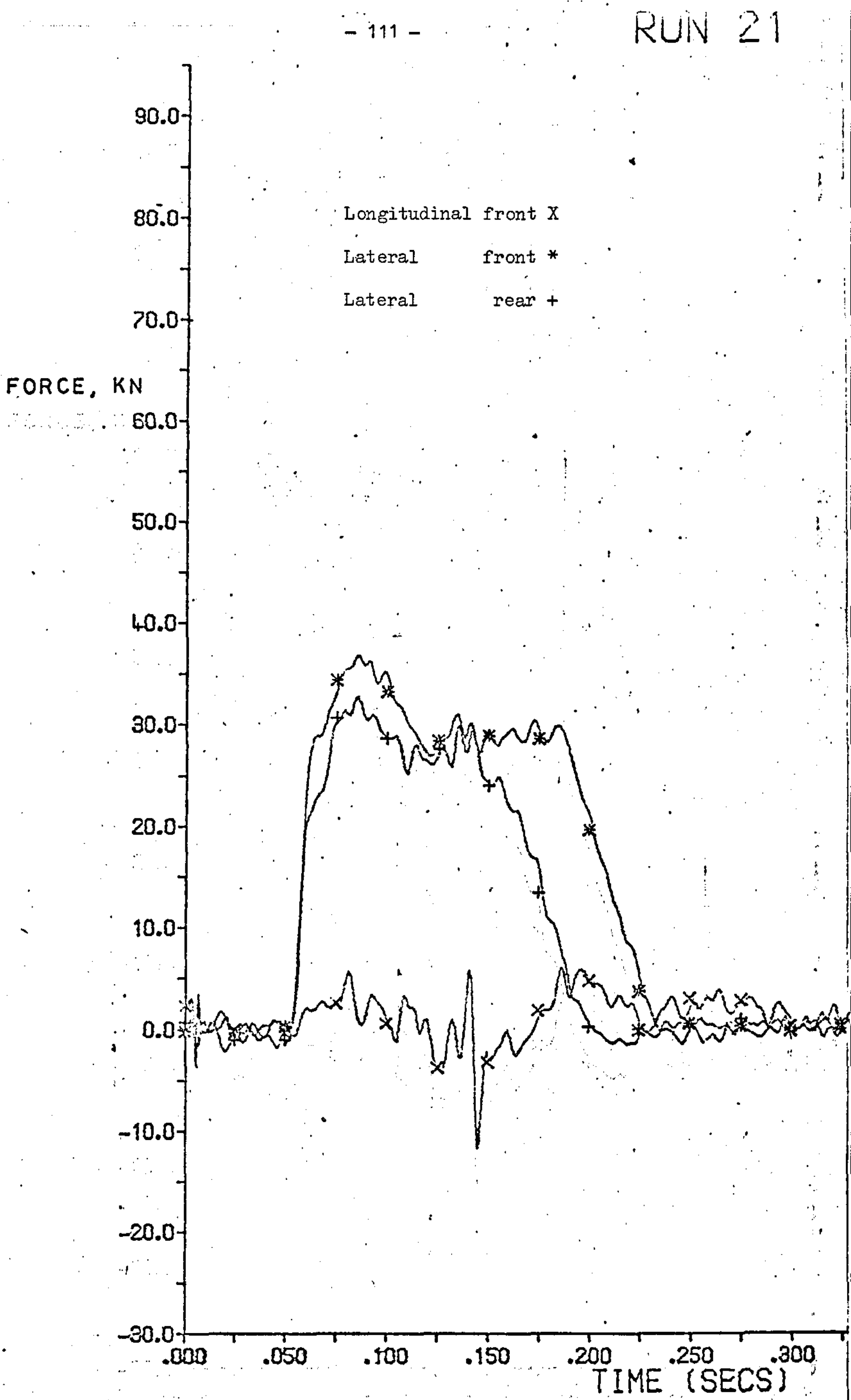

Fig.5.7. Sample plot of impact forces on frame

RUN 21

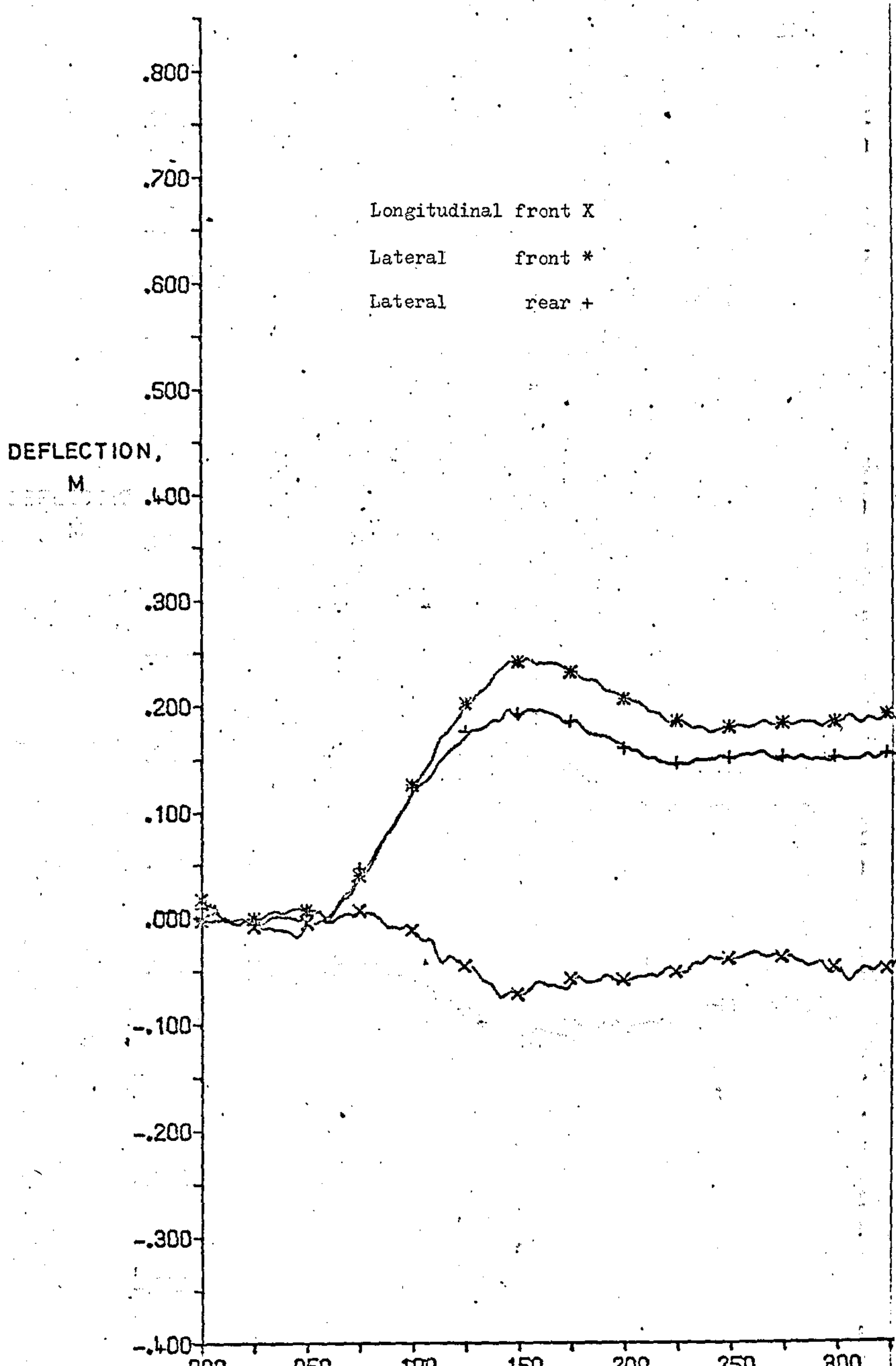

Fig. 5.8. Sample plot of frame deflections

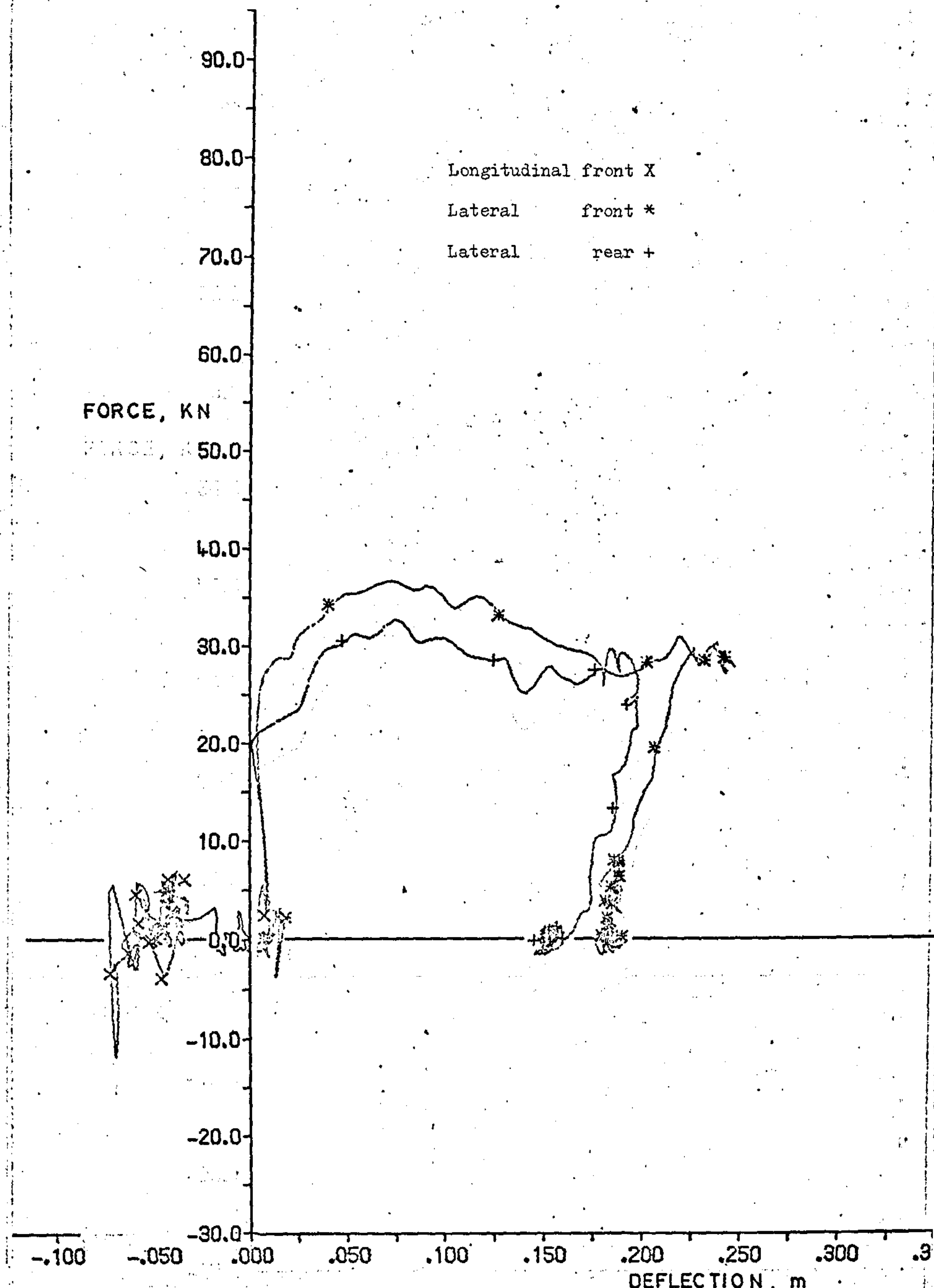

Fig. 5.9. Sample impact force/deflection plot

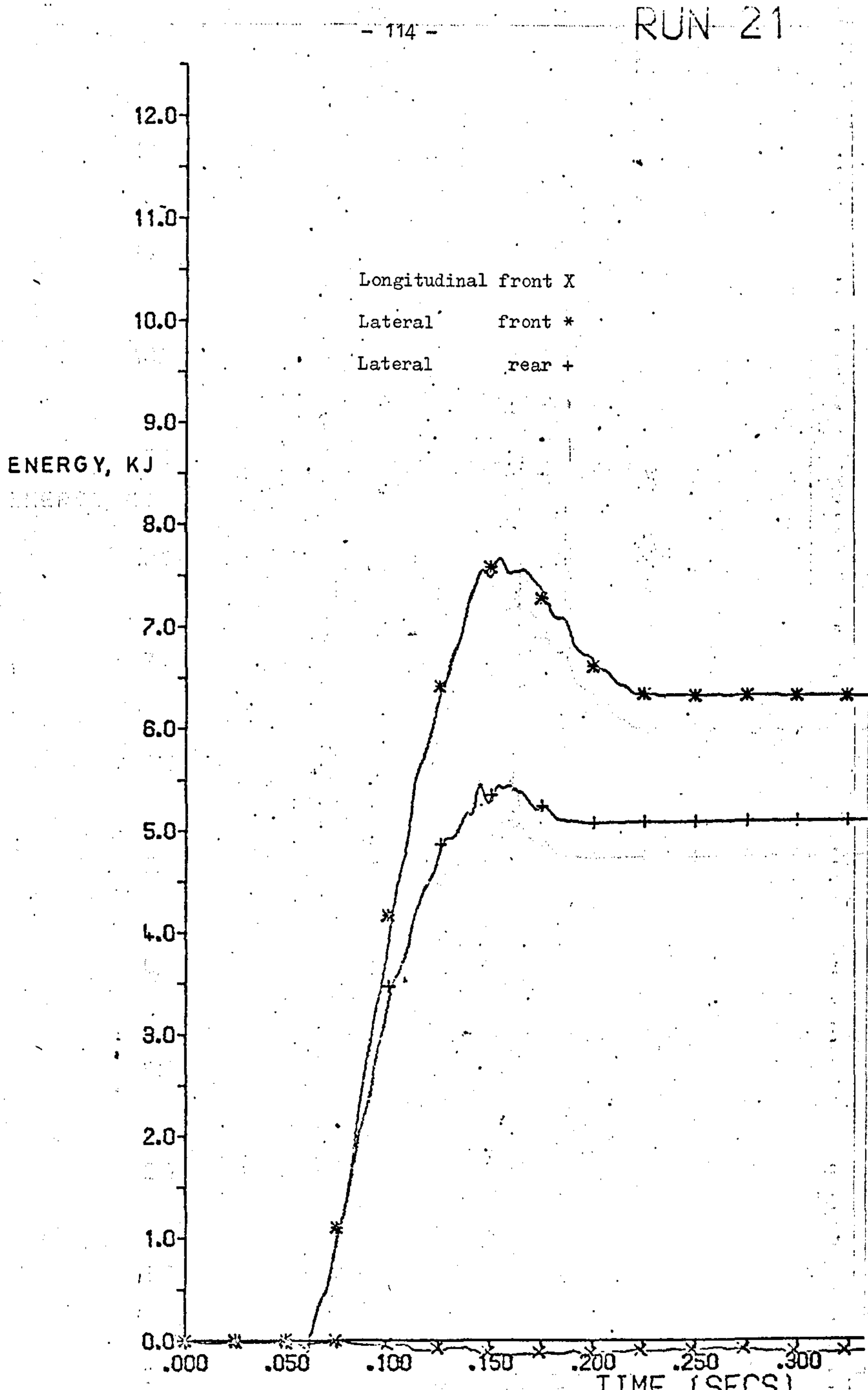

Fig. 5.10. Sample energy-time plot

Table 5.15. Maximum sideways energy absorbed by frame, kJ

Condition	Axle stop	Nominal α (Bank angle to vertical), degrees: 0	$7\frac{1}{2}$	15	$22\frac{1}{2}$	30	$37\frac{1}{2}$
Standard A	No		12.7, N.R.	15.9 B	1.4	N.R.	S 4.5
	Yes	15.5	10.3, 10.5	5.9, 7.3 C	8.6	11.8	
Ballasted (mass = 4015 kg + change in centre of mass and moment of inertia)	No		16.8		13.4		
	Yes		15.7 D		11.9 D		
Low friction (μ = 0.1 - 0.15) + wide cab (1.67 m)	No				13.5		
	Yes		13.0		14.6		
On concrete	No			14.5 E			
On concrete + low friction	Yes			22.2 D,E			
	No			N.R. D,E			
Higher speed (3 ms^{-1})	No		11.1				
Larger approach angle (γ = 8o)	No		11.3				
Wide cab (1.67 m)	Yes		6.2		3.5		
Wide track (1.65 m)	Yes				1.8		
Wide cab + (1.67 m) wide track (1.65 m)	Yes				7.8		

NOTES

A. The conditions referred to as standard are:

Tractor mass: 3065 kg
Surface dry: (μ = 0.8-1.0)
Cab width: 1.37 m
Track width: 1.55 m
Bar diameter: 42 mm
Speed DZ: 1.5 ms^{-1}
Approach angle: 4° (γ)
Landing surface: soil

B. Front of tractor on concrete.
C. Partial failure of rear wheel.
D. 48 mm diameter bar.
E. $\alpha = 17.7^{\circ}$ due to repositioning of plates.

Table 5.16. <u>Maximum longitudinal energy absorbed by frame, kJ.</u>

Condition	Axle stop	Nominal α (Bank angle to vertical), degrees: 0	$7\frac{1}{2}$	15	$22\frac{1}{2}$	30	$37\frac{1}{2}$
Standard A	No		0.6, N.R.	1.8 B	0.1	N.R.	S 1.4
	Yes	0.1	0.2, 0.1	0.5, 0.9 C	1.0	0.2	
Ballasted (mass = 4015 kg + change in centre of mass and moment of inertia)	No		4.0		3.4		
	Yes		0.3 D		0.9 D		
Low friction (μ = 0.1 - 0.15) + wide cab (1.67 m)	No				0.3		
	Yes		0.1		0.4		
On concrete	No			1.9 E			
On concrete + low friction	Yes			3.8 D,E			
	No			N.R. D,E			
Higher speed (3 ms^{-1})	No		1.1				
Larger approach angle (γ = 8°)	No		1.6				
Wide cab (1.67 m)	Yes		1.0		0.6		
Wide track (1.65 m)	Yes				0.0		
Wide cab + (1.67 m) wide track (1.65 m)	Yes				0.3		

<u>NOTES</u>

A. The conditions referred to as standard are:

- Tractor mass: 3065 kg
- Surface dry: (μ = 0.8-1.0)
- Cab width: 1.37 m
- Track width: 1.55 m
- Bar diameter: 42 mm
- Speed DZ: 1.5 ms^{-1}
- Approach angle: 4° (γ)
- Landing surface: soil

B. Front of tractor on concrete.

C. Partial failure of rear wheel.

D. 48 mm diameter bar.

E. α = 17.7° due to repositioning of plates.

Table 5.17. Ratio: $\frac{\text{(maximum side + maximum longitudinal energy)}}{\text{(energy at minimum vertical velocity, } \dot{y}_{0min}\text{)}}$, %

Condition	Axle stop	Nominal α (Bank angle to vertical), degrees: 0	$7\frac{1}{2}$	15	$22\frac{1}{2}$	30	$37\frac{1}{2}$
Standard A	No		22, N.R.	33 B	3	N.R.	S 13
	Yes	29	28, 20	17, 22 C	22	22	
Ballasted (mass = 4015 kg + change in centre of mass and moment of inertia)	No		N.R.		25		
	Yes		N.R. D		20 D		
Low friction (μ = 0.1 - 0.15) + wide cab (1.67 m)	No				25		
	Yes		24		28		
On concrete	No			26 E			
On concrete + low friction	Yes			40 D,E			
	No			N.R. D,E			
Higher speed (3 ms^{-1})	No		16				
Larger approach angle (γ = 8°)	No		28				
Wide cab (1.67 m)	Yes		13		8		
Wide track (1.65 m)	Yes				3		
Wide cab + (1.67 m) wide track (1.65 m)	Yes				17		

NOTES

A. The conditions referred to as standard are:

Tractor mass: 3065 kg

Surface dry: (μ = 0.8-1.0)

Cab width: 1.37 m

Track width: 1.55 m

Bar diameter: 42 mm

Speed DZ: 1.5 ms^{-1}

Approach angle: 4° (γ)

Landing surface: soil

B. Front of tractor on concrete.

C. Partial failure of rear wheel.

D. 48 mm diameter bar.

E. α = 17.7° due to repositioning of plates.

Table 5.15. The two maxima are reached in all cases at sufficiently close times to make this addition valid.

The corresponding longitudinal energies are given in Table 5.16. There is often a slight delay between the maximum sideways and longitudinal deflections but the error introduced in summing all the maximum energies is not significant, as the longitudinal values are almost all small proportions of the totals. The totals are expressed in Table 5.17 as percentages of the energies before impact from Table 5.11.

To give an indication of the relative magnitudes of the various dissipated energies, mean values over the set of 24 complete results are given below:

(i) Mean total energy difference between roll-off and final rest position: 72.5 kJ (Standard Deviation 10.1 kJ). Of this, 67.9 kJ (SD 9.1 kJ) is due to the height difference and 4.6 kJ to the initial velocity.

(ii) Mean difference between energy just before impact and at final rest: 53.5 kJ (SD 9.9 kJ). Of this, 10.2 kJ (SD 5.8 kJ) is due to the height difference.

(iii) Mean energy absorbed by the frame: 11.3 kJ (SD 5.5 kJ).

The mean energy changes are summarised in Table 5.18.

Table 5.18. Mean energy changes, kJ. Values in brackets are percentages of total change, 72.5 kJ

	During overturning		During impact		Total
Potential Energy	−58	(−80)	−10	(−14)	−68 (−94)
Kinetic Energy	+39	(+53)	−43	(−60)	−5 (−6)
Dissipation					
Sliding friction, etc	+19	(+26)			+19 (+26)
Absorbed in frame			+11	(+16)	+11 (+16)
Other (soil, tyres, wheels etc)			+42	(+58)	+42 (+58)
Total	19	(26)	53	(74)	73 (100)

Note: Row and column totals not always 100% due to rounding.

Energy applied in standard tests

To provide a basis for comparison, the energies applied to frames in present pendulum impact test standards (12, 13, 15, 16) and in proposed static test standards (17) are given below. The static test energies are at present approximately 50% of the pendulum energies on the basis that this is the average proportion absorbed by the frame; these figures are still under discussion but are likely to remain within the range 50 ± 10%. As a means of comparison with energies absorbed in the overturning experiemnts the static test energies are therefore more appropriate.

(i) Pendulum test

$$E_{side} = 2 \times 9.8067 \ (125 + 0.15m)$$

for $m = 3065$ kg (unballasted) $E_{side} = 11.47$ kJ

for $m = 4015$ kg (ballasted) $E_{side} = 14.26$ kJ

(ii) Static test

for $m = 3065$ kg $E_{side} = 5.74$ kJ

for $m = 4015$ kg $E_{side} = 7.13$ kJ

For the 26 overturning tests in which reliable measurements are available the maximum sideways energy is greater than the corresponding static test energy in 22 cases and greater than the pendulum energy in 11 cases. The highest value (22.2 kJ in test 30, low friction onto concrete) is nearly four times the static energy or twice the pendulum energy.

It was expected that these experiments, chosen for their severity, would yield high absorbed energies but these results are a little surprising in view of the fact that the rear wheel absorbed significant energy in all tests, and the soil in most. Overall, however, the findings are not inconsistant with estimates of the energy absorbed in real accidents in relation to that applied in standard tests (21).

5.4. DISCUSSION

A preliminary discussion of the experimental results in isolation was included in the NIAE Departmental Note (71) covering this part of the work, which was written before the full computer simulation results were available. Some trends with parameter variation were noted but few could be fully explained without the mathematical models, and it is more appropriate in this thesis to treat these aspects in relation to the simulation results, in section 7 and 8. Several conclusions are relevant here, however, and these are given below:

(i) These experiments have, overall been successful in providing data for validating the mathematical models. A considerable amount of time and effort has been expended in getting these results, due partly to the complex equipment and instrumentation involved. It is inevitable that breakdowns and partial failures occur but the need for complete sets of data and the cost of tests has placed a high premium on reliability. A significant proportion of analysis time has been spent in overcoming experimental inadequacies. It is arguable that the overall time could have been reduced by repeating some of the tests. However, the damage resulting from the final tests onto the concrete surface was much greater than expected, and extensive repairs would have been required after the last test.

An alternative way of increasing the proportion of directly useable data would have been the adoption of greater measurement redundancy. One example is the spare frame displacement channel and an other is the use of accelerometers. A third film camera and automatic control of the tractor would also have helped. All these would have needed extra effort in preparation, calibration and during the tests but, in hindsight, some of them might have been worthwhile.

The proportion of data successfully recovered is, however, reasonably high; this also applies to the repeatability of tests. Overturning experiemnts are notoriously difficult to reproduce and it is considered that these tests are significantly better in this respect than any others previously carried out in realistic conditions. The initial expectations, however, proved to be rather optimistic, and a more balanced experimental design concentrating on fewer parameters might have yielded more significant trends. Since the results do not need to stand alone, this is of less importance, and the models should help to explain some of the variations. A more appropriate design could probably have been adopted if the models had been available at the outset.

(ii) In the condition studied, with a maximum bank height of about 2.5 m, the frame does not hit the ground significantly before other parts of the tractor. The mean proportion of impact energy absorbed by the frame was 21% and the maximum 40%. The mean proportion of total energy absorbed by the frame was 16%.

(iii) Despite the foregoing, the absolute amount of energy absorbed was significantly higher than in equivalent Standard Tests. The sideways energy absorbed was greater than the energy applied according to draft static test standards in 22 out of the 26 experiments for which reliable measurements were available. The highest absorbed energy was nearly four times the static test energy. High values were expected from the severe conditions, and the results are reasonably consistent with estimates of energy absorbed in the most severe, real accidents.

(iv) The statistical tests confirm that the tractor falls significantly more rear-down (greater θ_{ymax}) when the front axle is allowed to pivot normally than when it is fixed by the axle stop. The effect on pitch angle θ_x is also significant but probably less important, since the tractor strikes the ground at a roll angle θ_z of around 90°. There are also weakly significant effects on roll angle and velocity, but not on horizontal or vertical linear velocities. These results add some confidence in the treatment of overturning behaviour by a two-dimensional mathematical model.

6. STRUCTURAL ANALYSIS OF THE EXPERIMENTAL SAFETY FRAME

6.1. INTRODUCTION

A typical force-deflection curve is shown in Fig. 6.1. The gradual transition from elastic to plastic regions is typical of non-annealed mild steel in bending; annealed material or axial loading usually results in a more clearly defined yield point, perhaps with some reduction of stress immediately after yield as discussed in section 6.3 below. The slope of the curve during recovery is similar to that in the elastic region during loading; when expressed as force per unit deflection it is the elastic stiffness. If the stress continues to increase gradually after yield, as is the case in Fig. 6.1, this is due to increased strength from cold working, known as strain-hardening. The energy absorbed at any stage in the loading is given by the area under the curve up to that point.

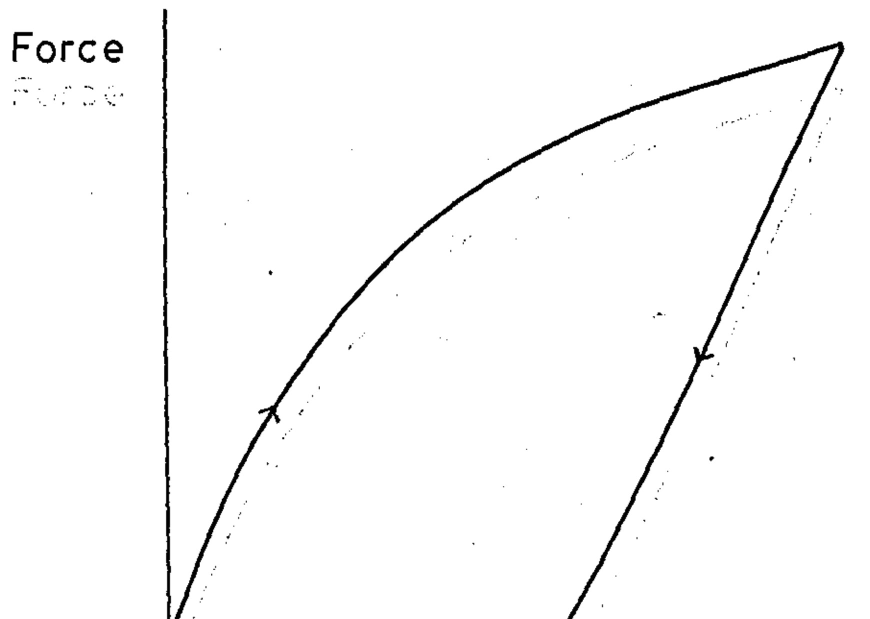

Fig. 6.1. Typical force-deflection behaviour of a simple mild steel structure

As the speed of loading is increased beyond a rate equivalent to "static" conditions two effects may appear: (i) change in yield strength and (ii) change in dynamic behaviour due to inertia of the material elements. The yield effect results in higher yield strength with increased strain-rate, the elastic stiffness and general shape of the curve remaining unaltered. This is relevant to safety cab impacts, where the yield strength may be up to 30% higher than in static conditions, and is discussed more fully below. The inertia effect where shock waves in the material change the strain distribution and deformed shape, is important only at much higher rates of loading, such as in the impact of shells and bullets. It can be ignored for safety cab impacts; for example, the frame impact velocities measured in the overturning experiments were only about 6 m/s.

6.2. PREVIOUS WORK

Yield enhancement in tension and bending

The plastic behaviour of simple structural elements under axial and bending impact has been studied extensively and comprehensive reviews are available (72, 73). For the purpose of this thesis a general outline of the fundamental results will be adequate.

The enhancement of yield at high strain-rates was first quantified by Manjoine (74) from results of tensile tests on axial specimens. The independent variable he chose was mean strain rate in the elastic phase, and this or its effective inverse, the time-to-yield, have been used by investigators ever since. The mechanism by which yield enhancement takes place is not fully understood and in cases where the strain rate varies significantly during elastic loading it is not clear whether the mean value is the most relevant. No studies are known in which other values have been compared, such as the strain rate at the point of yielding which may be more important than the mean rate.

Other workers have extended Manjoine's findings to cases of simple bending such as cantilevers (75 - 77). Parkes made the important distinction between low velocity impacts and those in which the inertia of the beam affected the behaviour (75). While high velocity impacts resulted in plastic strain throughout the length of the beam, giving it a curved final form, the permanent deformation after low velocity impacts was restricted to a discrete bend at the root, the rest of the beam remaining straight as in static tests. This pattern is referred to as a plastic hinge.

The reduction in stress immediately following yield was studied by Rawlings (77) who used the terms upper and lower yield stress (Fig. 6.2). The upper value, which is generally of less practical significance, was found to be more sensitive to strain rate, while the lower showed a very similar logarithmic relationship to strain rate to that found by previous workers (Fig. 6.3). Rawlings also presented this relationship in a way which is easier to use in subsequent analysis (Fig. 6.4), based on values measured by several experimenters.

Research on frames at NCAE

Ashburner's work on the behaviour of simple model portal frames and cubes made from $\frac{1}{4}$ in square bar (73) was the starting point for the present study. The four models of the deformation process he investigated are described by the force deflection relationships shown in Fig. 6.5. Ignoring the elastic phase and yield enhancement (Figs. 6.5a and b) proved unrealistic, but the effect of strain-hardening (Fig. 6.5d) was found to be negligible and the behaviour of Fig. 6.5c represented adequately the experimental results. The elastic and plastic phases of this behaviour were then treated separately.

The elastic stiffness was predicted with fair agreement by analysis based on the slope-deflection equations and taking into account the torsional rigidity of the members. The time-to-yield in model pendulum impact tests was calculated by several methods of varying sophistication.

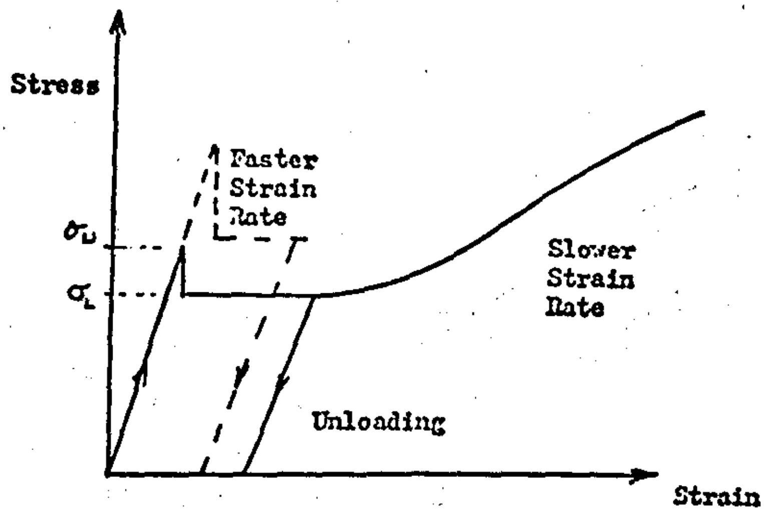

Fig.6.2 Effect of increasing strain rate on upper (σ_U) and lower (σ_L) yield stress investigated by Rawlings

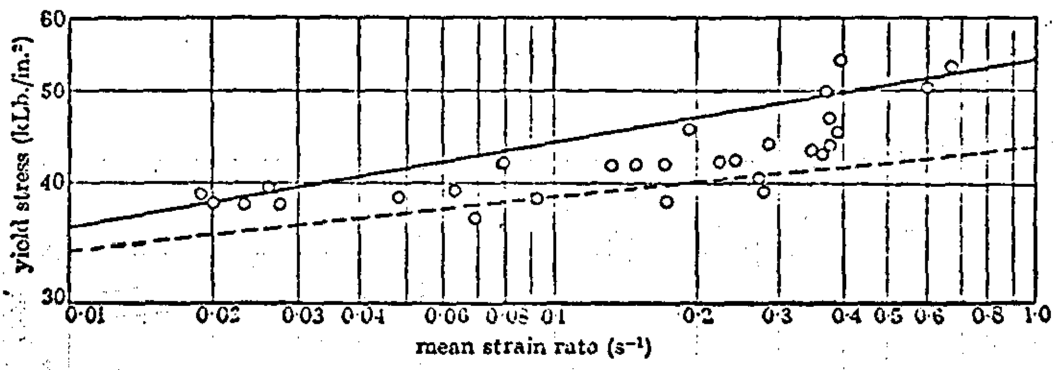

Fig.6.3 Effect of strain rate

o Lower yield stress (Rawlings)
--- Axial tests (Manjoine)
—— Relation assumed by other investigators on results of axial tests

A = -0.1

T = 0.17 sec

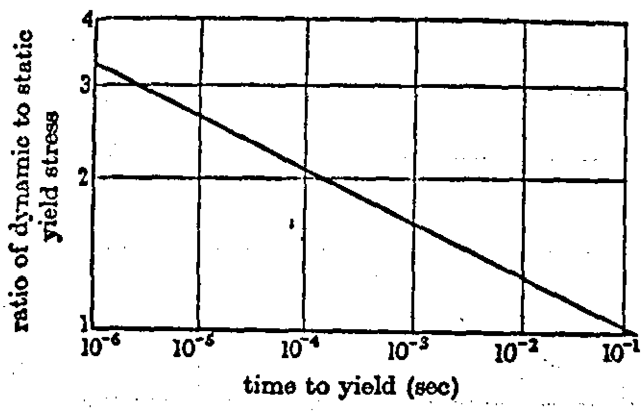

Fig.6.4 Effect of strain rate expressed in terms of time-to-yield. Logarithmic relationship assumed by Goldsmith and others

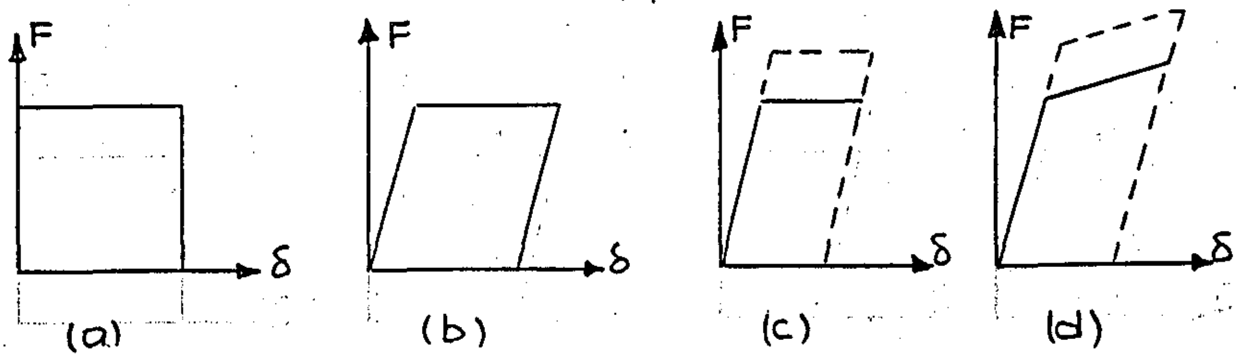

Fig.6.5 Force-deflection relationships assumed by Ashburner

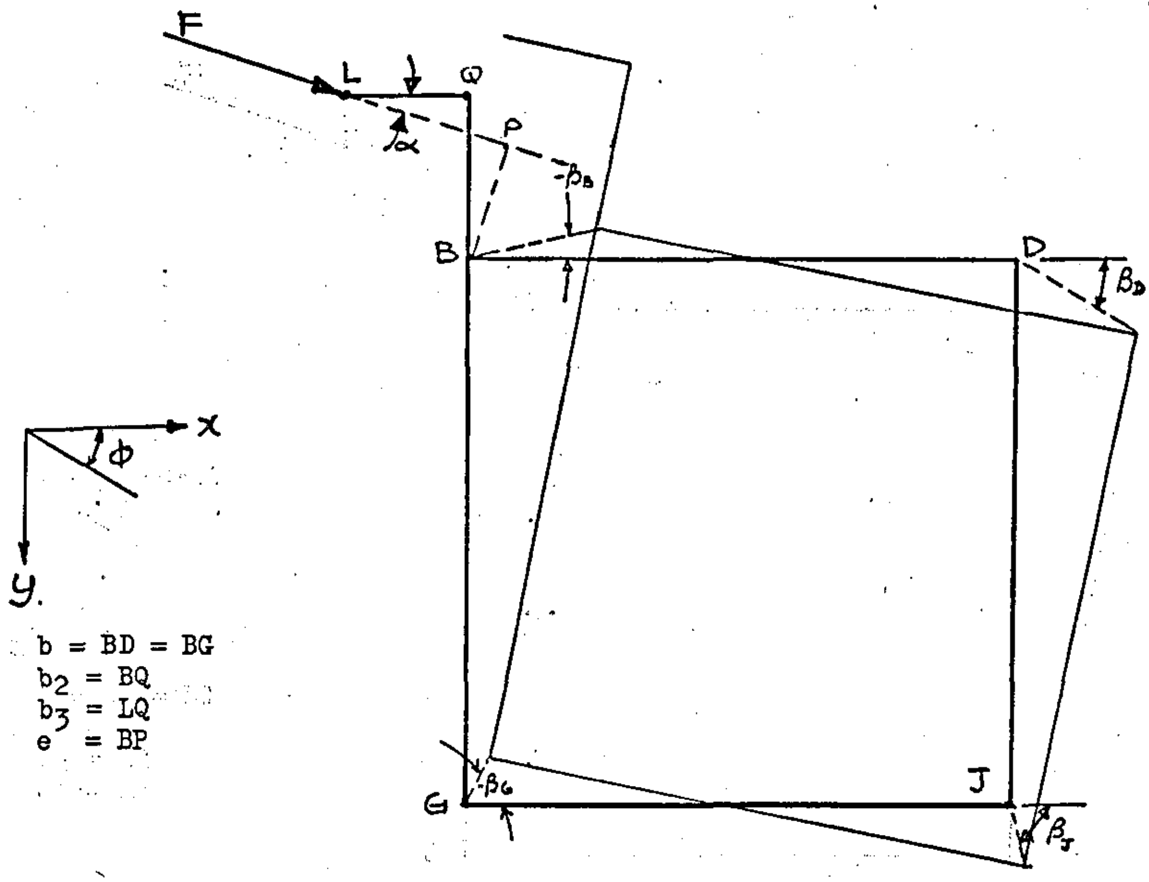

b = BD = BG
b_2 = BQ
b_3 = LQ
e = BP

Fig.6.6 Deflection of NIAE frame in plan view

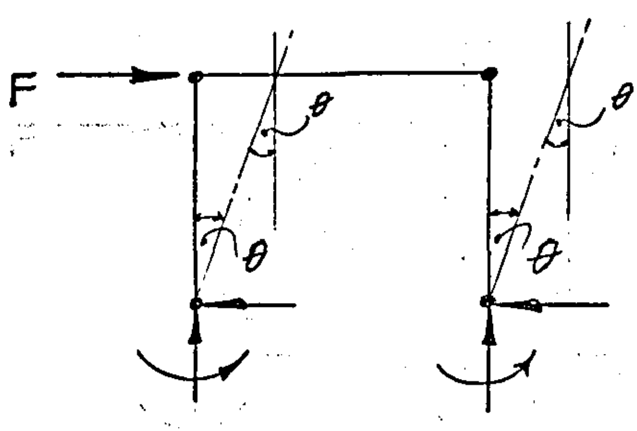

Fig.6.7 Portal frame

The simplest, assuming constant velocity to yield, was found to give reasonable estimates of yield enhancement assuming the relationship given in Fig. 6.4. The more complex methods based on the equation of motion were therefore not needed, although a comparison of the results of these methods in isolation is not given.

Two material constants were measured in static tests on portals and cantilevers: the static plastic moment is the bending moment at which the elastic limit is just reached by all fibres across the yielding section; the strain hardening coefficient is the increase in this moment for unit angular rotation of the plastic hinge. Dynamic plastic moments were calculated by applying the yield enhancement ratio found from the elastic analysis to the static moment. A simple analysis allows the collapse load to be determined by assuming a collapse mode defined by the positions of the plastic hinges. Elastic and plastic deflections follow from consideration of the input energy and the linearised form of the force deflection curve.

In this way Ashburner obtained quite good agreement between predicted and measured values in a wide range of conditions on annealed and non-annealed material. Although three-dimensional cubic frames were included in his investigations, the collapse modes assumed allowed then to be treated in the plastic phase as effectively a combination of two-dimensional portals. Asymmetrical loading analysis was based on superposition, which was admitted to be not strictly applicable but did lead to excellent agreement with experimental results in the cases studied.

6.3. ANALYSIS

The prediction of the behaviour of the NIAE experimental frame follows Ashburner's general technique described above. The elastic stiffness is calculated by classical methods and used in conjunction with the impact velocity to predict the time-to-yield. Yield enhancement is then found from the relationship in Fig. 6.4 and allows calculation of the dynamic plastic moment Mp.

There are important detail differences which affect the complexity of the approach and the reliability of the results:-

(a) Because of the size of the members and lack of facilities at NIAE no static tests were carried out. The static plastic moment was therefore calculated from the material yield strength, measured in tensile tests on small specimens.

(b) The determination of the elastic stiffness was simplified by assuming deflection to be restricted to the four uprights, the rest of the frame being rigid. Offset of the point of application of load provided additional complexity.

(c) The collapse mode could no longer be considered as a combination of collapse of plane frames. The reduction in collapse load due to asymmetrical loading was described by a "skew factor", which was found by an iterative technique.

Assumptions

The analysis rests on the following assumptions whose validity will be examined later:-

(a) No elastic or plastic deformation takes place other than in the four uprights.

(b) The inertia of the top frame and uprights can be ignored.

(c) There is a known, precise yield point which is reached by all fibres across the section of all plastic hinges at the same time.

(d) Deflections are small compared with frame dimensions, resulting in no change of geometry or loading direction during deformation.

(e) The impact velocity remains constant up to yield.

(f) Yield enhancement follows the simple relationship to time-to-yield given in Fig. 6.4.

(g) The dynamic plastic moment remains constant after yield i.e. strain hardening coefficient is zero.

(h) The rubber pad described in Section 6.4. has no effect on the behaviour.

(i) The energy determined from the pendulum lift height is totally absorbed by the frame.

6.3.1. Elastic phase

Corner displacements

The top rigid frame BDJG (Fig. 6.6.) has three degrees of freedom all within its plane: two of translation and one of rotation. The three independent co-ordinates are chosen as X_B, y_B and y_D. *

Then: $$\phi = \frac{y_D - y_B}{b} \quad - \text{ for small } \phi \qquad -(6.1)$$

$$x_D = x_B \quad -(6.2) \qquad x_G = x_B - b\phi = x_B + y_B - y_D \quad -(6.5)$$

$$y_G = y_B \quad -(6.3) \qquad x_J = x_G = x_B + y_B - y_D \quad -(6.6)$$

$$y_J = y_D \quad -(6.4)$$

The displacement of point L in the direction of F is given by

$$\delta_L = x_B\cos\alpha + y_B\sin\alpha + e\phi$$

$$= x_B\cos\alpha + y_B\sin\alpha + \frac{e}{b}(y_D - y_B) \qquad -(6.7)$$

*Co-ordinate system given in Fig. 6.6 and notation are specific to this section: see 'Notation'.

Forces and moments

In the elastic phase the forces can be obtained by superposition from the forces acting on the four portals separately. If the top and base frames are infinitely stiff and axial forces on the uprights are neglected each portal can be considered as a pair of double encastré beams.

The deflection of one beam is $\frac{Fh^3}{12EI}$ so that

for one portal $\frac{F}{x} = \frac{24EI}{h^3}$ -(6.8)

Taking the displacements of the four portals from equations (6.2) to (6.5) the four forces becpme:-

$$F_{xB} = \frac{24EI}{h^3}.x_B \quad -(6.9) \qquad F_{yB} = \frac{24EI}{h^3}.y_B \quad -(6.10)$$

$$F_{xG} = \frac{24EI}{h^3}.(x_B + y_B - y_D) \quad -(6.11) \qquad F_{yD} = \frac{24EI}{h^3}.y_D \quad -(6.12)$$

The moment resulting from the twist in each bar is given by $\frac{GJ\phi}{h}$, so that the total torque is

$$TQ = \frac{4GJ.(y_D - y_B)}{hb} \quad -(6.13)$$

<u>Equations of equilibrium</u>

<u>Resolving in x direction</u>: $F\cos\alpha = F_{xB} + F_{xG} = \frac{24EI}{h^3}(2x_B + y_B - y_D)$ -(6.14)

<u>Resolving in y direction</u>: $F\sin\alpha = F_{yB} + F_{yD} = \frac{24EI}{h^3}(y_B + y_D)$ -(6.15)

<u>Taking moments about B</u>: $-F_{xG}.b + F_{yD}.b + \frac{4GJ}{hb}(y_D - y_B) = F.e$

$$\therefore \frac{24EIb}{h^3}(-x_B - y_B + y_D + y_D) + \frac{4GJ}{hb}(y_D - y_B) = F.e$$

$$\therefore x_B + y_B - 2y_D + \frac{4GJh^3}{24EIb^2h}(y_B - y_D) = -\frac{h^3}{24EI}.\frac{Fe}{b} \quad -(6.16)$$

Put $Q1 = \frac{h^3}{24EI}F$, $Q2 = \frac{GJh^2}{6b^2EI}$ in (6.14), (6.15) and (6.16):-

$$\left.\begin{aligned} \text{then } 2x_B + y_B - y_D &= Q1\cos\alpha \\ y_B + y_D &= Q1\sin\alpha \\ x_B + (Q2+1)y_B - (Q2+2)y_D &= -Q1\frac{e}{b} \end{aligned}\right\} -(6.17)$$

Solving for x_B, y_B, y_D :-

$$x_B = \left(\frac{-2\frac{e}{b} - (2Q2 + 3)\cos\alpha + \sin\alpha}{-4.(1 + Q2)} \right) . Q1 \qquad -(6.18)$$

$$y_B = \left(\frac{2\frac{e}{b} + \cos\alpha - (2Q2 + 3)\sin\alpha}{-4.(1 + Q2)} \right) . Q1 \qquad -(6.19)$$

$$y_D = \left(\frac{-2\frac{e}{b} - \cos\alpha - (2Q2 + 1)\sin\alpha}{-4.(1 + Q2)} \right) . Q1 \qquad -(6.20)$$

Substituting for x_B, y_B and y_D from (6.18), (6.19) and (6.20) in (6.7):-

$$\frac{-4\ (1 + Q2)}{Q1} \cdot \delta_L = -2\frac{e}{b}\cos\alpha - (2Q2 + 3)\cos^2\alpha + \sin\alpha . \cos\alpha$$

$$+2\frac{e}{b}\sin\alpha + \sin\alpha.\cos\alpha - (2Q2 + 3). \sin^2\alpha$$

$$+\left(-2\frac{e}{b} - \cos\alpha - (2Q2 + 1)\sin\alpha - 2\frac{e}{b} - \cos\alpha + (2Q2 + 3)\sin\alpha \right)\frac{e}{b}$$

giving the elastic stiffness:-

$$k = \frac{F}{\delta_L} = \frac{24EI}{h^3} \left(\frac{1 + Q2}{\frac{Q2}{2} + \frac{3}{4} + \frac{e}{b}\left(\cos\alpha - \sin\alpha + \frac{e}{b}\right) - \frac{1}{2}\sin\alpha\cos\alpha} \right) \qquad -(6.21)$$

$$\text{where } Q2 = \frac{GJh^2}{6EIb^2} \qquad -(6.22)$$

$$\text{and} \quad e = b_2\cos\alpha - b_3\sin\alpha \qquad -(6.23)$$

Equation (6.21) expresses the elastic behaviour of the structure in terms of the stiffness of a spring at L acting in the direction of F that could replace the frame.

6.3.2. Plastic phase

Collapse load

Without strain-hardening or geometry changes the forces and moments are constant throughout the plastic phase. The collapse load, which is the force at the loading point during plastic deformation, can be found most easily by equating the energy it generates in displacing the frame to the strain energy absorbed in deflecting the plastic hinges. Thus in general:-

$$F_c \cdot \delta_p = \sum M_p \theta \qquad -(6.24)$$

Under plastic collapse the structure is equivalent to a mechanism and the number of plastic hinges is therefore one greater than the number of redundant reactions. The location of hinges may be found by considering the most highly stressed point in an elastic analysis, limiting the stress there to the yield stress and finding the next point to reach yield. This process is repeated until all hinges are found.

In the case of the simple portal shown in Fig. 6.7, for example, there are six reactions and three equations of equilibrium. Hence there are three redundant reactions and four plastic hinges needed for collapse. Their positions are clearly at the point of maximum bending moment at the corners and fixings. Here all angles θ are the same and there is a simple relationship between δ_p and θ in equation (6.24) allowing F_c to be found directly:-

$$\delta_p = h\theta \qquad \sum M_p \theta = 4M_p \theta$$

$$\therefore \; F_c = \frac{4M_p}{h} \qquad -(6.25)$$

Equally, in the cubic frames analysed by Ashburner (73) the position of the hinges and the geometry of the frame result in a similar relationship (Fig. 6.8), the plastic behaviour being equivalent to that of two portals:-

$$\delta_p = h\theta \qquad \sum M_p \theta = 8M_p \theta$$

$$F_c = \frac{8M_p}{h} \qquad -(6.26)$$

Equation (6.26) would also describe the behaviour of the NIAE experimental frame in the two particular loading conditions shown in Fig. 6.9. In general, however, the directions of deformation of the four corners is different, the individual values of θ are different and there

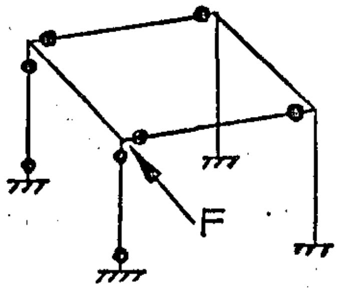

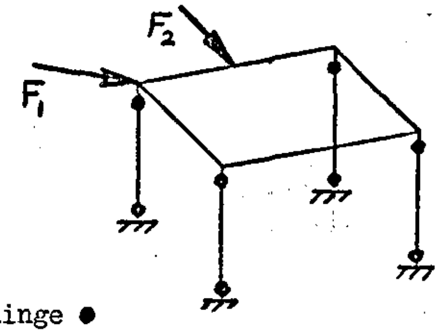

Plastic hinge ●

Fig.6.8 Collapse mechanism of Ashburner's frames

Fig.6.9 Collapse mechanism of frame with rigid top under two alternative symmetrical loading conditions, F_1 and F_2

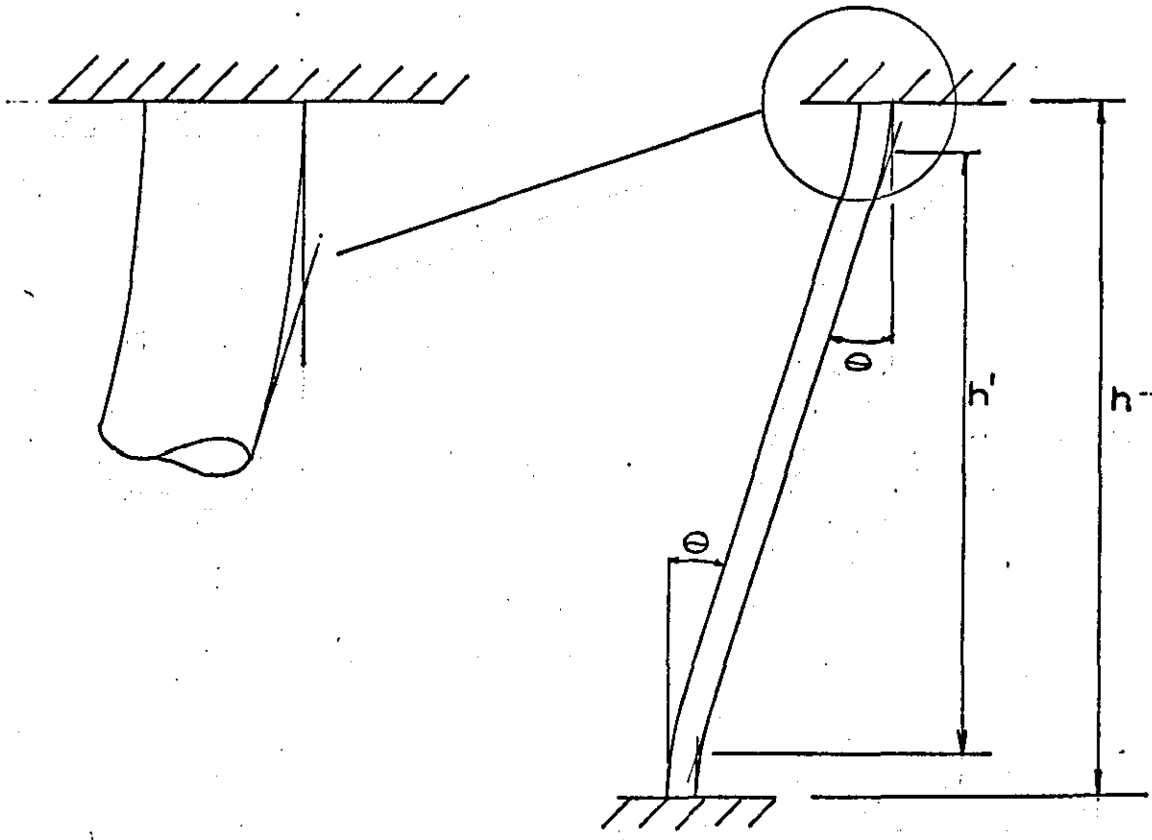

Fig.6.10 Effective position of hinges displaced from root

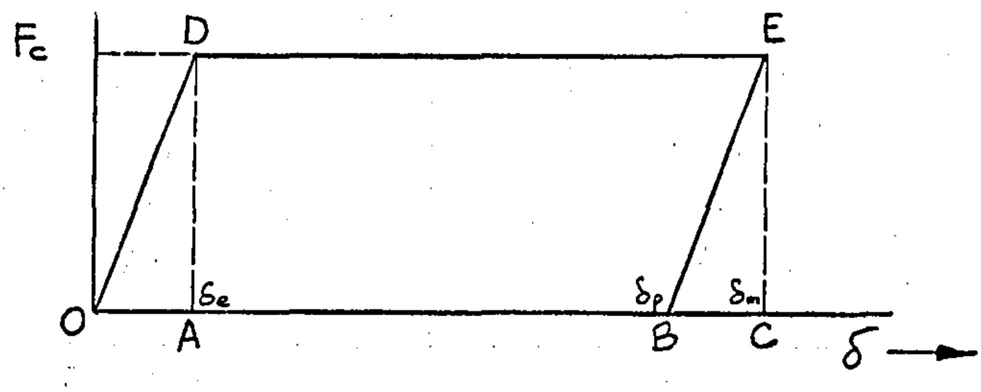

Fig.6.11 Relationship of area, energy force and displacement

is no simple relationship between them and δ_p.

Since all the uprights are of equal length and section the linear deflections of the corners are related to the rotations in the hinges (Fig. 6.10).

$$\theta_i = \frac{\delta_i}{h'} \qquad -(6.27)$$

It is necessary to use h', the effective length of uprights in the NIAE frame in place of h because the ratio of length to diameter is only about 20 compared with about 40 for Ashburner's frames. The effective position of the hinge is therefore significantly displaced from the root.

There are eight hinges so the summation in (6.24) is from 1 to 8, but the two values of θ_i at each end of an upright are both equal to the value of δ_i/h' for that corner, thus

$$\sum_{i=1}^{8}\theta_i = \frac{2}{h'} \cdot \sum_{i=1}^{4}\delta_i \qquad -(6.28)$$

Equation (6.24) then becomes, with M_p constant for all members:-

$$F_c = \frac{2M_p \sum_{i=1}^{4}\delta_i}{h' \quad \delta_p} = \frac{8M_p}{h'} \quad Q_s \qquad -(6.29)$$

$$\text{Where } Q_s = \frac{\sum_{i=1}^{4}\delta_i}{4\delta_p} \qquad -(6.30)$$

Equation (6.30) defines a "Skew factor" Q_s which depends on the asymmetry of the loading condition. Thus in the two cases in Fig. 6.9, Q_s is unity and equation (6.29) becomes identical to (6.26).

Skew factor

Since the plastic moment is assumed to be constant the force on the top frame due to each upright will be constant and its line of action will be opposite to the direction of deflection of that upright. For any deflected form the directions β of deflections of the corners can be expressed in terms of three co-ordinates x_B, y_B and y_D, as in the elastic phase (Section 6.3.1, Fig. 7):-

$$\tan\beta_B = \frac{y_B}{x_B} \qquad (6.31) \qquad \tan\beta_G = \frac{y_G}{x_G} \; \frac{y_B}{x_B + y_B - y_D} \qquad -(6.33)$$

$$\tan\beta_D = \frac{y_D}{x_D} = \frac{y_D}{x_B} \qquad (6.32) \qquad \tan\beta_J = \frac{y_J}{x_J} = \frac{y_D}{x_B + y_B - y_D} \qquad -(6.34)$$

The resistance forces P of the four uprights are assumed to be in equilibrium with an externally applied force system which in general will be two forces and a moment. Replacing these by three forces in the three deflection co-ordinates and resolving:-

<u>x - direction</u>:- $F_{xB} = P\cos\beta_B + P\cos\beta_G + P\cos\beta_J + P\cos\beta_D \qquad -(6.35)$

<u>y - direction</u>:- $F_{yB} + F_{yD} = P\sin\beta_B + P\sin\beta_G + P\sin\beta_J + P\sin\beta_D \qquad -(6.36)$

<u>Moments about B</u>:- $F_{yD}.b = -P\cos\beta_G.b - P\cos\beta_J.b + P\sin\beta_J.b + P\sin\beta_D.b \quad (6.37)$

from (36) and (37) $F_{yB} = P(\sin\beta_B + \sin\beta_G + \cos\beta_J) \qquad -(6.38)$

The forces required, however, are those at L together with a new force F_{yD1} at D to maintain equilibrium. These are obtained by further resolution:-

$$F_{xL} = F_{xB} \qquad (6.39) \qquad F_{yL} = \frac{F_{y1}.b + F_{x1}.b_2}{b + b_3} \qquad -(6.40)$$

$$F_{yD1} = F_{yD} + \frac{F_{y1}.b_3 - F_{x1}.b_2}{b + b_3} \qquad -(6.41)$$

In a given impact at L the values that are known are the ratio F_{yL}/F_{xL}, which is $\tan\alpha$, and F_{yD1}, which is zero. It is not possible to solve equations (6.31 - 6.41) directly for these conditions but for a given deflection at B a value of y_d that makes $F_{yD1} = 0$ can be found by iteration.

A computer program, STAF6, to carry out thos procedure is described in Appendix 6.1. For a given angle β_B and unit deflection at B the program determines the deflection y_D which defines the collapse mode and the forces F_{xL} and F_{yL} in terms of P. From these are obtained α and the resultant force F_L. The skew factor is then given by

$$Q_s = \frac{F_L}{4P} \qquad -(6.42)$$

The values of β_B, y_D and Q_s are plotted against α in Fig.6.12 for the Mk I frame in range $-90^\circ < \alpha < 90^\circ$. The behaviour in the other two quadrants is similar but of only academic interest. When α is between -70° and -20° no solution is found by STAF6 because in this range the collapse mode is such that the frame rotates about J. The force at J is lower than the collapse force P and hence the plastic deflection at J is zero. In this mode β_B is -45° and y_D is zero, and the collapse load F_L can be found directly by taking moments about J:-

$$F_L \cos\alpha.(b + b_2) - F_L \sin\alpha.(b + b_3) = P\ (b + b + b\sqrt{2})$$

$$\text{giving } Q_s = \frac{F_L}{4P} = \frac{b\ (2 + \sqrt{2})}{4(b + b_2)\cos\alpha - 4(b + b_3)\sin\alpha} \qquad -(6.43)$$

Confirmation that $F_J < P$ can be obtained by resolving:-

$$x - \text{direction:} \quad F_{xJ} - 1 - 1/\sqrt{2} \quad = \quad - F_L \cos\alpha \qquad -(6.44)$$

$$y - \text{direction:} \quad F_{yJ} + 1 + 1/\sqrt{2} \quad = \quad - F_L \sin\alpha \qquad -(6.45)$$

That the discontinuity in the change of mode shape with α does not result in a discontinuity in the change of Q_s can be seen in Fig. 6.12.

Yield enhancement

On the basis of Ashburner's findings the assumption of constant velocity up to yield appeared to be appropriate (73). The impact velocity is found from the lift height of the pendulum:

$$V_P = \sqrt{2g\ l} \qquad -(6.46)$$

giving the time to yield $\quad t_y = \dfrac{\delta_e}{V_P} \qquad -(6.47)$

where $\quad \delta_e = \dfrac{Fc}{k} \qquad -(6.48)$

thus $\quad t_y = \dfrac{Fc}{k\sqrt{2g\ l}} \qquad -(6.49)$

The static plastic moment M_{ps} is plastic modulus multiplied by the static yield stress and for solid circular bar is given by:-

$$M_{ps} = \frac{1}{6}\ d^3\ \sigma_o \qquad -(6.50)$$

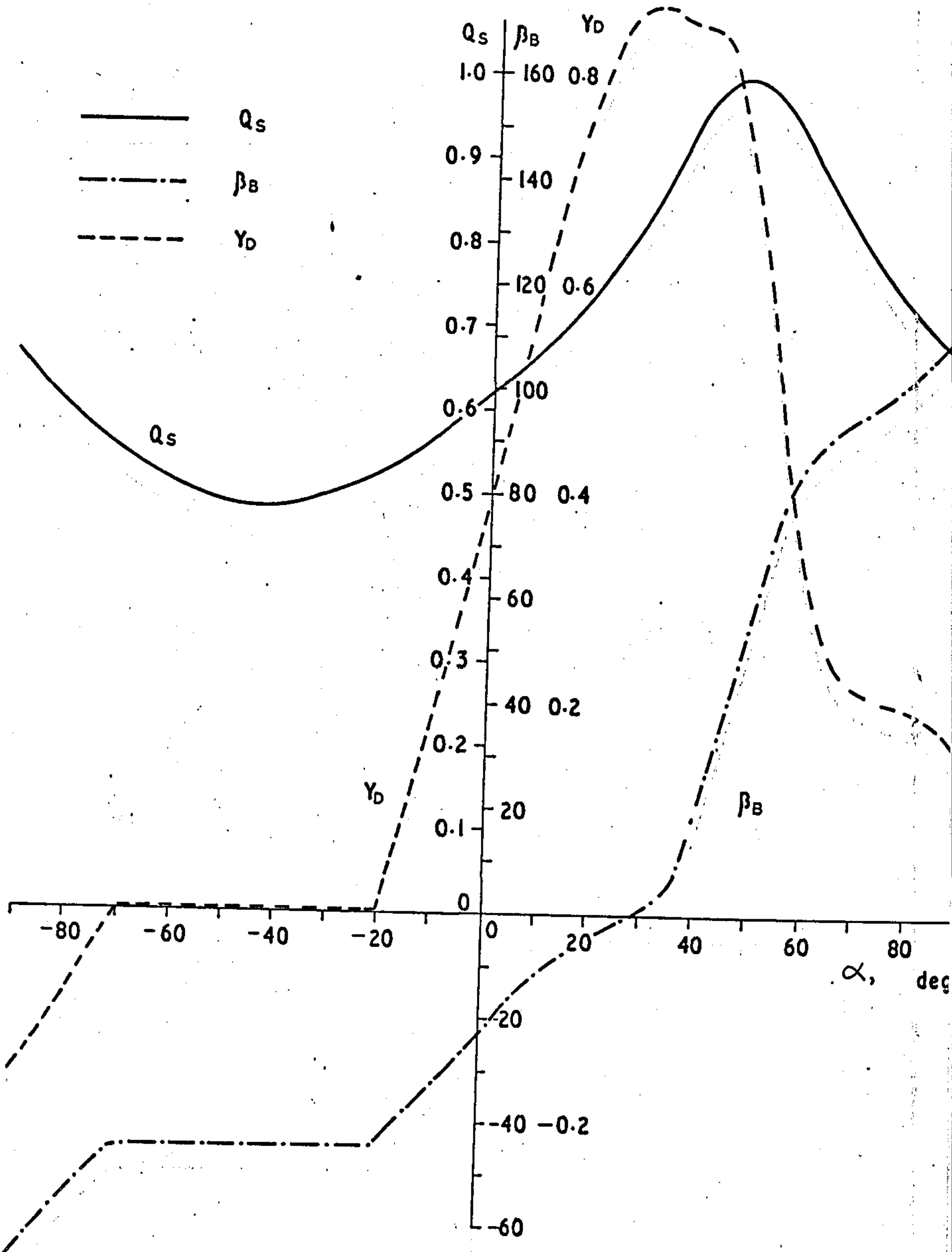

Fig.6.12 Variation of skew factor, Qs, angle of displacement at B, β_B and displacement of Y_D with angle of impact, α

REF. T.D. 3940

This static moment is multiplied by the ratio of elevated/static yield stress to give dynamic plastic moment M_p. This step is assumed to be valid if the yield enhancement ratio is less than 1.5, even though the strain rate varies across the section (73). Yield enhancement behaviour shown in Fig. 6.4 can be expressed as:-

$$\frac{M_p}{M_{ps}} = \frac{\sigma}{\sigma_o} = \left(\frac{t_y}{T}\right)^A \qquad -(6.51)$$

where T and A are material constants. Ashburner calculated A to be -0.1 and T 0.17 from data presented by Goldsmith (78). The value of A calculated from Fig. 6.4 agrees with this while T becomes 0.13. The accuracy with which these values represent the behaviour in a particular experiment should not be overestimated, however, as they are derived from averages of individual test results which themselves vary a fair amount.

Substituting for Fc in (6.49) from (6.29) and then for t_y in (6.51):-

$$M_p = M_{ps}\left(\frac{8M_p \cdot Q_s}{h'k\, V_p T}\right)^A$$

$$\text{i.e. } M_p = \left(M_{ps}\right)^{\frac{1}{1-A}} \cdot \left(\frac{8\,Q_s}{h'k\, V_p T}\right)^{\frac{A}{1-A}} \qquad -(6.52)$$

from which F_c can be found by (6.29).

Deflections

Assuming the idealised force-deflection curve of Fig. 6.5c, the deflections are simply found from the collapse load and input energy. Referring to the labelled diagram in Fig. 6.11:-

Input energy E_w = Area ODEC = OAD + ADEC

$$E_w = \tfrac{1}{2} F_c\, \delta_e + F_c\, \delta_p = \tfrac{1}{2} F_c \cdot \frac{F_c}{k} + F_c\, \delta_p$$

$$\text{Hence final deflection } \delta_p = \frac{E_w}{F_c} - \frac{1}{2}\frac{F_c}{k} \qquad -(6.53)$$

$$\text{elastic deflection } \quad \delta_e = \frac{F_c}{k} \qquad -(6.54)$$

$$\text{and maximum deflection } \delta_m = \frac{E_w}{F_c} + \frac{1}{2}\frac{F_c}{k} \qquad -(6.55)$$

6.4. EXPERIMENTAL METHOD

Mounting of experimental frame for impact tests

The base frame with uprights and top frame (Fig. 4.1) was removed from the tractor and fixed securely to the floor. Although pendulum impact tests to British and International Standards are carried out with the frame mounted on the tractor this results in some energy being dissipated in the tyres and lashing ropes. Fixing the frame directly to the floor ensures that a high proportion of the input energy is absorbed in the frame. To reduce the impact load on the floor rails the long axis of the base frame was fixed roughly parallel to the impact direction and the top frame rotated to receive impact from what would be the front. Since the mounting centres of the uprights form a square this change in relative position had no effect on the structural behaviour. The tests were carried out at an impact direction α of 6 degrees to the frame for convenience of mounting.

Measurements and recording

The instrumentation system designed for overturning experiments was used in these tests, although not all of the twelve channels were needed. Channels 1 to 3 are load cells sensing the impact force in three perpendicular directions; 7 to 9 are linear displacement transducers (LDT) measuring deflections corresponding to the three degrees of freedom of the top frame; 11 is an accelerometer fixed to the frame near the load cell with sensitive axis in the impact direction and 12 another accelerometer with similar alignment fixed to the pendulum weight. The accelerometers were duplicating information from the load cells but also indicated differences in the movements of the weight and frame during impact due to bouncing.

Permanent deformation was also recorded manually. Before and after each test the vertical projections of the four corners of the top frame on the base frame were measured using a plumb line. Scale drawings in the two positions constructed from these measurements enabled deflections of any point to be determined.

In addition a cine film at 64 frames/second recorded the displacements in the direction of the impact.

<u>Protecting the load-cells from inertial peaks</u>

Earlier experiments had shown that the initial impact of the pendulum weight gave rise to a large force pulse due not to the resistance of the uprights but to the inertia of the top frame. The load cells are designed to withstand forces of 220 kN, which is higher than the collapse load of any frame likely to be used in the experiments but not as high as the initial peak force in typical pendulum impacts.

For these tests the impact face of the weight was covered with a rubber pad to reduce the peak force. The pad was in the form of a sandwich of 12 mm hard rubber sheet between two pieces of 12 mm plywood, the overall size being 300 x 300 mm. The pad makes contact on impact with a convex dome of spherical radius 250 mm fixed to the load cell. This and the ply distribute the load through the rubber. The aim was to reduce the peak force without allowing a significant amount of energy to be lost in hysteresis and permanent deformation. The force pulse was certainly lower using the pad and there was no danger of overloading the cells in these tests. It was still present, however, and was followed by bouncing and loss of contact, indicated by the zero force immediately following the pulse. This created some problems in analysis.

It was originally intended to estimate the energy loss by double-integrating the difference between the two accelerometer signals to give the pad deflection, plotting this against the force and measuring the area under the curve. The likely reliability of the result obtained from such a procedure was considered not to be high enough to justify the effort involved, however, and the energy loss was assumed to be negligible.

6.5. TESTS ON THE MK I FRAME

The Mk II frame, with its lighter top, different end fixings and different geometry, was used in all the overturning experiments. Most of the laboratory impact tests were carried out before the change from Mk II, however, to validate the structural analysis (79). The results of these tests are therefore reported first, followed by confirmation of the behaviour of the Mk II on the basis of a further, single test.

The results analysed here are from impact test series L4, carried out on 16th and 17th April 1973, and L5 on 2nd August 1973. An additional test, L6, was made to investigate the mode of collapse on 24th September 1973.

Series L4 consisted of five impacts at successively greater pendulum lift heights using the same frame without straightening the uprights between tests. The lift heights were 1, 1, 4, 12 and 12 inch (25, 25, 102, 305, 305 mm) from which the 4 inch and first 12 inch blow were selected for analysis. A single 18 inch (457 mm) blow was used in both L5 and L6.

6.5.1. Results

Displacement measurements

The permanent displacements measured by plumb-line for all three tests are given in Table 6.1 and a comparison of the three methods for one test in Table 6.2.

Table 6.1

Permanent displacements measured by plumb-line

Test	Permanent deflections, mm												
	B			G			J			D			L
	x	y	δ	x	y	δ	x	y	δ	x	y	δ	δp
L4/3	27	-15	31	5	-15	16	4	5	6	25	5	26	31
L4/4	100	-40	108	24	-45	51	18	30	35	96	35	102	112
L5	151	19	152	67	15	69	61	98	115	145	104	178	177
L6	165	-42	170	26	-56	62	13	79	80	150	93	177	196

Table 6.2

Displacements in test L5 measured by three methods

Method of measurement	Displacement at LDT in dircetion of force, mm	
	Plastic	Maximum
Plumb line	150	-
UV trace	146	200
Cine film	160	218

Load deflection curves

From the UV recordings the values of force and displacement were measured at small time increments for each test using the calibrations given in Appendix 6.2. The bouncing and frame vibration in the initial elastic phase of the impact reduces the accuracy of the readings up to yield. Attempts were made to average visually the peaks that are present; an automatic measuring technique might have been an advantage, although the problem has also been found by other workers. (73)

The measured deflections were those at the LDT at the centre of member BD in the direction of the force. Since deflections in the directions of the other two degrees of freedom were relatively small it was assumed for simplicity that the measured deflection was proportional to the deflection at the impact point. The ratio of these deflections after the test was found from the plumb-line measurements and this ratio taken to apply throughout the impact. This assumption is likely to be valid in the plastic phase but will only be true in the elastic phase if the mode of deformation is the same in both.

The load-deflection curves are shown in Figs.6.13-6.15. In the 4 in. lift impact the permanent deflection is small compared with the total, and although yield has occurred the full plastic moment had probably not been developed at all the hinges. The other two tests show a more clearly defined plastic region. In all cases the elastic unloading curve is better behaved than the loading one but both show the evidence

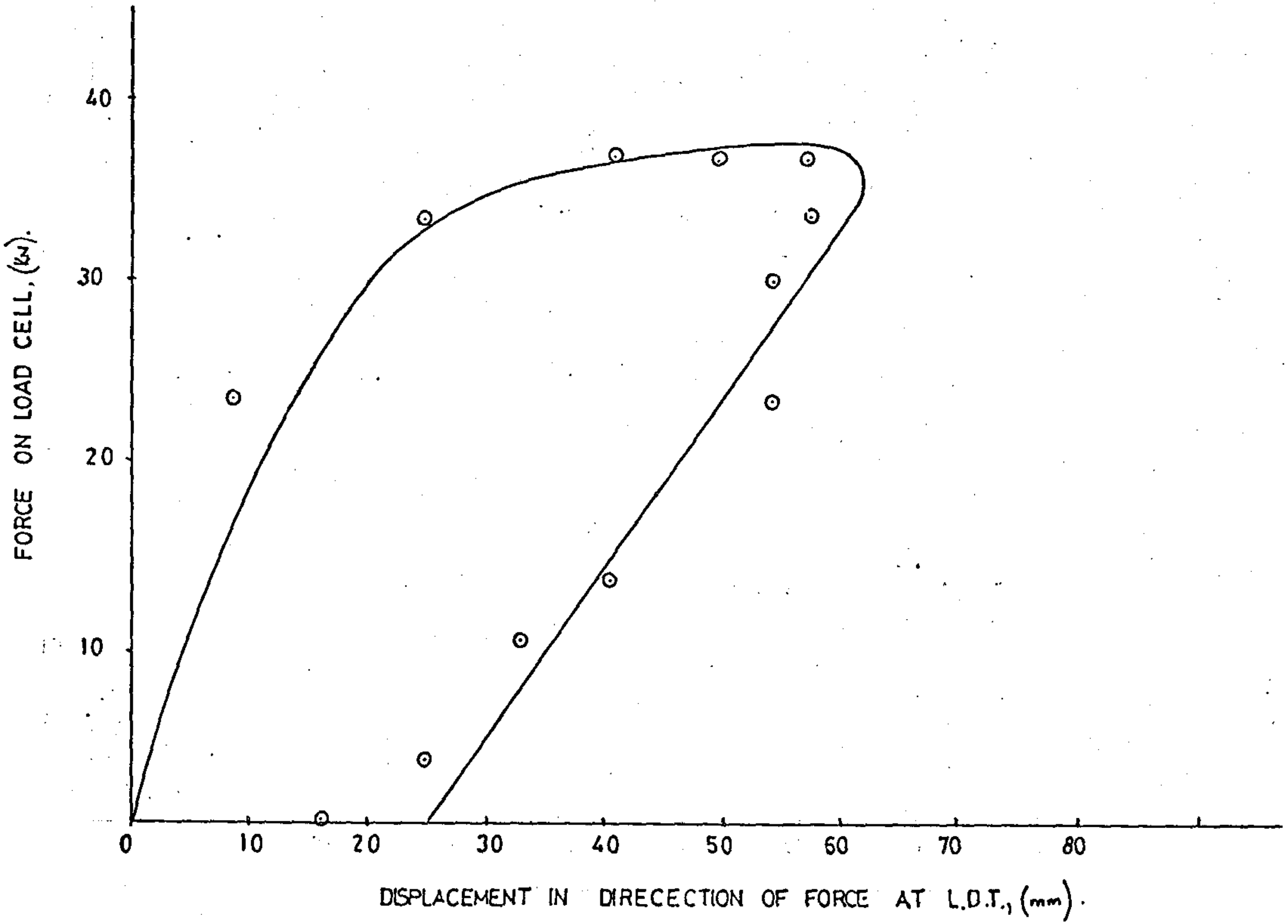

Fig.6.13 Force deflection curve, test I4/3

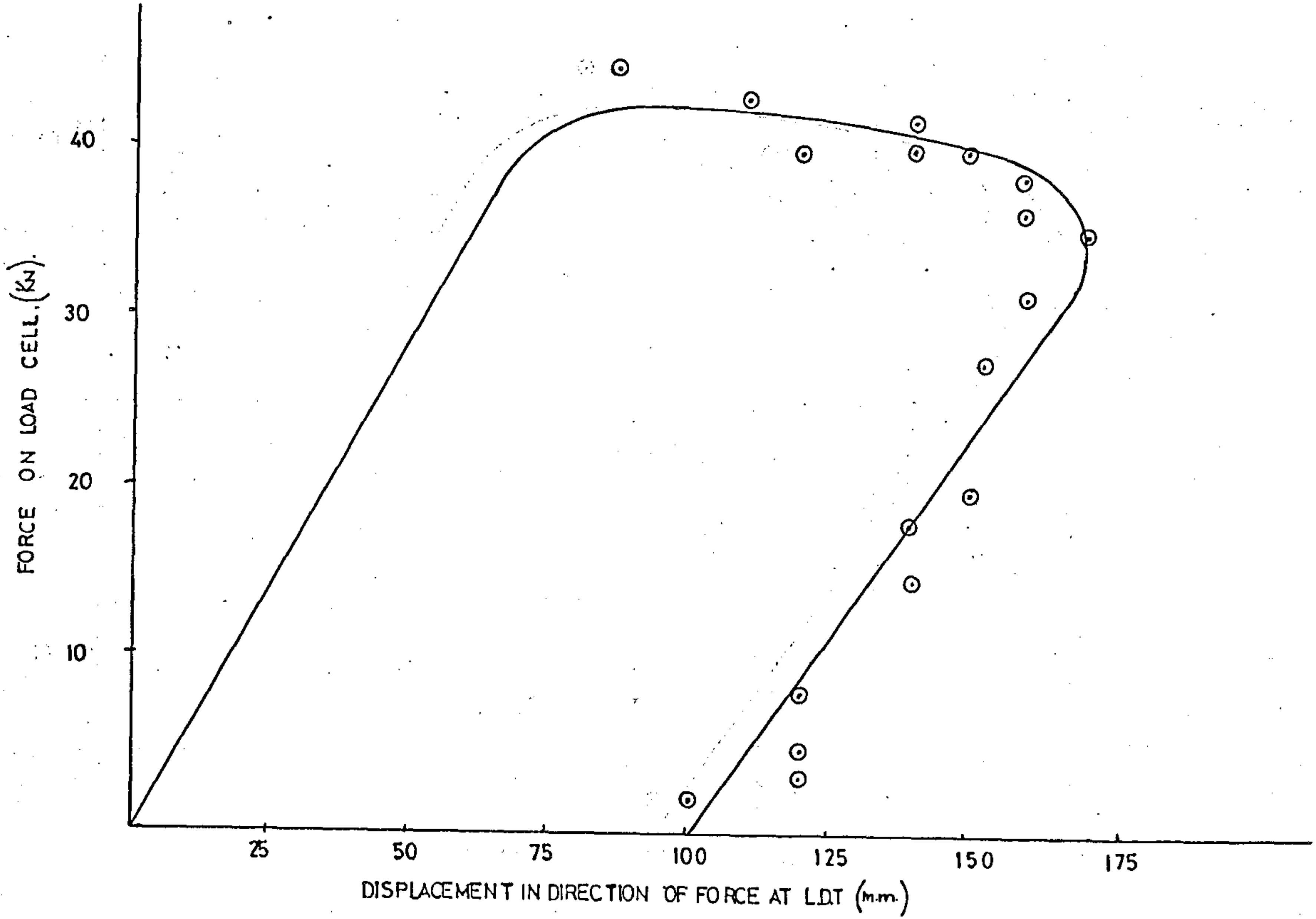

Fig.6.14 Force-deflection curve, test L4/4

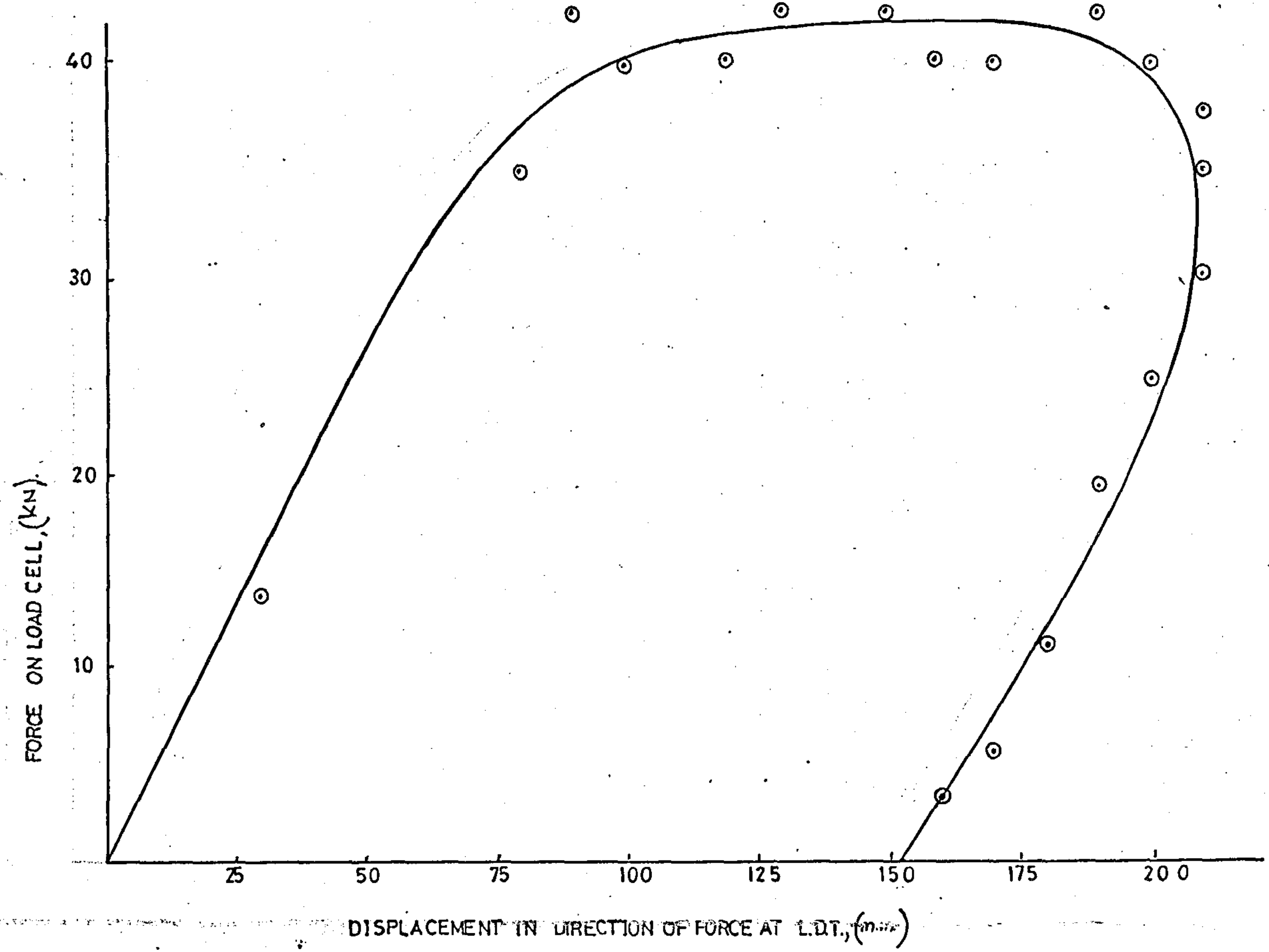

Fig.6.15 Force deflection curve, Test L5

of vibration and a gradual transition between elastic and plastic phases. The general form of the curves, particularly that for the 18 in. impact, validates the assumed behaviour shown in Fig. 6.5c.

Collapse mode

The final deflected forms in the four tests are shown in plan view in Fig. 6.16. The collapse mode in test L5 is somewhat different to that in tests L4/3 and L4/4. The repeat 18 in. blow (L6) shows behaviour similar to L4/3 and L4/4, and the mode of L5 may therefore be considered to be unrepresentative.

A simple way of visualising the collapse mode independent of the amount of deflection is to plot the position of the centre of rotation. This is not an instantaneous centre, whose position will change slightly during the deformation, but the point about which the top frame could be rotated from its initial position to reach the final position.

The centres of rotation for the four tests are shown with the predicted positions in Fig. 6.17. The effect of finite deflections can be seen in the difference between two predicted points, and within this range the predicted position and measured position for L4/3, L4/4 and L6 are grouped quite closely. The point for L5 is however significantly removed from this group. Further evidence of the difference is given by the values of skew factor in Table 6.3.

No explanation can be found for this but it is possible that the pendulum weight could have been oscillating sideways during its swing, giving a slightly different impact direction. Alternatively, there could have been an error in the displacement measurement.

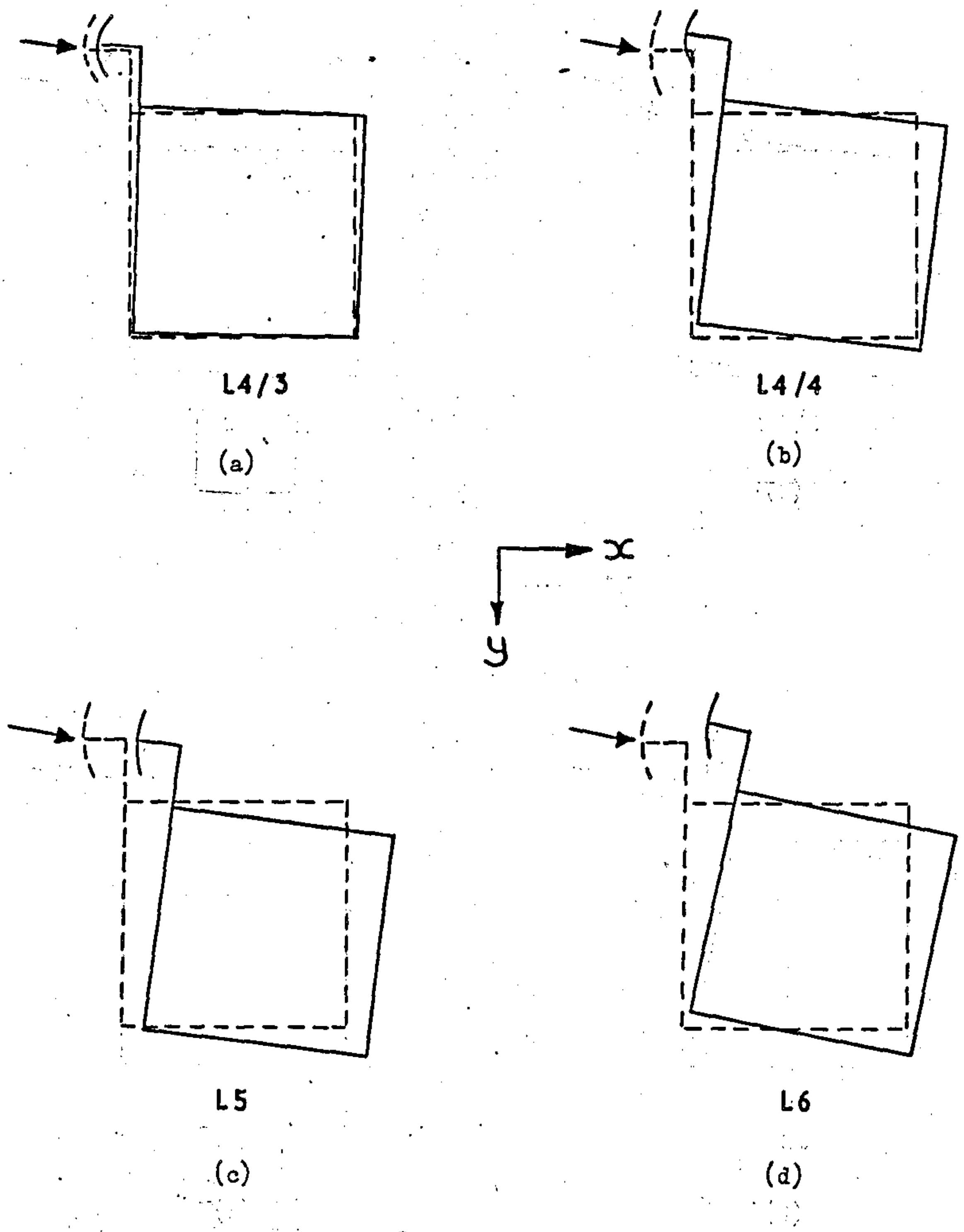

Fig.6.16 Collapse mode ---- initial position of frame
—— final position of frame

- 149

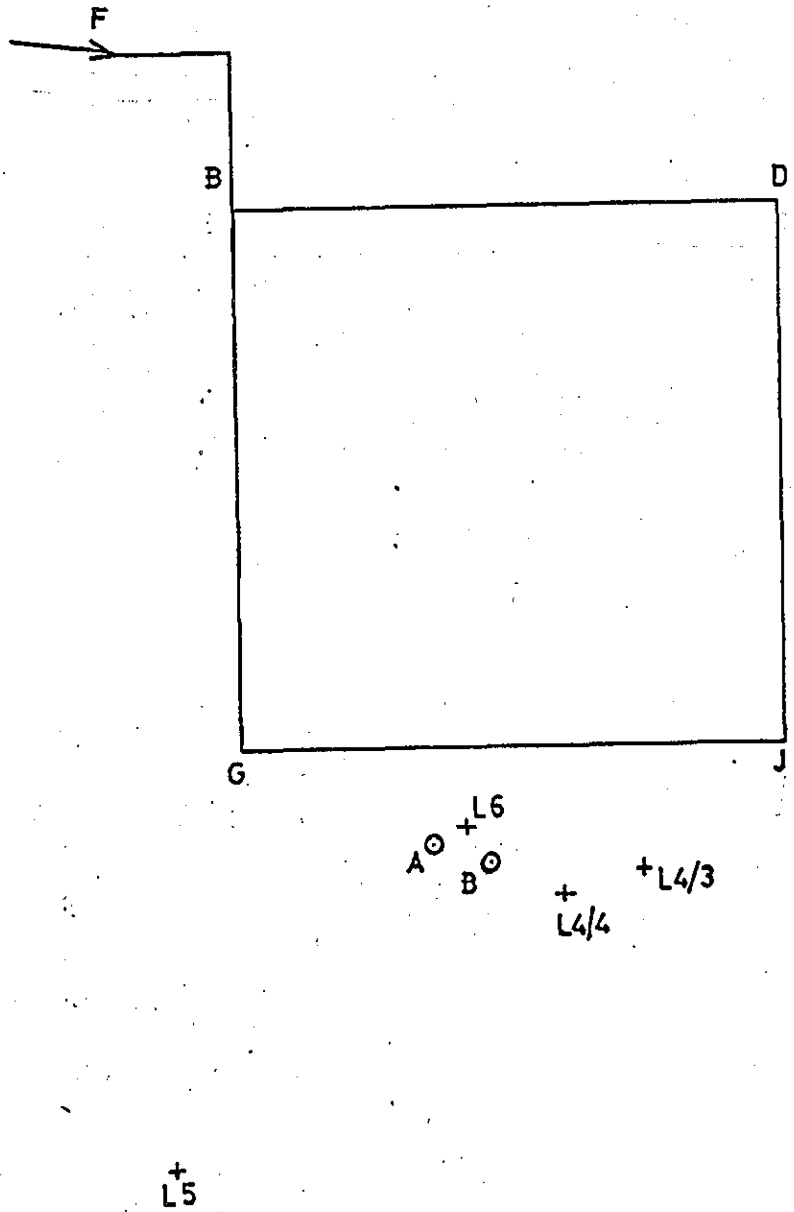

Fig.6.17 Centres of rotation
⊙ Predicted A - infinitessimal deflections
B - realistic deflections

+ Test data

Table 6.3

Collapse mode

		Skew factor, Q_s	Angle of movement of B, β_B, deg	Relative defl. of D y_D/δ_B
Predicted by STAF6		0.65	- 16	0.52
Measured in tests	L4/3	0.64	- 29	0.16
	L4/4	0.66	- 22	0.33
	L5	0.73	+ 7	0.68
	L6	0.62	- 14	0.55

Forces and deflections

The forces and deflections obtained by scaling the load deflection curves of Figs. 6.13-6.15 are given in Table 6.4, together with values predicted by the methods given in Section 6.3. The static yield stress σ_o of 410 MN/m^2 was found by tensile tests carried out by Materials Testing Section on specimens cut from the bars as described in Appendix 6.2.

In addition the predicted elastic stiffness is compared with an experimental value determined from

$$k = \left(\frac{\delta_m - \delta_p}{F_c}\right)_{\text{measured}}$$

Table 6.4

Measured and Predicted Force, Deflection and Stiffness

Test No.	Collapse Force F_c kN		Deflection, mm				Stiffness kN/mm	
			Permanent		Maximum			
	Measured	Predicted	Measured	Predicted	Measured	Predicted	Measured	Predicted
L4/3	36	38	34	35	78	70	0.82	1.09
L4/4	41	40	118	132	189	169	0.57	1.09
L5	42	41	175	203	242	240	0.63	1.09
L6	-	41	192	203	-	240	-	1.09

The total energy absorbed up to the point of maximum deflection was calculated from the area under the force-deflection curves. These values are based on the deflection ratio assumption and are therefore only approximate but they are given for completeness in Table 6.5.

151 -

Table 6.5

Energy

Test no.	Impact Energy, J	
	Measured from graph	Calculated from pendulum lift height
L4/3	2258	1993
L4/4	6425	5978
L5	8450	8967

6.5.2. Discussion

Elastic stiffness

The predicted value of 1.09 kN/mm is significantly higher than the measured values given in Table 6.4. Stiffness cannot be measured very reliably in dynamic tests of this kind however, mainly because of the scatter of points in the elastic phases due to vibration. Ashburner (73) found similar difficulties although his values based on the unloading elastic phase showed better agreement than those in Table 6.4. Two main explanations are suggested to account for the discrepancy:-

(a) The mass of the top frame is significant compared with that of the pendulum weight, about 14%. This will affect the equation of motion of the impact and hence alter the time-to-yield. In addition, however, the measured force is that between the pendulum and the frame rather than the nett resistance of the uprights, so that it will include a mass acceleration term.

(b) The assumed relationship between deflections at the loading point and at the LDT may result in significant errors in the elastic phase.

Collapse force

The measured and predicted values of F_c in Table 6.4 agree to within the accuracy of the experimental techniques.

- 152

The accurate prediction of skew factor given in Table 6.3 validates the simple method used to determine the effect of asymmetry of loading. While this is a satisfactory technique for analysing the behaviour of the present frame it may not be suitable for handling more complex structures. The assumptions of idealised elasto-plastic behaviour without strain-hardening may also be restrictive in some circumstances.

Ashburner's conclusion that yield enhancement can generally be calculated assuming constant pendulum velocity up to yield has been shown to apply in most of these tests. This assumption may, however, be the cause of the slightly higher ratio of predicted/measured force in test L4/3 than in the others. In this test little plastic deformation took place and the predicted amount of energy absorbed elastically was 33% of the total, compared with only 12% in L4/4 and 8% in L5 and L6. The pendulum velocity would therefore be significantly lower at yield than at impact in test L4/3. The average velocity, governing the time-to-yield, would be less different, but the change in either final or average velocity would probably be enough to account for the small error in F_c.

The calculated yield elevations of 1.2 to 1.3 are in general agreement with expectations.

Deflections and energy

The predicted permanent deflections are higher than the measured values by 3%, 12%, 16% and 6% respectively for the four tests. Although this agreement is not so close as that for the forces, part of the difference can be explained by dissipation of input energy in other ways, such as movement of pendulum suspension, noise, pendulum rotation etc. Energy measurements given in Table 6.5 do not help to assess the proportion absorbed by the frame, probably because of the inadequate measurements of force and deflection in the elastic phase. Measurements in very similar conditions in Sweden (63), however, indicate that 95% of the energy calculated from the pendulum lift height is likely to be absorbed in the frame. Permenent deflections predicted on this basis are given in Table 6.6

and show excellent agreement with measured values, bearing in mind the unrepresentative collapse mode in test L5. Maximum deflections agree less well because of the problems of the elastic measurements.

Table 6.6

Deflections calculated assuming input energy is 95% of pendulum potential energy

Test no.	Energy, J	Delfection, mm				
		Permanent			Maximum	
		Measured	Predicted	Difference	Measured	Predicted
L4/3	1893	34	33	- 3%	78	68
L4/4	5679	118	125	+ 6%	189	161
L5	8519	175	192	+ 9%	242	229
L6	8519	192	192	0%	-	229

6.6. TESTS ON THE MK II FRAME

The main effect on the analysis of the change from Mk I to Mk II was the different load cell mountings. Referring to Fig. 6.6, b_2, the lateral offset is reduced from 204 mm to zero. The change in extension b_3 from 147 mm to 326 mm has less effect.

The manual analysis of one force and one displacement signal with scaling assumptions, used in section 6.5, was replaced by a complete digital analysis of both horizontal forces at impact and all three displacement signals. Recordings from an accelerometer on the pendulum weight were also analysed to verify the impact force. A version of the program AN14PL was modified to take account of the different orientation of the top frame in the laboratory and overturning tests[80].

Test L7, carried out on 25th March 1974 was nominally identical to L5 and L6, with a pendulum lift height of 18 in (457 mm). The horizontal angle α between frame axis and impact direction was 7° instead of the previous 6°. The frame upright height was 1137 mm and the effective height between plastic hinges h^1 assumed to be 1081 mm.

There were two shortcomings in the deflection measurements partly due to the lapse in time before analysis:

(i) The initial frame position was not verified before impact and the datum for the physical measurements of final position had therefore to be assumed. In addition there was some ambiguity in the precise position of the measurement points.

(ii) The position of the mechanical zero of the displacement transducers was intermediate between two positions for which calibrations were subsequently carried out, and was not accurately recorded. The calibration coefficients were interpolated.[80]

Since all three displacement transducers were fitted the final position and mode shape could be determined independently from the physical measurements. The limitations above should not account for more than 5% error in the transducer results; this is consistent with results from photographic records (Table 6.7).

Table 6.7. Permanent displacement of the top frame transducer mounting (Channel 9) in the x direction (7° to impact)

From physical measurement after test	181 mm
From displacement transducer recording	166 mm
From photographs	175 mm

6.6.1. Results and discussion

Collapse mode

The values of skew factor, Q_s direction of movement of the upright nearest impact, β_B and the deflection y_D for the new frame geometry are shown in Fig. 6.18. These were calculated as before using the program STAF6. In this case the discontinuities caused by a mode of pure rotation about J ($-69^{\circ} < \alpha < 20.7^{\circ}$) are accompamied by others ($43.5^{\circ} < \alpha < 68.3^{\circ}$) due to rotation about D. These second discontinuities may have been present in the previous configuration but if so they were too small to be recognised. Modes of pure rotation about the other two uprights, B and

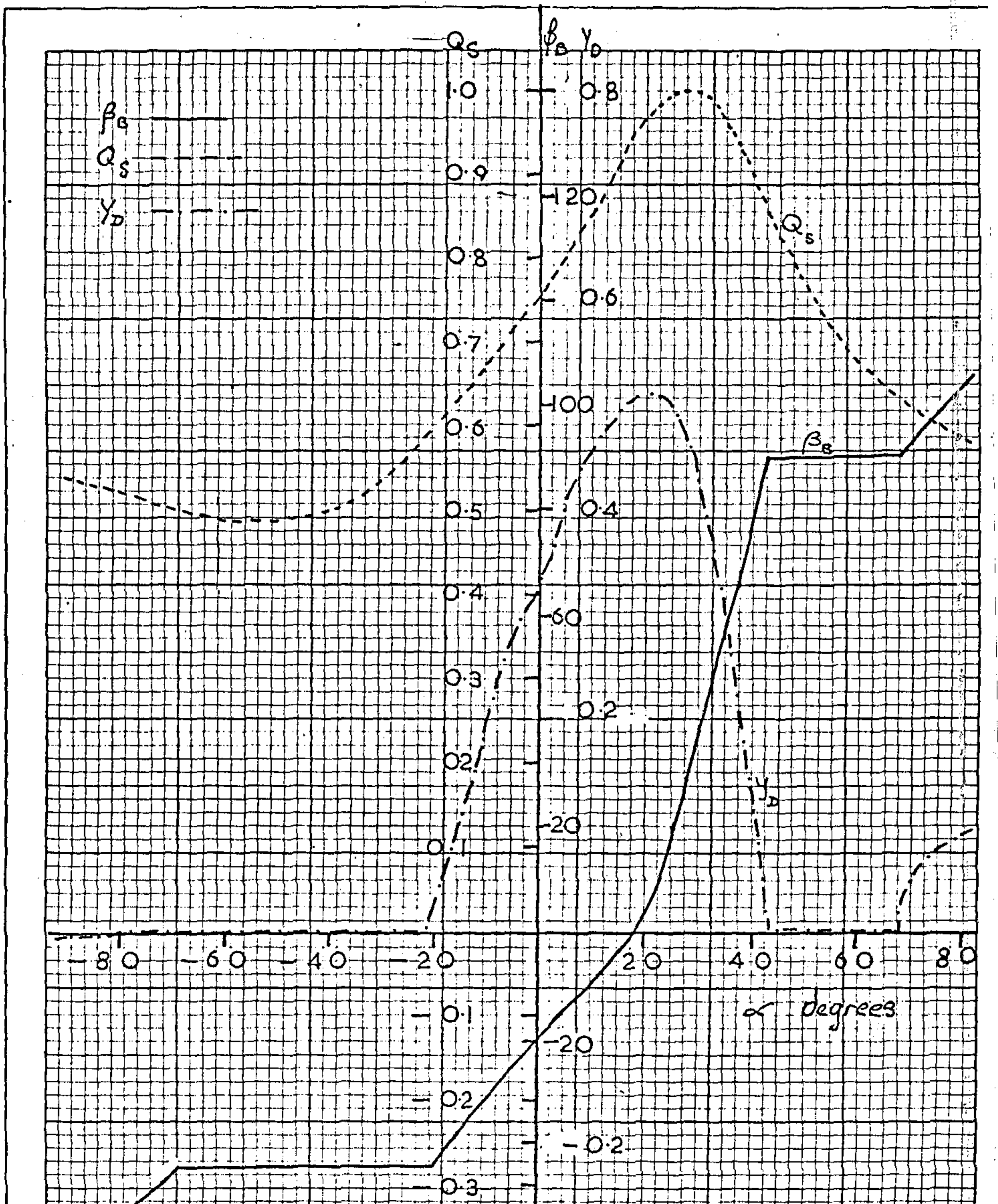

Fig.6.18 Predicted variation of skew factor, Q_s, angle of displacement at B, β_B, and relative displacement at D, y_D with angle of impact α

G are also theoretically possible in general but do not occur in the present loading configuration. The equations describing pure rotation modes are given in Appendix 6.3.

The relavant values of mode parameters are given with the test results in Table 6.8.

Table 6.8. Collapse Mode

	Skew factor Q_s	Angle of movement of B, β_B, deg	Relative defl. of D y_D/δ_B
Predicted by STAF6	0.83	−13	0.43
Measured by transducers	0.82	− 6	0.37
Physical measurements	0.82	−12	0.26

The close agreement of predicted and measured skew factor, as found before, is particularly gratifying in view of the importance of this parameter in describing the structural behaviour. The reduced load cell offset in the new frame has the additional practical benefit of reducing the variation of Q_s with α in the region around $\alpha = 0$. Since α is poorly defined in the overturning experiments this reduces unknown sources of variations in structural behaviour.

The measured and predicted deflected forms agree quite well (Fig.6.19). The effective centres of rotation, however, are not so close as in the previous tests, reflecting the smaller measured than predicted frame rotation.

In addition to the prediction of plastic mode shape, the behaviour in the elastic mode was calculated from equations (6.18 - 6.20), and the equivalent centre of rotation is also shown in Fig. 6.19. An attempt was made to anlyse the test mode shape in the form of a continuous plot of instantaneous centre. The erratic behaviour during elastic loading and, particularly, the inability of the technique to cope with movements in near pure translation, however, produced results which did not help to clarify the pattern of movement. Even so, it was apparent that maximum

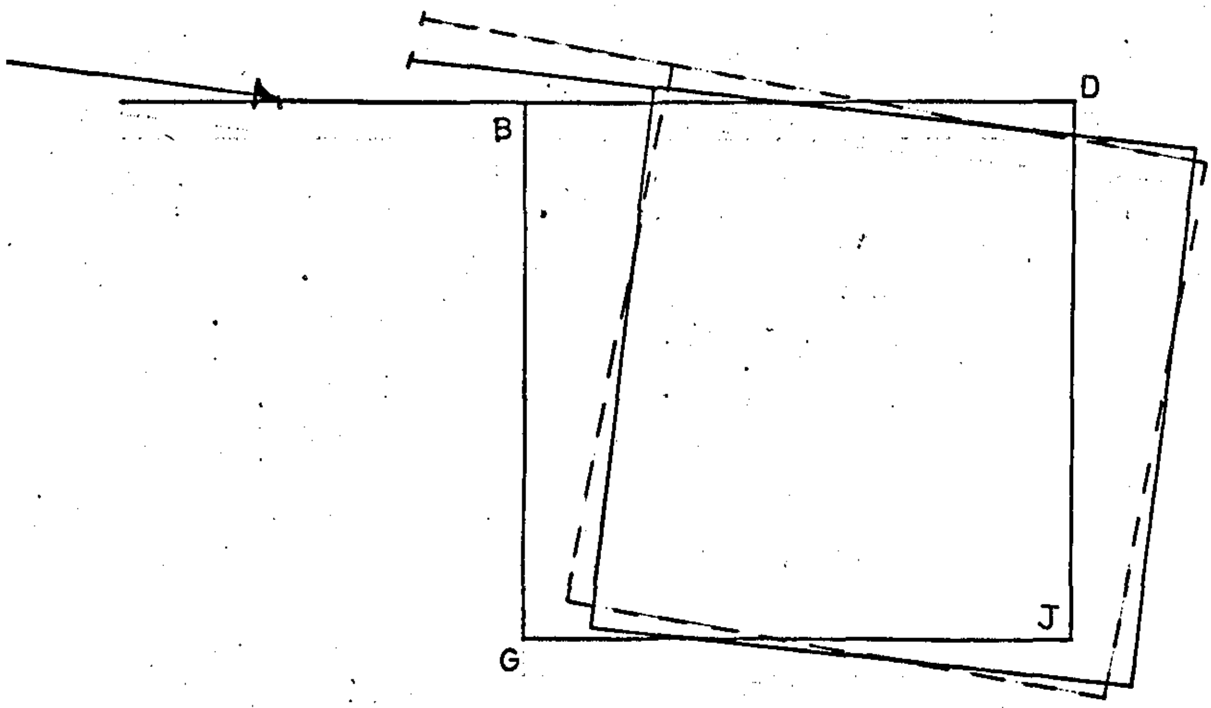

Fig.6.19 Final deflected forms: measured ———
predicted - - - -
and equivalent centres of rotation.

deflections in different directions were not reached at the same times and transitions between pure elastic and plastic regions were complex.

Forces and deflections

The force-deflection curves in the direction of, and perpendicular to the impact are given in Fig. 6.20. The normal smoothing (Section 5.3.1.) was used with a nominal cut-off frequency of 148 Hz. Bouncing at initial impact is evident. The force calculated from the pendulum accelerometer showed good agreement and is omitted for clarity. The force perpendicular to the impact direction remains fairly small and there is negligible absorption of energy in the frame in this direction, although an unknown amount is dissipated in sliding friction at the pendulum contact face.

To see how far the general elastic behaviour during loading differed from that during recovery the analysis program was run with a nominal cut-off frequency (70) of 20 Hz (Fig. 6.21). This smooths the bouncing during initial impact giving a load-deflection shape not dissimilar to that expected in a static loading test. This is encouraging, although the effect of bouncing on, particularly, the yield enhancement, is quite unknown.

The close approximation of Fig. 6.21 to the idealised elasto plastic behaviour (Fig. 6.5c) is also encouraging. The theoretical analysis ignores rounding of the curve due to gradual development of yield, both across the upright sections and among the four different uprights. This is apparently justifiable for the overall force deflection behaviour in spite of the complex mode shape pattern.

The predicted and measured values are given in Table 6.9.

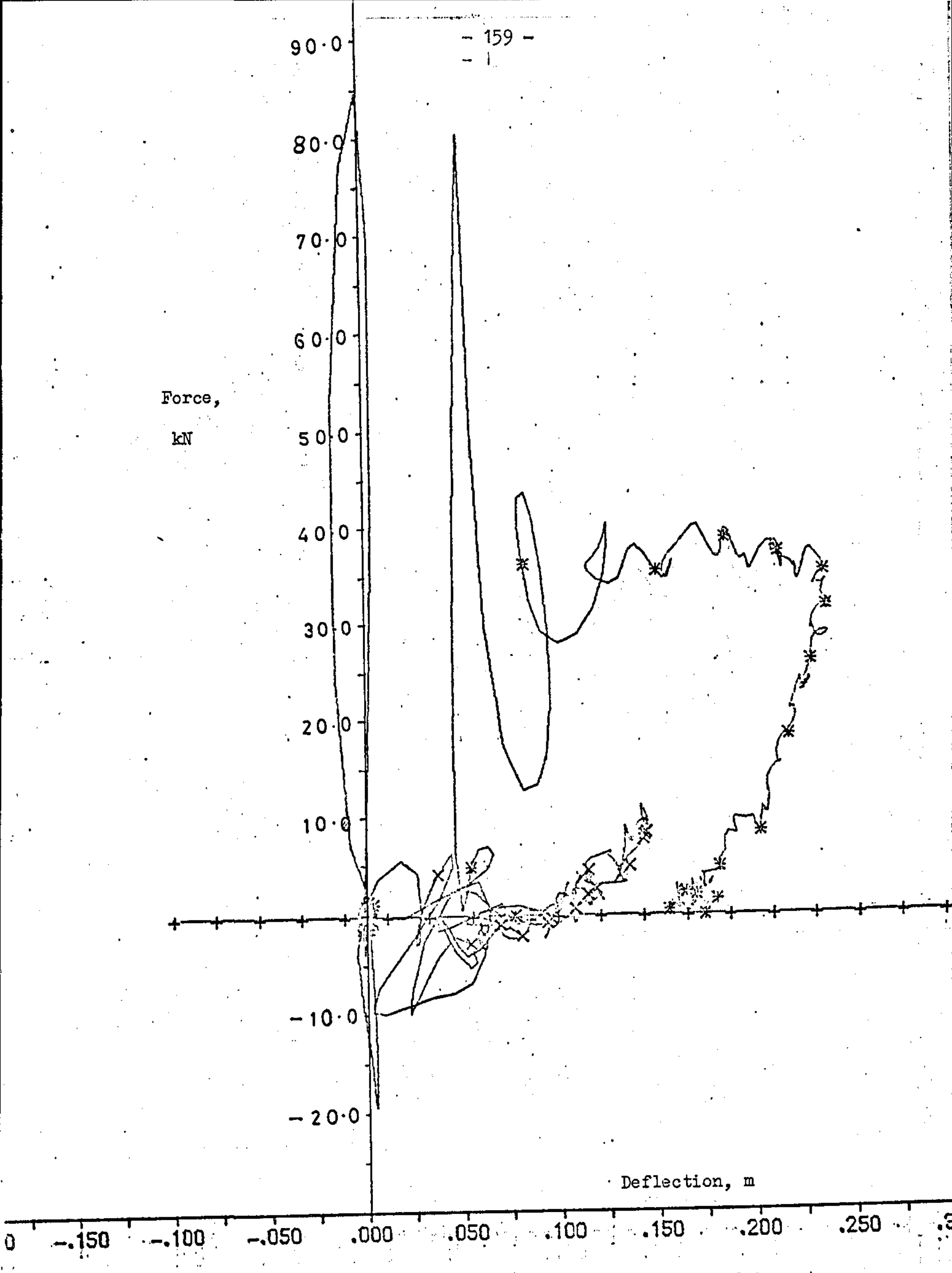

Fig.6.20 Force-deflection behaviour in direction of impact.

Data filtered at 148 Hz cut-off frequency.

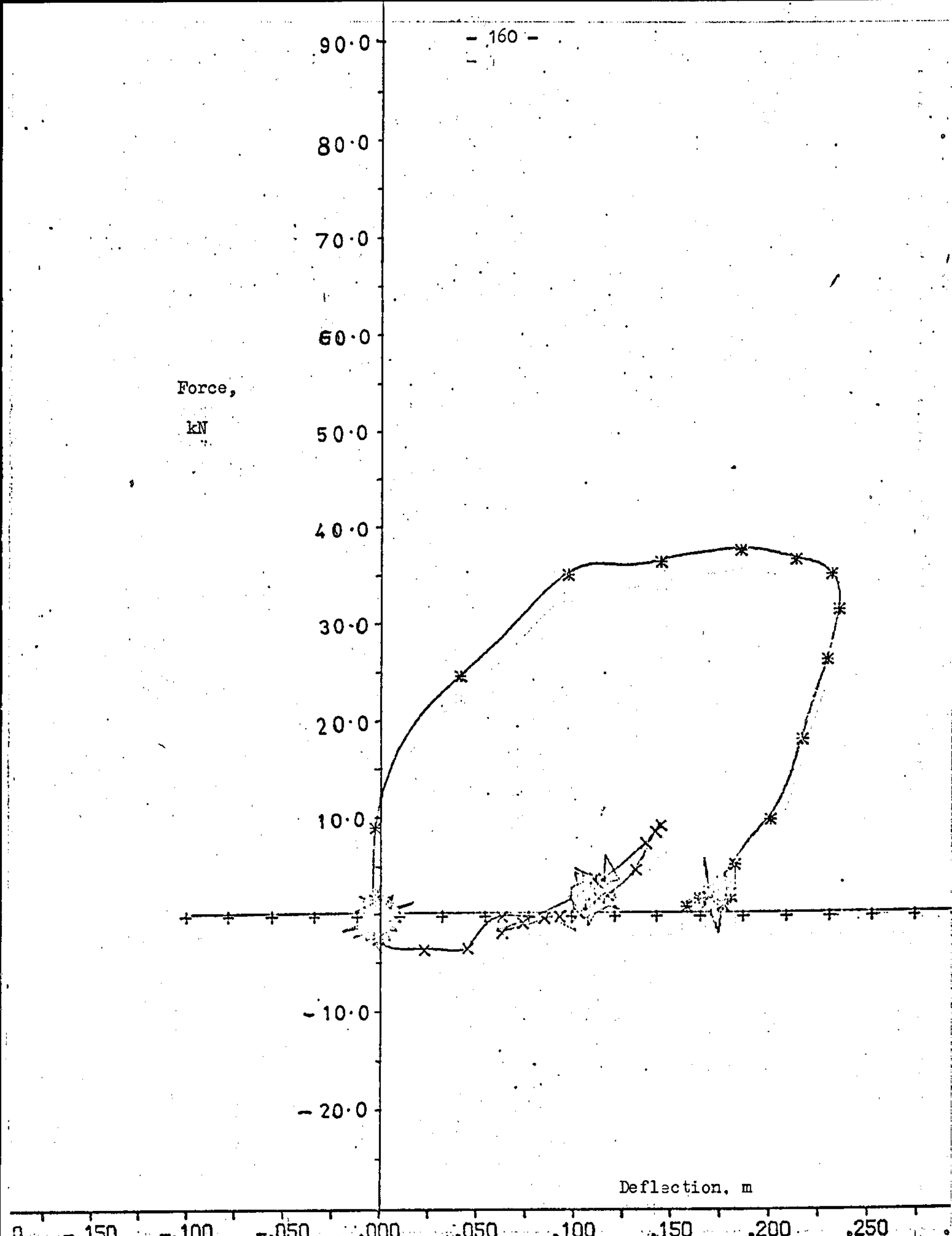

Fig.6.21 Force-deflection behaviour in direction of impact.

Data filtered at 20 Hz cut-off frequency.

Table 6.9. Forces, stiffness, delfection and energy

	Collapse force F_c, kN	Elastic stiffness, kN/mm	Deflection in direction of force, mm		Energy, kJ
			Permanent	Maximum	
Predicted*	39.5	0.85	192	239	8.52
Measured+	38	0.65	162	235	7.65 (Total instan-tanecus)

*Assuming input energy is 95% of pendulum potential energy; static yield stress 410 MN/m^2; strain rate sensitivity constants as in section 6.5.

+From transducer recordings.

As in the previous results, collapse load is predicted well. Elastic stiffness, measured as the gradient of the straight part of the unloading curve, is again significantly lower than the predicted value. The agreement is slightly better than for tests L5 and L6 with the heavier top frame, reinforcing the conclusion that inertia forces may be the main cause of the difference. The effect of the finite elastic stiffness of the top frame (section 6.3) is too small to contribute significantly to the error (see 4.1.4 and ref. 62).

The measured deformation is 15% less than predicted. Part of the difference may be due to the inaccuracies in the displacement measurements; if these are scaled according to the photographic measurements, assuming the mode shape is correct, the permanent deflection becomes 171 mm - still 11% less than predicted. It appears that less than 95% of the pendulum potential energy is being absorbed in the frame, although it is difficult to account for the remainder. In the previous tests the value of 95% was found to be appropriate and although there were differences in the mode of deformation these were not expected to be great enough to cause significant changes in the proportions of energy dissipated. The most important difference may be movement of the loading face in the direction perpendicular to impact. This implies loss of energy either in friction or in sideways pendulum velocity.

The initial bouncing is an area of poorly defined behaviour which will be altered by the top frame mass but no explanation of how this affects the energy absorbed is forthcoming.

6.7. CONCLUSIONS

(a) Simple techniques have been developed to predict collapse forces and deflections of the NIAE experimental safety frame under impact. The accuracy obtained is high enough to allow the structural behaviour to be defined for the simulation studies of tractor overturning.

(b) Predicted stiffness showed poor agreement with experimental measurements. Some difficulty is expected in dynamic measurements of this kind but the main cause is probably the high mass of the frame, which was not included in the analysis and does not allow true elastic forces to be measured directly.

The measured elastic stiffness was still significantly lower than the predicted value for the lighter, MK II frame but the discrepancy was slightly smaller than in the tests on the Mk I.

(c) The collapse mode under assymetrical loading was successfully predicted by a simple iterative method.

(d) The techniques used to predict collapse forces and deflections of the Mk I experimental frame under impact have been applied with similar success to the Mk II frame. The skew factor, the main parameter describing both force and deflection behaviour, was predicted to change from 0.65 to 0.83 due to the change in frame geometry. The measured change was from

0.64 to 0.82 (discounting one of the four earlier tests which gave unrepresentative behaviour).

The predicted permanent deflection, on the other hand, was more in error than before. It appeared that only about 85% of the pendulum potential energy was absorbed in the frame compared with 95% in the earlier test. No clear reason can be found, but energy dissipated in lateral motion due to the different mode of deformation may be the main cause.

7. VALIDATION OF THE OVERTURNING AND IMPACT MODEL

The results of the 30 overturning experiments were used to validate the models. At the outset of the study it had been intended that the individual variable time histories should form the main basis for comparison. This proved to be a satisfactory method of interpreting the general behaviour and typical cases presented in 7.2. below show good agreement between experimental and simulated results. The time histories are of fairly complex form, however, and the effects of parameter variation are small in many cases and may be masked by subtle effects of the tyre friction relationships discussed in 7.1. The overall comparisons between simulation and experiment are therefore presented in section 7.3. without direct consideration of any but the most important parameters. A parameter sensitivity analysis based on the simulation is presented in section 8.

7.1. TRIAL SIMULATIONS

Before running the simulations with the parameters appropriate to each of the experiments, several trials were run to investigate the effects of those tyre and structural characteristics which were less precisely known.

In addition, it was necessary to consider the effects of the two-dimensional nature of the model. The main limitation is the inability to predict pitch and yaw motions but the experiments had shown that these were generally small, particularly when rigid front axle stops were fitted to prevent the axle from rotating about its longitudinal pivot . The tractor centre of mass is towards the rear, about two-thirds of the weight being carried by the rear tyres. The most appropriate method of ensuring consistency between tyre forces and weight was therefore to treat the two dimensional model as a simulation of the part of the tractor weight supported by the rear tyres. In resisting roll motion, however, the front tyres contribute relatively little, particularly when the front axle is free to pivot. For the moment of inertia in roll, the value for the whole tractor was therefore considered to be most suitable (Appendix 7.1).

The effects of these inertial parameters were studied in the initial trials and the relationships assumed above were found to give the best agreement with the experimental results.

7.1.1. Tyre behaviour

The tyre side force model depends on three parameters, limiting coefficient of friction, cornering stiffness and relaxation length, together with a slip angle relationship of the type given in Appendix 7.2. Four parameters, vertical and lateral stiffness and damping, describe the tyre vibrational behaviour. All the parameters and the relationship were estimated from indirect measurements as described in Appendix 7.2. The effects of errors in these estimates was also investigated during the trial simulations. The effects of variation are quantified in the sensitivity analysis in section 8 but a discussion of the main findings is given below. To understand the causes of some of the highly sensitive, discontinuous effects it is necessary to consider the behaviour in detail.

The moment of the resultant force on the "upslope" tyre (point 9, Fig.3.3) acts in the negative θ direction for the whole time it is in contact with the surface (Fig.3.1) and its effect is to increase |roll velocity|. For the "downslope" tyre (point 10), however, the sense of the resultant moment depends on the coefficient of friction and the camber angle of the tyre to the surface. The position when the resultant force passes through the centre of mass is analogous to an unstable equilibrium, and further increase in |roll angle| will produce increasing |angular acceleration|. In the absence of oscillation of the tractor on its tyres this relationship is straightforward and the motion is relatively simple and well behaved, as was found in the early version of the model. Oscillation perpendicular to the surface affects the magnitude of the forces but lateral oscillation has the more complex effect of altering the friction angle and coefficient.

The biggest changes occur, however, when the perpendicular oscillation causes momentary loss of contact. In these circumstances the dynamic coefficient of friction is reset to zero in the model, as this was thought to represent the real behaviour. If contact is then remade the coefficient of friction increases gradually according to the relaxation length and slip angle relationships. This is a stick-slip phenomenon, but it is likely to occur only a small number of times during an overturn, if at all. A temporary loss of contact at a time when the roll moment is high therefore has a considerable effect on the roll acceleration in the period immediately following, and hence on roll velocity and angle throughout the rest of the overturn. The effect on vertical acceleration is generally the reverse of that on roll acceleration; increased side force on the downslope tyre increases |roll acceleration| and reduces |vertical acceleration|. In addition to this transfer of energy between coordinate motions, more is dissipated under higher side forces.

Thus small changes in tyre, or other parameters may alter the interaction between oscillation and the development of frictional forces, causing moderate changes in the behaviour; or they may result in temporary loss of contact when previously it had been continuous, causing large changes in the behaviour.

Normally, the upslope tyre remains in contact until it meets the chamfered edge of the bank (surface 2, Fig.3.6). It may loose contact at any point on surface 2 but at the latest it will do so at the junction with the bank slope, surface 3. The motion is generally well behaved during the initial part of the overturn when the upslope tyre is in surface contact but bounce/slip interaction has some affect on the rotational velocity at loss of contact, and hence on the ensuing dynamics. From that point, the forces at the downslope wheel determine the behaviour and it is here that the bounce/slip/roll angle relationships become critical, particularly under temporary loss of contact.

The bank angle α has a considerable effect on this sensitivity. With a steep bank (small α) the |roll velocity| is fairly high when the upslope wheel loses contact. The point of zero roll moment is passed quickly, the forces on the downslope tyre are relatively small and there is little liklihood of contact here being regained once it is lost. At larger α (shallower bank) the $|$roll velocity$|$ is smaller initially and the tractor may hover around the point of unstable dynamic equilibrium for longer. And the path that the downslope tyre would take in free flight is closer to the line of the bank slope, so the chance of intermittent contact at the critical time is much higher. The trial simulations confirmed that the behaviour became much more sensitive to many parameters as α was increased. Eventually, of course, a value of α is reached ($> 45^\circ$) when the tractor does not overturn at all but bounces back onto its wheels.

To ensure that the modelling of loss of surface contact was realistic, the simulation was run with suppression of the statements that reset the coefficient of friction to zero. This naturally reduced the sensitivity in some cases but the agreement with the experimental results was worse in almost all instances where intermittent contact was critical. It may be concluded not only that the reset to zero is correct, but that in general the intermittent contacts predicted by the model also occurred in the experiments. The detail shown in the films of the experiments was not sufficiently fine to confirm this independently. However, because intermittent contact can be very sensitive to parameters and its effects are so large, there are inevitably cases when the prediction and experiment do not agree. This is discussed in relation to the individual experiments in 7.3.

Relaxation length proved to be the most sensitive of the parameters and was unfortunately the least clearly defined. It was, however, encouraging to find that the conventionally assumed value equal to the rolling radius gave the best prediction, and this was used in all subsequent simulations.

The form of the side force/slip angle relationship had a much smaller effect, although there was some interaction with relaxation length. Again, the conventional relationship,(Appendix 7.2), was found to be the most suitable in cases where there was significant difference, at large α.

The other tyre parameters had little effect within the range of likely error of their estimated values, and these were therefore accepted. It had been expected that small changes in tyre stiffness, for example, would have significant effects on behaviour by changing the positions of normal force minima in relation to roll angle, and perhaps by altering the phase relationship between roll and linear oscillations. These changes were noted in the results but no large effects on overall behaviour were found.

7.1.2. <u>Impact parameters</u>

The force/deflection characteristics of the ROPS are covered in section 6. Measurement and modelling of rear wheel and soil characteristics are described in Appendices 7.3 and 7.4. The least well defined impact parameters were the effective areas of tyre and rim, the damping coefficient and the soil friction.

The reasonable minimum effective areas of tyre and rim are sufficiently large to cause only small soil deformation under the rim collapse force. The majority of the energy in these impacts is therefore absorbed in the rim, so changes in the areas have only small effects on the overall energy distribution and hardly any on the ROPS energy.

The ROPS was known from the laboratory impact tests to be very lightly damped. The true damping coefficient would be too small to have any significant effect, so a value of zero was assumed. In the case of the rim, however, deflection causes a considerable amount of movement in bolted joints in addition to the deformation of the material. The model had provision for velocity dependent damping only, which probably does not describe accurately that at the rim. Furthermore, the recovery curve after loading was dissimilar to the elastic loading curve, and could be represented only approximately by the single recovery line of the model.

The damping coefficient and recovery stiffness could be estimated only intuitively and by comparison of the impact motion with that found in the experiments. The same applies to a large extent to the soil friction. The coefficient of friction due to pure sliding on the soil surface is probably about 0.10 - 0.15[81] but the effect of penetration was assumed to raise it to between 0.5 and 1.0. Soil friction and rim damping and recovery all affect the motion during and after impact, and have some effect on the energy absorbed in the ROPS. Even with the most extreme values of these parameters that seemed inuitively reasonable, the amount of bouncing, assessed by peak reversals of vertical and roll velocities, was generally rather greater in the simulations than in the experiments.

Three explanations are suggested to account for this. Firstly, the front of the tractor is very rigid and little energy is recovered from its impact with the soil. This has only a small effect on the vertical recovery velocity at the rear, as could be seen on the film, but the simulated vertical velocity applies to the centre of mass, which is not at the rear. In roll, the front impact may have more effect in resisting bouncing, although the impact points are fairly close to the vertical plane through the centre of mass. Secondly, the soil deformation is not reset to zero after the first impact in the bank overturn model, although it is in the multiple roll version. In the bank case, subsequent impacts occur in approximately the same places, on already deformed soil. Some shift in position does occur, however, and energy dissipated in compressing undeformed soil results in greater reduction of rebound velocity. And finally, a coulomb friction representation of the rim damping would probably be more appropriate and could be expected to reduce the amount of bouncing.

The values selected from the trial simulations for these parameters were:

Tyre and rim areas: each 0.2 m^2 at top and bottom.

Rim damping coefficient: 20 kNs/m, which is equivalent to 38 % critical damping for support of the rear mass on one side of the rim, or 53 % for support on both sides.

Soil coefficient of friction: 0.5.

7.6. GENERAL COMPARISON OF DYNAMIC BEHAVIOUR

A complete set of time-histories showing linear and angular displacements, velocities and energies for one experiment and its simulation is

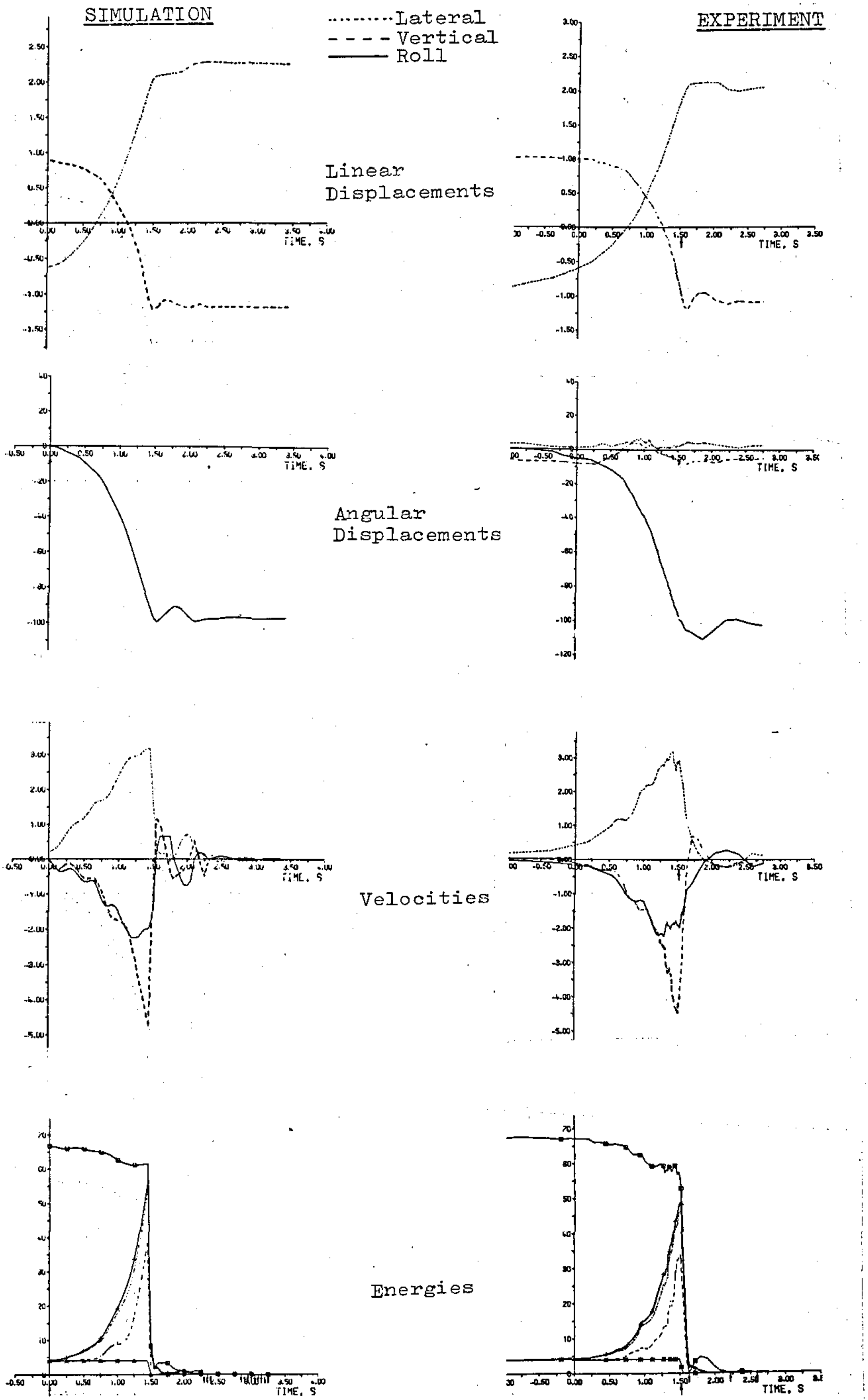

Fig. 7.1 Sample results for one overturn (run 22)
For full legend see Figs 5.3 - 5.6.

given in Fig. 7.4. The kinetic and potential energies are plotted cumulatively to show the changing distribution; the gradual fall in the top line indicates dissipation in sliding friction and impact.

The most important variables are the velocities, and these are shown for different bank slopes, α, in Figs. 7.2 - 7.7 representing experiments in "standard" conditions. The effect of bank friction μ_s can be seen by comparing Fig. 7.5 (limiting μ_s = 1.0) with Fig. 7.1 (limiting μ_s = 0.14).

The overall comparison of simulated and experimental results is good, both in shape and in absolute levels. The comparisons are generally better for low μ_s than for high, which is to be expected in view of the relative effects of gravity, which is well defined, and tyre friction, which is much less so.

7.2.1. Initial behaviour

The first part of the overturns when the downslope wheel is still on the chamfered edge of the bank is the least well predicted. (Figs. 7.2-7.7) The chamfer was necessary to prevent fouling of the tractor underside on the edge and represents a slope of 45^o, on which the tractor is fairly stable. The reasons for the discrepancies are:

(i) The nominal start of the overturn, when the downslope tyre leaves the flat surface of the platform, was difficult to define from the films of the experiments. The effect of this error is an overall shift on the time scale.

(ii) The lateral ($\dot{x}$) velocity at time = 0 was incorporated as an initial condition in the model but no reliable method was found of simulating in two dimensions the effect of the initial yaw angle. The initial behaviour in the simulation is controlled by the build-up of tyre friction in response to this lateral

SIMULATION EXPERIMENT

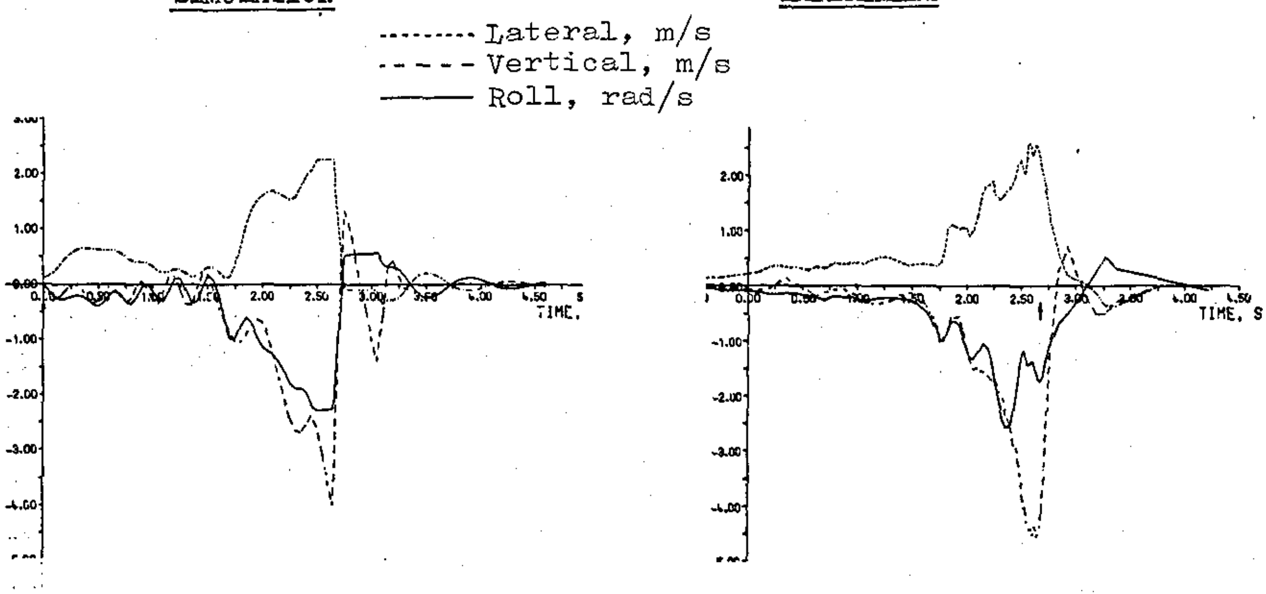

Fig. 7.2 Velocities for Run 16. Bank angle 1.0 deg.

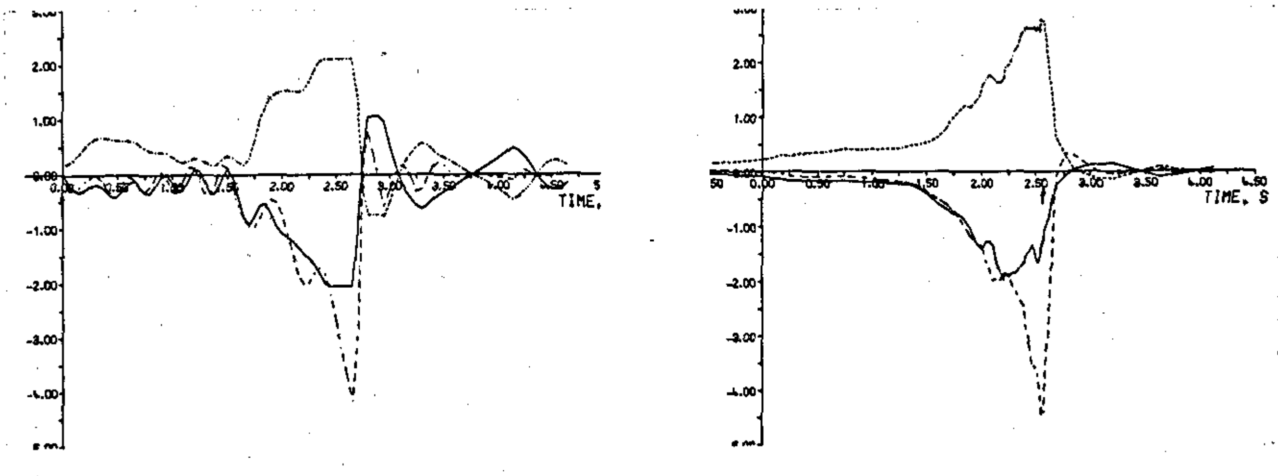

Fig. 7.3 Velocities for Run 20. Bank angle 7.4 deg.

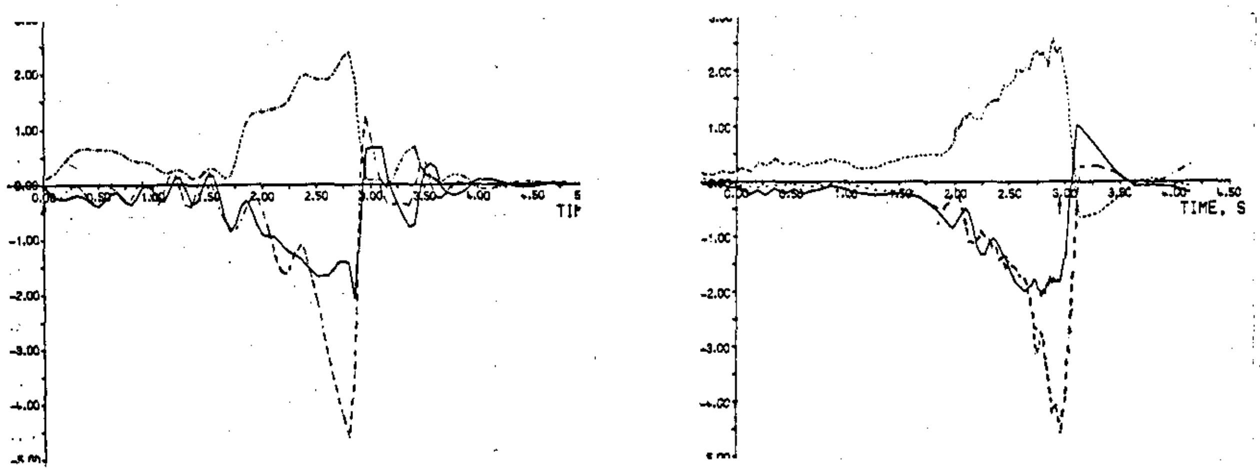

Fig. 7.4 Velocities for Run 4. Bank angle 15.1 deg.

SIMULATION EXPERIMENT

·········· Lateral, m/s
- - - - - Vertical, m/s
——— Roll, rad/s

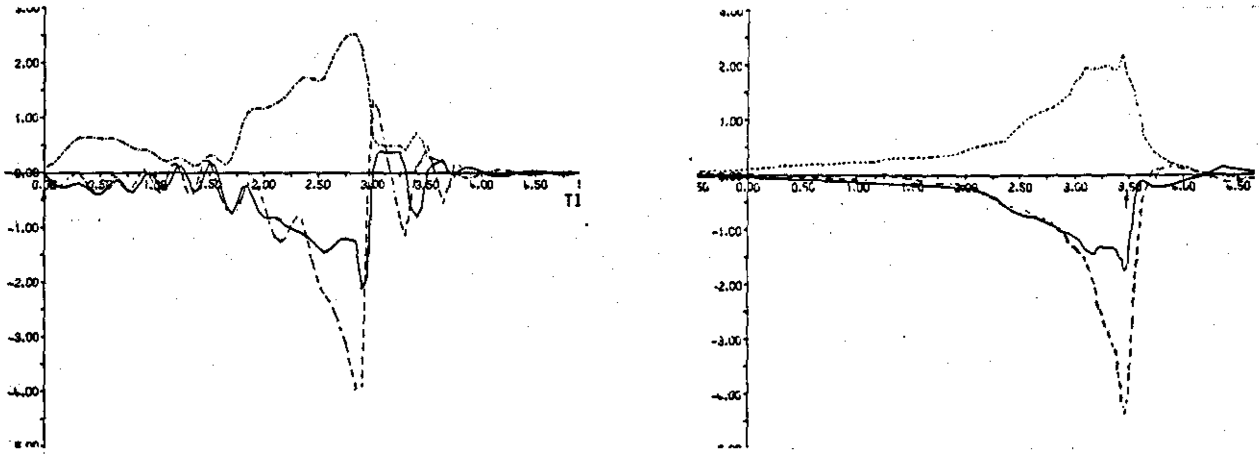

Fig. 7.5 Velocities for Run 19. Bank angle 21.4 deg.

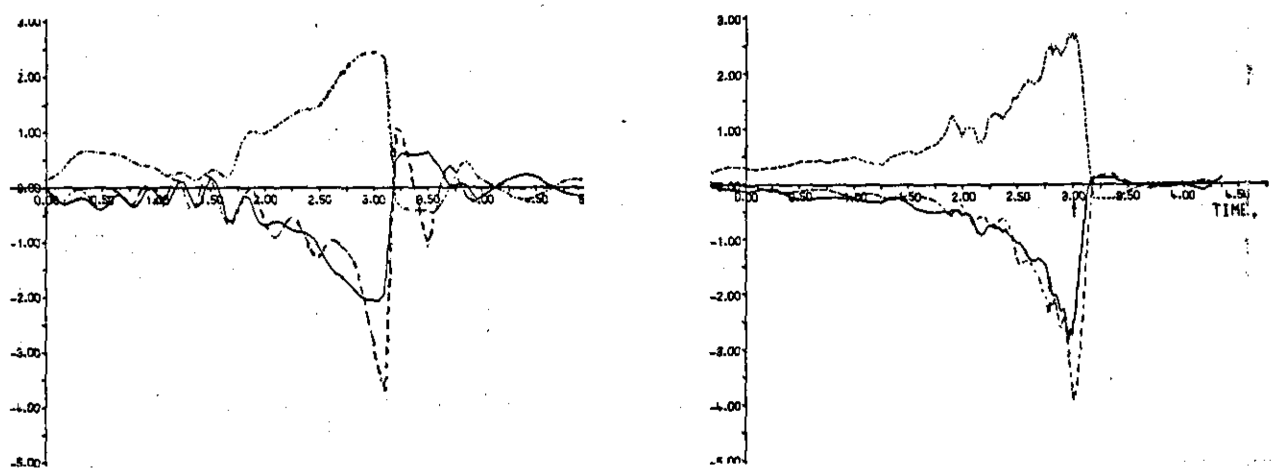

Fig. 7.6 Velocities for Run 7. Bank angle 29.3 deg.

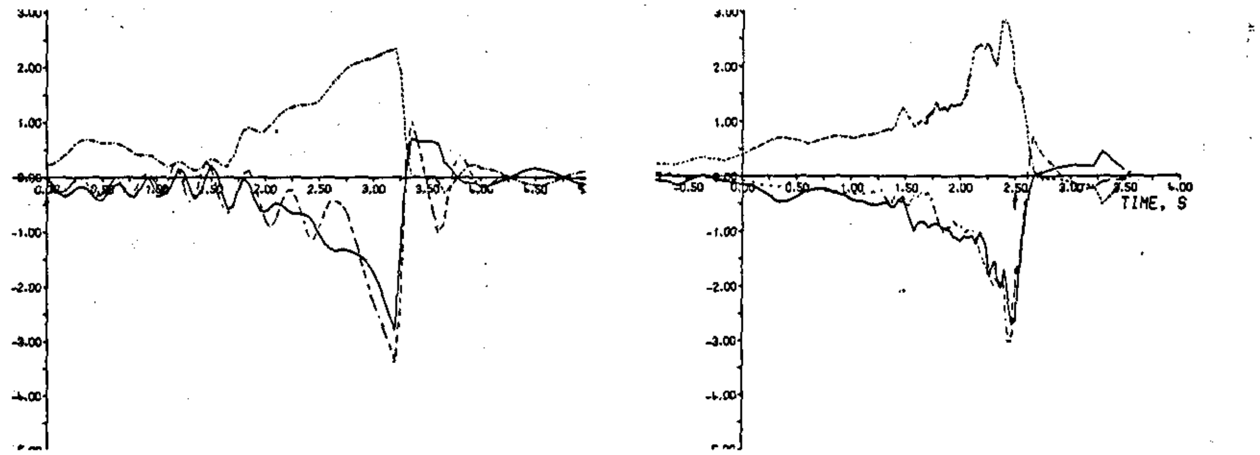

Fig. 7.7 Velocities for Run 6. Bank angle 37.9 deg.

velocity and to the downward path of the tyre. In the experiments, however, the small yaw angle resulting from the approach angle γ of the tractor to the bank edge allowed the tyre to move gradually down the slope even under infinite friction. An attempt was made to model this effect by defining the origin of the side force/slip angle (ψ) relationship as $\psi = \gamma$ instead of $\psi = 0$. This was not satisfactory because the experimental effect appears to cease when the tyre leaves the chamfer for the slope proper, or in some cases, earlier, due to the effect of the front wheels. It might be possible to improve the simulation by setting the origin to $\psi = \gamma$ initially but forcing a gradual change to $\psi = 0$ as the downslope tyre moves down the chamfer, but this was not tested.

(iii) The real tyre envelopes the edges between surfaces and gives a gradual transition of supporting forces. The model does not include this effect and the transients cause ringing, evident in the vertical and roll velocities in all simulations.

(iv) The films of the experiments were analysed before the simulation predictions were available. The digitising interval was varied throughout each run using a criterion of roughly equal movement of tractor marker points at each step, to minimise analysis time. Overturning movement was slow at the beginning and the course steps selected could have missed the effects of tyre oscillation particularly after application of smoothing. There was some variation of digitising interval between runs.

Apart from the differences in oscillation and initial rate of change of velocities, all the simulations show an early peak in lateral ($\dot{x}$) velocity which was absent from most of the experimental results but could just be detected in a few. If the tractor slides down a uniform 45° slope it does not overturn, in most cases. The peak in lateral velocity is due to the oscillation on the tyres caused by the transition from the level surface, combined with the effect of friction build-up. That it does not generally occur in practice can be explained only by the effects of approach angle and tyre envelopment described in (ii) and (iii) above.

7.2.2. Tyre oscillation

During the main part of the overturn, after the downslope tyre has moved from the chamfer onto the slope proper, oscillation is present in both predicted and experimental results (Figs.7.1-7.7). The amplitudes and frequencies of the oscillations do not change much between simulations but the experiments show considerable variation in both. In most cases the amplitudes of measured roll and vertical velocity oscillations are similar to those predicted. The frequency of the predominant oscillations in these directions generally agree with the expected value of about 3 Hz determined from the combined vertical tyre stiffness, although the wave form is often much less clearly defined in the experimental results than in the simulations (e.g. Fig.7.6b). In the lateral direction a low frequency oscillation (1.5 - 2 Hz), corresponding to the combined lateral stiffness, is generally evident in both simulations and experimental results, but the latter often have superimposed a waveform similar in amplitude and frequency to the vertical and roll oscillations (Fig. 7.2b).

These ride vibration modes are clearly excited by transients, where the limitations of the model have been explained. Further complications arise from tyre non-linearity and from the coupling of oscillations on the front tyres. Also, the expected frequencies quoted are those of the rear mass supported by the two rear tyres, but in the later stages of overturning only one tyre is in contact and the expected frequencies would be lower by a factor of $\sqrt{2}$. Spectral analysis of the results has not been carried out and would be of doubtful validity because of the short record length; it might, however, provide qualitative evidence of the contribution of vibration in the expected modes.

Before the predictions were available it had been imagined that much of the experimental oscillation was due to stick-slip. This phenomenon was indeed found in the simulations but its effects were very clear and quite different from the continuous oscillation. The delay associated with tyre relaxation also interacts with lateral oscillation, but this is not thought to be a significant factor. It is possible that partial stick-slip occurred in the experiments without being predicted by the relatively simple tyre model, but the good general agreement indicates that the main cause of oscillation is simple ride-mode vibration.

Finally, there is a nice distinction in the definition of slip angle that could have some bearing on the behaviour. The slip angle is defined in the model as the arctangent of the transverse velocity across the surface divided by the forward velocity. The transverse velocity is calculated from the instantaneous velocity of the point in the wheel plane corresponding to the undeformed tyre contact point. As an alternative, the transverse velocity of the contact point itself may be used, the difference between the two being the velocity of tyre deformation. At first sight, the true contact point velocity might seem more appropriate but it is the effective angle of the wheel plane that is quoted in published tyre data. In the steady state the two are identical; under changing conditions, the difference is presumably reflected in the relaxation behaviour.

The two alternatives were tested in the trial simulations. The differences in overall behaviour and oscillation were generally small, although where loss of contact was affected at large α they were sometimes significant. The use of the contact point velocity without the relaxation relationship caused irretrievable instabilities in the solution of contact point equations.

7.2.3. The effect of intermittent contact

The biggest discrepency caused by erroneous prediction of loss of contact occurred in run 12 (Fig.7.8). The parameters affecting overturning were very similar to those of run 19 (Fig. 7.5) and the overall behaviour shown by the experimental results is also similar. The simulation, however, predicted temporary loss of contact twice in run 19 but only once in run 12, resulting in considerable differences in vertical and roll velocities after a time of about 2.5s.

These differences help in interpreting the results of other runs. Three types of behaviour may be differentiated in the latter part of the overturn when the upslope tyre has lost contact:

(i) The downslope tyre remains in contact up to ground impact. Roll moment remains negative (i.e. clockwise in Fig. 3.1), and roll velocity continues to increase up to impact (Figs. 7.6-7.8).

(ii) The downslope tyre loses contact completely. Roll moment is zero and roll velocity is constant up to impact (Figs. 7.2 and 7.3, simulation only).

(iii) The downslope tyre loses contact temporarily. On renewed contact the angle of friction remains small and the roll moment is positive, causing a reduction in |roll velocity| from the peak when contact was lost (Figs. 7.2, 7.3 and 7.8 (experimental); Figs. 7.4 and 7.5 (both)).

Earlier in the overturn the upslope tyre is still in contact and provides a negative roll moment. Temporary loss of contact at the downslope tyre then has much less effect.

The experimental behaviour at $\alpha = 0$ (Run 16, Fig. 7.2b) is influenced by the tractor underside fouling the edge of the platform, despite the chamfer. This provides a transient that increases the oscillation on the tyres leading to behaviour of type (iii) above, which conflicts with the prediction. The final oscillation between 2.5s and impact is an analysis

SIMULATION EXPERIMENT

.... Lateral, m/s
------ Vertical, m/s
———— Roll, rad/s

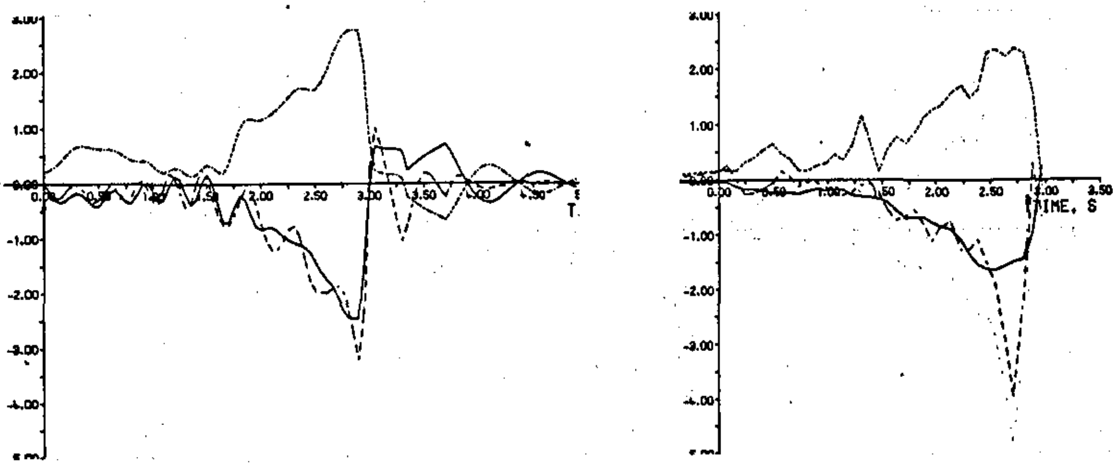

Fig. 7.8 Velocities for Run 12. Bank angle 22.9 deg.

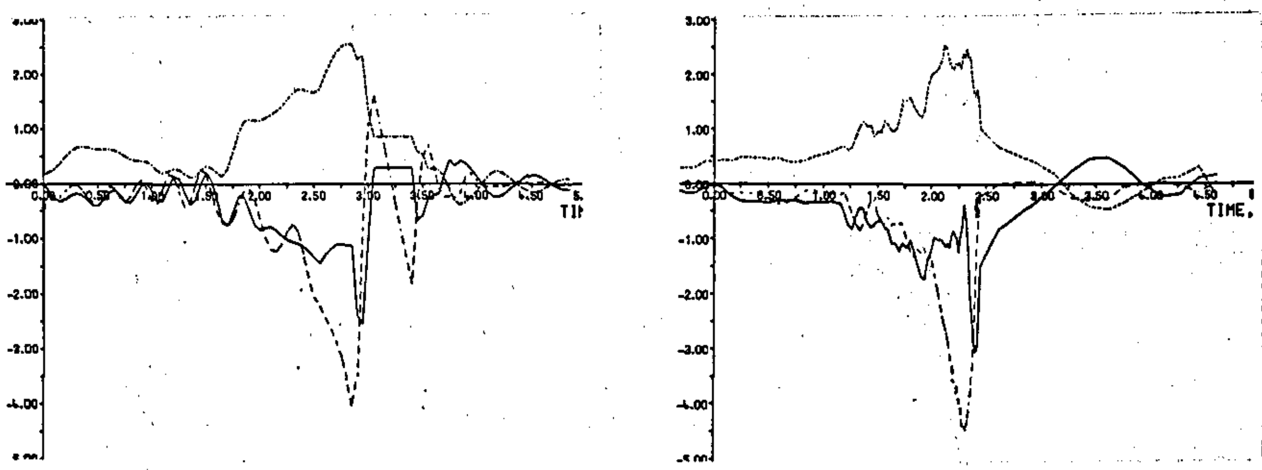

Fig. 7.9 Velocities for Run 1. Bank angle 22.9 deg.

error, probably due to inaccurate measurement of roll angle; there is no contact in this period and the roll velocity must be constant.

7.2.4. Initial impact point

In most of the overturns the top side of the tyre/rim and the ROPS (points 2, 4, 8, Fig.3.3 impact the ground at about the same time, causing a rapid decrease in vertical and roll |velocities| (Figs.7.1-7.3, 7.6 and 7.7) In some cases, however, the roll angle at impact is less and the wheel hits the ground before the ROPS, particularly at the intermediate bank slopes of 15° and $22\frac{1}{2}^{\circ}$. If the bottom of the wheel impacts first (points 6, 10, Fig. 3.3), the high negative roll moment results in a peak |roll velocity| immediately before ROPS impact (Fig.7.9). If the top of the wheel hits first, the friction force generated by the ground impact also gives a negative roll moment, but of lower magnitude (Figs.7.4a, 7.5).

7.2.5. Behaviour during impact

The velocities are not predicted as well during impact as before it (Figs.7.2-7.9). In general, the simulations show higher peaks of shorter duration than the experimental results. The displacements, however, are in better agreement (e.g. Fig. 7.1).

These effects have been discussed in general in 7.1.2. In addition, the following aspects are relevant:

(i) The rim damping coefficient effects not only the vertical force at the rim but also the lateral force due to soil friction. This influences the roll moment and subsequent roll motion. Although coulomb friction cannot easily be incorporated into the model, more accurate simulation might have resulted from a steeper elastic recovery stiffness for the rim, together with lower viscous damping.

(ii) The elastic stiffness of the ROPS was assumed to be the value predicted by structural analysis. The value measured in the laboratory impact tests was significantly lower; had this been used instead, the elastic ROPS energy would have been higher and the impact time longer. Roll oscillation after impact would probably then have been of lower frequency, as in the experimental results, because of the greater effect of wheel forces during this longer ROPS impact.

(iii) The mass of the top frame supported by the structural uprights was included in the measurement of tractor roll moment of inertia; it is therefore assumed in the simulation to contribute to the inertia of the "rigid" part of the tractor. During impact, however, this mass is displaced laterally relative to the tractor and appears between the stiffness of the uprights and that of the ground. Most of the kinetic energy due to lateral velocity (in tractor coordinates) of this mass is dissipated in soil deformation. This probably results in a longer impact and lower roll oscillation.

7.2.6. The effect of bank angle, α

The differences in general behaviour evident in Figs. 7.2 - 7.7 are surprisingly small. The duration of the main overturning phase, between the point where the downslope tyre leaves the chamfer and impact, increases steadily with increasing α. The only other noticeable effect is a reduction of peak |roll velocity| between $\alpha = 0$ and $15^\circ - 22\frac{1}{2}^\circ$, followed by an increase at larger α. This is caused by the unstable dynamic equilibrium being reached at a lower roll angle with increasing α, as discussed in 7.1.1, together with the effect of intermittent contact, discussed in 7.1.1. and 7.2.3.

A variation not evident from the figures is the final resting position of the tractor. The simulations predicted that the downslope tyre (point 10) would remain on the bank slope in runs 6 ($\alpha = 30$) and 7 ($\alpha = 37\frac{1}{2}$); in run 5 ($\alpha = 30$) it was found to "rattle" in the corner between the slope and the ground (Appendix 3.1); in all other cases, the wheel lay flat on the ground after impact. All these predictions were confirmed by the experimental results.

The experimental results have been summarised in terms of instantaneous values of the dynamic variables after a fall in the height of the centre of mass (y_g) of 1.5m from its initial value. The reasons for the choice of this measure and its limitations are described in 5.2.3. These results are given in Fig. 7.10, together with the predictions, for those tests in which "standard" conditions apply to the parameters affecting overturning. The effects on roll velocity noted above are apparant in both predicted and experimental values, and these are reflected in the roll angles. Lateral and vertical velocities show neither such clear effects nor such good agreement. although the trends of predicted and experimental results are similar but displaced with respect to α. The causes of the discrepencies in run 16 ($\alpha = 0$) and run 12 ($\alpha = 22\frac{1}{2}$) have already been explained in 7.2.3.

7.2.7. <u>The effects of other parameters</u>

Bank friction (Figs.7.1 and 7.5) has the expected effects of reducing overturning time, particularly in the initial phase, and increasing all the velocities. It is perhaps surprising that such a large change in limiting friction (0.14 to 1.0) changes the velocities by only 20 - 30%. This further demonstrates the importance of ride motions, tyre relaxation and intermittent loss of contact in influencing the overall behaviour.

The effect of a wider track is shown in Fig.7.11(run 18) and of changes in the inertial parameters due to ballasting in Fig.7.12(run 25). Behaviour in standard conditions at the bank slope of $22\frac{1}{2}^{\circ}$ applying to both these cases is shown in Fig.7.5.

Increased track width has a similar effect to increased bank slope, and for the same reasons given above (Figs.7.6 and 7.7). The relatively small changes in centre of mass position and moment of inertia had little effect on the overall behaviour, but the increased mass caused some change in tyre

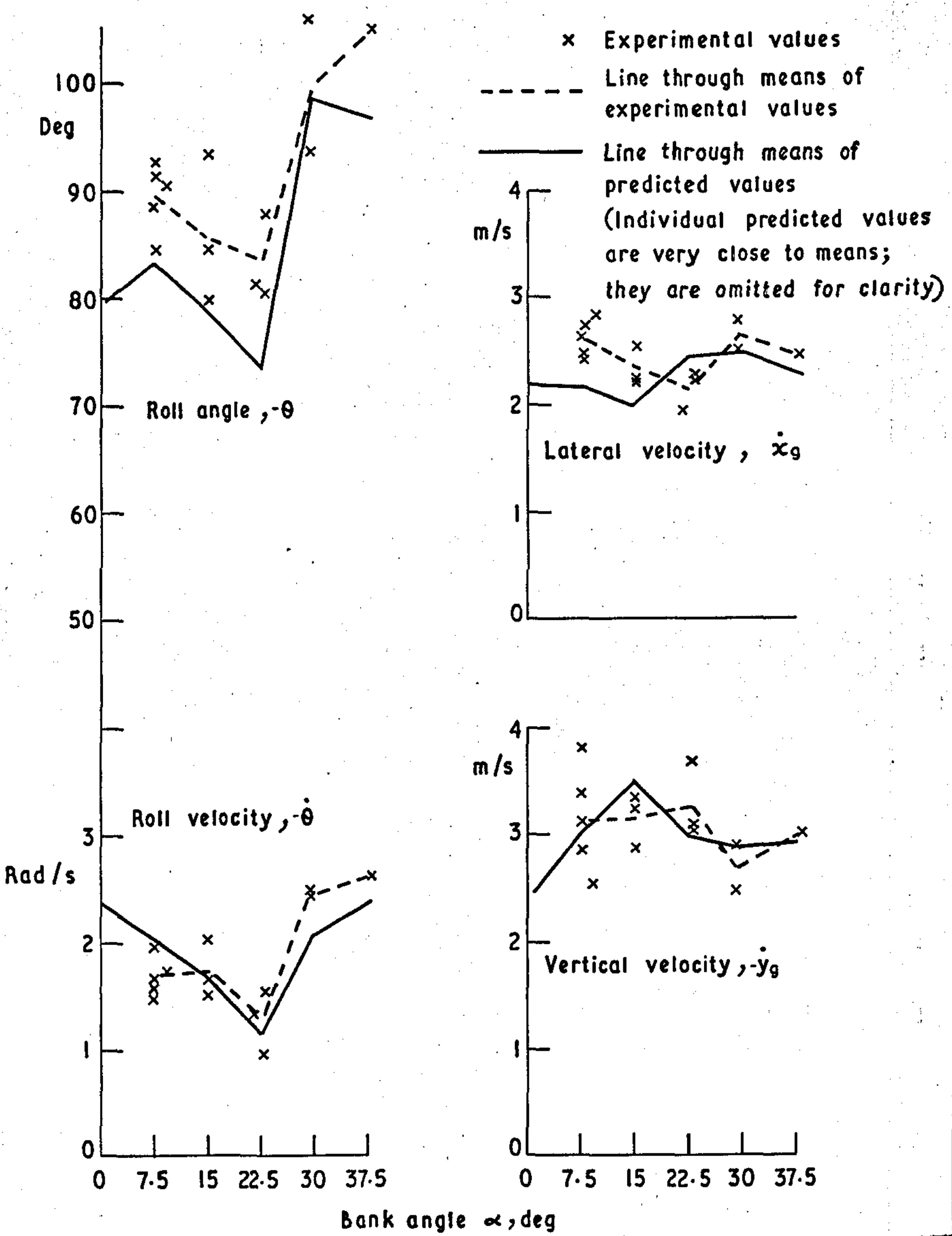

Fig. 7.10 Values at a centre-of-mass fall of 1.5m vs. α, for overturns in 'standard' conditions. (Nos 1-12, 16, 19, 20, excluding experimental values for No 16 and predicted values for No 12, as explained in the text)

SIMULATION EXPERIMENT

.... Lateral, m/s
- - - - - - Vertical, m/s
———— Roll, rad/s

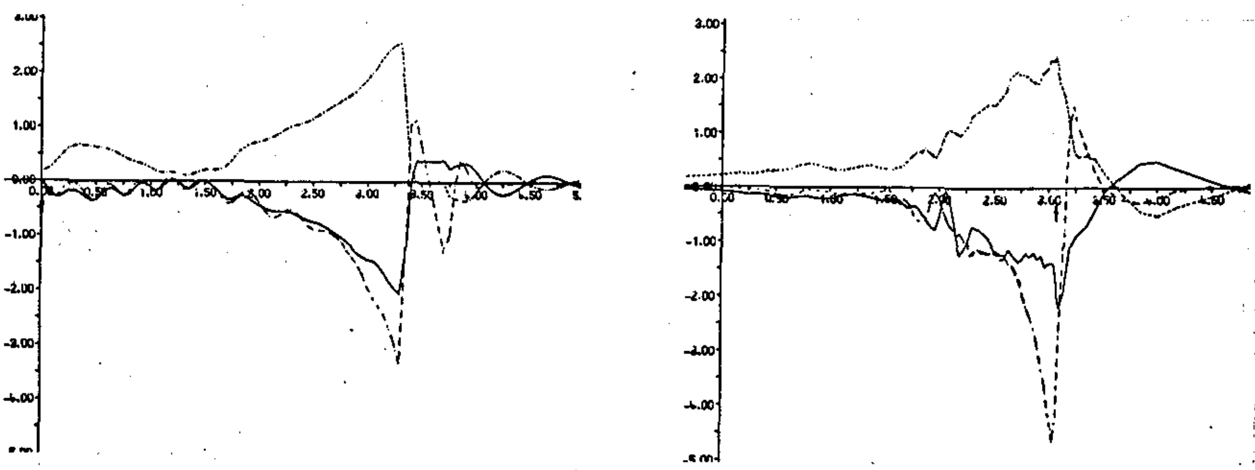

Fig. 7.11 Velocities for Run 18. Wide track, bank angle 21.4 deg.

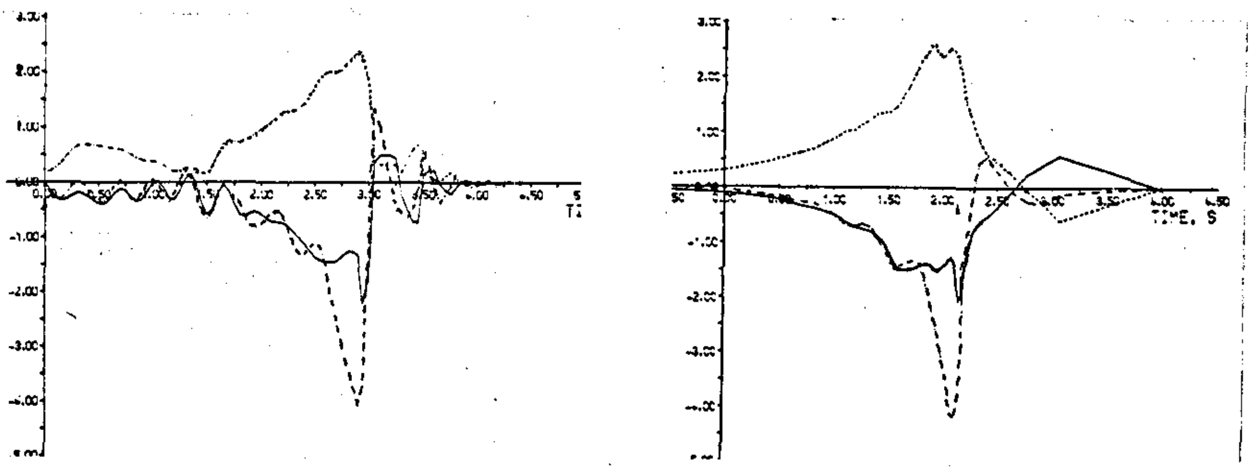

Fig. 7.12 Velocities for Run 25. Ballasted, bank angle 21.4 deg.

oscillation and impact behaviour.

7.2.8. Experimental variation

Two further examples of behaviour in standard conditions are included to help put the above comparisons in perspective. The nominal overturning conditions in Fig.7.13 are the same as those in Fig.7.3 ($\alpha = 7\frac{1}{2}^{\circ}$) and in Fig.7.14 the same as those in Fig.7.4 ($\alpha = 15^{\circ}$) except for the front axle stop. Differences are evident, particularly in the amount of oscillation.

Considerable care was taken in the control of the experiments, and repeatability is thought to be better than in any similar tests. Even so, it is apparant that forward speed and steering movements were not controlled as precisely as they should have been to provide the most reliable results. In addition, the film analysis technique was only just capable of giving resolution in time and displacement adequate for the determination of velocity.

7.3. QUANTITATIVE COMPARISONS

The instantaneous variable values have already been presented for the "standard" conditions as a function of bank slope in Fig.7.10. It is not practicable to do this for other parameters because of the very small number of experiments in which each was varied from its standard value. In addition, many parameters had only small effects in relation to that of, for example, the bank height, which was measured but not closely controlled. Instead, instantaneous predicted values are plotted against their experimental equivalents for all runs in Figs.7.15-7.22. Values at a centre-of-mass fall of 1.5 m are shown in Figs.7.15 (roll angle), 7.16 (roll velocity), 7.17 (lateral velocity), 7.18 (vertical velocity) and 7.19 (kinetic energy). Values at impact are shown in Figs.7.20 (roll angle) and 7.21 (total energy above that in final resting position). The maximum instantaneous energy absorbed in sideways deformation of the ROPS is shown in Fig. 7.22.

The causes of the disagreements in runs 12, 16, 17 and 18 have already been explained; some other cases deserve special mention:

SIMULATION EXPERIMENT

.... Lateral, m/s
- - - - - Vertical, m/s
———— Roll, rad/s

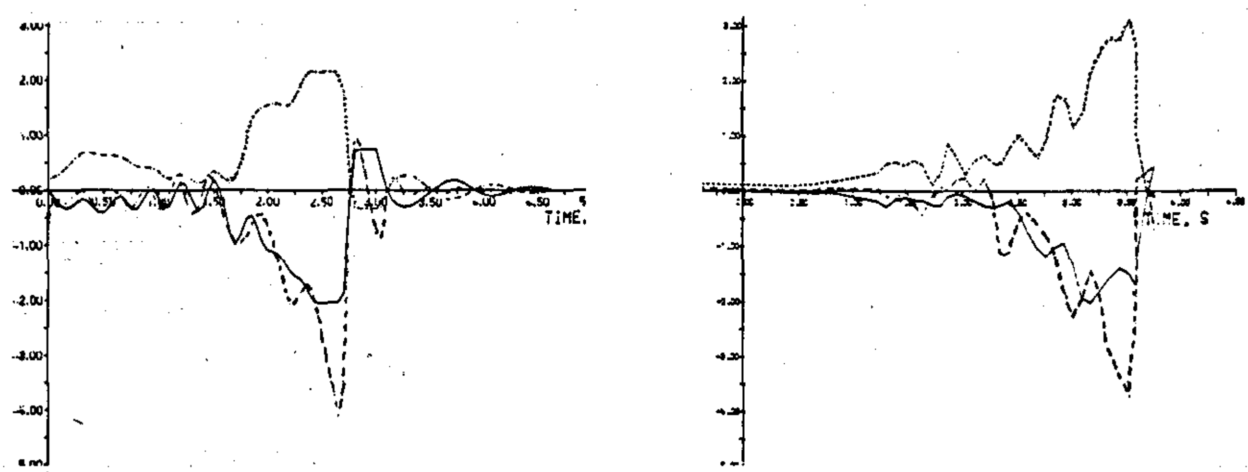

Fig. 7.13 Velocities for Run 11. Bank angle 7.7 deg.

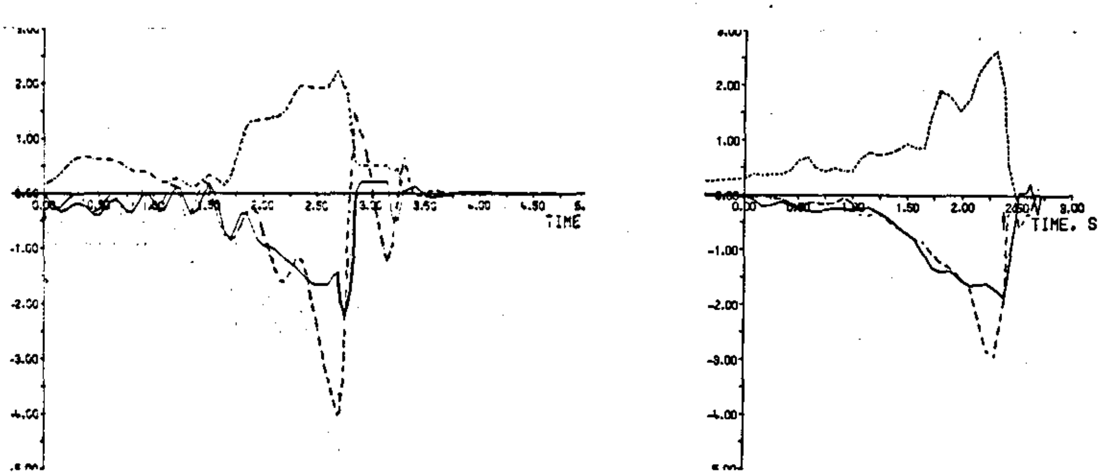

Fig. 7.14 Velocities for Run 9. Bank angle 15.1 deg.

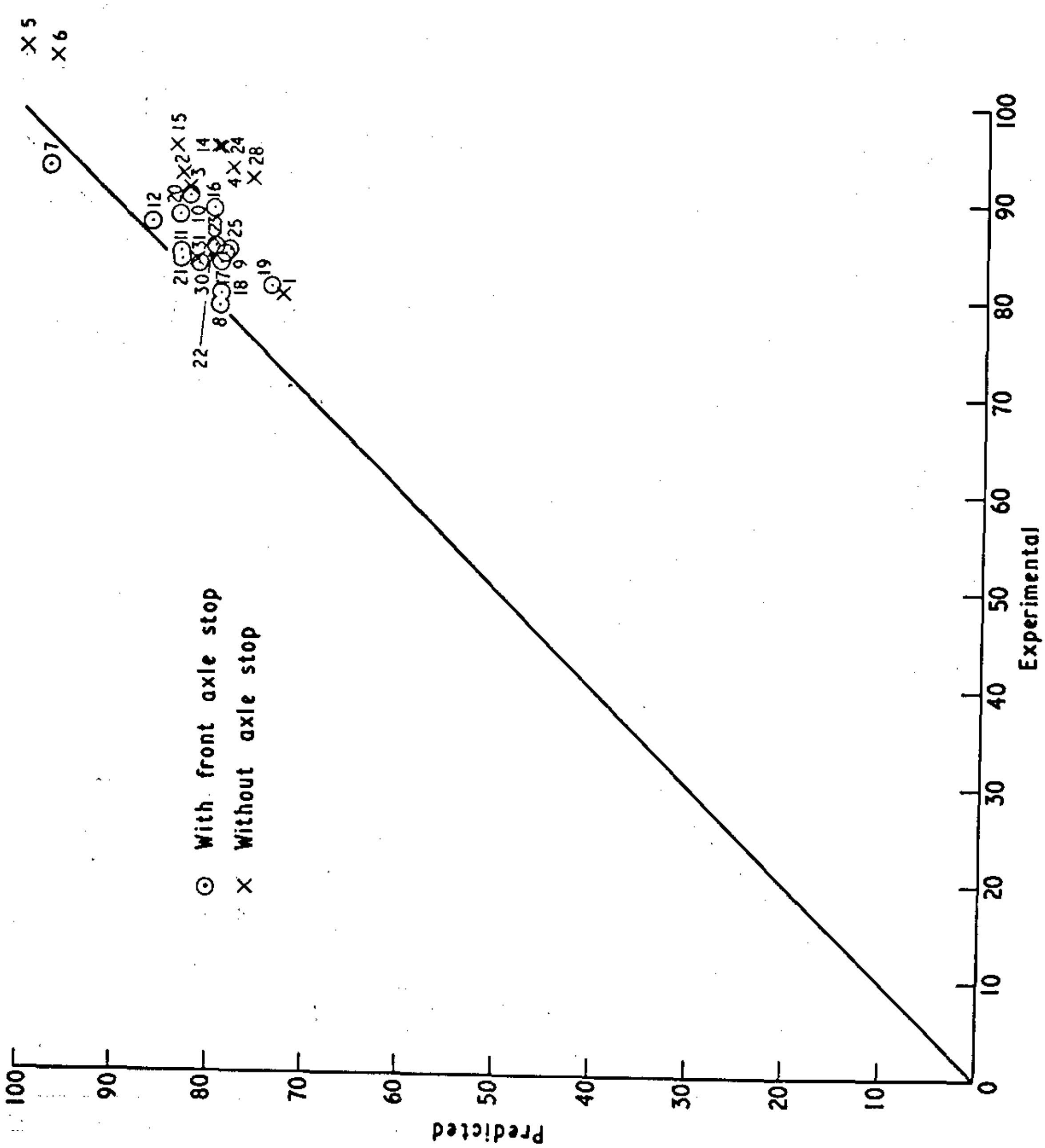

Fig. 7.15 Roll angle at a centre-of-mass fall of 1.5m.(deg)

O With front axle stop

X Without axle stop

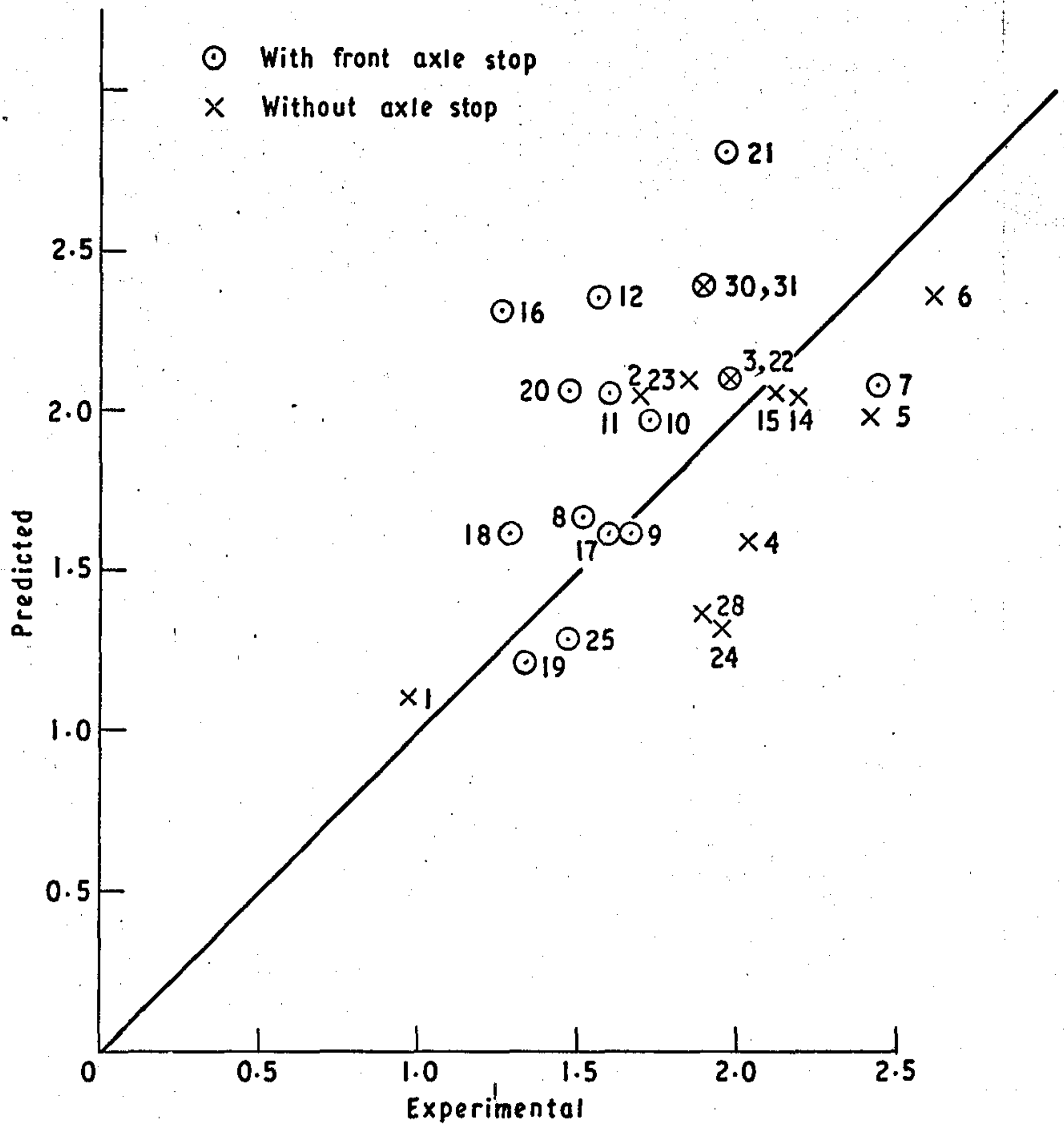

Fig. 7.16 Roll velocity at a centre-of-mass fall of 1.5m. (rad/s)

O With front axle stop

X Without axle stop

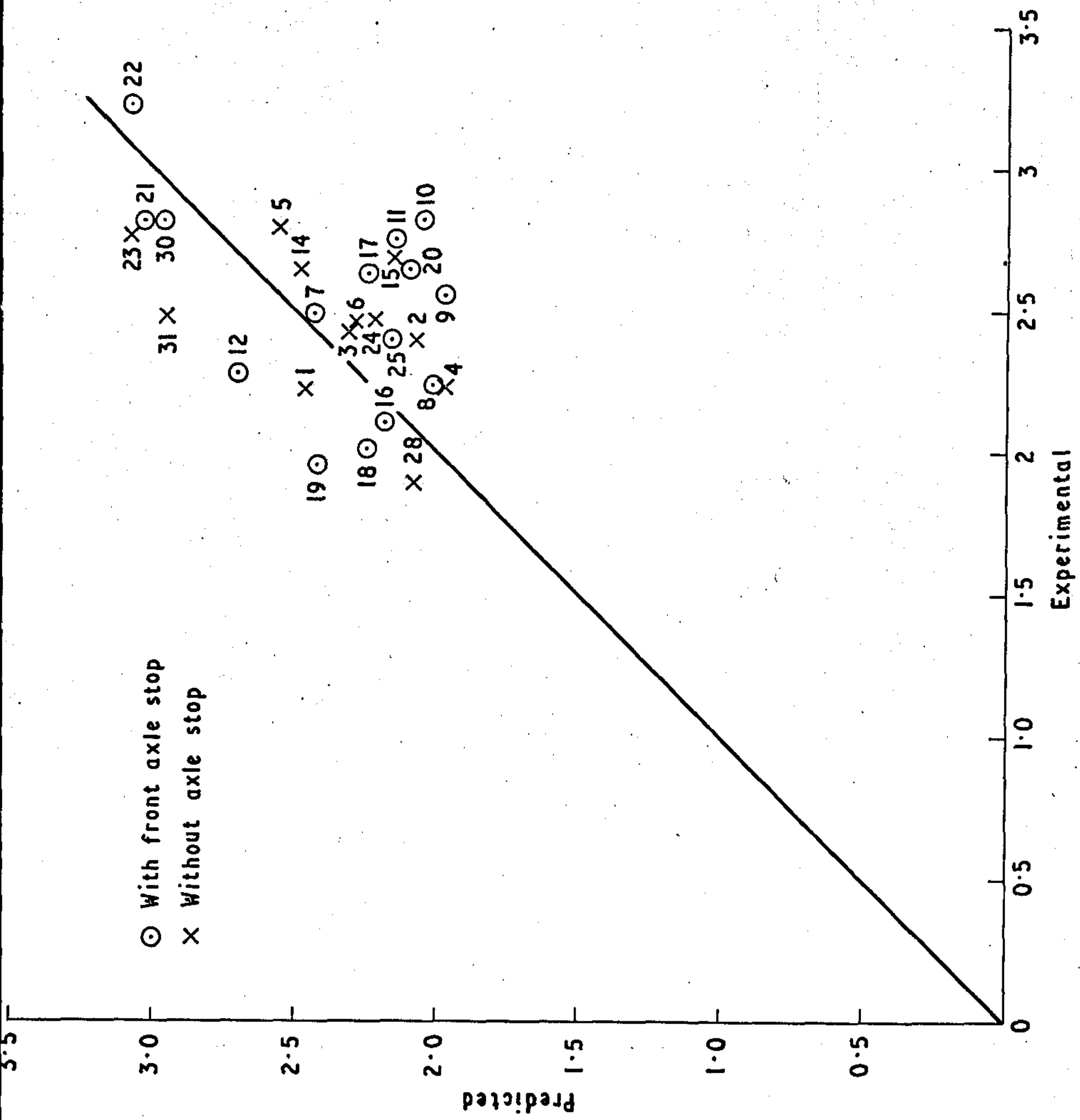

Fig. 7.17 Lateral velocity at a centre-of-mass fall of 1.5m. (m/s)

O With front axle stop

X Without axle stop

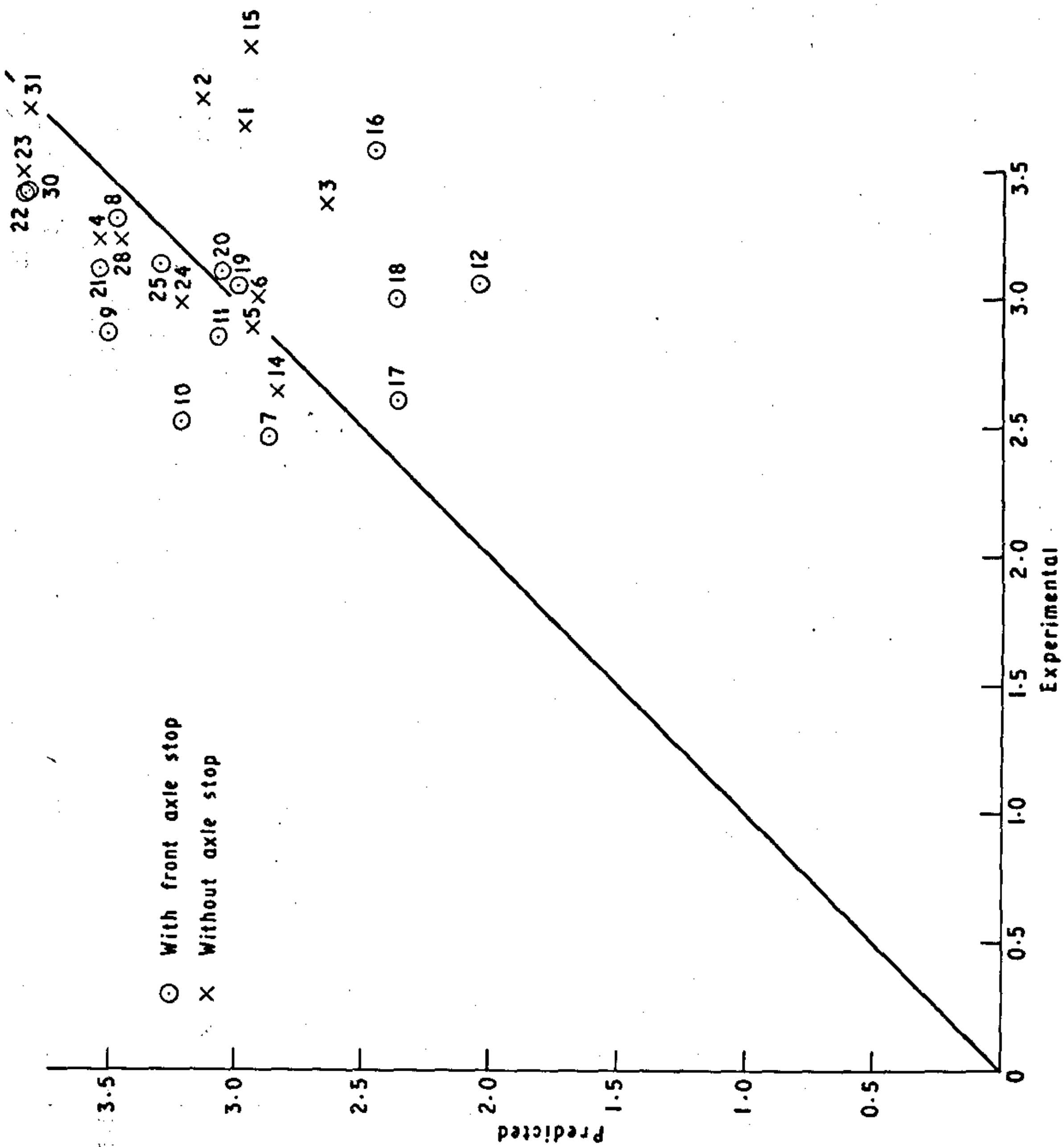

Fig. 7.18 Vertical velocity at a centre-of-mass fall of 1.5m. (m/s)

O With axle stop

X Without axle stop

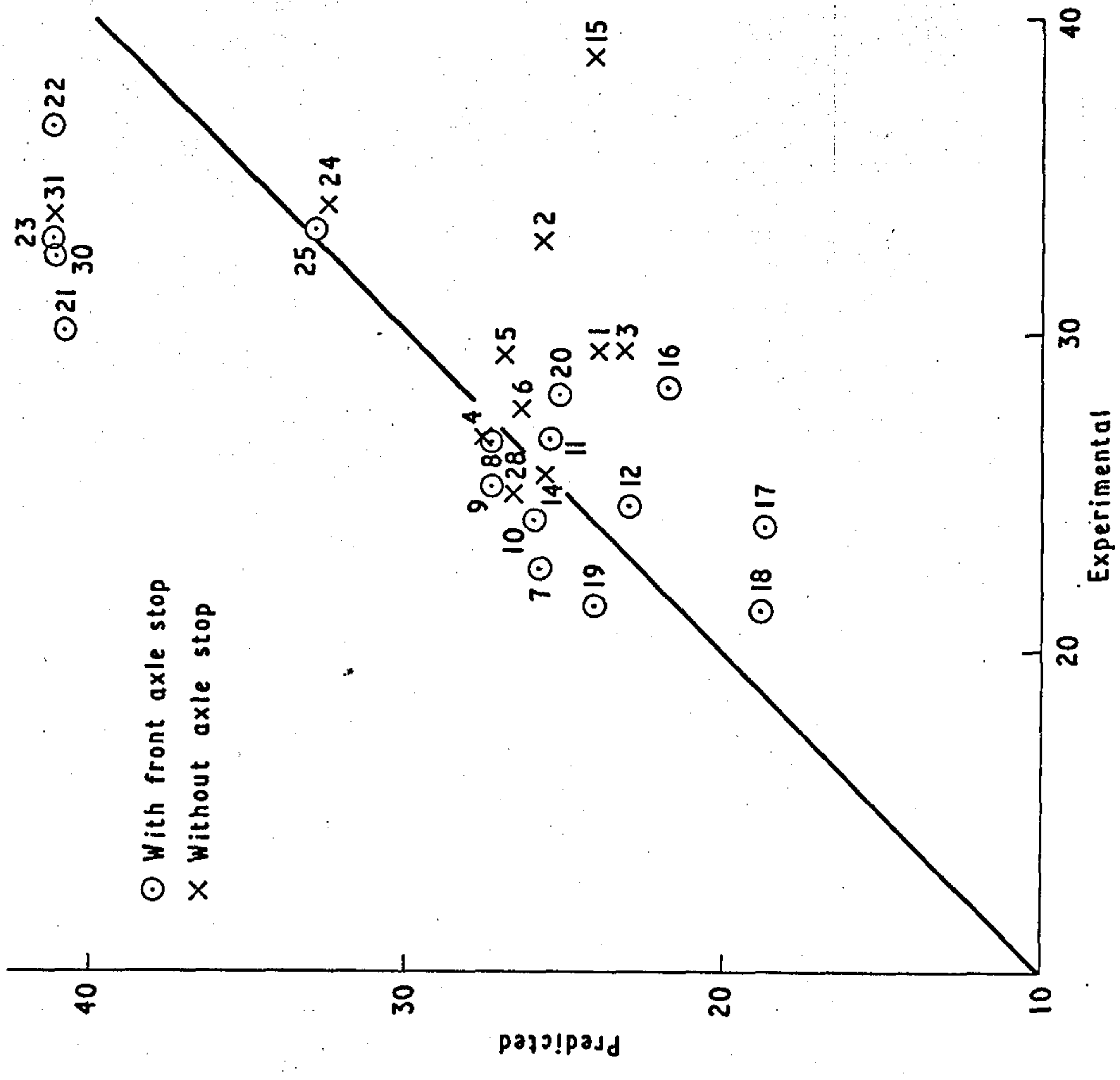

Fig. 7.19 Kinetic energy at a centre-of-mass fall of 1.5m. (kJ)

O With front axle stop

X Without axle stop

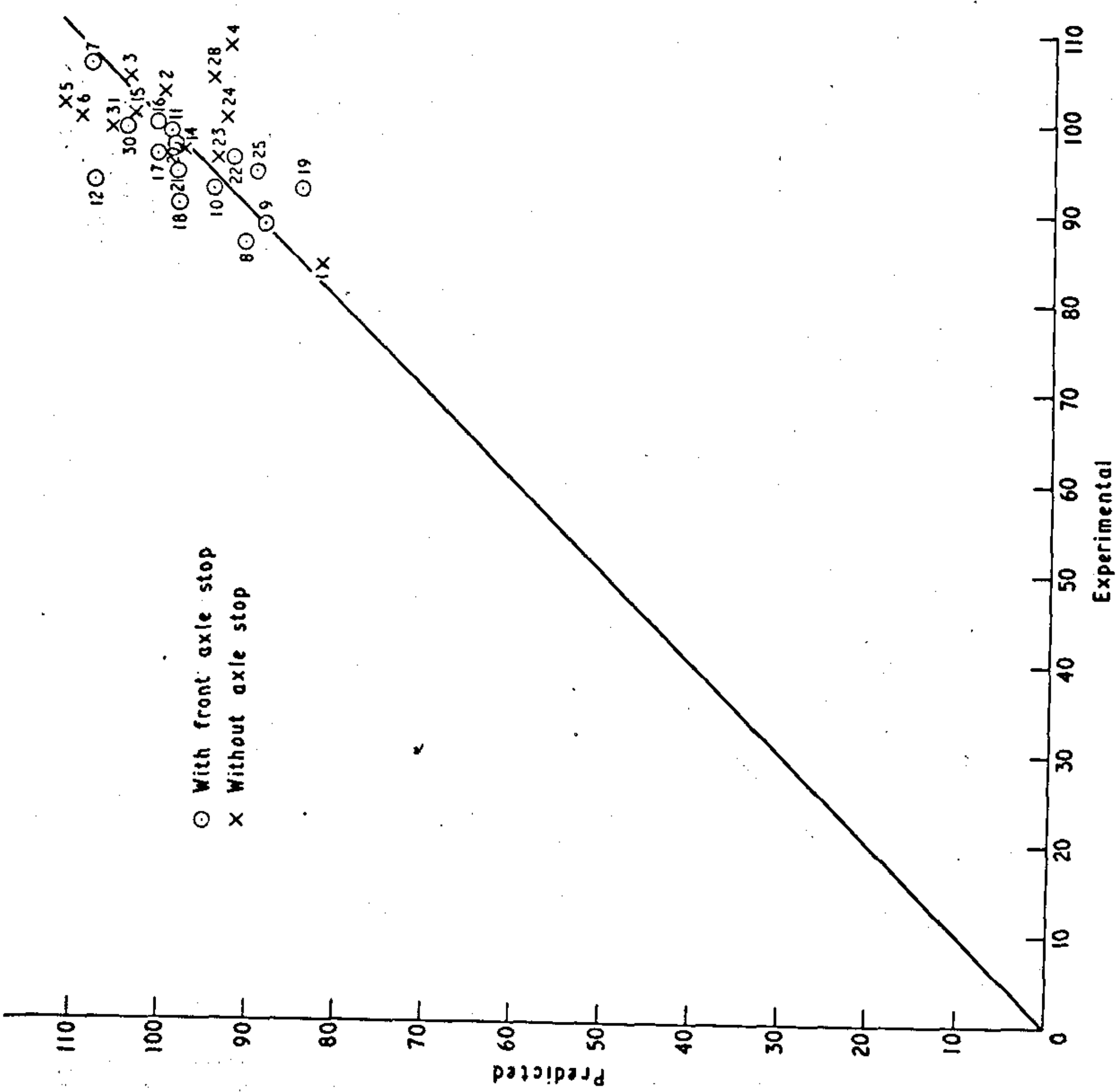

Fig. 7.20 Roll angle at impact (deg.)

O With front axle stop

X Without axle stop

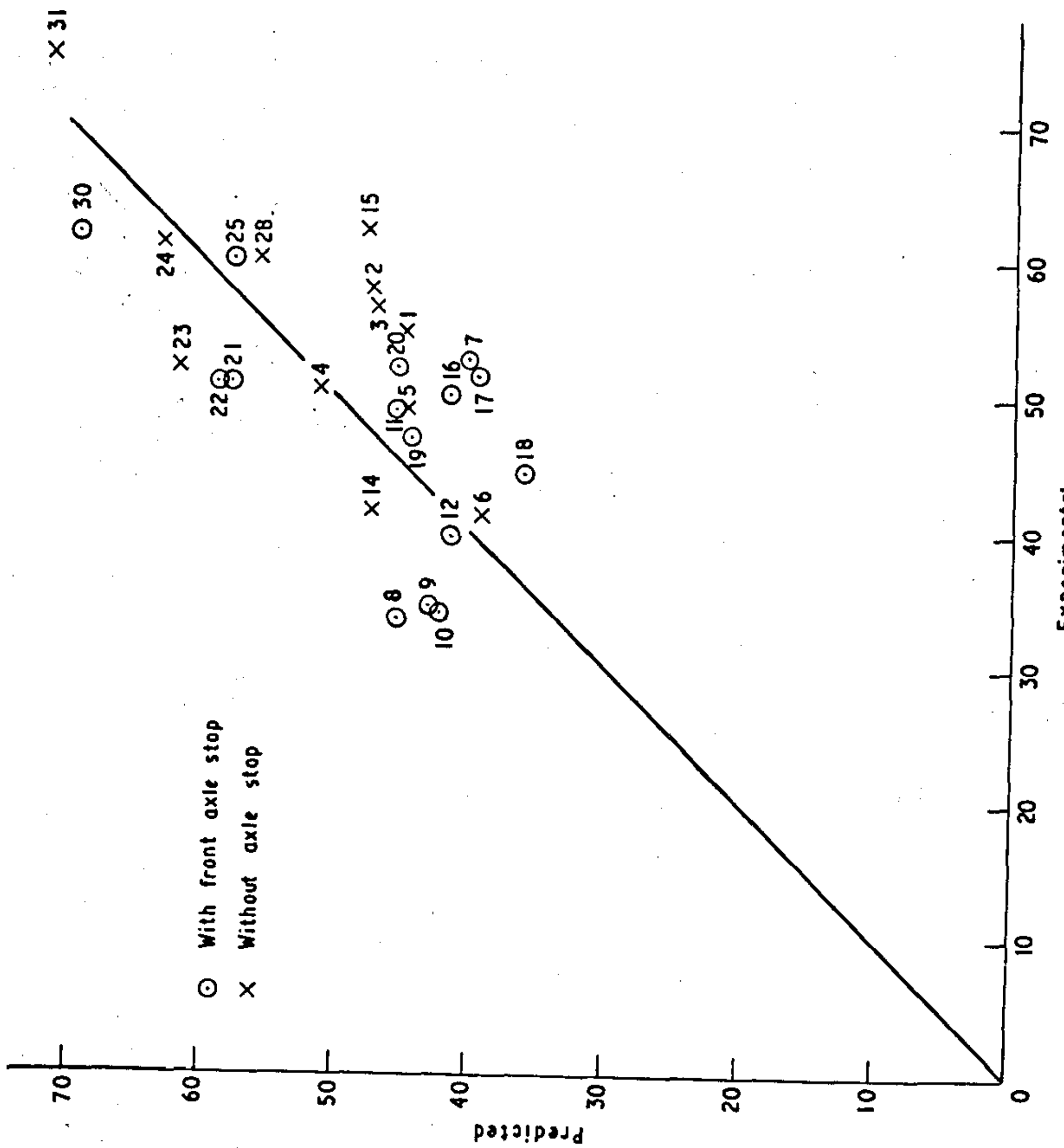

Fig. 7.21 Total energy at impact above that at final rest (kJ)

O With front axle stop

X Without axle stop

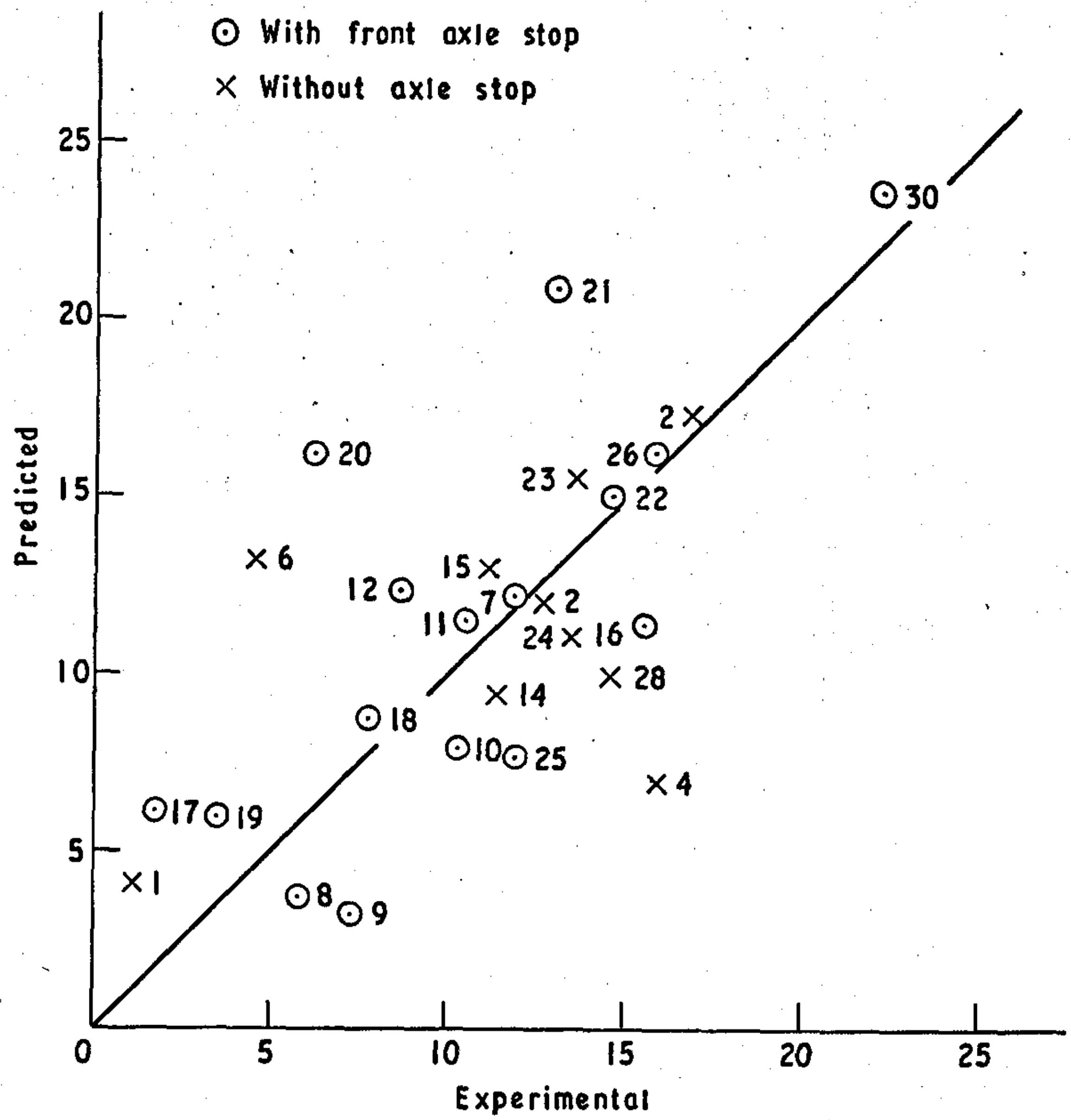

Fig. 7.22 Maximum instantaneous energy absorbed in sideways ROPS deformation (kJ)

O With front axle stop

X Without axle stop

(i) Differences in temporary loss of contact between test and simulation are also responsible for disagreement in roll angle in runs 4 and 24, and for disagreement in vertical and roll velocities in runs 20 and 21. In these cases, the energy absorbed is affected by these differences in overturning behaviour.

(ii) Instantaneous values compare well in general but there are cases when they happen to fall on the peak of an oscillation in the simulation and not in the experiment, or vice versa. This is the cause of disagreement in lateral velocity in runs 10, 11, 19 and 23, in vertical velocity in runs 10 and 22, and in roll angle and velocity in run 28.

(iii) In some experiments, particularly the first few, the yaw angle at impact was relatively high. Impact occurred slightly earlier than would otherwise have been the case, and the ensuing behaviour was more influenced by the forces at the front of the tractor. This is the cause of low angles at impact in runs 5 and 6, and may be responsible for disagreement in absorbed energy in these cases and in run 1 (energy was not recorded in run 5 because of an equipment fault)

(iv) In the one experiment at twice the standard forward speed, run 15, the measured vertical and lateral velocities are significantly higher than the predicted values (Figs. 7.17 7.18). It appears from the film of the experiment and from the measured yaw velocity that the driver applied a late steering correction while the downslope wheels were on the chamfer. Normally, small steering adjustments made while the tractor approached the edge were sufficient to ensure an appropriate path, and no further changes were made once the overturn had begun. In this case, however, it had become apparant that the tractor would overshoot the overturning area, because of the higher speed, unless late action was taken.

The large yaw angle combined with higher forward speed gave a high initial lateral velocity. This caused premature loss of contact, which largely explains the difference in predicted and measured velocities.

7.3.1. Statistical tests

Visual inspection of Figs.7.15-22 indicates that the comparisons are sufficiently good to justify being tested statistically. The choice of a suitable test, however, is complicated by two features of the results:

(i) The effect of parameter variation was much smaller than had been expected, giving a small range of values about the mean for most variables.

(ii) Neither the set of experimental values nor the set of simulated values can be considered as a truly independent variable. The predicted set is chosen conventionally, but in this case it is subject to errors in parameters, which have been seen to result in effects of similar magnitude to errors in measurement or initial conditions in the experiments.

Without these limitations, a linear regression would be the obvious method of obtaining a measure of correlation. To illustrate the problem, consider a set of experiments and simulations with nominally identical conditions but in the presence of parameter and measurement errors. This would result in a cluster of points randomly distributed about a "true" value, of which both the simulated and experimental values were estimates.

Linear regressions would not be significant and yet, if the errors were small, the agreement must be good.

The coefficient of variation is a measure which overcomes this difficulty but interpretation of the value obtained is only intuitive. An alternative in this case is to fit a linear regression which is forced through the origin. This could be expected to provide an appropriate solution to the above example but caution is needed in interpreting the level of significance. Normally, a fit through the origin is accepted only if the intercept found in a natural regression is not significantly different from zero.

Finally, because the real case is not so extreme as the hypothetical example, it is possible to fit natural regressions. No method of giving equal weight to errors in both variables x and y is available in classical statistics but a technique sometimes used is to take a geometric mean of the slopes found by regressing y on x and x on y.

Results of these three types of analysis for the most important variables are given in Table 7.1.

These results confirm that the correlations are significant. The mean slopes are similar for the two types of regression, except for lateral velocity, and the values are close to unity. Not surprisingly, the regressions forced through the origin pass very close to the centroid of the points, $\bar{x}$, $\bar{y}$. The coefficient of variation for ROPS side energy is rather large, but this is expected because it is additionally subject to errors in impact, whereas the other variables include only errors during overturning.

All the data were used to calculate these statistics. The correlations would, of course, have been better after the removal of "rogue" data, where disagreement was known to have been caused by shortcomings in the experiments or analysis.

TABLE 7.1

Statistical tests of the comparison between predicted (x) and experimental (y) values for all tests

	Roll Angle $-\theta$, deg	Roll Velocity $-\dot{\theta}$ rad/s	Lateral Velocity $\dot{x}_g$, m/s	Vertical Velocity $\dot{y}_g$, m/s	ROPS Side energy, kJ
1. Natural Regressions					
Mean x (simulation)	82.1	1.916	2.404	3.110	11.68
Mean y (experiment)	88.8	1.786	2.496	3.182	10.82
Slopes(i) y on x	0.655	0.365	0.391	See Note (ii)	0.627
Slopes(i) x on y	1.675	2.285	1.935		1.420
Slopes(i) Mean	1.048	0.914	0.870		0.944
Significance	P<0.001	P<0.05	P<0.01		P 0.001
2. Regressions forced through the origin					
Slopes(i) y on x	1.080	0.907	1.025	1.006	0.877
Slopes(i) x on y	1.085	0.956	1.045	1.033	0.985
Slopes(i) Mean	1.082	0.931	1.035	1.019	0.929
Significance	P<0.001	P<0.001	P<0.001	P<0.001	P<0.001
3. Coefficient of variation(iii)					
	10%	24%	16%	16%	37%

Notes (i) The slopes quoted are y/x in all cases

(ii) The intercepts from natural regressions were significant ($P < 0.05$) for all variables except vertical velocity; in this case the results for the natural regressions are omitted.

(iii) Coefficient of variation is defined as $\dfrac{\sqrt{\Sigma(y-x)^2}}{\Sigma(\bar{x}+\bar{y})/2} = \dfrac{2n\sqrt{\Sigma(y-x)^2}}{\Sigma x + \Sigma y}$

7.3.2. Energy absorbed in impact

The energy absorbed in sideways deformation of the ROPS is the most important result of this study, and it was the only part of the absorbed energy that could be measured in the experiments.

Soil deformation was not measured directly but may be estimated in some cases from photographs. In hindsight it is unfortunate that an attempt was not made to overcome the problems of irregular soil surfaces to obtain estimates on site.

Soil deformations predicted by the simulations are in general significantly less than the estimates from photographs. This may be due partly to inadequate measurement of soil strength, but the inertia of the top frame, mentioned in 7.2.5, is thought to be the main cause. If all the kinetic energy due to the top frame's lateral velocity, in tractor coordinates, is assumed to be absorbed in the soil, the additional deformation calculated from soil strength largely accounts for the difference in typical estimated and predicted values.

The addition to the predicted soil deformation energy must be accompanied by a reduction in other energies. If the top frame lateral inertia is considered separately in this way, the effective mass and roll moment of inertia of the tractor must be reduced by the appropriate amounts, and energy absorbed by the wheel, and particularly by the ROPS, would be expected to be smaller. Energy absorbed in sliding friction may also be affected.

It is not valid to run the simulations directly with the smaller tractor inertial parameters, because these apply only in impact and not during overturning. In any case, other impact parameters were adjusted empirically, as described in 7.1.2. and 7.2.5. A lower value of rim damping coefficient, as suggested, would probably have increased the ROPS energy in most cases. In addition, the proportion of total mass ascribed to the rear of the tractor in the simulations (see 7.1) was appropriate to the vertical plane containing the rear axle. This is clearly suitable in impact as well as in overturning as far as forces on the tyre and rim are concerned. The mid point of the two ROPS impact points, however, is further forward by about 17% of the wheelbase, and this must affect the proportion of kinetic energy due to linear velocities that is absorbed in the ROPS.

The slopes of the regressions in table 7.1 indicate that, on average, the measured ROPS sideways energy was 93% of the predicted value. It is not certain what combined effect the above limitations would have on this value but it is likely that the predicted energy would turn out to be slightly lower, rather than slightly higher than the measured one, if they could be taken into account. For the simulations to be valid it is necessary that the absolute level of predicted energy is reasonably accurate, but it is more important that the effect of parameter changes is correct. The limitations have a broadly similar effect in all cases, and may therefore be accepted without seriously weakening the power of the model.

7.4. GENERAL DISCUSSION

There are no generally accepted standards for judging the adequacy of simulations of this type. Clearly, less close agreement can be expected in this case, where the dynamic behavior is very complicated and the validation involved full scale experiments, than in simpler, laboratory studies. The comparisons described above, however, show that the model is capable of predicting both qualitative and quantitative effects found in the experiments.

The final criterion for acceptance must relate to the model's intended purpose. The main requirement was the prediction of the effects of parameter changes in a particular kind of overturn, and the results give confidence in the model's ability to do this. The effects of, for example, yaw angle cannot be predicted but equally it would be an enormous task to attempt to simulate every possible type of overturn.

The two-dimensional nature of the model certainly restricts its scope and does have some limitations in describing the behaviour in the present experiments, even though this was itself predominately two-dimensional. It is considered, however, that the limited knowledge of tyre and impact parameters has at least an equal effect, and that a three-dimensional model would have corrected only some of the discrepencies.

experiments, even though this was itself predominately two-dimensional. It is considered, however, that the limited knowledge of tyre and impact parameters has at least an equal effect, and that a three-dimensional model would have corrected only some of the discrepencies.

8. PARAMETER SENSITIVITY ANALYSIS

After development and validation, the model was put to two main uses: an investigation of the effect of parameter variation, described here, and simulations using data for individual real tractors, described in the next section. The sensitivity analysis was needed to enhance the understanding of the behaviour given by the study of individual simulations; it was also important, however, because of the limited accuracy to which some parameters were known, particularly in the case of real tractors.

8.1. OUTPUT VARIABLES

The most important variable was the energy absorbed in deformation of the ROPS. This gave only a limited description of the complex overturning and impact process, however, and a more informative picture was obtained from the distribution of energy dissipation.

The kinetic energy (KE) at the start of a simulation was generally very small (< 0.1 kJ)*. The simulations were not halted until 2s after impact to allow bouncing motion to cease, and the final KE was also generally negligible. Thus the energy input was the loss of potential energy (PE) in falling down the bank, which depended not only on the bank height but also on the difference between the height above ground of the centre of mass at the beginning, when the tractor was upright, and at the end, when it was on its side and supported by the deformed wheel and ROPS. These heights varied slightly according to the simulation conditions, but the differences were generally small.

---

*Initial KE was that due to lateral velocity as tractor approaches bank edge; KE due to tractor forward speed was not included in the two dimensional simulation, but was typically about 2 kJ in the experiments.

The distribution of energy was classified as follows (the shorthand notation used in the figures is given in parentheses:

(i) Energy dissipated in sliding friction between tyres and bank surfaces (μ_B).

(ii) Energy dissipated in tyre damping + energy stored in elastic tyre deformation (up to impact) (TYRE).

(iii) Energy dissipated in sliding friction between tractor points (ROPS, wheel, tyre) and soil (μ_s).

(iv) Total energy dissipated in soil vertical deformation at all impact points (SOIL).

(v) Energy dissipated during impact in tyre and wheel deformation and damping + difference in energy stored in elastic deformation between final value and value at impact (WHEEL).

(vi) Energy dissipated in ROPS deformation (ROPS).

The sum of these energies was less than the PE loss calculated from the total tractor weight, because the simulations applied to the rear part of the tractor, as explained in section 7; the difference was the implied total energy dissipation at the front part (figure notation: FRONT). (The internal energy balance for the simulated inertia was automatically checked as descibed in 3.5.3).

Energy (ii) above was small but it was excluded from (v) to allow clear distinction between the energies dissipated before and after impact.

To acheive an overall energy balance, the dissipations (iv), (v) and (vi) due to deformation were the net final values, taking account of elastic recovery. The most important ROPS energy was that at maximum deflection, but since the energy recovered elastically was fairly constant between simulations, the final energy was a satisfactory measure for comparisons in most cases.

8.2. PARAMETERS

There were about fourty parameters that could influence the behaviour. Some, such as bank slope and height and parameters governing the tyre side forces, were effective only during the overturning phase; others such as ROPS, wheel and soil structural characteristics affected only the impact behaviour; and a third class, the tractor inertias and geometry, were important in both.

Even with the economy of simulation, it was not practicable to study the effect of many parameters in combination. The basis of the sensitivity analysis was a small number of "standard" conditions typical of those studied experimentally. Each parameter was then varied in turn for several values on either side of its standard value.

For the parameters which influenced the overturning phase, six standard conditions were chosen, representing bank angles (α) of $0 - 37\frac{1}{2}$ in $7\frac{1}{2}^{\circ}$ steps. It was hoped that this would help to average the effects of discontinuities due to loss of tyre contact and provide an overall indicator of parameter sensitivity, in addition to showing the variation with α.

A single standard set of conditions (designated by "A") was adequate for most parameters which affected only the impact dynamics, since these were generally well behaved. In these cases, the simulations were started with the tractor in free flight just above the soil, with position and velocity vectors approximately equal to those at the end of the overturning phase with a $7\frac{1}{2}^{\circ}$ bank angle.

The roll angle of the tractor at impact had an important bearing on the effect of some parameters, however, and in these cases two standard sets of impact conditions were used (designated by "C" and "D"), identical except for impact roll angle. If simulations with different initial roll angles had been started immediately before impact, the initial centre of mass heights, and hence potential energies, would not have been the same. This applied equally to simulations with different ROPS width, for example. The input energies were therefore equated by starting these simulations with a uniform centre of mass position, high enough to be significantly before impact in all cases; resulting variation of impact velocity was accepted as of less importance than variation of input energy.

TABLE 8.1

Standard parameter values and initial conditions for sensitivity study

(a) Values common to all standard conditions

Bank height	:	2.25m
Centre of mass height	:	0.894m
Track width	:	1.54m
Tyre height (dia)	:	1.44m
Tyre width	:	0.29m
Rim height (dia)	:	0.91m
ROPS height	:	2.26m
ROPS width	:	1.372m
Rim deflection limit	:	0.2m
Tractor mass	:	3065 kg
Effective rear mass	:	1960 kg
Polar moment of inertia	:	1255 kg m^2
Vertical tyre stiffness	:	400 kN/m
Lateral tyre stiffness	:	120 kN/m
Vertical damping coefficient	:	3 kNs/m
Lateral damping coefficient	:	1 kNs/m
Rim collapse force	:	26 kN
Rim elastic stiffness	:	179 kN/m
Rim damping coefficient	:	20 kNs/m
Cone indices: at surface	:	632 kN/m^2
at 76 mm	:	1186 kN/m^2
at 152 mm	:	1309 kN/m^2
at 229 mm	:	1400 kN/m^2
Effective impact areas: ROPS	:	0.1 m^2
Tyre point	:	0.2 m^2
Rim point	:	0.2 m^2
Limiting coefficient of soil friction	:	0.5

TABLE 8.1 continued

(b) Initial conditions in impact study

dif impact roll angle

		A	B	C	D
Height of centre of mass, y_g, m	initial	-1.222	-0.971	-0.606	
	at impact	-1.236	-0.985	-1.246	-0.951
Vertical velocity, $\dot{y}_g$, m/s	initial	-4.50		-3.0	
	at impact	-4.53		-4.64	-3.66
Roll angle, θ, deg	initial	-104.0	-119.0	-83.0	-108.0
	at impact	-104.3	-119.3	-102.2	-121.6
Roll velocity, $\dot{\theta}$, rad/s		-2.0			
Lateral velocity, $\dot{x}_g$, m/s		2.25		2.35	

Notes: (i) Values at impact are close to initial values for A and B simulations, but vary with conditions for C and D.

(ii) Standard ROPS lateral collapse force and elastic stiffness in A and B, and in overturning phase simulations were 41.24 kN and 1.329×10^6 N/m respectively, determined from the standard ROPS upright bar diameter of 0.042 m and length of 1.045m. In C and D, they were set at 30.06 kN (tractor weight) and 1.0×10^6 N/m respectively so that they could be varied independantly without reference to bar diameter. Vertical collapse force and stiffness were effectively infinite in all standard conditions.

TABLE 8.1 continued

(c) Parameters and conditions relating to overturning phase

Bank slope, angle to vertical:	:	0, $7\frac{1}{2}$, 15, $22\frac{1}{2}$, 30, $37\frac{1}{2}$ d
Limiting coefficient of tyre/bank friction	:	1.0
Tyre relaxation length	:	0.72 m ($\simeq$ rolling radius
Normalised cornering stiffness	:	4.4 rad^{-1}
Forward speed	:	1.5 m/s
Approach angle to bank edge	:	6 deg

The standard parameter values and sets of initial conditions are given in Table 8.1. Most relate to the the tractor used in the experiments and are generally typical of a medium size, 3000 kg tractor. The tyre/bank friction behaviour and soil strength are also taken from the experiments; these may be less typical but this is not important, and the effects of their variation are included.

The standard ROPS parameters allow flexibility only in sideways deformation, the vertical stiffness being effectively infinite. This is a close representation of the behaviour of the experimental structure and is fairly realistic in describing normal ROPS, except under very large deformations. The experimental ROPS is typical in forming plastic hinges at the tops and bottoms of the upright members. Sideways deformation then approximates to that of a parallelogram mechanism, and the high initial resistance to vertical forces becomes smaller as the angle of deformation increases. The present model does not include this relationship between effective vertical and lateral stiffness, which are assumed independant, but it would not be difficult to incorporate a relationship in an enhancement to the program.

8.3. THE EFFECT OF IMPACT VELOCITIES AND INERTIAS

Variation of the initial conditions at impact provides the greatest insight into the impact behaviour, and this will be covered before the effects of parameter variation.

The standard conditions used were A and B (Table 8.1). The two sets were used to demonstrate the effect of impact roll angle, but since the requirement in this case was for control of velocity at the moment of impact, the initial centre of mass heights in the two sets were different.

8.3.1. Energy distributions

The effects on final energy distribution of variation in initial lateral velocity, $\dot{x}_o$, vertical velocity $\dot{y}_o$ and roll velocity $\dot{\theta}_o$ are shown in Figs. 8.1., 8.2. and 8.3 respectively. The variable ranges were chosen to cover the extremes found in the experiments, although for $\dot{x}_o$ and $\dot{\theta}_o$ the results at velocities down to zero are also given (dashed lines).

These figures and the later ones of the same format are presented as cumulative energy distributions: the curves are the boundaries between each contribution. In most cases, the uppermost-boundary is a line of nearly constant energy, equal to the loss of PE and deviating only because of variation in the final rest position. Where the initial velocities or inertias are varied, as in Figs. 8.1–8.3., the upper boundary is not constant, reflecting the variation in input energy. The energy contributions are denoted in the shorthand form listed in section 8.1. The standard parameter or variable values are shown by short arrows on the axis.

The overall effects apparent in Figs. 8.1–8.3 confirm expectations:

(i) Wheel and tyre deformation absorbs a considerable amount of energy when the tyre and ROPS make nearly simulations impacts (condition A). In most of the condition B simulations, the ROPS reached maximum deflection before the wheel touched the ground and the energy absorbed by the wheel and tyre was much less. The ROPS energy was slightly higher in these cases, but most of the difference was accounted for by increased energy in soil deformation and friction.

(ii) The main effect of initial lateral velocity is on the energy absorbed in sliding friction (Fig. 8.1).

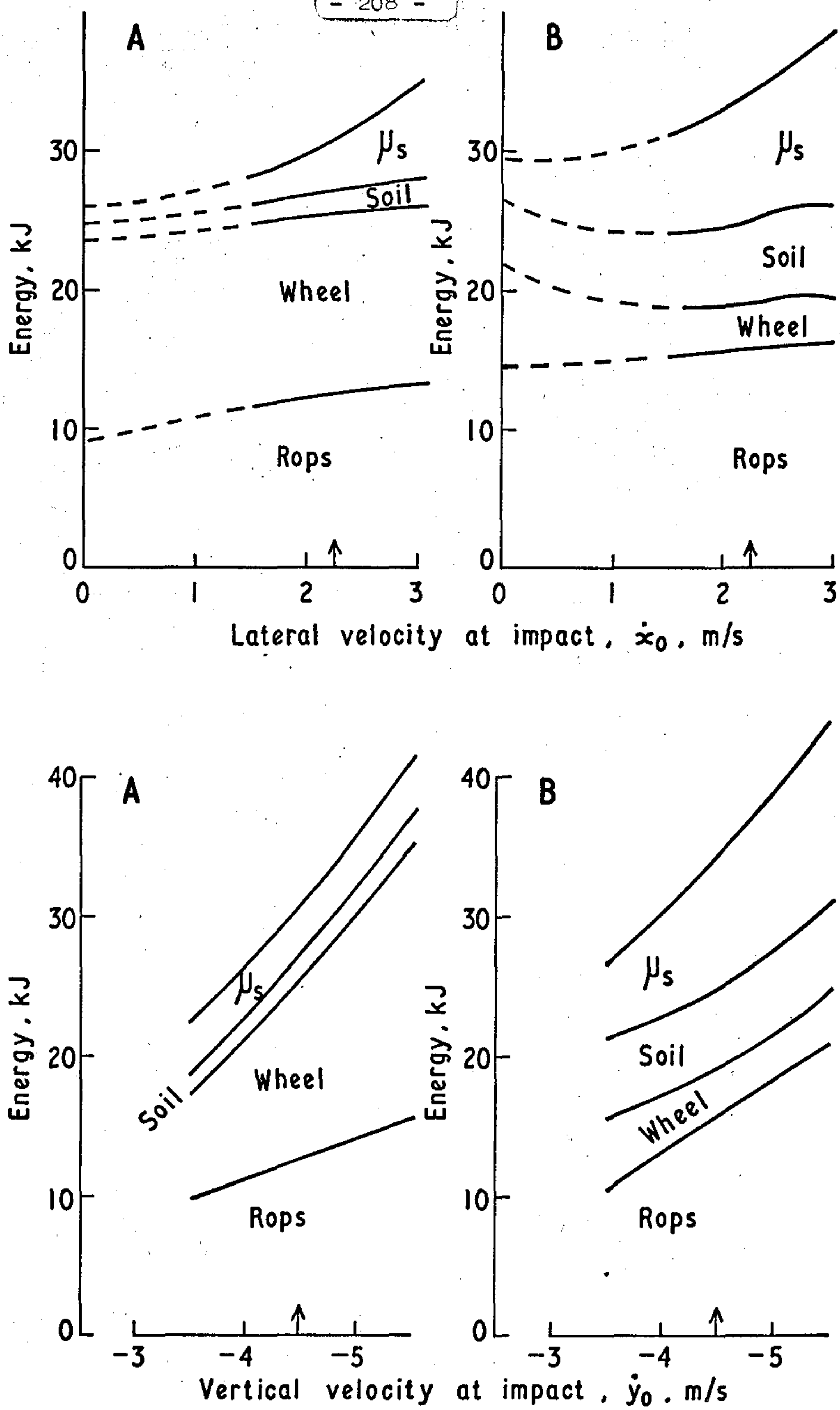

Fig. 8.1 (top) and 8.2 Sensitivity of energy distributions to lateral and vertical impact velocities.

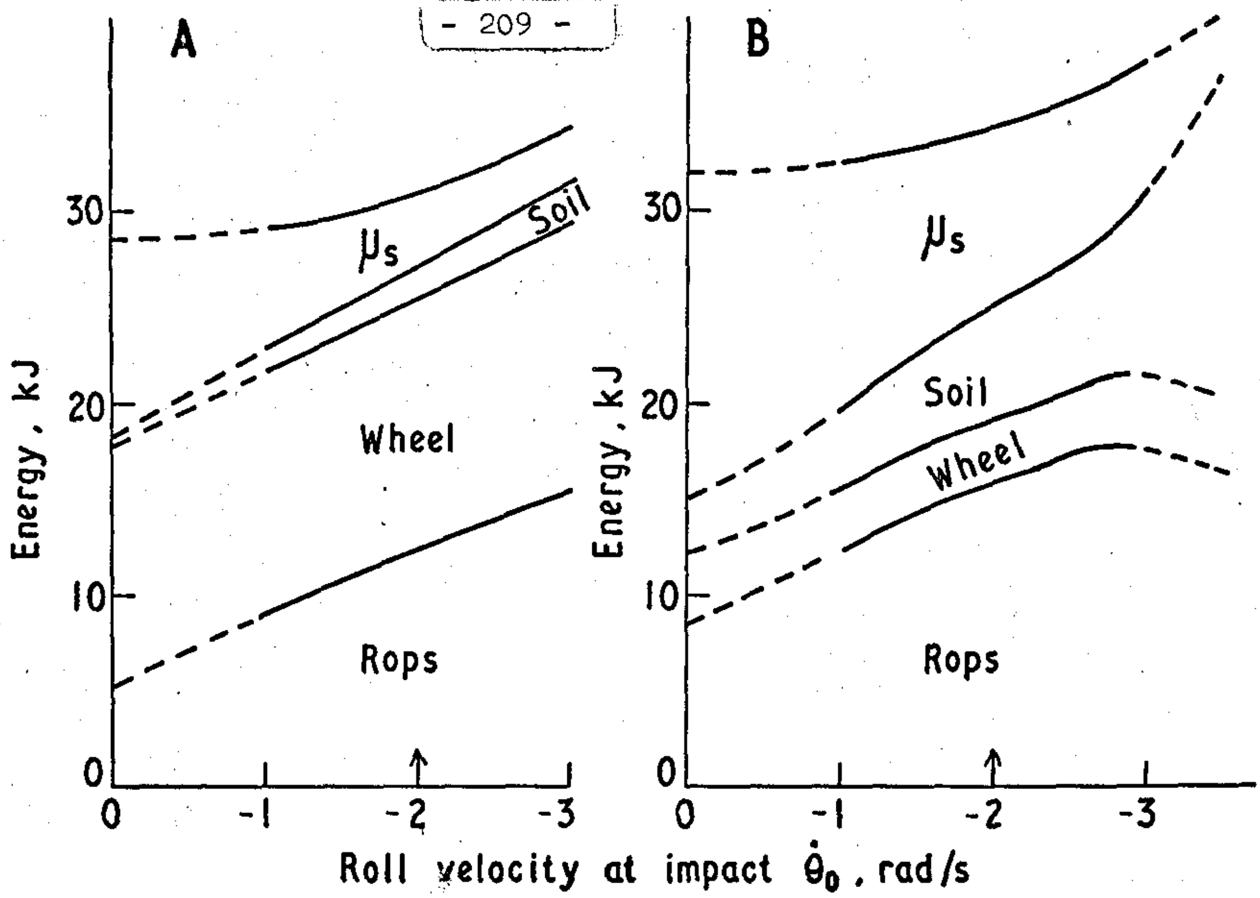

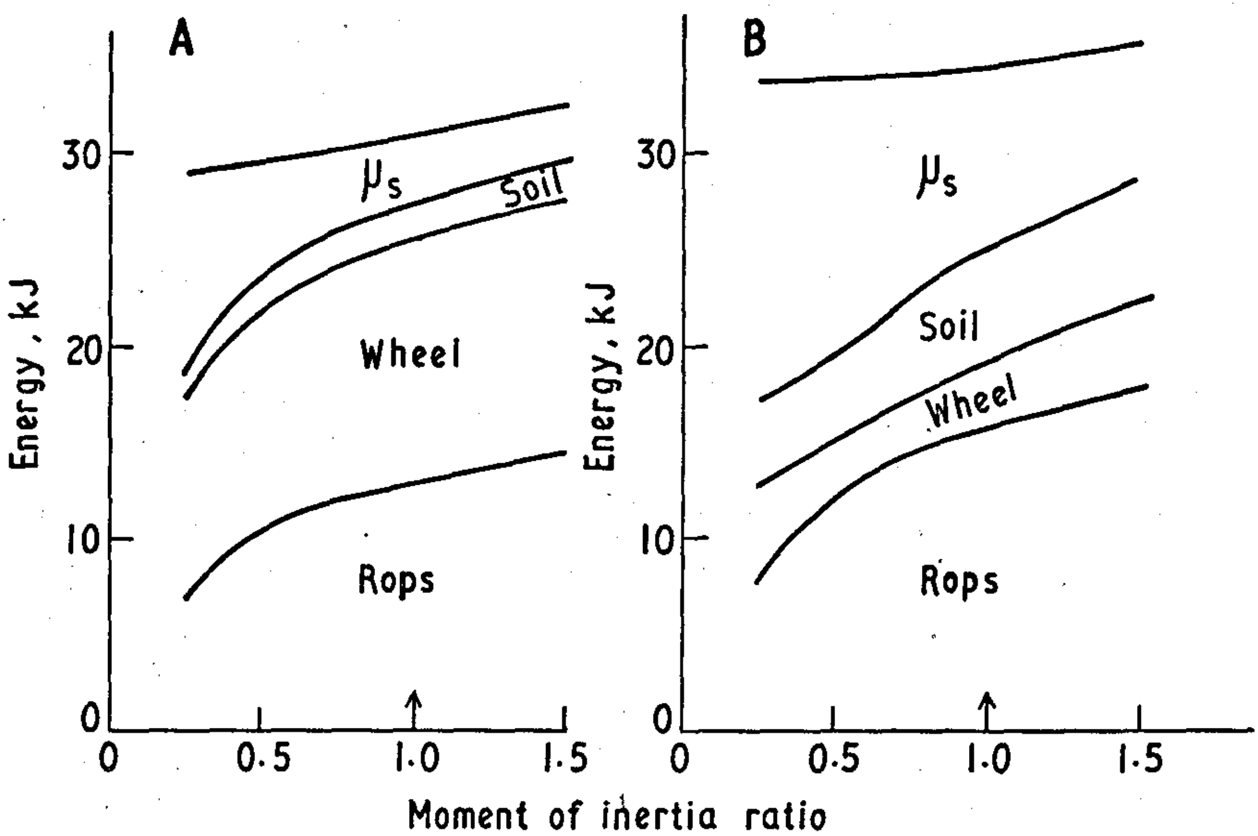

Figs. 8.3 (top) and 8.4 Sensitivity of energy distributions to impact roll velocity and moment of inertia.

(iii) Energy due to variation in initial vertical velocity is shared about equally between wheel and ROPS in condition A, but is absorbed mainly by the ROPS in B (Fig. 8.2).

(iv) Increase in impact roll velocity causes an increase in ROPS energy but a decrease in energy absorbed in friction (Fig. 8.3). At low roll velocity, the sliding velocity of the contact points is positive throughout impact, with the standard initial lateral velocity of the centre of mass. When the roll velocity is high the sliding velocity is negative; during a simulation with high initial roll velocity, the sliding velocity is negative at the start, but increases and becomes positive as the roll velocity drops during impact. The lower mean sliding velocity results in the reduction of energy absorbed in friction.

The energy distribution for variation of roll moment of inertia is given in Fig. 8.4. The scale is the same as that for impact roll velocity (Fig. 8.3) when each variable is expressed as a ratio of its standard value; the scales in the two figures then transform to identical scales in initial angular momentum about the centre of mass. The effects of variation would be expected to be fairly similar, and the figures show that this is so. The differences between them are due to differences in impact time available for absorption of PE and of KE due to the linear velocities, as will be explained later.

8.3.2. Energy absorbed as a function of kinetic energy at impact

The quantitative effects of variation of parameters which do not alter the initial KE will be apparant from the energy distributions. In cases such as Figs.8.1-8.4, however, the interpretation is made more difficult by variation of input energy, especially as the amount of this variation is different for each of the four variables. To provide a common basis for comparison, the results are repeated in Figs. 8.5 and 8.6 using a total initial kinetic energy as the independent variable, and energy absorbed in

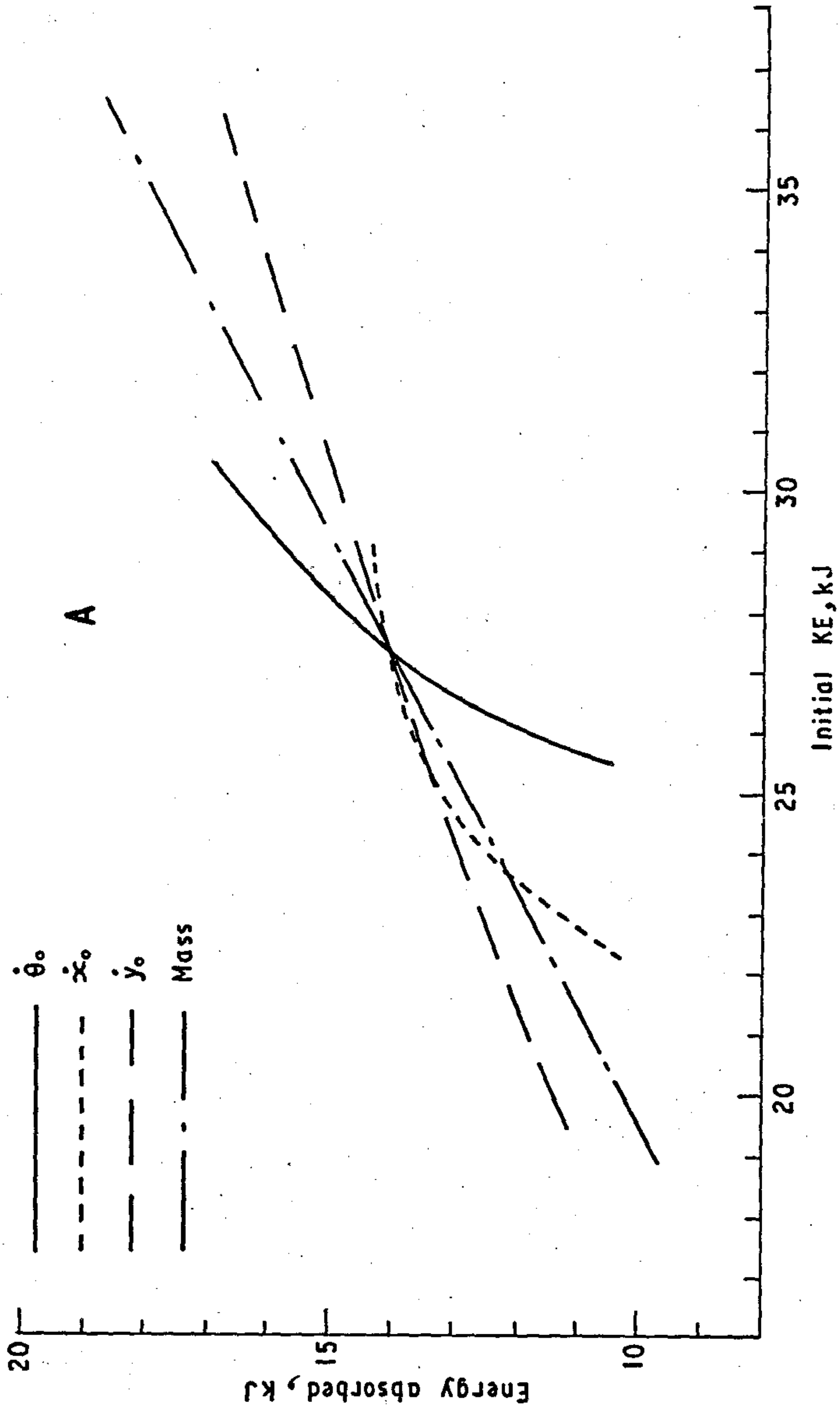

Fig. 8.5 Sensivity of ROPS sideways energy to impact velocities and mass: conditions A.

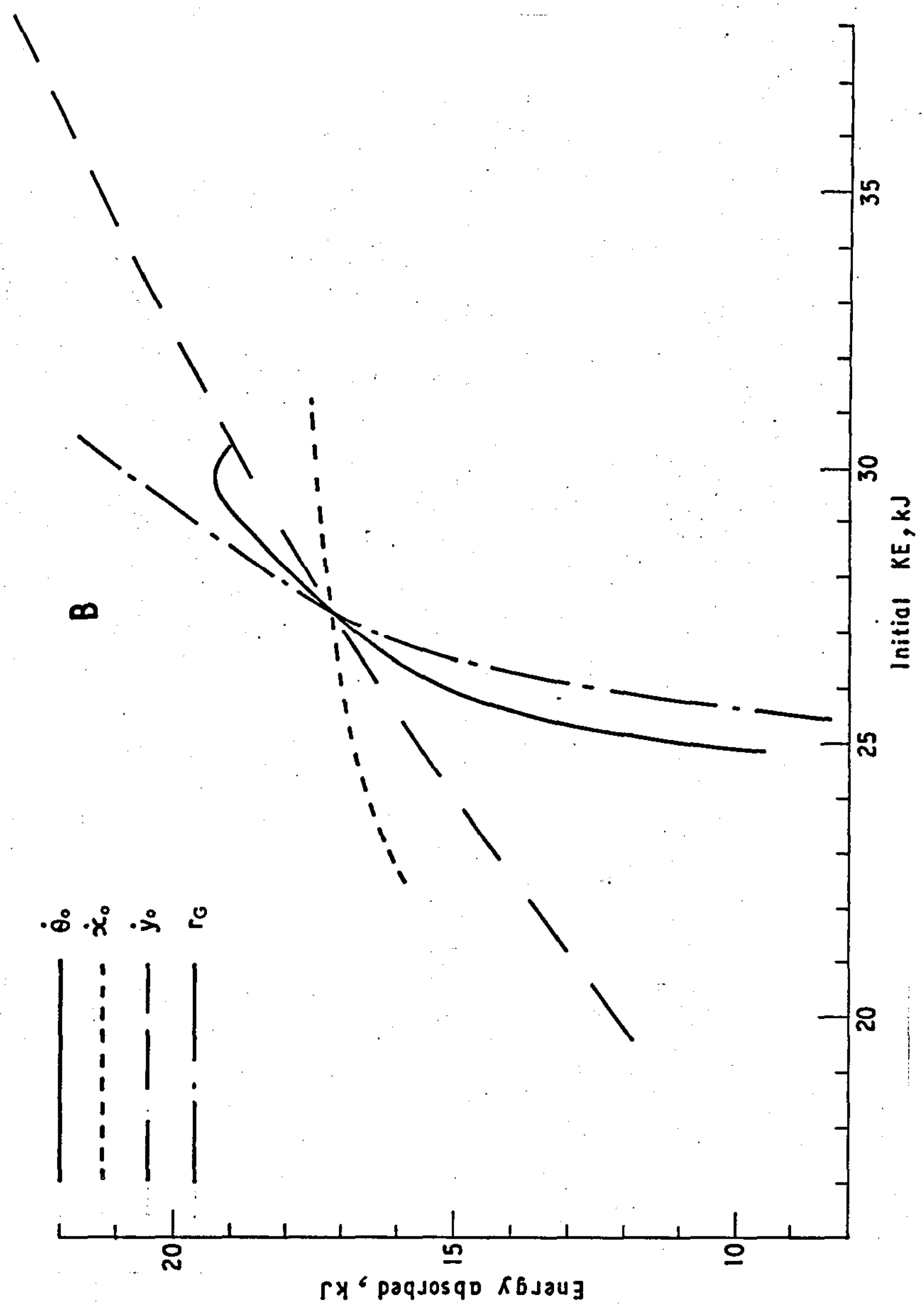

Fig. 8.6 Sensitivity of ROPS sideways energy to impact velocities and moment of inertia: conditions B.

the ROPS at maximum sideways deflection as the dependent variable. The curve for moment of inertia in condition A is almost identical to that for roll velocity when plotted in this way, and has been omitted; a curve for mass is included in this case but not for B, to preserve clarity.

The effects of combinations of the most important variables, roll and vertical velocity, are presented as carpet plots in Figs. 8.7 and 8.8. The general similarity of the shapes of these curves provides further evidence of the lack of discontinuities in the impact behaviour. In condition B, absorbed energy reaches a maximum at an impact roll velocity of about 2.75 rad/s for all values of initial vertical velocity (Fig. 8.8). An indication that sliding friction is responsible for this effect is given by Fig. 8.9. When friction is absent the slopes of the roll velocity and moment of inertia curves remain more constant, and show no signs of approaching zero over the ranges covered. With friction, the reduction in ROPS energy beyond $\dot{\theta}_o \simeq 2.75$ is accompanied by an increase in energy absorbed in soil deformation (Fig. 8.3). The presence of friction increases the angle between the resultant soil force and the ROPS collapse force (Fig. 8.10) when the sliding friction velocity is positive; this is the case after the first moments of impact, even at high roll velocity, as explained in (iv) above. The larger angle between these forces requires a larger vertical soil force than when friction is absent. In the conditions chosen, this force becomes high enough at $\dot{\theta}_o = 2.75$ to fall into the range of the next line in the soil force/deformation characteristic. This line has a lower stiffness than the previous one, so the soil deformation energy increases much more rapidly with $\dot{\theta}_o$ than would otherwise be the case.

Clearly, this type of behaviour depends strongly on the chosen conditions of soil friction and strength.

The relationships between the curves for impact roll velocity and moment of inertia also deserve comment, because there are important differences even though the general shapes are similar.

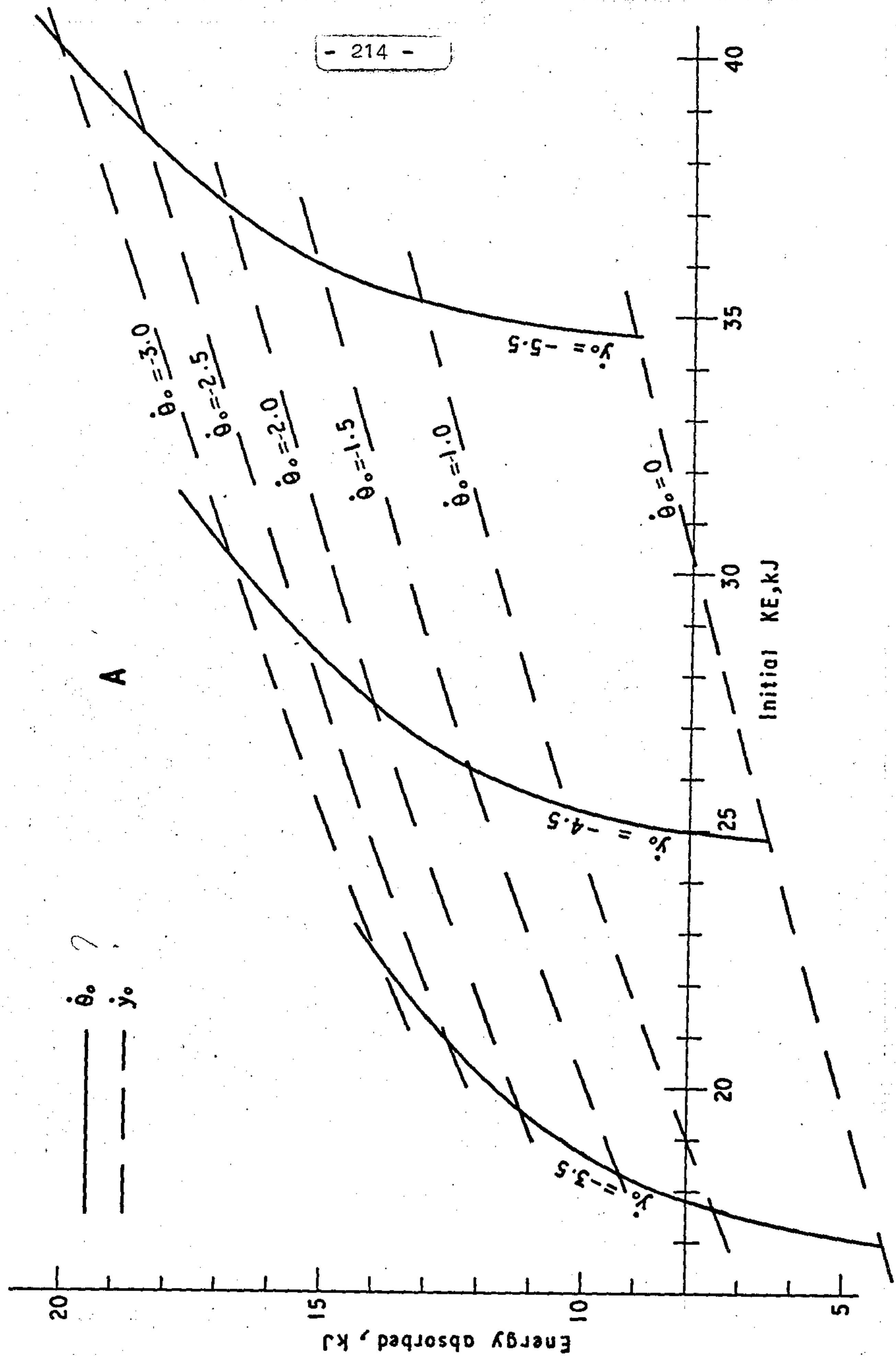

Fig. 8.7 Sensitivity of ROPS sideways energy to vertical and roll impact velocities as carpet plot: conditions A

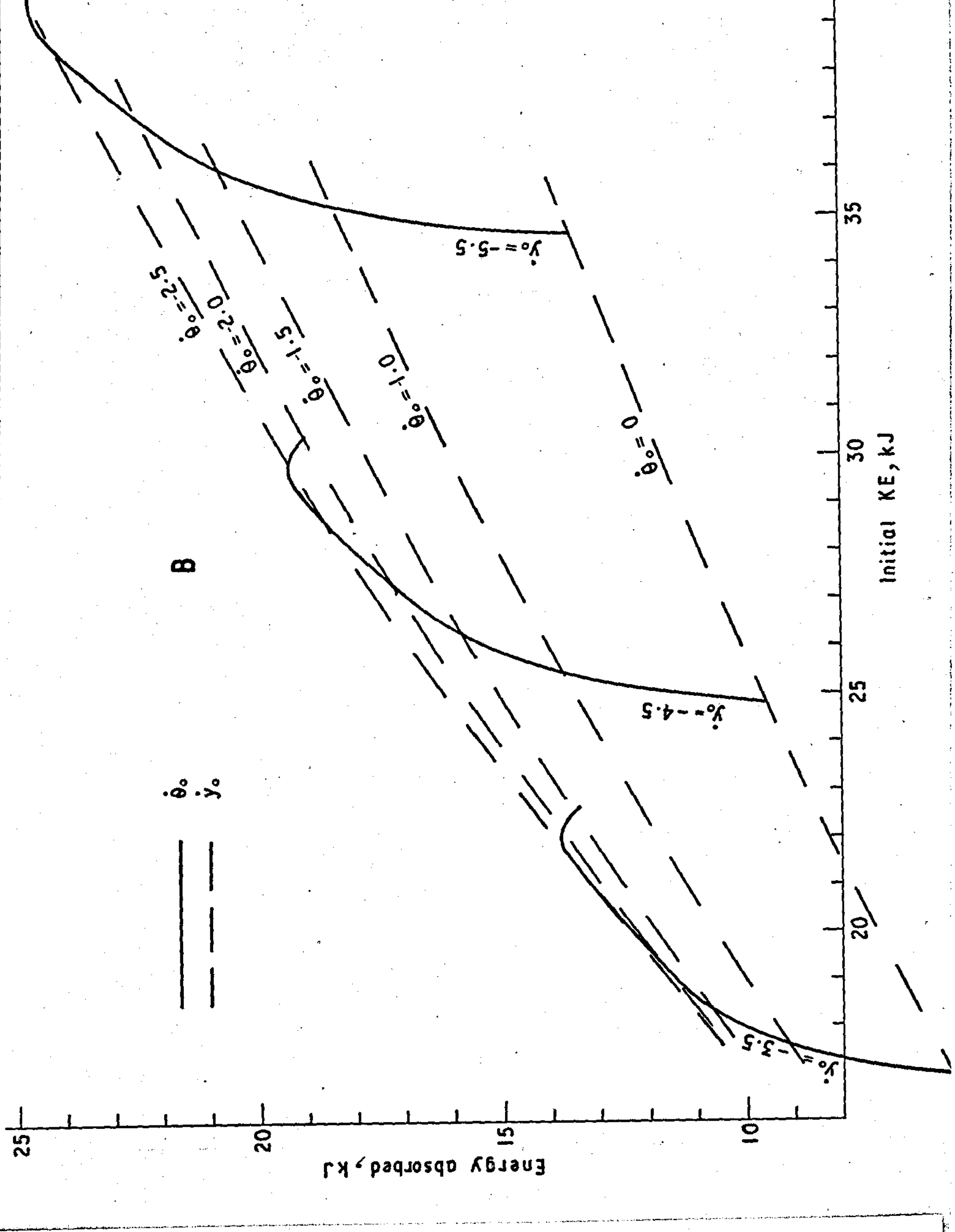

Fig. 8.8 Sensitivity of ROPS sideways energy to vertical and roll impact velocities as carpet plot: conditions B

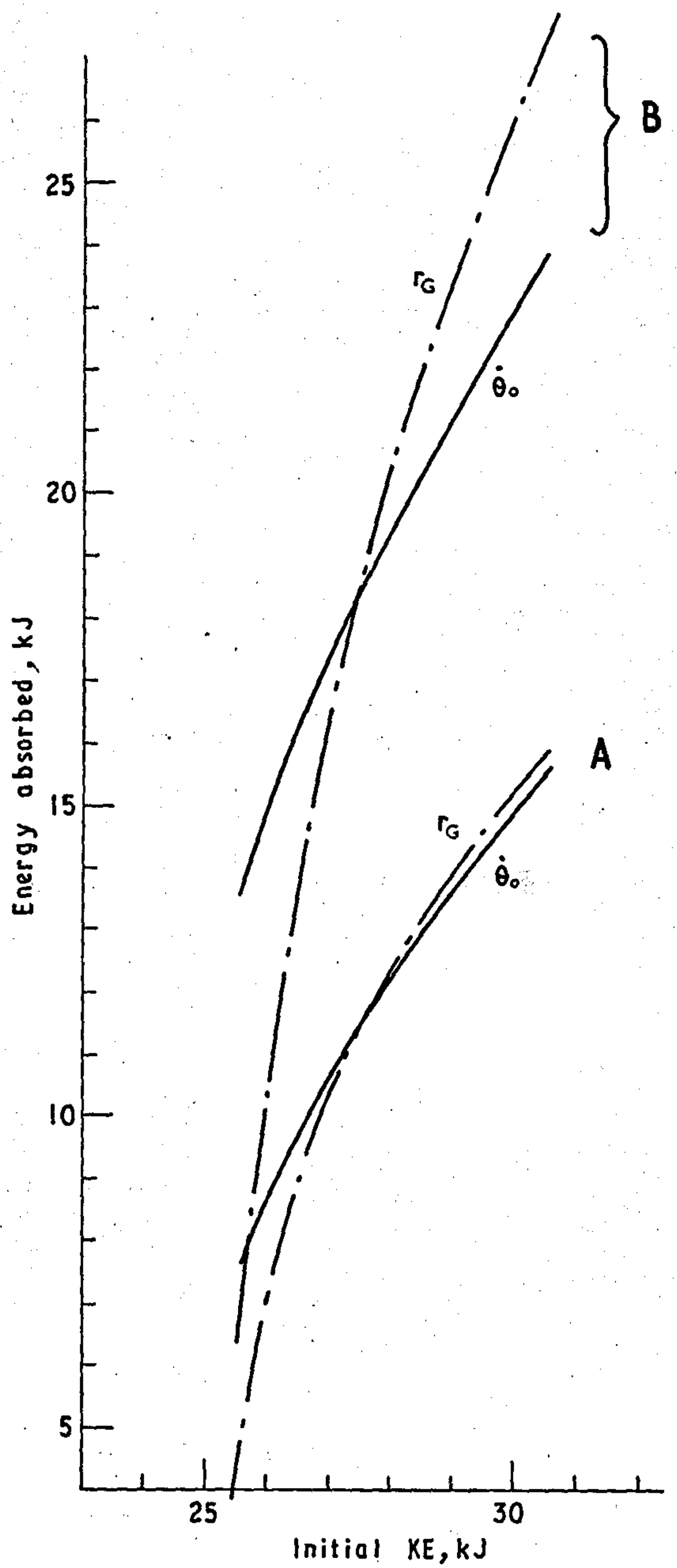

Fig. 8.9 Sensitivity of ROPS sideways energy to impact roll velocity and moment of inertia under low friction.

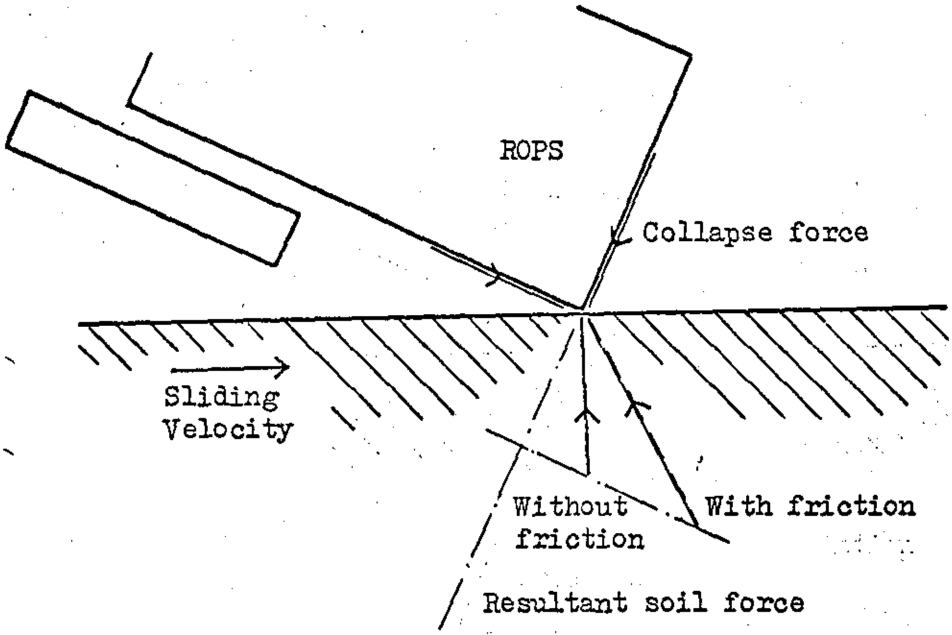

Fig. 8.10 The effect of friction on the normal soil force.

The equivalence of the angular momentum scales in Figs.8.3 and 8.4 is convenient but takes no account of the component of angular momentum due to the movement of the centre of mass around the instantaneous centre of rotation. Also, the energy due to initial angular velocity is proportional to the product of velocity and momentum.

The effect of moment of inertia may be considered as having two components: the part of the initial rotational energy absorbed, and the part of the linear energy absorbed. For a given initial energy, the duration of impact is longer with a high inertia and low velocity than with a high velocity and low inertia. Hence increasing inertia has more effect on the amount of linear kinetic energy absorbed than increasing velocity. In the extreme, reducing the roll velocity to zero allows some of the linear kinetic energy to be absorbed in the ROPS because of the inertial resistance, whereas zero inertia results in zero energy.

The foregoing applies to condition B, but in A the wheel absorbs much of the linear kinetic energy and the difference between the roll velocity and moment of inertia curves is smaller over most of their range (Figs. 8.5 and 8.9).

8.3.3. Sensitivity coefficients

The sensitivities may be quantified in terms of the change in the dependent variable for unit change in the independent variable. The simplest measure is the slope of the curve, and where the units for both axes are the same, as in Figs. 8.5-.8, the resulting non-dimensional sensitivity coefficient is easy to interpret. A non-dimensional coefficient may be obtained whether or not the units are the same if the changes are expressed as ratios of the absolute values, thus:

$$\text{Relative sensitivity coefficient} = \frac{\Delta y}{y} \Big/ \frac{\Delta x}{x} \simeq \frac{x}{y} \cdot \text{slope}$$

This is more appropriate in many cases and may also be more powerful in revealing the effect of proportionate changes. The relationships between the sensitivity coefficients for the different curves in Fig. 8.5 are unchanged by expressing them as proportions if all the slopes are multiplied by the same ratio of coordinates of the common point. The same applies to the curves of Fig. 8.6, but the comparisons between the two sets would be altered because of the different y values of the two common points. More importantly, is the total initial kinetic energy the appropriate independent variable? If the component of kinetic energy due to the relevant variable is selected instead, such as rotational kinetic energy for the rotational velocity curve, the shape and slope remain the same but the removal of a constant from the abscissae has a major effect on the relative sensitivity coefficient (Table 8.2).

TABLE 8.2

Sensitivity coefficients Q for the effect of lateral, vertical and roll velocities at impact, and moment of inertia on maximum energy absorbed in ROPS, in standard conditions

	Q_A Absolute coefficient = slope	Q_{RT} Relative coefficient based on total kinetic energy	Q_{RC} Relative coefficient based on component of kinetic energy
Condition A (Fig. 8.5)			
Lateral velocity, $\dot{x}_o$	0.24	0.47	0.09
Vertical velocity, $\dot{y}_o$	0.33	0.65	0.47
Roll velocity, $\dot{\theta}_o$	1.25	2.44	0.22
Moment of inertia, I_z	1.28	2.49	0.23
Condition A, with $\mu_s = 0$ (Fig. 8.9)			
Roll velocity, $\dot{\theta}_o$	1.59	3.85	0.35
Moment of inertia, I_z	2.23	5.39	0.50
Condition B (Fig. 8.6)			
Lateral velocity, $\dot{x}_o$	0.20	0.32	0.06
Vertical velocity, $\dot{y}_o$	0.60	0.95	0.69
Roll velocity, $\dot{\theta}_o$	1.15	1.81	0.17
Moment of inertia, I_z	1.88	2.98	0.27
Condition B, with $\mu_s = 0$ (Fig. 8.9)			
Roll velocity, $\dot{\theta}_o$	2.09	3.11	0.29
Moment of inertia, I_z	4.11	6.12	0.56

- 220 -

Expressing the sensitivity coefficients in these three ways gives insight into an apparant paradox that is central to the performance of ROPS. Because the ROPS impact point is fairly high above the tractor centre of mass, it offers a high resistance to rotational inertia but little to vertical inertia at impact, when the roll angle is around 90°. Thus a large part of the energy due to change of roll velocity is absorbed by the ROPS (Q_A = 1.25, condition A) but only a small part of that due to vertical velocity change (Q_A = 0.33, condition A). The roll velocity contributes to only a small part of the total initial kinetic energy, however, so when expressed as sensitivities relative to a change in the component energies, vertical velocity (Q_{RC} = 0.47) appears to be more important than roll velocity (Q_{RC} = 0.22). The same phenomenon may be appreciated by studying the absolute ranges of ROPS energy in Figs.8.2, 8.3 and 8.5. Although the proportion of rotational energy absorbed is clearly higher, the absolute changes are less than those when vertical velocity is varied.

The severity of the bank type of overturn is due to the high vertical impact velocity. The simulations show that even when the ROPS reaches its maximum deflection before significant energy has been absorbed in the wheel (condition B), only a limited amount of the energy due to vertical velocity is absorbed in the ROPS. The height of the ROPS above the centre of mass and the relatively low moment of inertia and rotational velocities prevent the collapse of structures that are capable of absorbing only a small amount of the total energy. This applies only to ROPS with high vertical stiffness; the importance of this parameter will be covered later.

The relationships noted between the sensitivity coefficients for condition A apply also in condition B (Table 8.2). Comparing B with A, the roll velocity coefficients are slightly lower, presumably because of the larger angle between the ROPS collapse force and the vertical (Fig. 8.10). The vertical velocity and moment of inertia coefficients are considerably higher because of the absence of the effect of the wheel during ROPS impact.

All the lateral velocity sensitivity coefficients are small.

Finally, the curve for mass variation (Fig.8.5) is very close to a straight line through the origin. Radius of gyration was held constant for these simulations, so the moment of inertia increased with the mass and the linear behaviour was expected.

8.4. PARAMETERS THAT AFFECT ONLY IMPACT

Moving in the direction from the particular to the general, those parameters affecting only impact will be covered next, before those requiring simulations of complete overturns.

These parameters fall into three classes:-

(i) Geometrical parameters

(ii) Structural parameters describing the wheel and tyre

(iii) Structural parameters describing the ROPS and soil

The standard impact conditions C and D were used for (i) and (iii) to show the effect of impact roll angle (Table 8.1). Since the wheel/ROPS energy relationship is most important under simultaneous impact, (iii) were studied only in condition A, which is very similar in effect to C.

Final energy distributions only are presented because the total input energy is substantially constant in each case and both qualitative and quantitative effects are apparant from these figures. The small number of data points in most cases leads to some uncertainty, so they are connected diagrammatically by straight lines rather than the smooth curves of Figs. 8.1-8.4.

Impact roll angle

Initial roll angle is the only difference between conditions C and D; the effect of variation within the range of these values is shown in Fig. 8.11 Because of the need to start simulations at the same centre-of-mass height, as explained in 8.2, the variation of impact roll angle is accompanied by some variation of velocities and centre of mass height at impact but the effects are small (Table 8.1).

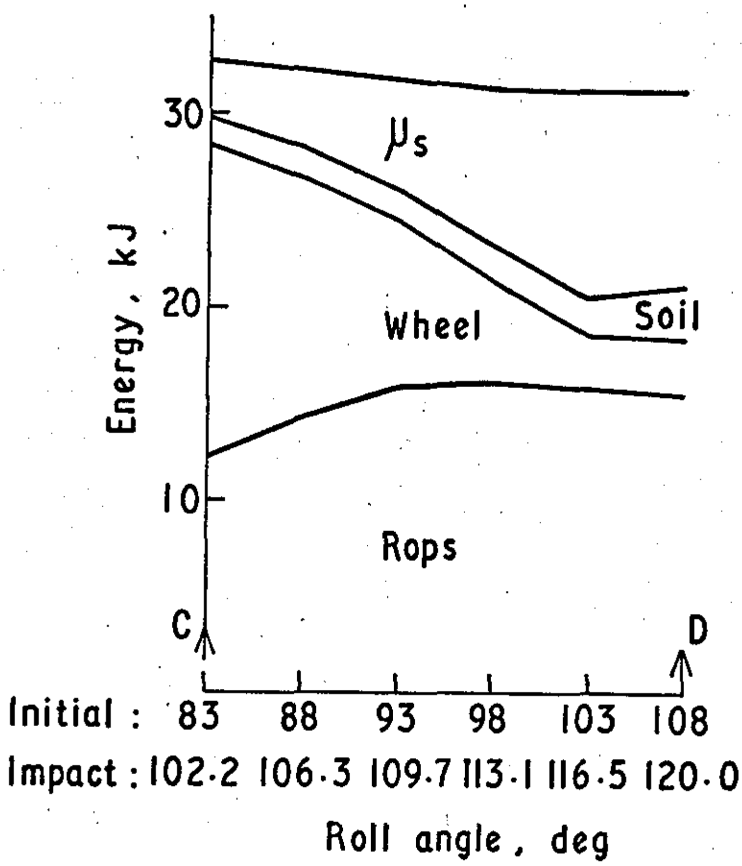

Fig. 8.11 Sensitivity of energy distributions to impact roll angle: range between conditions C and D.

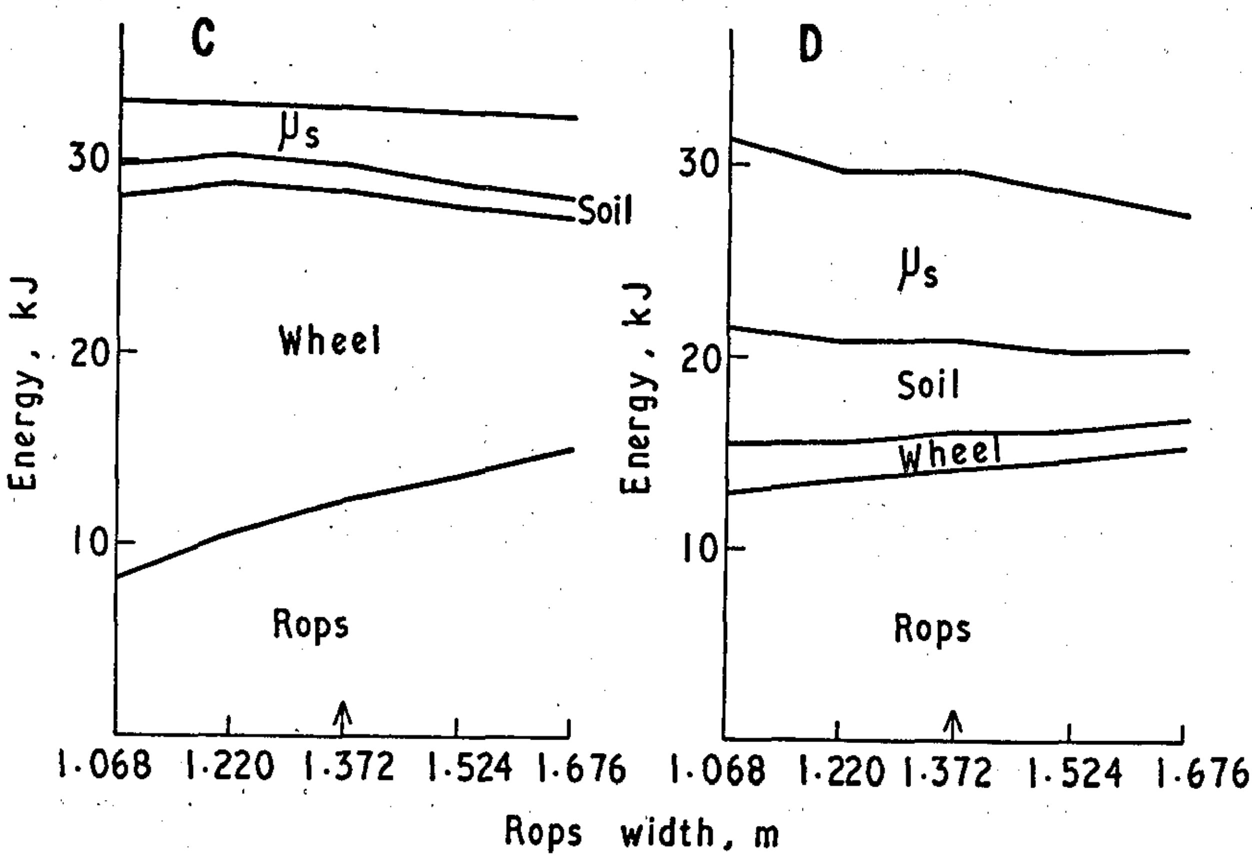

Fig. 8.12 Sensitivity of energy distributions to ROPS width

Less energy is absorbed by the wheel as impact roll angle increases, as expected. At impact roll angles up to about 110° the energy in ROPS sideways deformation and sliding friction both increase but beyond this the ROPS energy reaches a maximum because of the angle between the forces (Fig.8.10). This is consistent with the findings in conditions A and B reported above. The ROPS sideways energy would continue to decrease with further increase in impact roll angle up to 180°, accompanied by increase in soil deformation energy, just evident in Fig 8.11, for the reasons already given.

ROPS width

Increasing the width of the ROPS (Fig.8.12)has a similar effect on the relationship between ROPS and wheel impact to increasing the impact roll angle, but the angles between the forces remains unchanged. Thus in condition C, the ROPS energy continues to increase at the expense of wheel energy without reaching a maximum. In condition D, where the wheel absorbs little energy, the effect of ROPS width is small. The slope of the uppermost line in D is due to change in PE corresponding to the relationship between centre-of-mass height and the impact point at the ROPS.

Increase of track width (not presented) has the opposite effect in impact to increase of ROPS width in condition C and negligible effect in D.

ROPS height

A higher ROPS offers more resistance to angular momentum and less to vertical momentum. The nett effect on ROPS energy of increased height is a slight increase under condition C and negligible change under D (Fig. 8.13). This is consistant with the relationship between the sensitivity coefficients in the two conditions in Table 8.2.

The change in the proportions of energy in soil deformation and sliding friction under D are due to the effects of change in sliding velocity of the contact point.

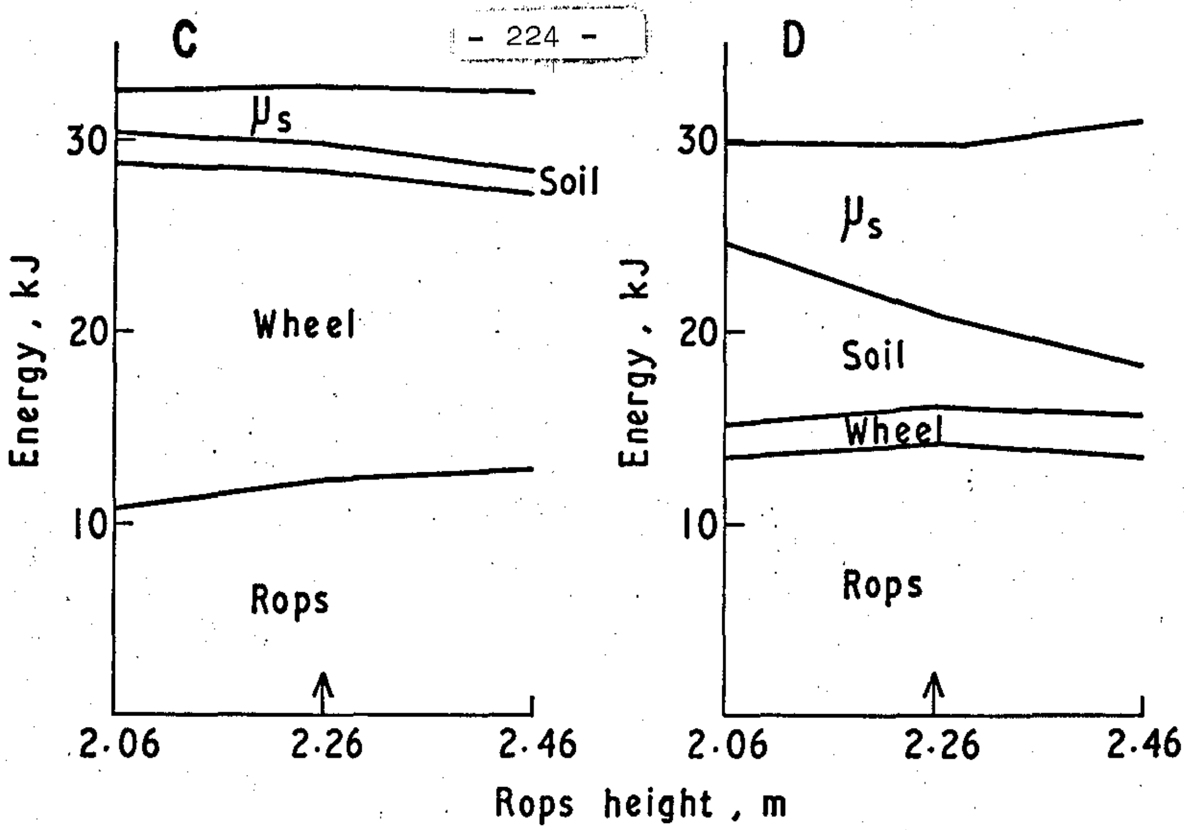

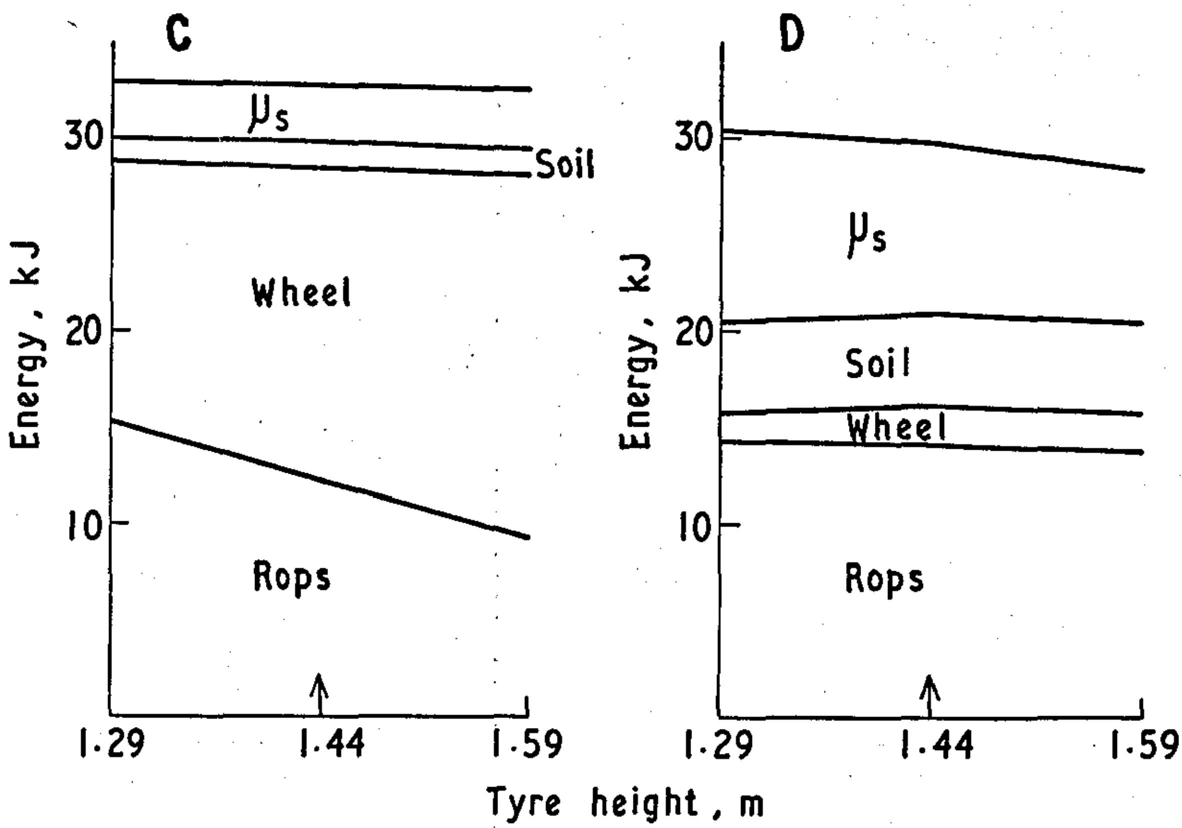

Figs. 8.13 (top) and 8.14 Sensitivity of energy distributions to ROPS height and tyre (with rim) height.

Wheel height

Tyre and rim height are varied together in Fig. 8.14 maintaing a constant tyre depth: the tyre forces are relatively low, and the main effect shown is due to the variation of rim height. As this increases the upper rim contact point offers more resistance to angular momentum and, in condition C, impacts the ground successively more in advance of the ROPS. The two effects both increase wheel energy at the expense of ROPS energy.

The only significant effect in condition D is a slight reduction of total energy due to the change in final resting postion.

Wheel structural parameters

The wheel rim collapse force (Fig.8.15) and elastic stiffness (Fig.8.16) have negligible effects within the ranges covered.

Increasing the rim damping coefficient from zero to the standard value has the expected effect of increasing the energy absorbed by the wheel (Fig. 8.17. Further increase to twice the standard value causes sufficient increase in vertical force at the rim contact point to shift the soil structural characteristic to its next line. Soil deformation energy then increases while the wheel energy shows little change. The ROPS energy decreases gradually with increase in rim damping.

Changing the effective rim area has little effect (Fig.8.18) and is directly comparable to changing the rim collapse force (Fig.8.15). Effective tyre area has no effect (not presented) because of the low tyre stiffness.

Some discussion of the effects of these parameters has already been presented in 7.1.2. and 7.2.5.

ROPS elastic stiffness

The effect of reducing elastic stiffness to one fifth of its standard value is shown in Fig. 8.19. The energy absorbed at maximum ROPS deformation is also given because it varies in relation to final energy absorbed when elastic stiffness is changed.

Maximum ROPS energy is unaffected in condition D. It increases slightly with increasing stiffness in C because the more rapid rise of ROPS force

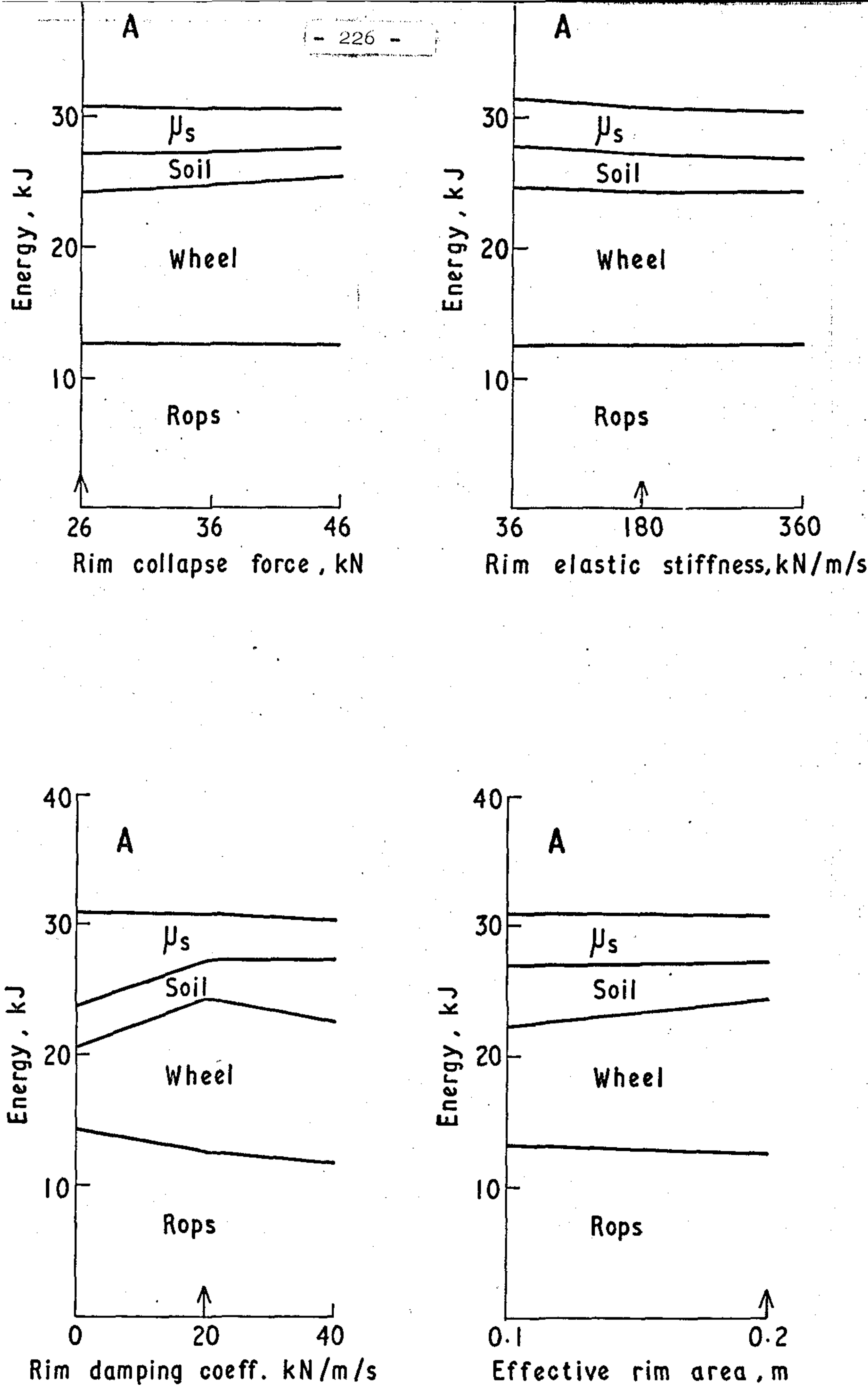

Figs 8.15 - 8.18 Sensitivity of energy distributions to rim parameters.

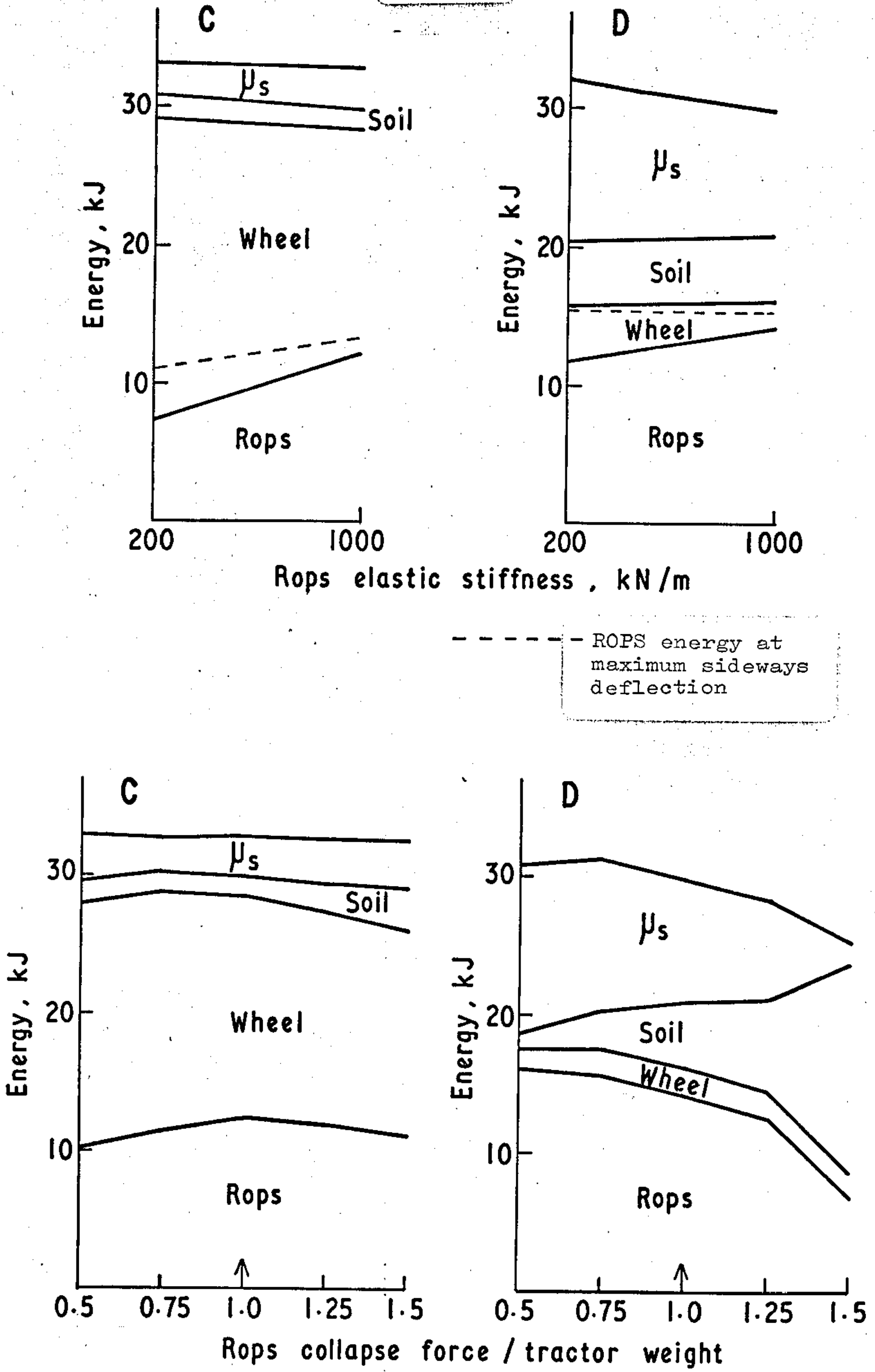

Figs 8.19 (top) and 8.20 Sensitivity of energy distributions to ROPS elastic stiffness and collapse force.

results in less energy absorption by the wheel during the first part of the impact.

ROPS lateral collapse force

The main effect of increasing ROPS strength (Fig.8.20)is to force greater deformation of the soil; more energy is absorbed in the soil and less in the ROPS with little effect on other energies. In condition C, however, there is a small effect on the relationship between wheel and ROPS impact similar to that when elastic stiffness is changed (Fig.8.19).

The reduction in total energy in condition D is due to tyre 10 making contact with the bank slope towards the end of impact, giving an unrealistic final position. The bank slope was not removed from these simulations by an oversight but the effect is not important; the absence of the slope would have allowed the friction energy to remain fairly constant with collapse force and other energies would be close to those shown.

Soil strength

Soil strength was changed by multiplying the force limits of all four structural lines (cone resistance in Table 8.1) by the same ratio of their standard values (Fig. 8.21). The effects are similar to those obtained by varying ROPS strength (Fig. 8.20) and rim strength (Fig. 8.15) but are shown over a wider range.

If the structural characteristics had been idealised rigid-plastic forms, with zero plastic stiffness, and the roll angle had remained constant during impact, these sensitivity curves would have been expected to contain step changes. Below a certain soil strength, for example, no ROPS deformation would occur, while above it, the soil would appear rigid to the ROPS. The gradual transition from zero ROPS energy to zero soil energy evident in Fig8.21 is due mainly to the shape of the structural curves. In addition, however, the angles between the component forces at impact affect both the sliding friction and the relationships between the force limits at structural line-changes for the two impacting members, such as ROPS and soil.

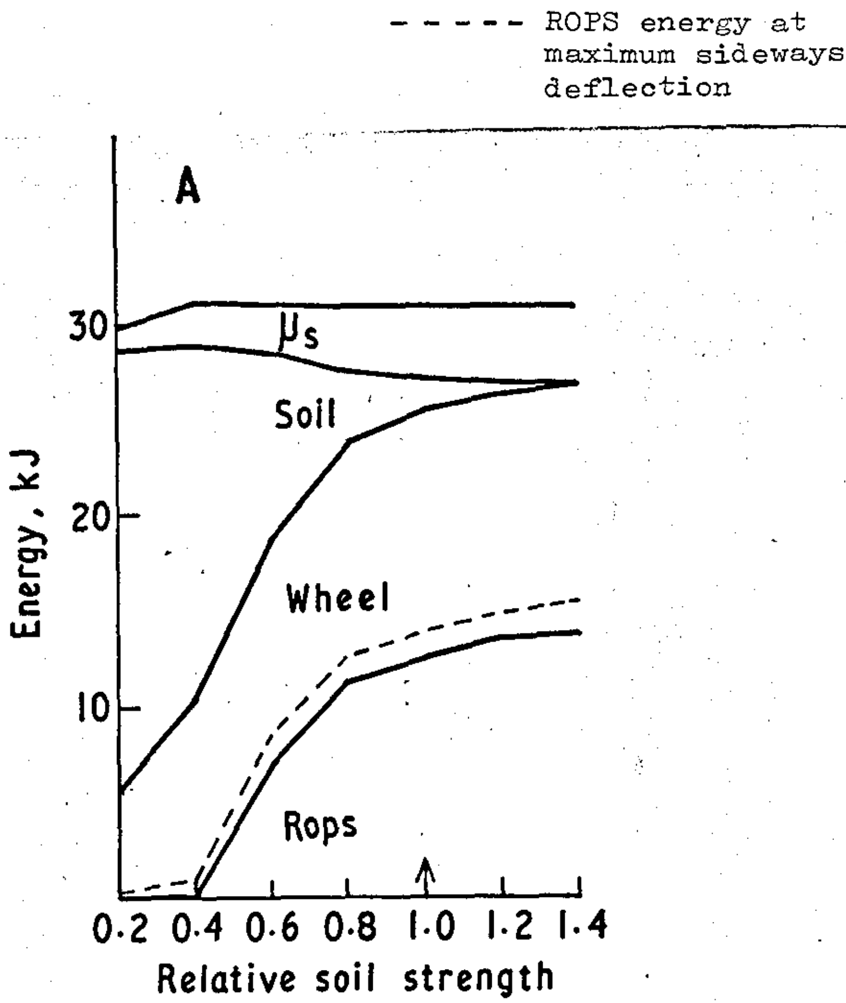

Fig. 8.21 Sensitivity of energy distributions to soil strength.

ROPS vertical collapse force and bank height

These parameters are presented together to show the relationship between them. Instead of energy distributions, the maximum ROPS energy in lateral and vertical directions are plotted against bank height in Fig.8.22 for three values of vertical strength.

The structural behaviour of typical ROPS under vertical loading has not been measured. Standard strength test procedures require only that a ROPS can support a force of twice the tractor weight, uniformly distributed across first the front, then the rear of the ROPS, after deformation due to horizontal impacts or loadings. The mounting arrangements of ROPS on tractors are generally strong and stiff; the main deflection under vertical loading normally occurs at the plastic hinges that have developed under horizontal loading, continuing the "parallelogram" mode of failure referred to in 8.2. above.

To a first approximation, a vertical strength of twice the weight at the front or rear is roughly equivalent to the same vertical strength at one side, for a symetrical, four-post ROPS. In each case, the force is reacted mainly by plastic hinges in two upright members, with some support from those in the other two. This is a considerable simplification because of the dependance of vertical strength on lateral deformation and on the strength of the horizontal members connecting the tops of the four uprights. After horizontal loadings in a typical laboratory strength test, the lateral deformations of all the upright members will be different. In addition, the simulation model does not include the interdependance of the vertical and horizontal characteristics. Despite these limitations, the results shown in Fig8.22 do give a strong indication of the importance of vertical strength.

Increasing bank height increases the roll angle and vertical velocity at impact (Fig.8.23). The kinetic energy has a direct influence on energy absorbed, while the impact roll angle alters the relationship between the energies absorbed in the lateral and vertical ROPS directions (Fig. 8.22).

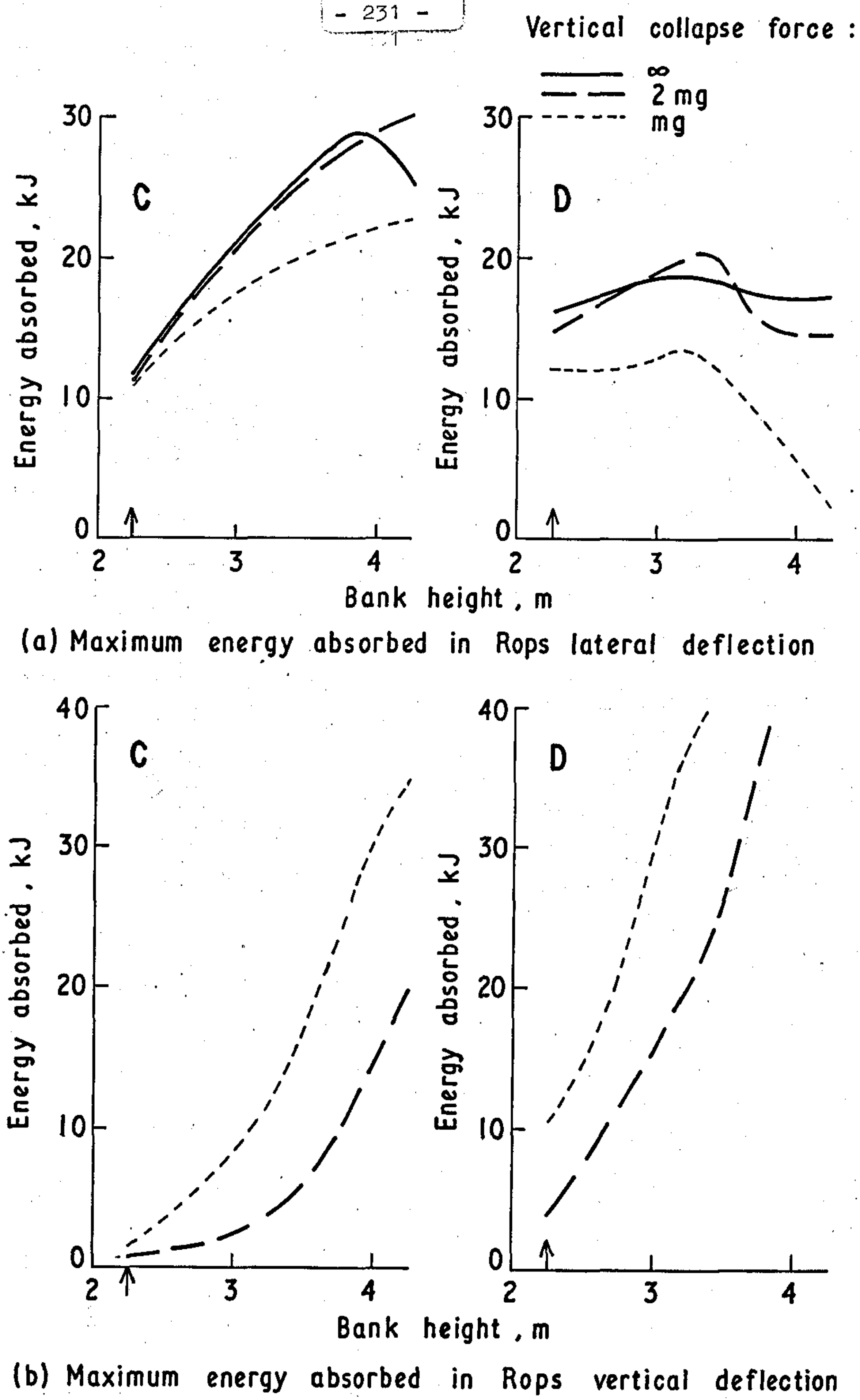

Fig. 8.22 Sensitivity of ROPS sideways energy (top) and vertical energy to bank height for different vertical collapse forces.

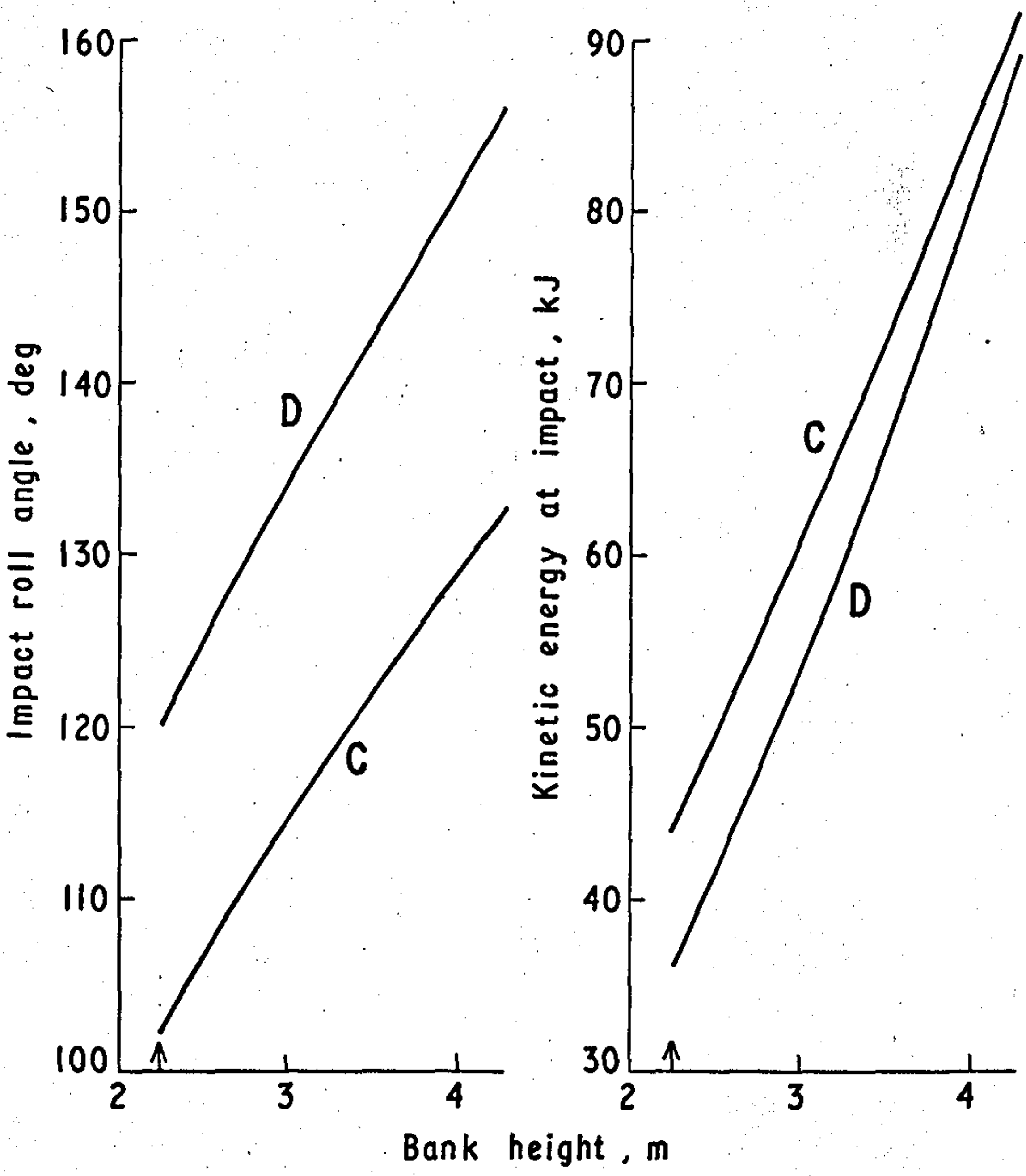

Fig. 8.23 Roll angle and kinetic energy at impact as a function of bank height for conditions C and D.

At impact roll angles beyond about 145°, depending on vertical strength and impact energy, the tractor does not fall back after impact but continues to roll; part of the energy is then not absorbed but retained as kinetic energy.

The approximately linear relationship between maximum deflection and energy absorbed gives an indication of the effects on driver protection.

An energy of 30 kJ is absorbed at about 400 mm vertical deflection when the collapse force is twice the weight or at about 700 mm when the force is equal to the weight. This occurs at bank heights of about 3.5 or 3.0 m respectively in condition D. Overturns down banks as high as this are certainly not common but do have a significant likelihood, particularly since the high roll angles of condition D are associated with shallower bank angles (higher α : see Fig.7.10). The magnitude of the deformations suggests a serious risk of a driver being crushed in such an accident.

8.5. PARAMETERS THAT AFFECT OVERTURNING

Apart from the bank angle, α , these parameters may be grouped in three classes:

(i) Tractor dimensions

(ii) Inertias and tyre structural parameters

(iii) Parameters governing tyre friction relationships and initial conditions

The effect of variation of each parameter was studied at six bank angles (see 8.2.). The results are presented as values at impact of the three most important variables, roll angle, roll velocity and vertical velocity, together with the energy absorbed in the ROPS at maximum deformation. In an attempt to show overall trends, the distributions of final energy are given as mean values of the results at the six bank angles. Again, the data points are connected diagrammatically by straight lines but the presence of discontinuities makes interpolation unreliable.

Track width

The results in Fig.8.24 are typical of many of those that follow, in showing considerable variation of trends at different bank angles, due to the complex effects on loss of tyre contact. The curves representing results at individual α are shown with different types of line to help interpretation; in many cases, overall trends are not apparant except from the mean energy distributions and the curves for each bank angle must be studied individually. The steeper banks ($\alpha = 0, 7\frac{1}{2}^{\circ}$) generally result in the most consistent loss-of-contact behaviour.

Increasing track width increases the roll angle at which dynamic unstable equilibrium is reached and reduces the roll moment of the weight about the downslope tyre at roll angles up to 90°. These are stabilising influences that would be expected to reduce all the velocities. In addition, however, the vertical velocity should be higher for a given roll velocity when the track is wider, because they are related kinematically when both tyres are in contact; and the track width will have effects on bounce motion and friction which would be difficult to predict.

The time to reach impact does increase with increasing track width for all bank angles (not presented); this is reflected in increased energy dissipation in tyre/bank friction (Fig.8.24). The roll and vertical velocities show slight overall downward trends, noticeable at low bank angles but masked by loss-of contact effects at higher ones.

The relationships between maximum ROPS energy and the impact variables are typical, and support the findings of the previous section. Where the shapes of the impact roll angle and roll velocity curves are the same, as they are in this case except at a bank angle of $37\frac{1}{2}^{\circ}$, these shapes will be approximately reproduced in the energy curves, modified slightly by the effects of vertical impact velocity. They are further transformed here by a slight downward trend due to the effect of track width during impact (the reverse of that due to ROPS width : see 8.4). This is evident from the energy distributions.

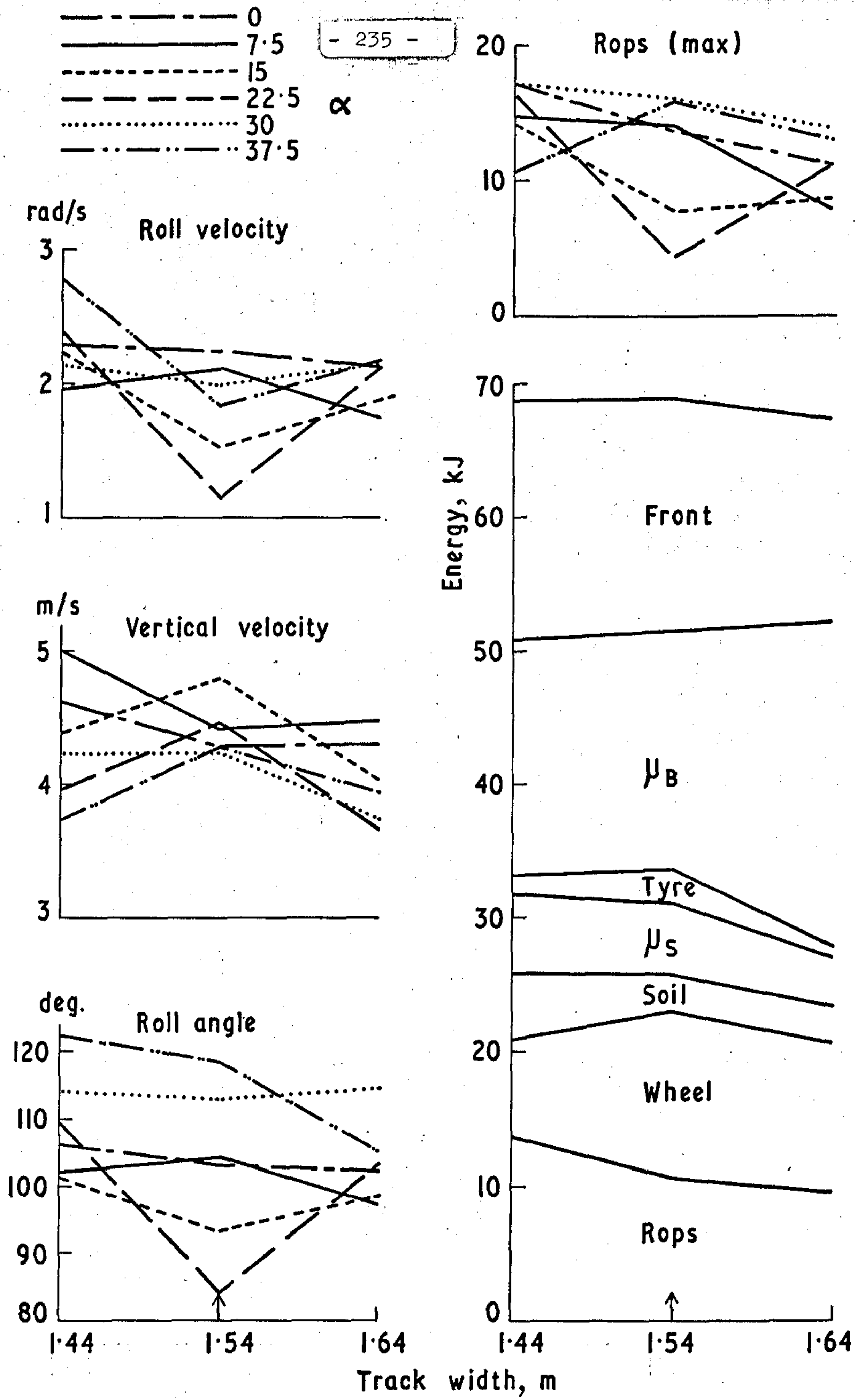

Fig. 8.24 Sensitivity to track width of variables at impact (left), and energy distributions (right).

Centre of mass height

Many of the effects of centre of mass height would be expected to be the reverse of those of track width and broadly, this is so (Fig. 8.25). Impact time and roll velocity show less variation, particularly at lower bank angles but the general trends of increased centre of mass height are the opposite to those of increased track width. The effects on energy distribution between wheel and ROPS during impact are consistent with those obtained by superimposing Figs 8.13 & 8.14 (ROPS height and wheel height). The slope of the uppermost (total) energy line is due to the change in initial potential energy.

Roll moment of inertia

It might be imagined that moment of inertia would have an important effect on the overall behaviour but consideration of the relative magnitudes of the parameters shows this not to be so. Forces at the tyres due to the product of roll acceleration and moment of inertia are generally of a lower order than those arising from the weight and linear accelerations. The main effects of changing moment of inertia therefore arise from the influence on loss-of-contact due to the change in roll oscillation frequency and amplitude.

At low inertia (Fig. 8.26) the oscillation amplitudes are generally small and contact is maintained under the control of the general overturning motion. Increase in inertia causes greater oscillation, which leads to contact being lost earlier and then renewed in some cases. The effect is greatest at large bank angles and leads to a reduction in |roll velocity| and an increase in |vertical velocity| (see 7.2.3.). At the highest inertia studied, loss of contact very early in the overturn modifies the ensuing behaviour to the extent that late loss-of-contact is often suppressed, giving a reversal of the above trend.

The relationships between maximum ROPS energy and the impact variables follow the typical case noted above, modified by the effect of moment of inertia during impact (see 8.3.). The overall effect on mean ROPS energy is small.

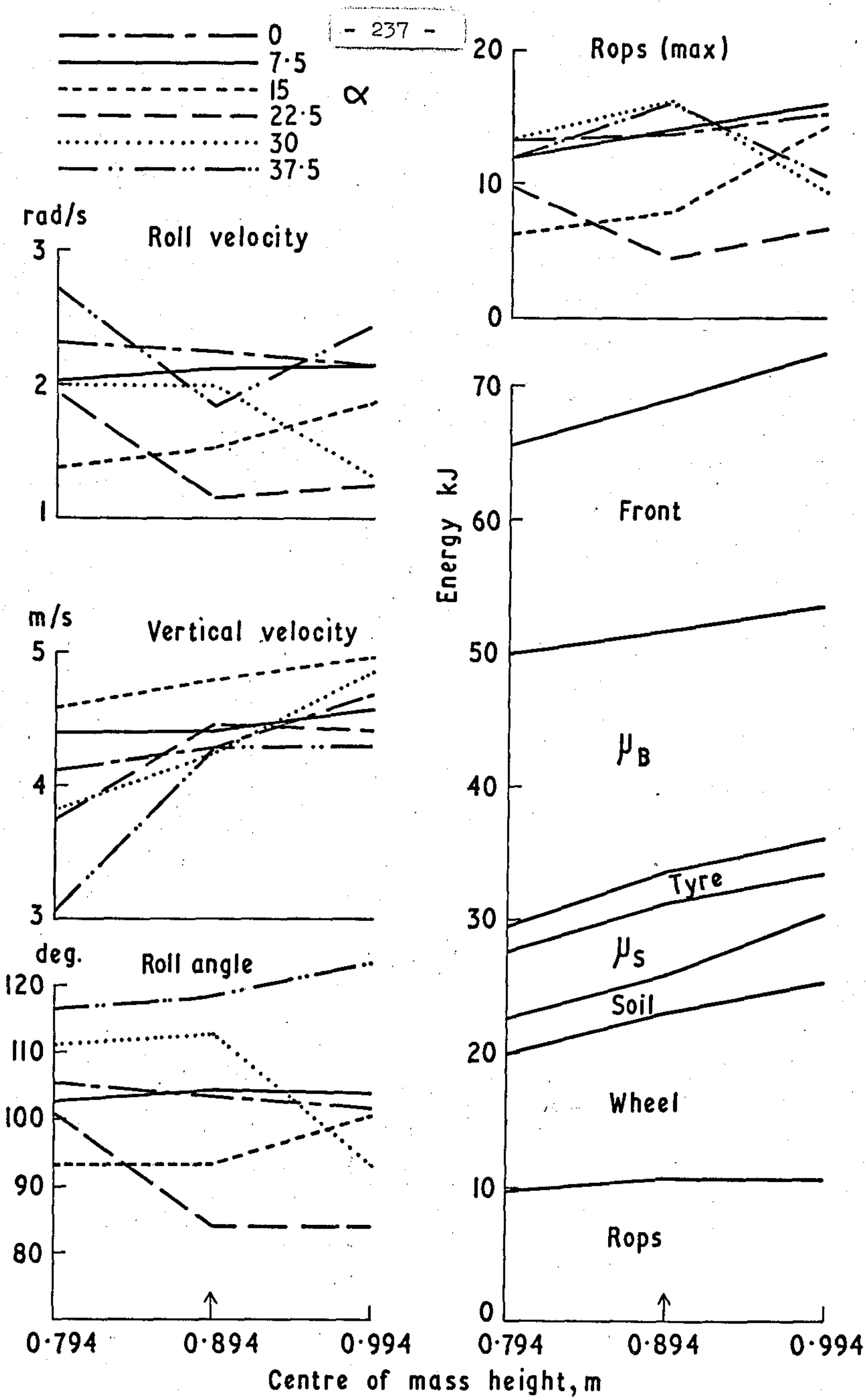

Fig. 8.25 Sensitivity to height of centre-of-mass of variables at impact (L) and energy distributions (R).

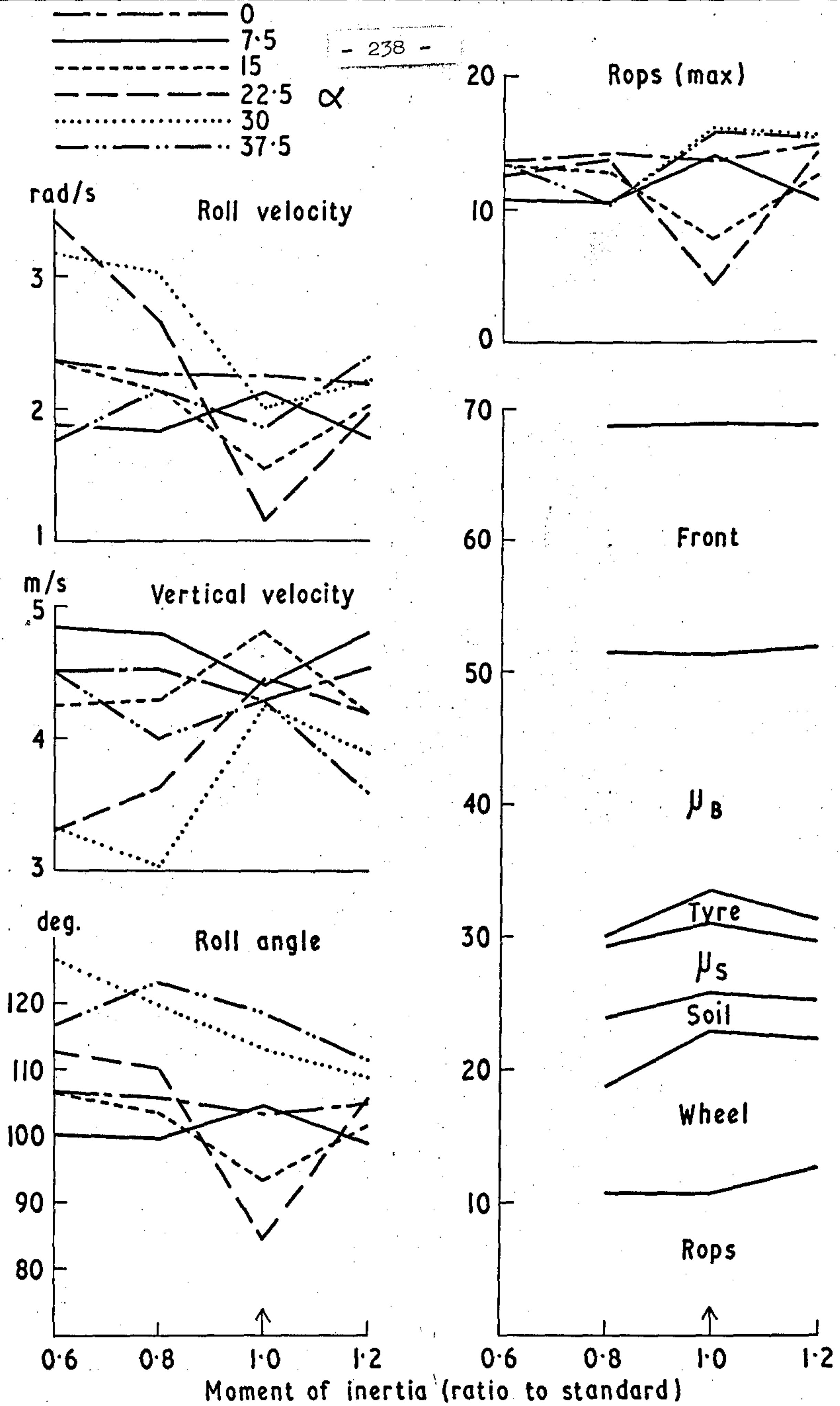

Fig. 8.26 Sensitivity to moment of inertia of variables at impact (left) and energy distributions (right).

Mass, tyre stiffness and damping

These parameters are treated together because their effects are related. The mass changes were made at constant radius of gyration, giving a constant ratio of mass to moment of inertia, in contrast to the changes discussed above. If mass, tyre stiffness and damping coefficients are all changed by the same ratio, all the forces are changed by this ratio and the dynamic behaviour remains unaltered. The parameters therefore influence the behaviour only by their effects on ride mode oscillation, and hence on loss-of-contact. The following effects would be expected by analogy with the effects of change in moment of inertia noted above:-

(i) Increase of damping coefficient has little effect on resonant frequency but should reduce oscillation amplitude. The resulting changes in loss of contact should increase impact roll velocity and reduce vertical velocity. The general trends in Fig.8.27 support this hypothesis.

(ii) Increase of mass reduces both resonant frequency and damping ratio. The effects should be similar to those of increasing moment of inertia and opposite to those of increasing damping. This is not evident in Fig.8.28

(iii) Increase of stiffness increases resonant frequency but reduces damping ratio. The effects are not predictable, and no general trends can be seen in Fig.8.29.

The energies in the three figures show the expected correllations with the variable values at impact. The distribution boundaries for mass variation (Fig.828b) are close to straight lines through the origin, although the bank friction energy increases less than in direct proportion to mass, and soil deformation energy more than in direct proportion.

Limiting coefficient of friction between tyre and bank

The effects shown in Fig.8.30 are almost entirely due to expected varations in overall kinematic behaviour with little influence of ride

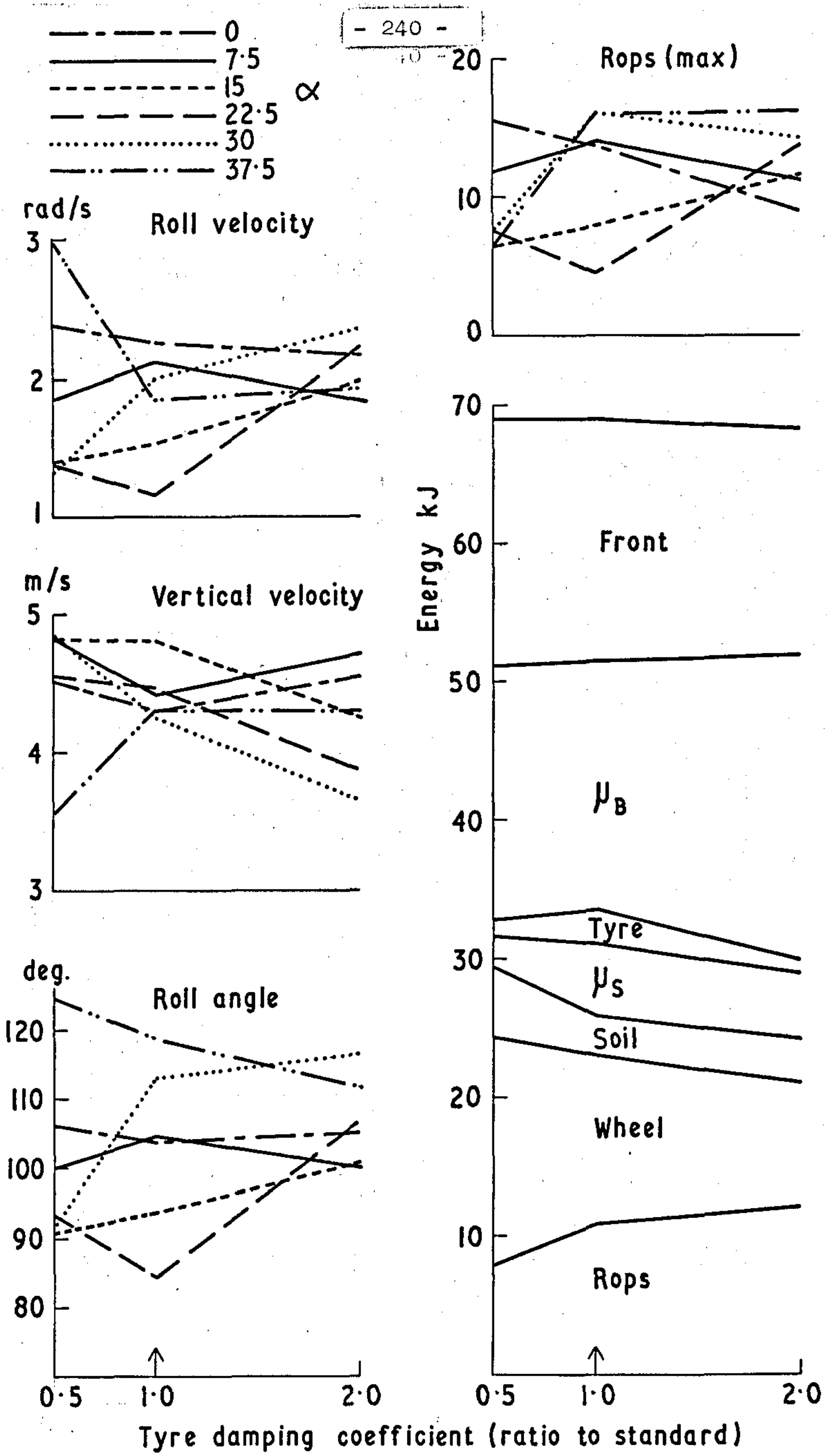

Fig. 8.27 Sensitivity to tyre damping of variables at impact (left) and energy distributions (right).

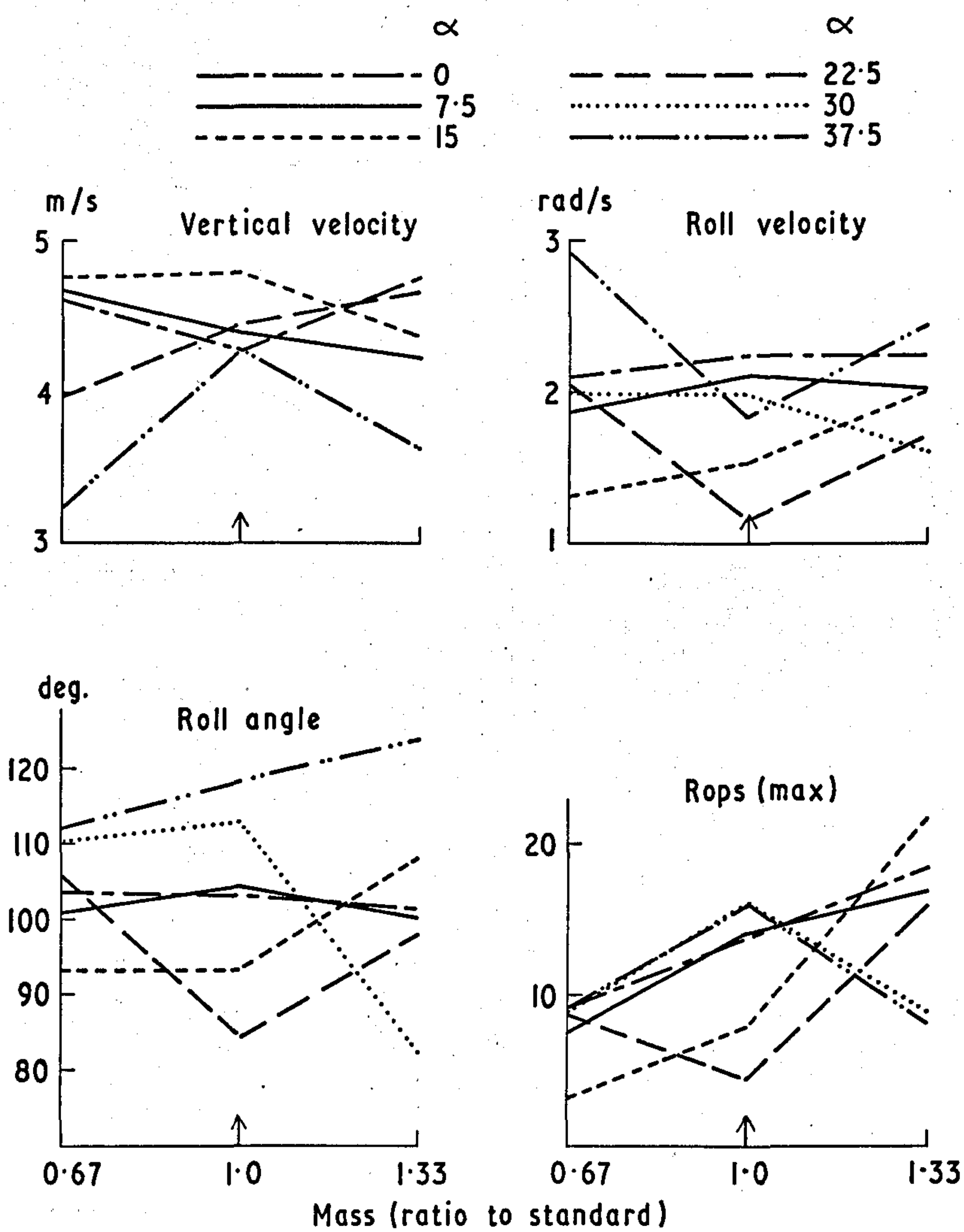

Fig. 8.28a. Sensitivity to tractor mass of variables at impact and maximum ROPS sideways energy.

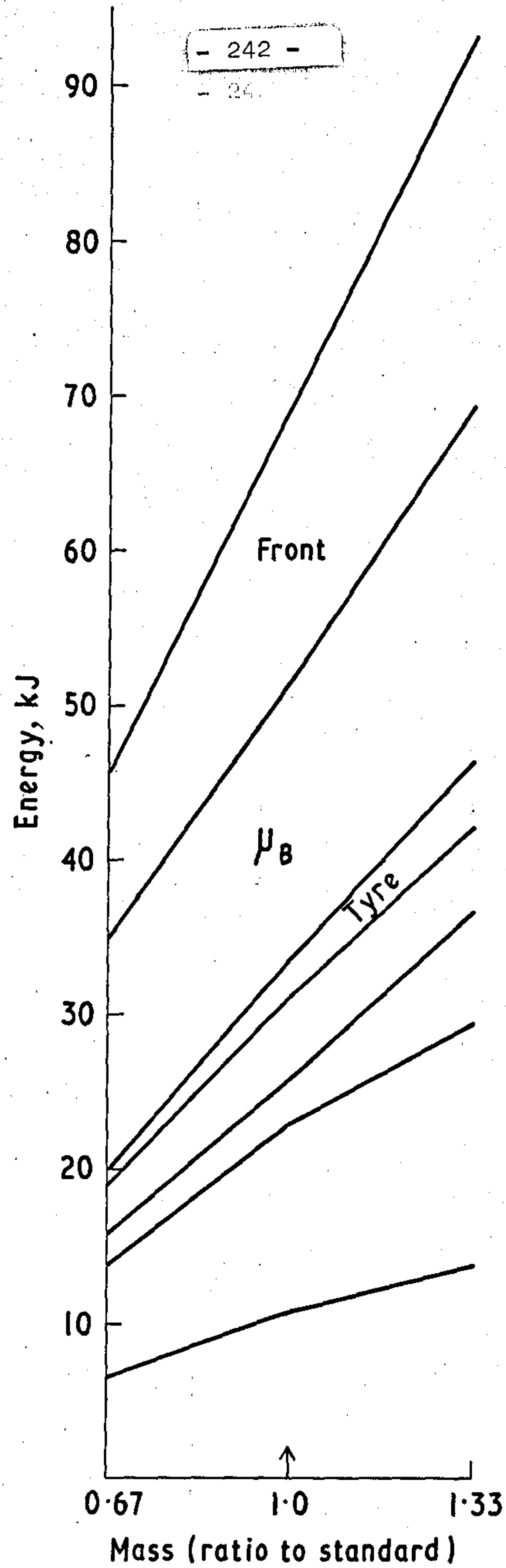

Fig. 8.28b Sensitivity to tractor mass of energy distributions.

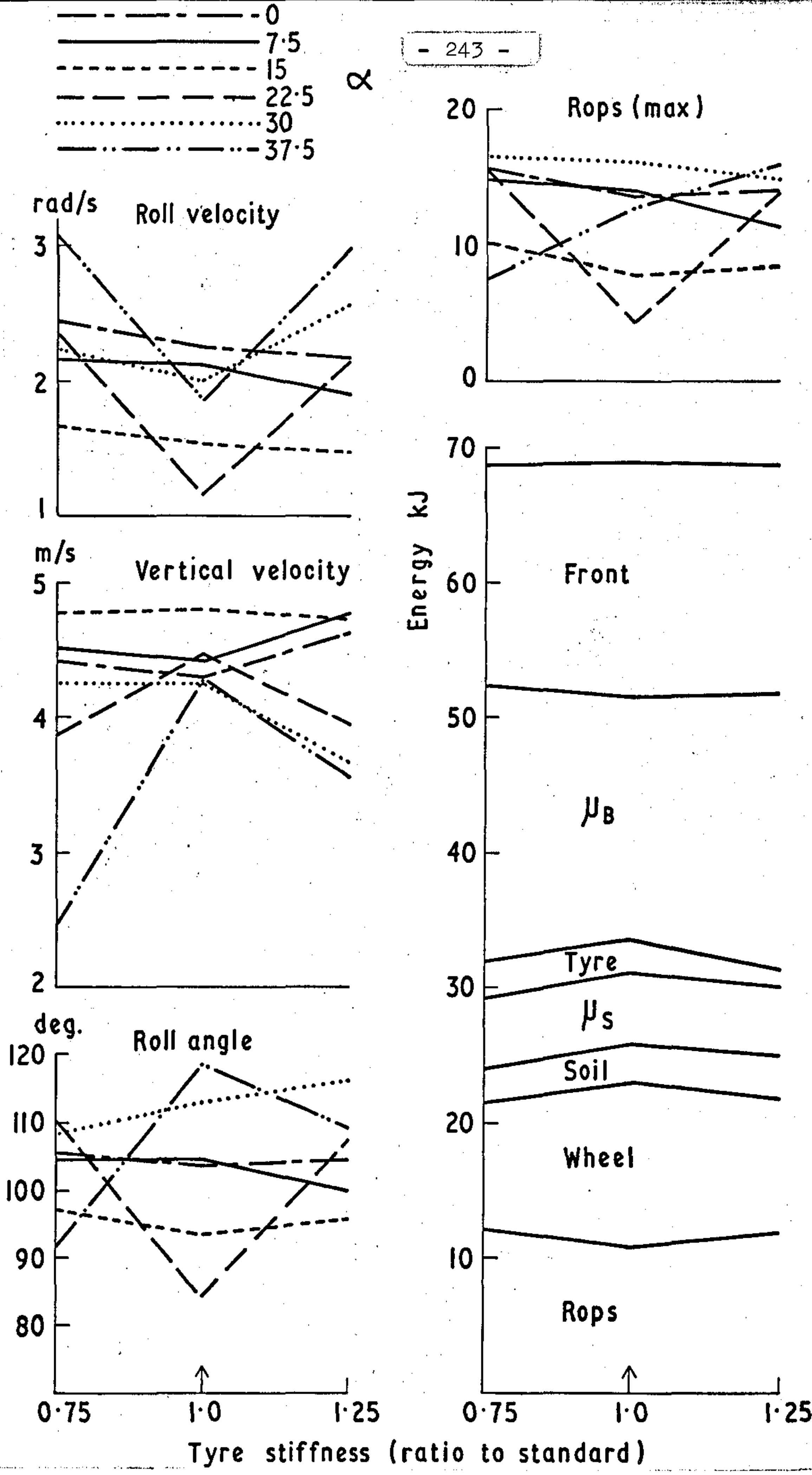

Fig. 8.29 Sensitivity to tyre stiffness of variables at impact (left) and energy distributions (right).

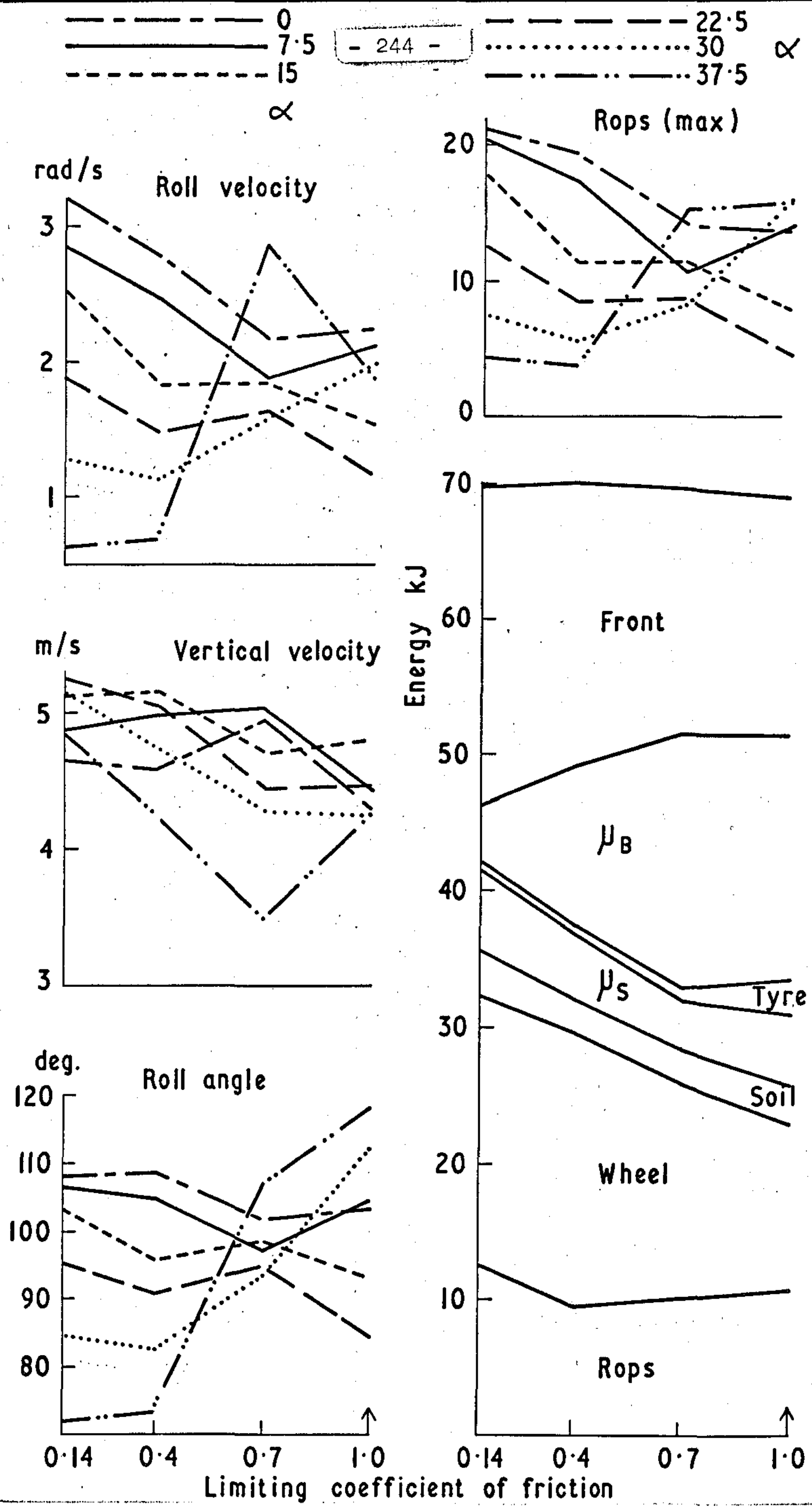

Fig. 8.30 Sensitivity to tyre/bank friction of variables at impact (left) and energy distribution (right).

mode oscillation and variations in loss of contact.

At bank angles up to $22\frac{1}{2}^{\circ}$ the accelerations are limited mainly by friction at the downslope tyre (point 10) in the first part of the overturn. As the roll angle increases the sliding velocity of tyre 10 decreases and friction at the upslope type (point 9) increasingly dominates the behaviour. Higher friction simply increases these retarding forces and results in lower roll and vertical impact velocities. In some cases the predominant reduction is in lateral velocity (not shown).

At the two higher bank angles, friction at tyre 10 continues to exert a major influence late in the overturn. Beyond the point of unstable dynamic equilibrium, increased friction exerts a higher roll moment, resulting in a higher impact roll velocity but a lower vertical velocity. Loss of contact reverses this trend only at a bank angle of $37\frac{1}{2}^{\circ}$, and sufficiently late in the overturn to have little effect on the trend of impact roll angle.

The ROPS energies relate to the impact variables as expected. There is little overall change because of the different effects at high and low bank angles. The largest influences are on energy dissipated in tyre/bank friction and energy absorbed in wheel deformation due to the effect of vertical impact velocity.

Cornering stiffness, relaxation length, forward speed and approach angle

Cornering stiffness, the initial slope of the side force/slip angle relationship, and relaxation length, the measure of delay in side force development, both have direct effects on tyre friction. Forward speed influences friction by affecting both the slip angle through its relation to sliding velocity and the development of side force through rolling distance. Forward speed also has a direct effect on initial lateral velocity. The angle of approach of the tractor to the bank edge affects only initial lateral velocity.

Increase in cornering stiffness or reduction in relaxation length lead to more rapid changes in side force. This might be expected to have similar but less pronounced effects to those of changing the limiting coefficient of friction. This is not generally evident in Figs.8.31 and 8.32, mainly because of the effects on loss of tyre contact, particularly at larger bank angles.

Clear trends with forward speed (Fig.8.33) cannot be expected in the absence of any with cornering stiffness or relaxation length.

Approach angle (Fig.8.34) has little affect at low bank angles; at high ones, changes in loss of contact lead to rather erratic behaviour.

The expected relationships between impact variables and ROPS energy are confirmed for all four parameters. Mean energy distributions are generally little affected but energy dissipated in tyre friction decreases with increasing relaxation length, which is consistent with the effect of limiting friction (Fig.8.30), and increases at the highest forward speed. In both cases the change in energy at impact is absorbed mainly in wheel deformation because of the effect of vertical velocity.

8.6. DISCUSSION

The relationships between energy absorbed in ROPS deformation and the parameters and conditions at impact have proved to be well behaved and amenable to explanation, at least qualitatively.

The variations of ROPS energy with impact roll angle, ROPS width and track width do not show rapid changes according to whether the ROPS or the wheel hits the ground first; rather, the effects are continuous because of the duration of impact. Similarly, the variations with vertical impact velocity and with the heights above the centre of mass of the ROPS and the top of the wheel are affected by interaction between the wheel and ROPS during impact. Of the variables at impact, only the lateral velocity has little effect on ROPS energy.

The ratio of ROPS-soil strength has a less continuous effect, with high sensitivity over a fairly narrow range. ROPS vertical strength has a

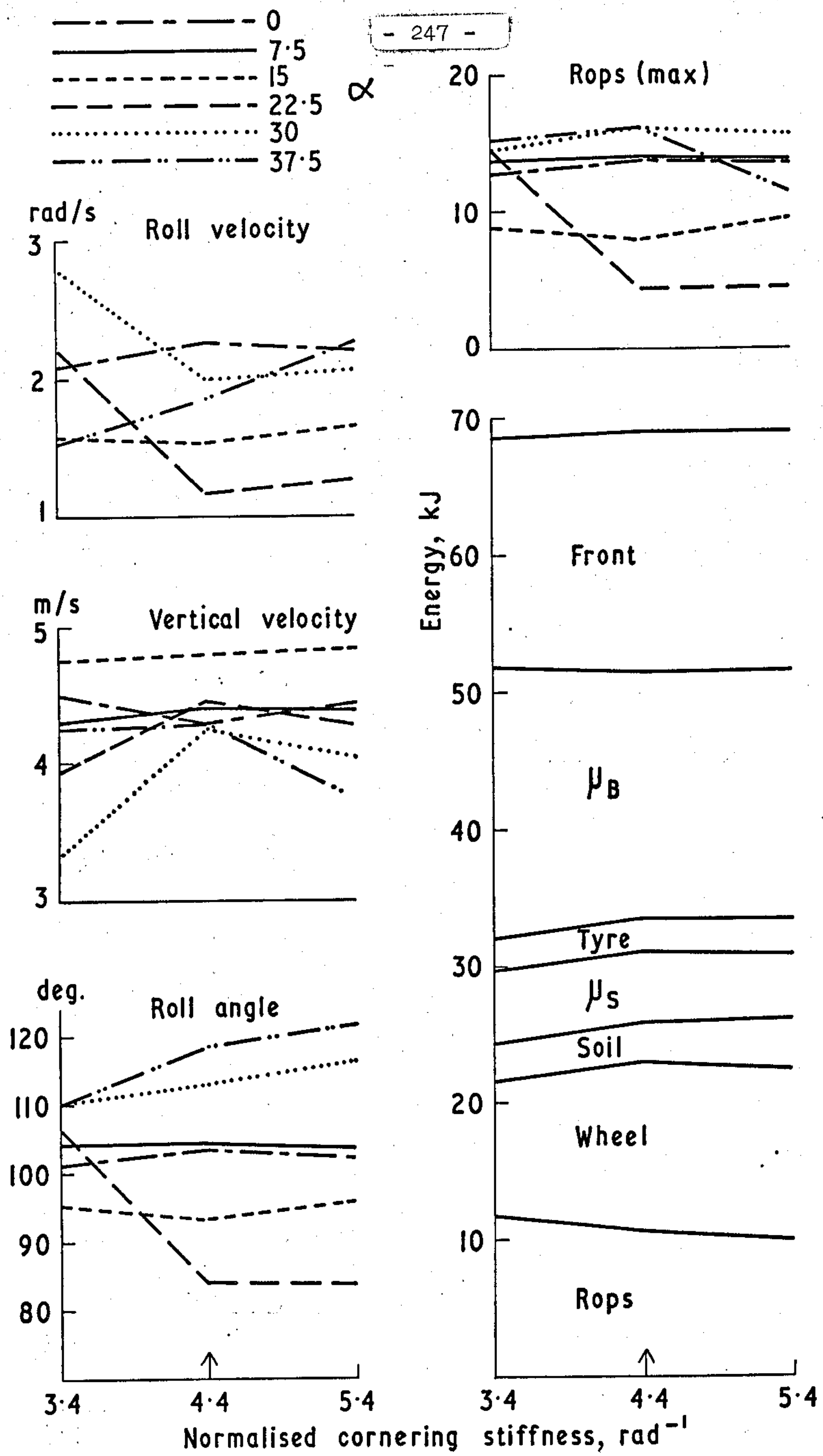

Fig. 8.31 Sensitivity to tyre cornering stiffness of variables at impact (L) and energy distributions (R).

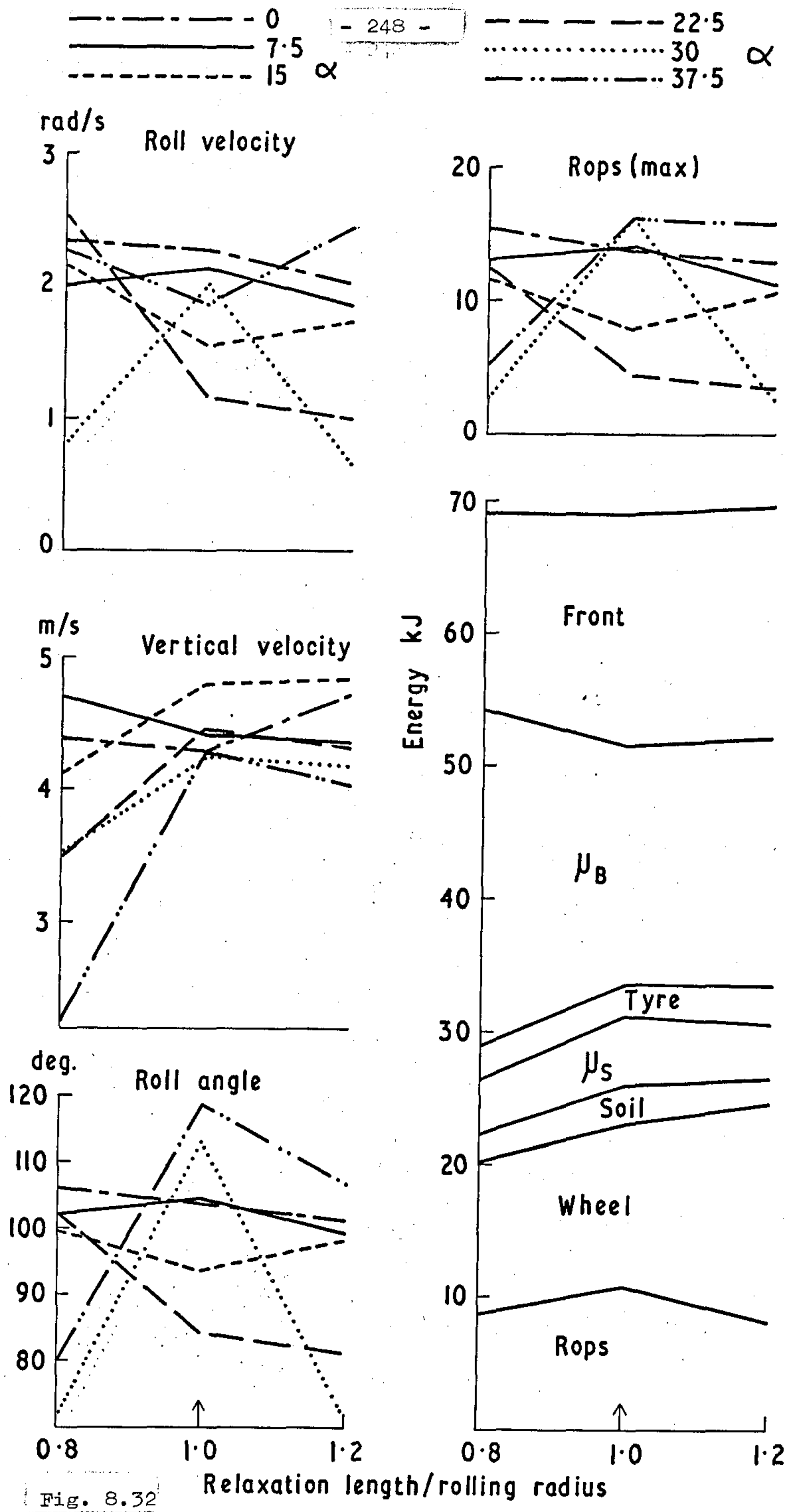
0
7·5
15
α
22·5
30
37·5
α
rad/s
Roll velocity
3
2
1
0
Rops (max)
20
10
0
m/s
Vertical velocity
5
4
3
70
Front
60
Energy kJ
50
μ_B
40
30
Tyre
μ_S
Soil
20
Wheel
10
Rops
deg.
Roll angle
120
110
100
90
80
0·8
1·0
1·2
0·8
1·0
1·2
Relaxation length/rolling radius

Fig. 8.32

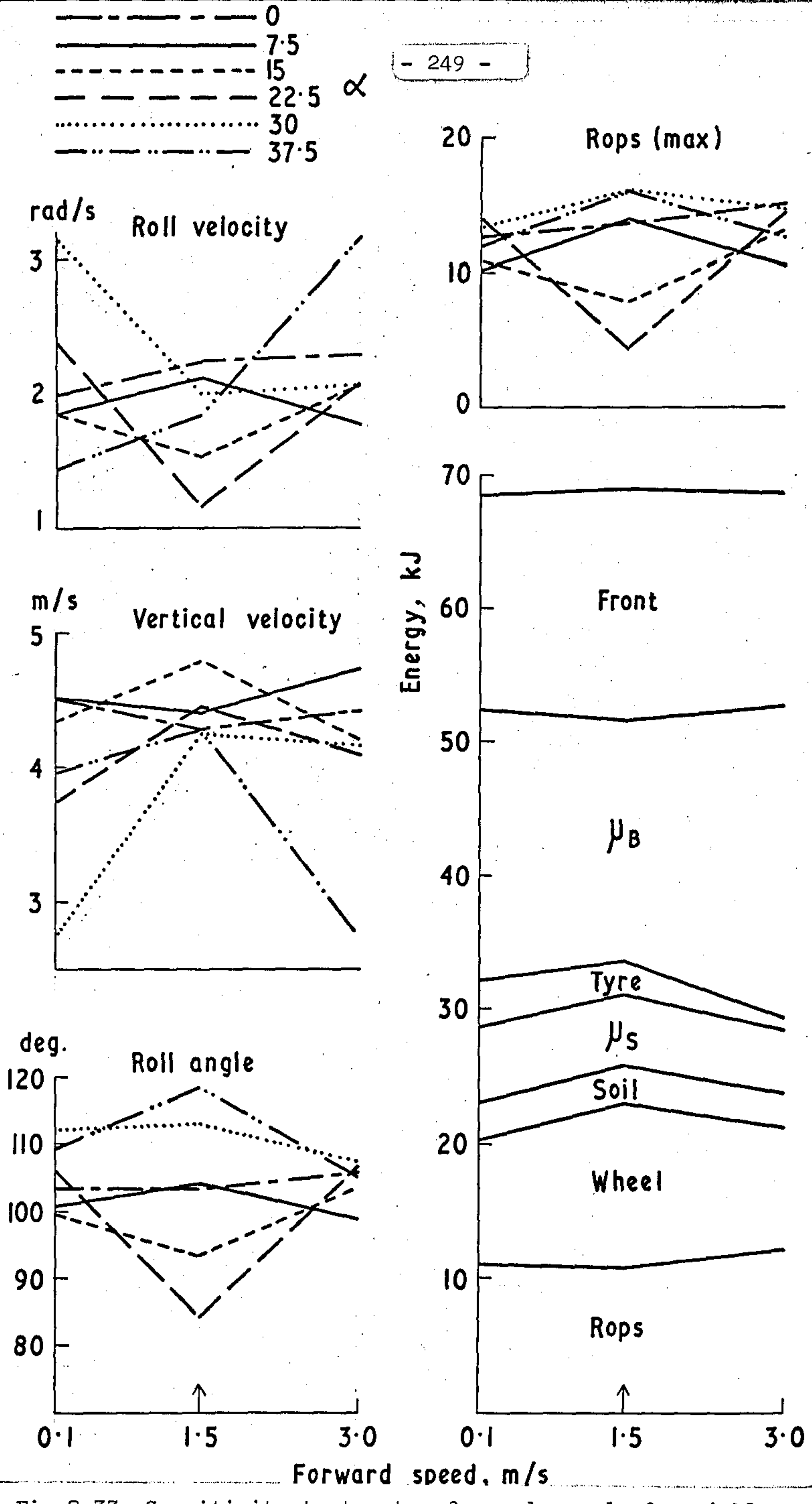

Fig 8.33 Sensitivity to tractor forward speed of variables at impact (left) and energy distributions (right).

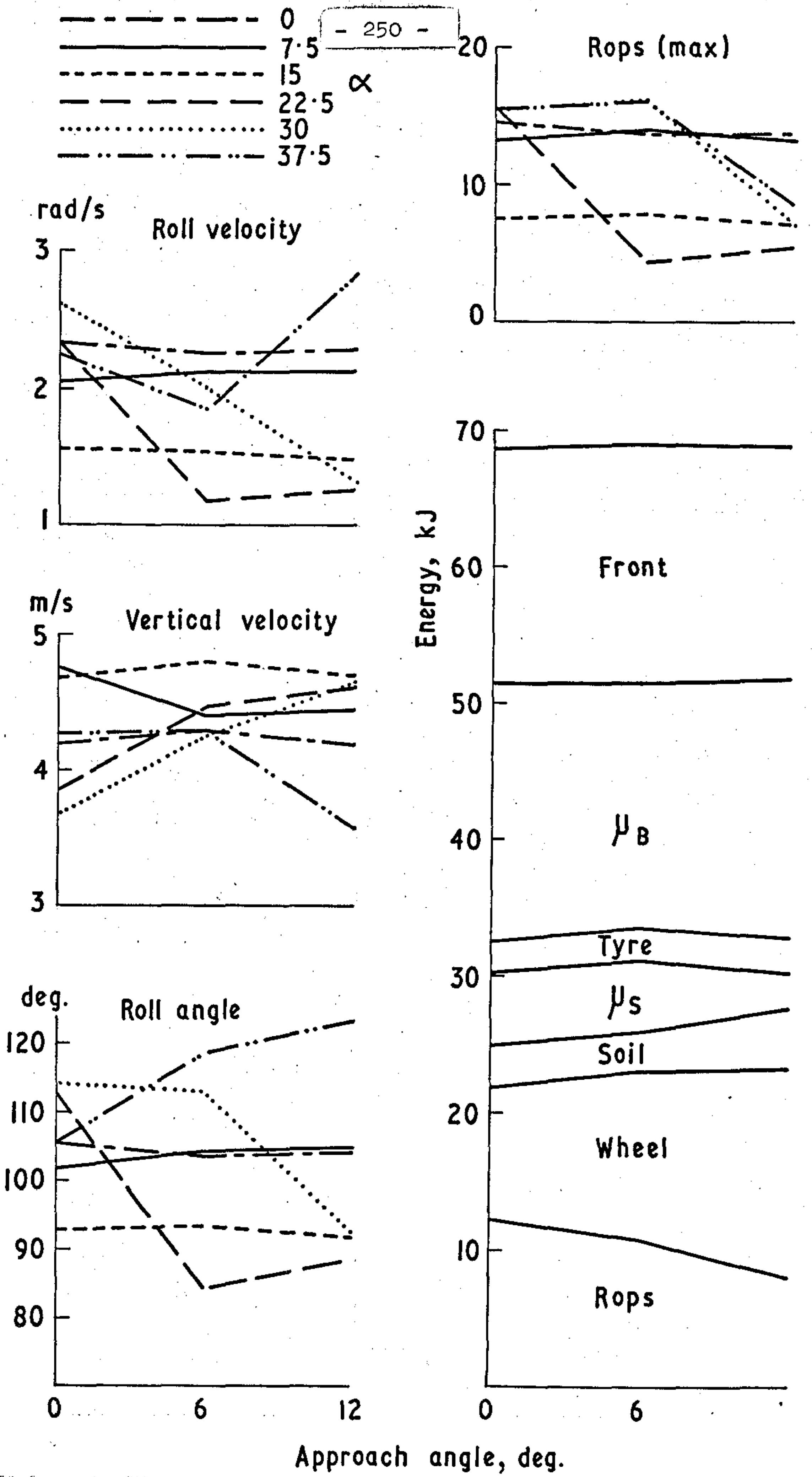

Fig. 8.34 Sensitivity to bank approach angle γ of variables at impact (L) and energy distributions (R).

major effect in simulations representing more severe accidents, with large impact roll angles and a high bank.

Damping coefficient is the only parameter describing the wheel structural behaviour that had a noticeable effect, and then mainly on the distribution of energy between wheel deformation and sliding friction.

The overturning phase is much less well behaved because of changes in loss of tyre contact. The causes are difficult to predict in many cases and the effects can be large. The experimental validation suggested that the effects predicted by the simulations were genuine, under the equivalent standard parameters. The reasons are understood in general terms of ride mode oscillation, which is affected by the continuous variation of tyre side force, but the explanation of why a particular loss of contact occurs in one simulation and not another, or occurs at a different time, would require much greater detail in the computer output. Values would be needed at fairly small time increments of all four component forces at each tyre (Fig.3.2), the corresponding deflections and their rates of change, the slip angles and nominal and instantaneous coefficients of friction, in addition to the variables describing the rigid body motion. There is little doubt that causes would become apparant, and investigation of the relationship between ride oscillation and dynamic friction would be of interest. Little benefit would result, however, in rationalising the effects on ROPS energy, which are fortunately fairly small overall, and the considerable effort that would be required is not justified in the present study.

Few parameters have much influence in the overturning phase on either the mean energy distributions or the individual values at low bank angles (the steepest banks). Track width, tyre damping coefficients and tyre friction parameters have some effect on both the energy dissipated in sliding friction and the variables at impact. At higher bank angles, the critical dependence of roll moment on roll angle at late loss of contact causes erratic behaviour in many cases but the overall effects on mean ROPS energy are generally small.

9. SIMULATIONS BASED ON DATA FROM REAL TRACTORS

The simulations reported in this section used data based on measurements of real tractors to find the relationship between ROPS sideways energy and tractor mass, for use in the development of standard strength test criteria.

Standards committees have shown an understandable reluctance to base ROPS strength test criteria on complicated formulae involving many parameters. The simplest analysis shows that several parameters are likely to influence overturning behaviour and the amount of energy absorbed in the ROPS, but only the tractor mass is included in present test formulae. The only exception is the formulae for rear impact or loading, which takes into account the pitch moment of inertia or an estimate of it based on the wheelbase. The lack of reliable evidence of the qualitative effects of different parameters largely justifies the simplicity of the formulae. Proposals have been made that simulations of the type described in this report could form the basis for energy determination for an individual tractor/ROPS combination, using the appropriate parameters. Any simulation , however, represents only a limited number of accident types, and it may be argued that such complex methods imply an overall realism that cannot be justified. In addition, they would be more difficult to implement in routine tests. One standard test method does use a simulation requiring many parameters, but it is related not to strength tests but to the determination of whether a tractor will continue to roll when overturned on a uniform slope. Using Scwanghart's analysis and computer program,(54) it is applied at present only in West Germany, although it has been proposed for inclusion in an EEC Directive.

The simulation described here is not therefore being recommended as a ready-made test criterion, and would be unlikely to be accepted as such. It was considered that the most directly useful information for standards committees would be the results of a large number of simulations based on data from real tractors. These simulations were run over a range of bank angles as before, to average out the effect of discontinuities and provide an indication of the variability.

Data on real tractors are not readily available. Some dimensional parameters and an estimate of ROPS strength could have been obtained from test reports but moment of inertia measurements and full tyre data are more scarce. Schwanghart has collated measurements of the basic parameters for a large number of tractors and the regression lines he fitted against mass were suitable for use in this study.(53) The averaging of relationships between parameters loses some precision in the simulations but is considered justifiable in view of the forgoing discussion, and of the only approximate estimates of other parameters.

9.1 Data

Regressions were taken directly from Sch wanghart for (Table 9.1) track width, centre of mass coordinates, rear tyre height and width, ROPS height and width, and roll moment of inertia. The track width is quoted as a minimum, but does not appear unduly small and is compensated by the larger tyre width common in Continental Europe. Longitudinal centre of mass position was used to calculate the effective rear mass. Rim height was determined from tyre height and width assuming a constant tyre depth/width ratio of 0.75.

ROPS sideways collapse force was assumed equal to tractor weight and the elastic stiffness was calculated to give a deflection of 100 mm at the elastic limit. Tentative evidence for these values was provided by an analysis of strength test report data. The ROPS was assumed to be vertically rigid for the simulations reported here, because of the lack of information on vertical strength.

All the structural characteristics for the rear tyres and wheels (elastic stiffnesses, damping coefficients and, for the wheel, collapse force) were assumed to be directly proportional to effective rear mass. The constants were selected to give the measured parameter values for the experimental tractor at a nominal rear mass of 2000 kg. The tyre stiffness relationships are probably reasonable in general (83) but the contribution of carcase stiffness for a particular tyre clearly depends on the size and type and will not be linearly related to nominal load. Wheel collapse force has been shown not

TABLE 9.1

Parameters based on real tractor data

Parameter	*Relation to tractor mass, m, kg	Parameter values for tractor mass, kg							
		1000	2000	3000	4000	5000	6000	7000	8000
Track width, m	1.202×10^{-4} m + 1.140	1.260	1.380	1.500	1.621	1.741	1.861	1.981	2.101
Centre of mass height, m	7.519×10^{-5} m + 0.588	0.663	0.738	0.813	0.889	0.964	1.039	1.114	1.189
– forward of rear axle, z_{gr}, m	8.453×10^{-5} m + 0.577	–	–	–	–	–	–	–	–
– behind front axle, z_{gf}, m	1.254×10^{-4} m + 1.044	–	–	–	–	–	–	–	–
Effective rear mass, m_r, kg	$z_{gf}/(z_{gf} + z_{gr})$	639	1268	1893	2512	3128	3741	4352	4962
Rear tyre height, m	1.113×10^{-4} m + 1.107	1.218	1.329	1.440	1.552	1.663	1.774	1.886	1.997
Rear tyre width, m	4.334×10^{-5} m + 0.259	0.302	0.345	0.389	0.432	0.475	0.519	0.562	0.605
ROPS height, m	1.236×10^{-4} m + 2.061	2.185	2.308	2.431	2.555	2.679	2.802	2.926	3.049
ROPS width, m	$2.0 \times 10^{-4} + 0.7$	0.900	1.100	1.300	1.500	1.700	1.900	2.100	2.300
Roll moment of inertia, kgm^2	$215.857e^{4.494 \times 10^{-4} m}$	338	530	831	1303	2042	3200	5016	7862
Rim diameter, m	Tyre height – 1.5 x tyre width								
Effective tyre area, m^2	Annulus area/4	0.176	0.217	0.263	0.313	0.366	0.424	0.485	0.550

*From ref.(53), updated by Schwanghart (Private communication)

TABLE 9.1 Continued

Parameter	Relation to tractor mass, m, kg	Parameter values for tractor mass, kg							
		1000	2000	3000	4000	5000	6000	7000	8000
Effective ROPS area, m^2	$0.1\ (m/3000)^{0.3333}$	0.0693	0.0873	0.100	0.110	0.118	0.126	0.132	0.138
ROPS side collapse force, kN	$9.8067 \times 10^{-3}\ m$	9.807	19.61	29.42	39.2	49.0	58.8	68.6	78.4
ROPS elastic stiffness, kN/m	$9.8067 \times 10^{-2}\ m$	98.07	196.13	294.20	392.27	490.33	588.40	686.47	784.54
RIM collapse force, kN	$0.018\ m_r$	11.50	22.84	34.07	45.22	56.31	67.35	78.35	89.32
Rim elastic stifness, kN/m	$0.24828\ m_r$								
Rim damping coefficient, kNs/m	$0.01\ m_r$	6.387	12.69	18.93	25.12	31.28	37.41	43.52	49.62
Tyre vertical stiffness, kN/m	$0.2\ m_r$	127.7	253.7	378.5	502.5	625.7	748.3	870.6	992.4
- damping coefficient, kNs/m	$1.5 \times 10^{-3}\ m_r$	0.958	1.903	2.839	3.768	4.692	5.612	6.529	7.443
Tyre lateral stiffness, kN/m	$0.075\ m_r$	47.9	95.1	141.9	183.4	234.6	280.6	326.5	372.2
- damping coefficient. kNs/m	$0.5 \times 10^{-3}\ m_r$	0.319	0.634	0.946	1.256	1.564	1.870	2.176	2.481

to be a sensitive parameter. Limitations of the use of wheel damping have been discussed (7.1.2, 7.2.5) but a coefficient proportional to mass should affect all tractors to about the same extent.

Tyre effective impact areas were calculated from the dimensions and those for the rim assumed to be the same, as in previous simulations. The effective area of the ROPS was assumed to be related to the standard value for the 3000 kg tractor according to the cube root of the mass, i.e. assumed proportional to ROPS length.

All other parameters, including bank height, soil strength and those describing the tyre friction relationships retained their values from the standard simulations.

The simulations based on fitted data were run for tractor mass between 1000 and 8000 kg in 250 kg steps. This represents an extrapolation of Schwanghart's regressions, which were obtained from data on tractors up to about 5000 kg.

9.2 Results

Energy absorbed in the ROPS at maximum sideways deformation is plotted against tractor mass for each bank angle in figs. 9.1–9.6, and for all combined in fig. 9.7. The method used to fit the curves was influenced by two observations: energy increases less than in direct proportion to mass and appears to be limited, particularly at low bank angles (figs. 9.1 & 9.2); and the points are not uniformly or normally distributed within the scatter band but lie predominantly in two groups (most noticeable at bank angles of $22\frac{1}{2}^{\circ}$ and above, and in the combined plot - figs. 9.3–9.7).

The falling slope of the energy-mass characteristic is due mainly to the fixed dimension in the terrain description - the bank height. Simulations of overturns on non-dimensional terrain, such as a uniform slope, give the opposite result of energy increasing more rapidly than in direct proportion to mass.[56] The linear dimensions of the tractor and ROPS increase roughly according to the cube root of the mass, for vehicles of the same shape and density (although they may be approximated over a limited range by straight

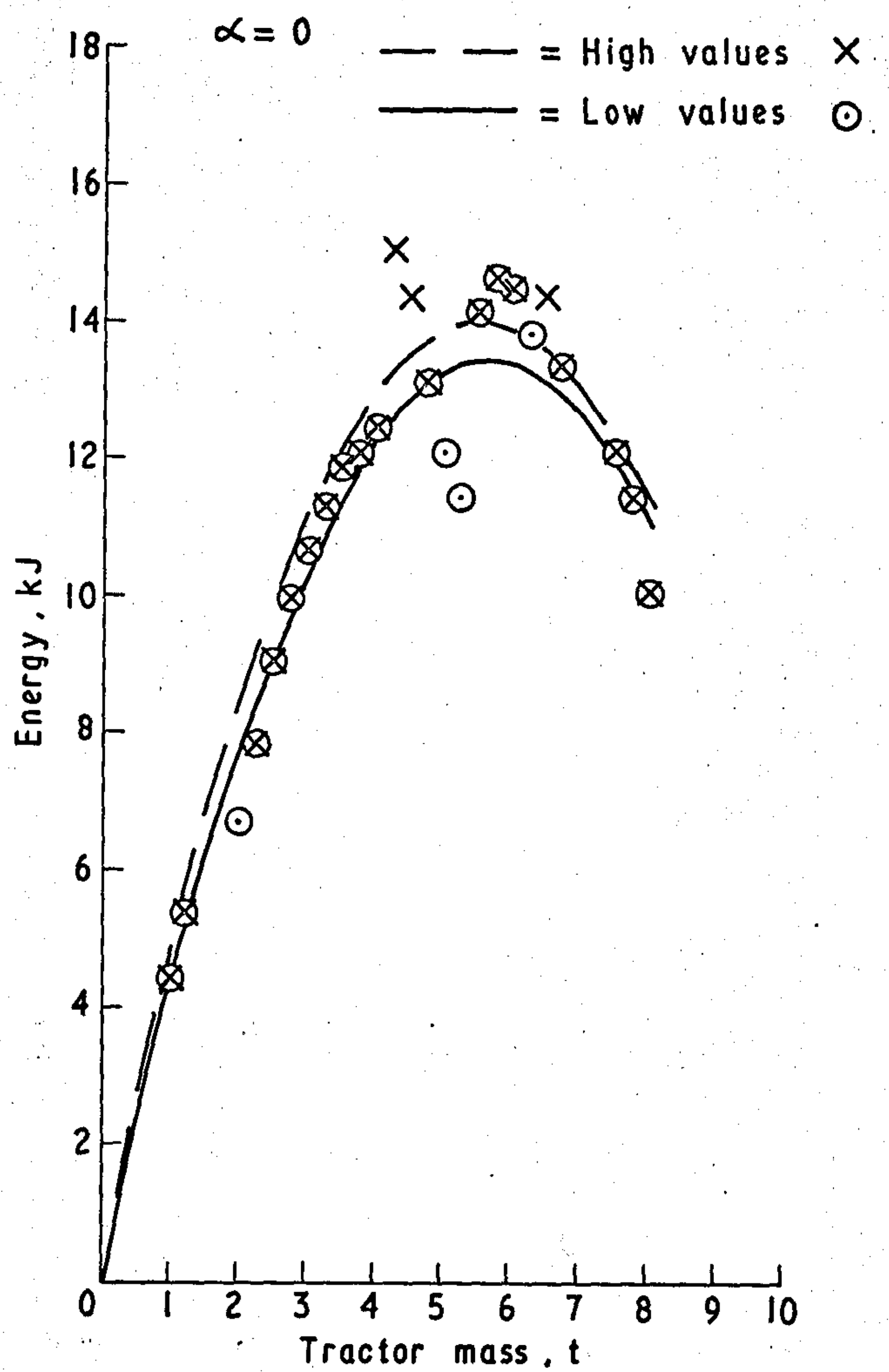

Fig. 9.1 Maximum ROPS sideways energy for simulations based on real tractor data: Bank angle 0°

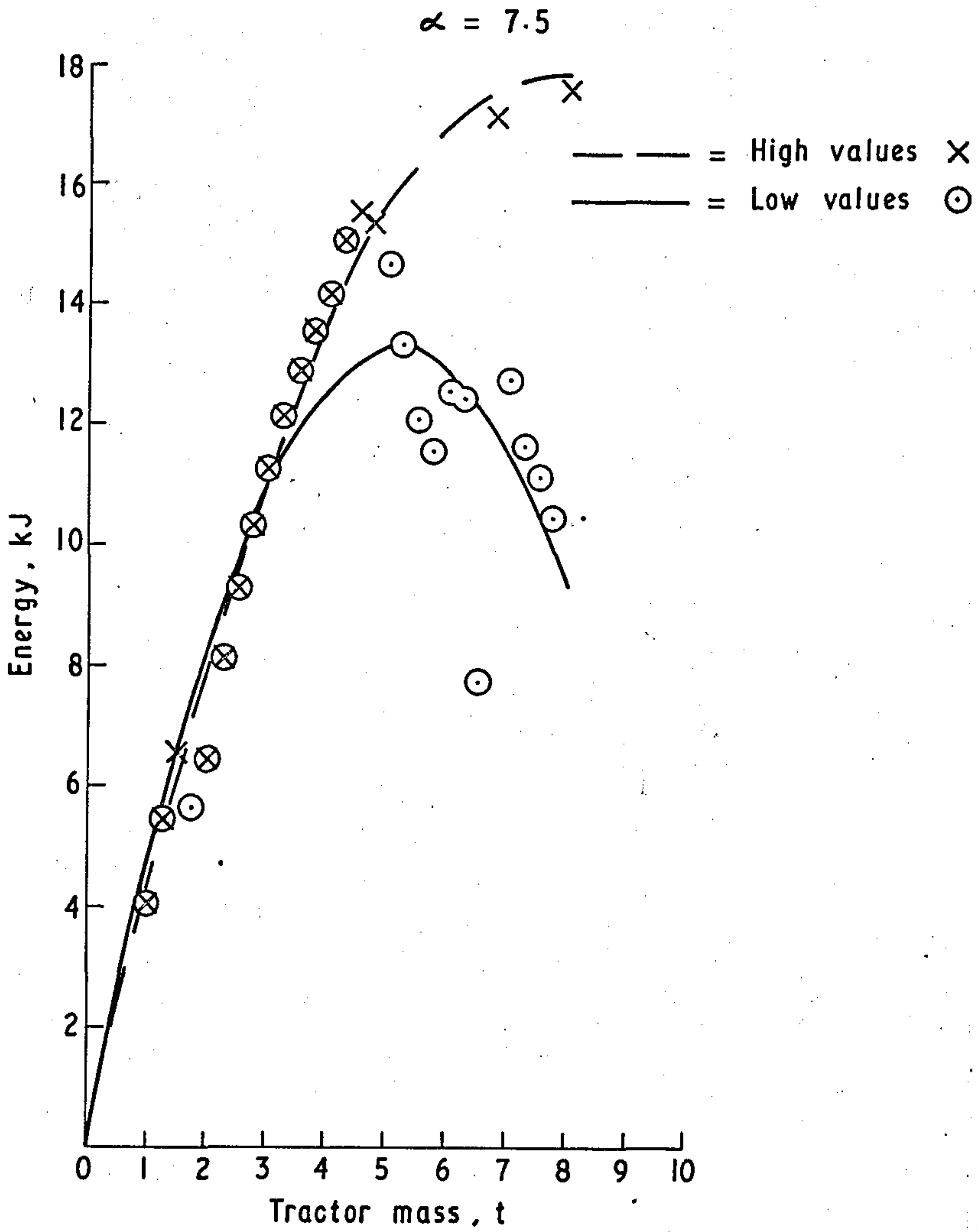

Fig. 9.2 Maximum ROPS sideways energy for simulations based on real tractor data: Bank angle 7.5°

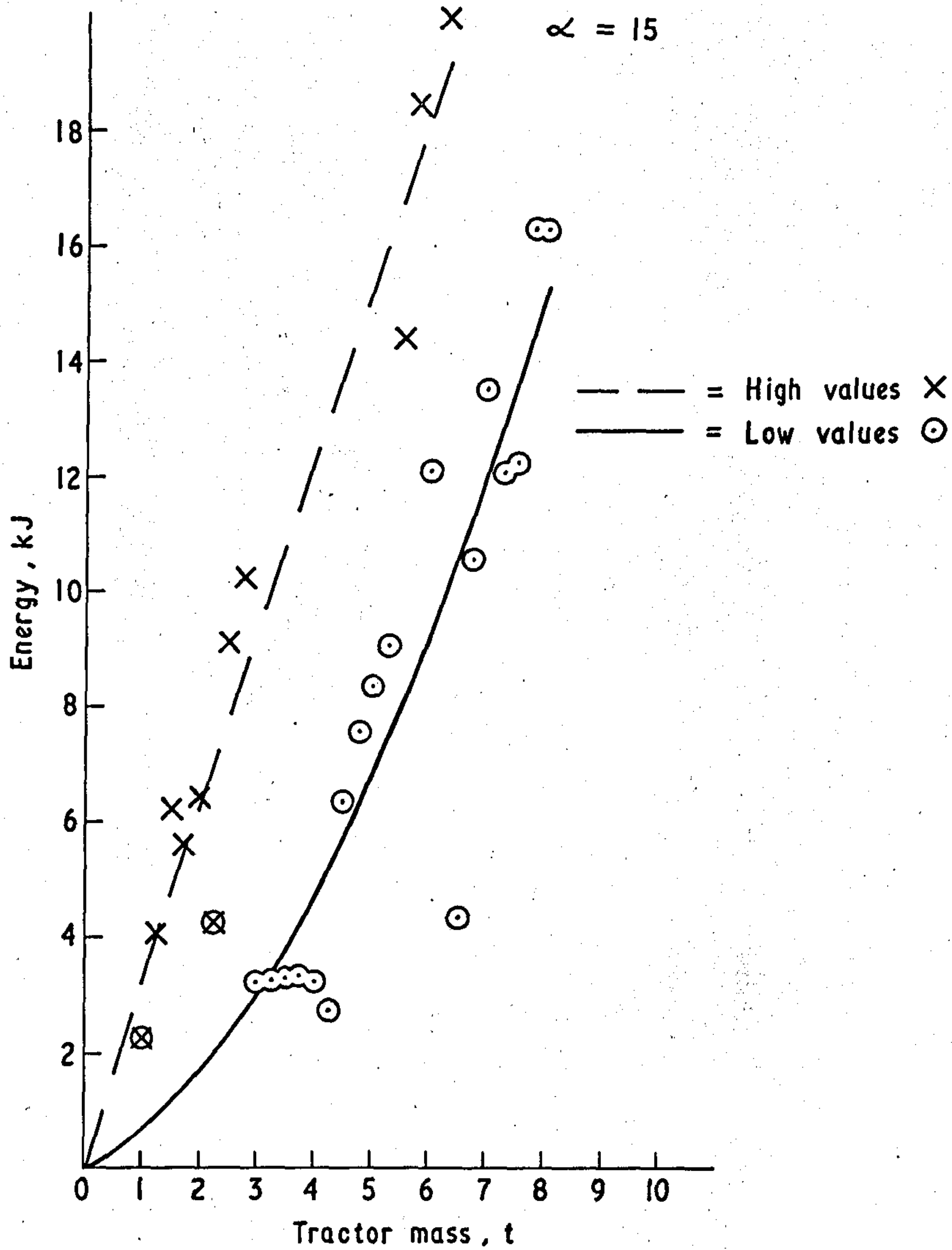

Fig. 9.3 Maximum ROPS sideways energy for simulations based on real tractor data: Bank angle 15°

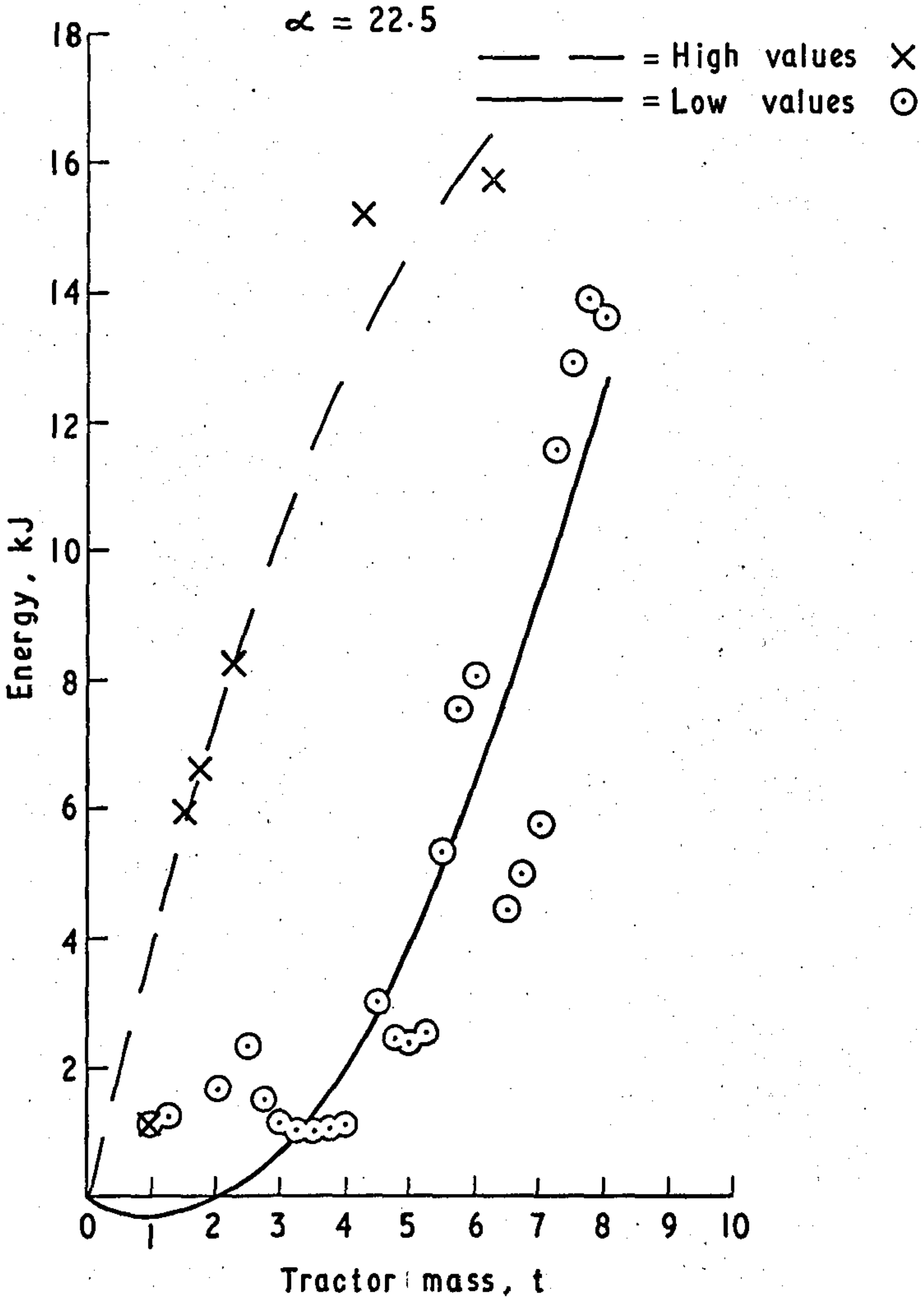

Fig. 9.4 Maximum ROPS sideways energy for simulations based on real tractor data: Bank angle 22.5°

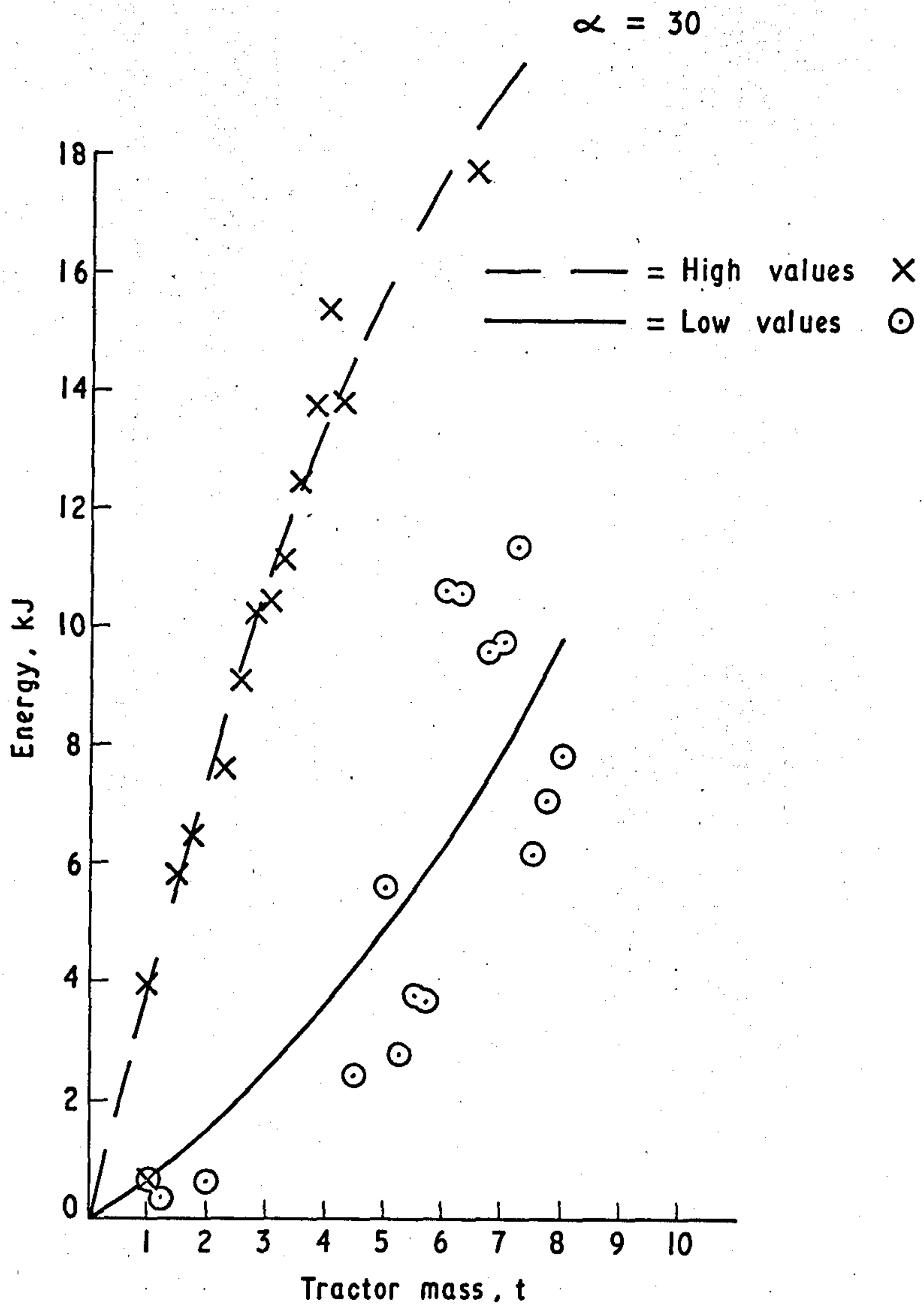

Fig. 9.5 Maximum ROPS sideways energy for simulations based on real tractor data: Bank angle 30°

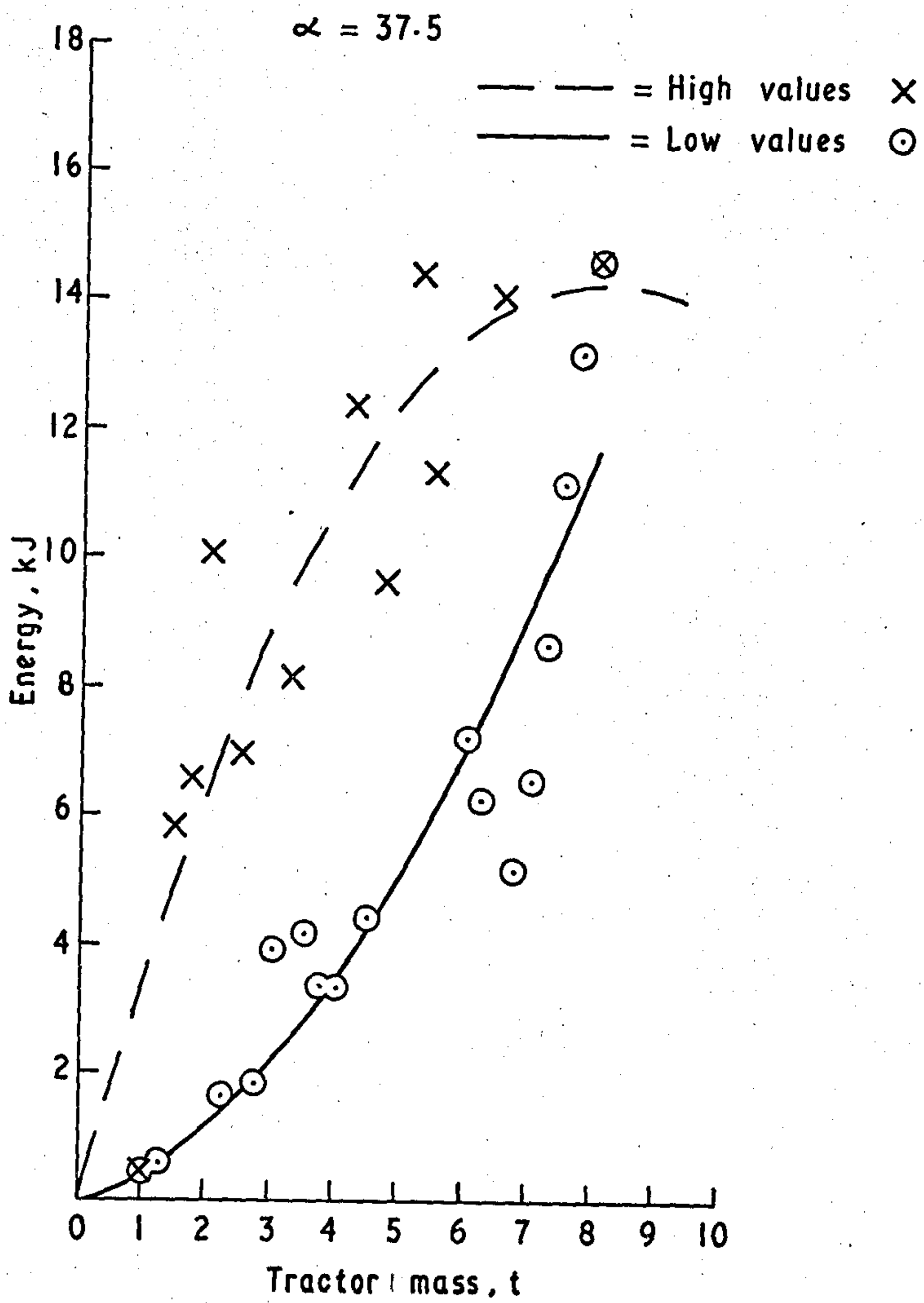

Fig. 9.6 Maximum ROPS sideways energy for simulations based on real tractor data: Bank angle 37.5°

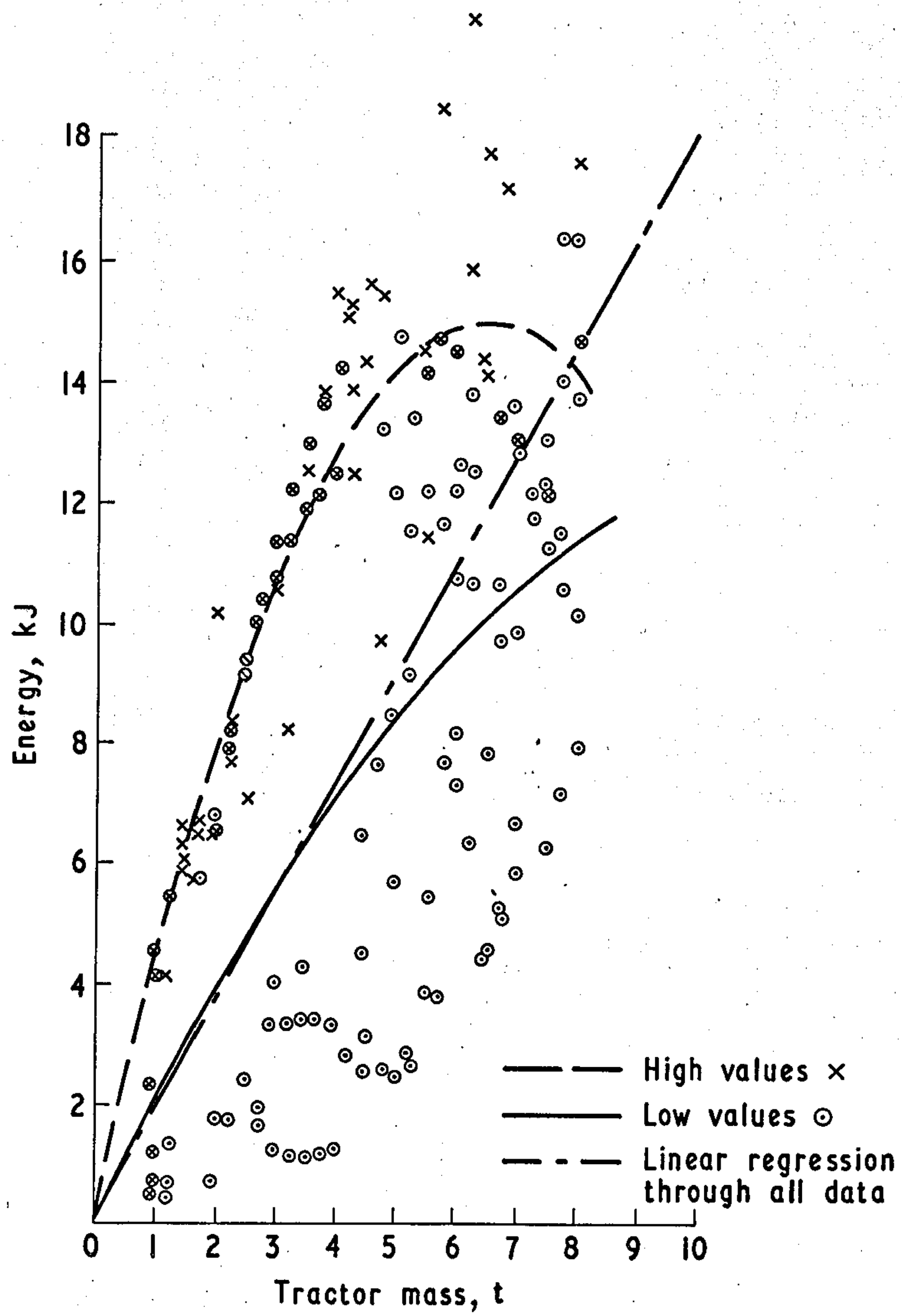

Fig. 9.7 Maximum ROPS sideways energy for simulations based on data from real tractors at 6 bank angles

lines). Where the terrain is non-dimensional, the height of fall of the centre of mass depends on the tractor size and the potential energy increases approximately to the 4/3 power of mass. For an overturn down a bank of fixed height, however, the height of fall varies less with mass and the roll angle at impact decreases as the track width increases. In the extreme, a tractor whose dimensions were very large compared with the bank would not overturn at all. The importance of impact roll angle velocity have been demonstrated in the sensitivity analysis.

The ratio of ROPS strength to soil strength is a secondary influence in both types of overturn. The effective ratio here increases to the 2/3 power of mass because of the effect of ROPS impact area; the influence on energy distribution is significant at masses over about 5000 kg, but is less important than the effect of impact roll angle.

The division of energy points into two groups appears to be caused by differences in tyre loss of contact, consistent with the difference between the simulations of experiments 12 and 19 (see 7.2.3.).

On the basis that these two sets are genuinely distinct, each data point was allocated to one or the other by inspection of the figures. Where the sets appeared to intersect, as in Fig.9.2 below a mass of 2500 kg, the points were allocated to both. A Second order polynomial was fitted to each of the two sets at each bank angle, since this appeared from the shape of the figures to be the most appropriate non-linear function. Curves were also fitted to the combined data of Fig.9.7. In all cases the regressions were forced through the origin on physical grounds. The polynomial coefficients obtained are given in Table 9.2.

This is entirely an ad-hoc approach and does not have the benefit of statistical rigor.

9.3. Discussion

This study has concentrated on the most severe types of overturn because these form the basis for strength test criteria designed to provide protection in a very high proportion of accidents. It may therefore be appropriate to

TABLE 9.2

Coefficients of polynomials fitted through the origin for energy in ROPS (kJ) at maximum sideways deformation vs tractor mass (t) (Figs. 67-73)

Bank angle, α, deg	Low energy points		High energy points	
	Coefficient of m	Coefficient of m^2	Coefficient of m	Coefficient of m^2
0	4.746	-0.4197	5.052	-0.4564
$7\frac{1}{2}$	5.147	-0.5004	4.669	-0.3054
15	0.477	0.1780	3.237	-0.0307
$22\frac{1}{2}$	-0.576	0.2687	4.281	-0.2625
30	0.575	0.0808	4.159	-0.2012
$37\frac{1}{2}$	0.267	0.1502	3.630	-0.2308
All α combined	2.129	-0.0987	4.602	-0.3542

	Both sets of data combined		
	Polynomial of degree:	Coefficient of m	Coefficient of m^2
All α combined	1	1.799	-
	2	3.001	-0.1972

to ignore those results in which loss of contact leads to low ROPS energy. The curves fitted the remainder, however, depend strongly on thegeneral parameters that were constant for all tractors - particularly on bank height and tyre friction and to a lesser extent on soil strength and friction. Increase in bank height would have greatest effect on larger, heavier tractors because of the relationship with impact roll angle discussed in 8.4.; the fitted curves are therefore illustrative and not of absolute significance.

If a statistically reliable distribution of accident bank height existed it would be possible to choose a value to assure any given level of protection; the same applies to other parameters. Accidents of the severity for which protection is required are so rare, however, that the parameters in this study are based on rather crude estimates. In addition, input energy in strength tests is related to protection only through the criteria of acceptable deformation, and it is unlikely that standards committees would allow a significant reduction in the generous zones of clearance adopted at present.

With these limitations it seems reasonable to take the linear regression through all the data points (Fig.9.7) as the basis for a sideways energy criterion in strength tests. The energy/mass relationship of 1.80 J/kg is surprisingly close to the value of 1.75 J/kg recommended by the EEC study group,[82] partly on the basis of simulations of overturns on a uniform slope. Since the two types produce characteristics with opposing curves, their combination in a single linear function appears to be logical, and the choice of a mean line rather than a maximum is justified by the zone of clearance considerations.

The analysis of this section has been restricted to sideways energy because of the assumption of vertically rigid ROPS. Vertical strength requirements must be concluded from the sensitivity analysis, although further simulations would be valuable.

10. SIMULATION OF MULTIPLE ROLLS

In a gentle roll on a uniform slope the axis of rotation changes direction continuously as the ground is impacted successively by the side of the front and rear wheels, the bonnet and the ROPS. The tractor rolls as a truncated pyramid, not continuing down the slope but turning about a point several metres in front of it. This simple type of overturn presents little danger to the driver.

There are conditions in which higher roll momentum or gravitational moment prevent such a large change in the direction of the axis of rotation: a steeper slope, higher roll velocity or inertia or different tractor geometry. If the energy is sufficient the tractor will continue to roll down the slope at increasing speed, probably without the bonnet touching the ground and without much deviation of the roll axis. The danger of the driver being crushed in the ROPS, or being thrown out and crushed by the tractor, is then much higher.

A three-dimensional model is needed to cover the most general behaviour, and Schwanghart's[53, 54] approximates to this by making assumptions about the changes in direction of the roll axis (see section 3.1). The present study is concerned with the more severe cases, however, when high speed multiple rolling occurs, and a two-dimensional model should give an adequate description of this behaviour. A two-dimensional model can determine whether a tractor will remain stable or continue to roll after the first ROPS impact, only if the longitudinal position of the centre of mass is behind the front of the ROPS. Schwanghart's results include such cases, which provide a basis for comparison with those obtained from the present model.

The bank overturning simulation program was modified to cover multiple rolls on a slope by simple changes to the terrain descriptors and initial conditions, together with some coding alterations to improve efficiency (Appendix 3.1). The program coped well with the continuing roll and successive impacts, and followed many complete rotations without numerical errors becoming significant. Execution time increased with simulation time but did not become excessive if the simulation was halted after 2-3 rolls, because of the small number of points in ground contact at any time.

The initial conditions were taken at the unstable equilibrium in which the centre of mass is vertically above the ground contact point at the down-slope tyre, with velocities chosen to give initial rotation about this contact point.

Preliminary trials at zero initial velocity on a 1:2.5 slope (21.8^{o}), the conditions used by Schwanghart, showed that parameters affecting soil friction forces and wheel recovery had a considerable influence on behaviour. A full investigation of these effects has not yet been carried out, but simulations using a reasonable set of parameter values gave results for non-continuous rolling criteria that compared well with Schwanghart's.

The NIAE study did not include multiple roll experiments, mainly because of the difficulty of conducting controllable and repeatable tests. Evidence from several films of overturning tests on long slopes carried out elsewhere, however, indicates conditions in which a tractor may become airborne after its first roll and then impact heavily on the ROPS without energy being absorbed in rear wheel deformation. Schwanghart report that the first impact on the ROPS in his side-slope overturning experiments was less severe than the second, i.e. after a further roll-over of the tractor.(84)

Conditions leading to this type of behaviour were found in the simulations. More work is needed to establish these conditions more precisely, but the general explanations are similar to those covering ROPS with moderate vertical strength in overturns down fairly high banks (8.4). There is little doubt that these two situations are the most critical for ROPS tested to present strength criteria.

11. CONCLUSIONS

A mathematical model of sideways overturning and impact has been developed which overcomes the limitations of previous treatments of impacts as pure impulses, by incorporating non-linear structural behaviour for each member at each impact point. The model is equally capable of handling general overturning motion through its ability to include tyre properties, and it could also be used in deterministic solutions to ride and other problems.

The model

The model is centred around the solution of the equations relating the forces and deflections at each contact point. In its present form it is written in two dimensions and depends on three assumptions: (1) all mass and inertia is concentrated in a "rigid" part of the body; (ii) each body point that makes contact with the ground is directly connected to this rigid part by defined structural characteristics in two directions, which are independent of relative displacements of other points; (iii) the instantaneous normal and tangential ground forces at each point are related by a coefficient of friction, which may vary continuously but only slowly with respect to the step interval in a numerical solution. These restrictions had little effect in limiting the model's ability to describe the behaviour studied here, and could be removed by further development.

The model was implemented as a computer simulation program in FORTRAN IV. This proved to be considerably more efficient than the use of CSMP, a language designed for the direct coding of simulation problems. The program contained extensive logical branching to cope with discontinuities in surface contact and structural characteristics, and was quite difficult to debug. A continuous energy balance check provided an indication of numerical accuracy, which was invaluable during development. The final version of the program was robust, and capable of simulating overturns down a bank and multiple rolls on a uniform slope, the two most important cases found in a survey of overturning accidents.

Overturning experiments

An experimental safety frame with variable structural characteristics was developed, and fitted to a medium size tractor. Impact force in three directions at both front and rear, and deformation of the frame, were sensed by special purpose transducers, and recorded on magnetic tape in an instrument van, via umbilical cables. A ramp was built to represent an overturning bank so that experiments could be carried out at different bank angles and surface friction, under closely controlled conditions. The tractor was driven using a simple remote steering system. Cine film was used to record the overturning motion, and analysed to give position and velocity coordinates in all six degrees of freedom.

Thirty overturning tests were carried out, with variation of tractor geometry and inertia, frame strength, bank angle, friction, and hardness of the ground impact surface. The effects of parameter variation on overturning and impact behaviour were generally less than expected from simple considerations, but some trends were evident and the results provided a sound basis for comparison with the simulations. In spite of some equipment problems, the overall reliability and repeatability were good considering the complex nature of the experiments.

Structural analysis

A simple method was developed to predict the elastic and plastic deformations of the frame under assymetric loading. Collapse force, deflections and mode shape showed good agreement with laboratory impact tests results, but elastic stiffness was less accurately predicted, possibly because of limitations in the measurement method.

Validation

The bank overturning simulation was validated by the results of thirty experiments. The simulations gave considerable insight into the behaviour during overturning and impact. In particular, complex relationships between ride-mode oscillation and the development of tyre friction forces had important effects on the behaviour. In some circumstances this led to temporary loss of contact at the downslope tyre. If contact was remade, the friction force had to build up again from zero as the tyre rolled forward, according to defined relationships between side force, slip angle and relaxation length. The tyre camber angle at loss of contact, which depended on roll angle and bank angle, had a critical effect on the ensuing behaviour; a rapid increase in either roll acceleration or vertical acceleration could result, depending on the conditions and parameter values. This sensitivity was generally confirmed by the experimental results and the overall agreement was good. Most major discrepancies were explained by loss-of-contact effects or recognised experimental shortcomings. Measured ride mode oscillation was qualitatively similar to that predicted but of smaller initial magnitude because of the effect tyre envelopment of surface edges, which was not included in the model.

Quantitative prediction of impact behaviour was satisfactory but not as good as the prediction of overturning behaviour. Energy absorbed in the ROPS showed quite good agreement but the simulations indicated less soil deformation and more bouncing motion than was observed. The limitations imposed by two-dimensional modelling were partly responsible but poorly defined parameters may be equally to blame. Soil strength and friction had not been measured adequately, and the structural characteristics of the wheel had been measured only under static conditions. The inertia of the top frame was thought to be the main cause of differences in soil deformation. Despite these limitations, the validation showed the model to be capable of predicting the effect of parameter changes, and generally established confidence in the simulation results.

Parameter sensitivity analysis

The model was used to investigate the sensitivity to parameter changes of the behaviour, and in particular of the energy absorbed in the ROPS; and to predict the results of overturns using data based on measurements from real tractors.

The effects of parameters that influenced overturning behaviour were obscured in many cases by the complex effects of loss of tyre contact. The effects of bank slope, limiting tyre/bank coefficients of friction, and track width were fairly clear and interrelated. A steep bank and low coefficient of friction resulted in the highest vertical velocities, as expected, but a bank slope of $30\text{-}37\frac{1}{2}^{\circ}$ to the vertical, with a higher coefficient of friction, was more likely to lead to high impact roll angle and roll velocity, the combination giving the highest absorption of energy in the ROPS. Most other parameters had little consistent overall effect on the overtunring motion.

The impact motion did not suffer from discontinuities and was much better behaved. The effects of parameter variation were clearer and more consistent, and even fairly small effects have been reported confidently. The energy absorbed in the ROPS was shown to be much more sensitive in general to impact energy in rotation than in translation, because the impact force at the ROPS typically has a large moment arm about the centre of mass. The component of impact energy due to rotational velocity is quite small, however, and the absolute effect of the component due to vertical velocity is just as important.

In general, most of the rotational energy is absorbed in the ROPS, and most of the translational energy in the wheel and soil, but it is the precise distribution of the large component due to vertical velocity that determines the severity of the ROPS impact. As expected, reduced track width, increased ROPS width or increased impact roll angle all reduce the amount of energy absorbed in the wheel and increase that absorbed in the ROPS. An upper bound to this variation generally occurs when the ROPS reaches maximum deflection before the wheel has hit the ground. If, however, the ROPS is relatively weak in its vertical direction, its ability to absorb impact energy due to vertical velocity increases dramatically at high impact roll angles. Instead of needing rotational inertia to transmit the forces of deformation, the ROPS becomes vulnerable to all the tractor's kinetic energy, and the likelihood of catastrophic collapse becomes significant. The simulations have shown that a ROPS which is very strong vertically and only just strong enough laterally to pass present standard tests, is unlikely to collapse far enough to crush the driver in any reasonable accident. One which only just meets present vertical strength standards, however, would be quite likely to do so in an overturn down a bank more than about 3m high. A multiple roll accident could also lead to these results, and although the simulations have tentatively confirmed this, they have not yet been run in enough multiple roll conditions to determine which are most severe.

The overall probability of a ROPS collapsing is too small to be established with any certainty, but the evidence is consistent with that obtained from the measurement of ROPS deformation in accidents[21].

Implications for standard strength test criteria

The data for simulations of tractors between 1000 kg and 8000 kg were taken from regressions of measured parameters against mass, since complete sets of individual data were not available. The simulation results again showed evidence of rather erratic, intermittent tyre contact, but their clarity was improved after subjective, visual separation into one class containing cases in which contact was fairly continuous, and another in which it was not.

The envelope of highest values of ROPS sideways energy, and the curves fitted through the higher energy class of data, both indicated a levelling off of energy as tractor mass was increased. This is opposite to the findings of studies of overturning on a uniform slope, where ROPS energy rises at a continually increasing rate with tractor mass. The tractor dimensions increase to a low power of mass and cause energy to increase more rapidly than in direct proportion to mass if the terrain is non-dimensional. In the bank overturn, the increase in tractor size must also be related to the fixed bank height, and the effect of larger track width, particularly, is to reduce the energy absorbed in the ROPS.

In a recommendation to standards committees combining the two sets of results it would be possible to take whichever was the larger at any tractor mass. In view of the restricted types of overturn covered, the limited knowledge of some parameters and the generous factor of safety inherent in the present standard zone of clearance, however, the mean line fitted through all the results of these simulations is probably more appropriate. The slope of this line, 1.80, is close to the value of 1.75 recommended by the EEC study group, partly on the basis of the simulation of overturning on a uniform slope. The units are absorbed energy at maximum sideways ROPS deflection, J, per tractor mass, kg.

The simulations based on real tractor data did not include vertically flexible ROPS because of the lack of structural information and the moderate bank height used. While the adequacy of present lateral strength test standards has been confirmed by the results of these and other simulations reported here, this is not so for vertical strength standards. The potential has been demonstrated for present ROPS to collapse vertically in very severe accidents (8.4 and 10). A vertical loading test procedure including an absorbed energy requirement in addition to a force limit would provide added assurance, but the best solution might be to replace the horizontal and vertical loadings by a single test in which the line of application of the force passes through the longitudinal axis containing the tractor centre-of-mass. This suggestion has already been made by the New Zealand authorities, and has the merit of simulating not the typical but the most severe accident conditions.

REFERENCES

1 M.A.F.F.
REPORT ON SAFETY, HEALTH, WELFARE AND WAGES IN AGRICULTURE.
H.M.S.O. LONDON (ANNUAL)

2 D.A.F.S.
AGRICULTURE IN SCOTLAND.
H.M.S.O. LONDON (ANNUAL)

3 MANBY, T.C.D.
DESIGN OF TRACTORS AND FARM MACHINES FOR SAFER OPERATIONS.
PROCEEDINGS OF SEMINAR OF SAFETY IN RURAL INDUSTRY. CANBERRA. MAY 1967.

4 MCKIBBEN, E.G.
THE KINEMATICS AND DYNAMICS OF WHEEL-TYPE FARM TRACTORS
AGRICULTURAL ENGINEERING VOL 8 NOS. 1-7 1927

5 MOBERG, H.A.
TRACTOR SAFETY CABS. TEST METHODS AND EXPEREIENCES GAINED DURING ORDINARY FARMWORK IN SWEDEN.
NATIONAL SWEDISH TESTING INSTITUTE FOR AGRICULTURAL MACHINERY, 1964

6 MOLNA, B.
THE TRACTOR ACCIDENTS AND FACTORS INCREASING OR DECREASING THE RISK OF SUCH ACCIDENTS.
NORWEGIAN INST. OF AGRIC. ENGNG. RESEARCH REPORT NO. 8. 1963

7 MANBY, T.C.D.
SAFETY ASPECTS OF TRACTOR CABS AND THEIR TESTING.
JOURNAL OF PROCEEDINGS OF INST. AGRIC. ENGRS., VOL 20. NO. 1. 1964.

8 MANBY, T.C.D.
TESTING OF SAFETY CABS.
N.I.A.E. SUBJECT DAY - TRACTOR OPERATOR COMFORT & SAFETY. OCT 1964

9 WATSON, M.
THE STRUCTURAL TESTING OF TRACTOR SAFETY FRAMES.
NEW ZEALAND AGRIC. ENGNG. INST., 1967, RESEARCH PUBLICATION R/1

10 BUCHER, D.H.
THE DESIGN AND EVALUATION OF A PROTECTIVE CANOPY FOR AGRICULTURAL TRACTORS.
ASAE PAPER NO. 66-625 DEC 1966

11 MANBY, T.C.D.
ENERGY ABSORBED BY PROTECTIVE FRAMES FOR DRIVERS WHEN TRACTORS OVERTURN REARWARD.
DEP. NOTE DN/TMPD/25/70,
NAT. INST. AGRIC. ENGNG. SILSOE, 1970 (UNPUBL)

12 O.E.C.D.
OECD STANDARD CODE FOR THE OFFICIAL TESTING OF SAFETY CABS AND FRAMES MOUNTED ON AGRICULTURAL TRACTORS.
OECD, PARIS, 1974.

13 BRITISH STANDARD. BS 4063:1973
SPECIFICATION FOR REQUIREMENTS AND TESTING OF PROTECTIVE CABS AND FRAMES FOR AGRICULTURAL WHEELED TRACTORS.
BRITISH STANDARDS INST. LONDON, 1973

14 AMERICAN SOCIETY OF AGRICULTURAL ENGINEERS
PROTECTIVE FRAME - TEST PROCEDURES AND PERFORMANCE REQUIREMENTS.
ASAE STANDARD ASAE S306.2. 1970
(EQUIVALENT TO SAE J334B)

15 I.S.O.
AGRICULTURAL WHEELED TRACTORS - PROTECTIVE CABS AND FRAMES - TEST METHOD AND ACCEPTANCE CONDITIONS
ISO DIS 3463.3, 1977

16 E.E.C.
COUNCIL DIRECTIVE OF 28 JUNE 1977 ON THE APPROXIMATION OF THE LAWS OF THE MEMBER STATES RELATING TO THE ROLL-OVER PROTECTION STRUCTURES OF WHEELED AGRICULTURAL OR FORESTRY TRACTORS.
OFFICIAL JOURNAL, VOL 20 NO L 220, 29 AUG. 1977.

17 CHISHOLM, C.J.
A COMPARISON OF STANDARDS FOR STATIC TESTS ON ROLL OVER PROTECTIVE STRUCTURES FOR AGRICULTURAL TRACTORS AND EARTHMOVING MACHINERY.
DEP NOTE DN/E/719/4600, NAT. INST. AGRIC. ENGNG. SILSOE, 1976 (UNPUBL).

18 I.S.O.
EARTHMOVING MACHINERY - ROLL OVER PROTECTIVE STRUCTURES - LABORATORY TESTS AND PERFORMANCE REQUIREMENTS.
ISO 3471 - 1975 (E), 1975.

19 NORDSTROM, O.
SAFETY & COMFORT TEST PROGRAM - SWEDISH APPROACH.
ASAE PAPER NO. 70-105 1970

20 APPEL, H.; FIALA, E.; HESSE, G.
COST/BENEFIT ANALYSIS OF RESTRAINT SYSTEMS, SAFETY STANDARDS AND VW SAFETY VEHICLE.
A.T.Z. MARCH 1973, VOL 75,NO 3 P85

21 CHISHOLM, C.J.; SEWARD, P.C.
THE CORRELATION BETWEEN DAMAGE TO ROLL-OVER PROTECTIVE STRUCTURES IN TRACTOR OVERTURNING ACCIDENTS AND IN STANDARD TESTS.
DEP NOTE DN/E/674/4600, NAT. INST. AGRIC. ENGNG. SILSOE, 1976 (UNPUBL).

22 CHISHOLM, C.J.
DESIGN AND TEST CRITERIA FOR TRACTOR SAFETY CABS.
PROJECT PAPER TE/71/1425, NAT.INST. AGRIC. ENGNG.
SILSOE, 1971 (UNPUBL).

23 WILLSEY, F.R.; LILJEDAHL, J.B.
A STUDY OF TRACTOR OVERTURNING ACCIDENTS.
A.S.A.E. PAPER NO 69-639, DEC 1969

24 BAKER, L.D.; STEINBRUEGGE, G.W.
A TRACTOR OVERTURN STUDY.
A.S.A.E. PAPER NO. 72-615, 1972.

25 MARPLES, V.
AN ANALYSIS OF TRACTOR ACCIDENTS IN ENGLAND & WALES 1967-69.
OCCUPATIONAL SAFETY AND HEALTH, 1(4), JULY 1971.

26 WHITAKER, J.R.
AN ANALYSIS OF OVERTURNING ACCIDENTS WITH SAFETY CABS.
TRACTOR ERGONOMICS SUBJECT DAY, PAPER NO. 6.
NAT. INST. AGRIC. ENGNG. REPORT NO.10, SILSOE, 1973.

27 INTERNATIONAL STANDARDS ORGANISATION.
STATISTICS ON FATAL ACCIDENTS CAUSED BY TRACTOR UPSET.
DOCUMENT ISO/TC23/SC3/WG1(SECR.-16)39, SEP 74.

28 INTERNATIONAL STANDARDS ORGANISATION.
ANALYSIS OF A STATISTICAL SAMPLE OF FARM TRACTOR ACCIDENTS IN THE FIELD.
DOCUMENT ISO/TC23/SC3/WG1(FRANCE-1)35, AUG 74.

29 INTERNATIONAL STANDARDS ORGANISATION.
TRACTOR OVERTURNING ACCIDENTS IN SWEDEN 1959-73
DOCUMENT ISO/TC23/SC3/WG1(SWEDEN-4)40, SEP 74.

30 ORGANISATION FOR ECONOMIC COOPERATION & DEVELOPMENT
ACCIDENTS INVOLVING AGRICULTURAL TRACTORS FITTED WITH PROTECTIVE DEVICES AGAINST OVERTURNING.
OECD DOCUMENT DAA/T/1213, PARIS, SEPT 1973.

31 CHISHOLM, C.J.
A SURVEY OF 114 TRACTOR SIDEWAYS OVERTURNING ACCIDENTS IN THE U.K. - 1969 TO 1971.
DEP. NOTE DN/TE/238/1425,
NAT. INST. AGRIC. ENGNG., SILSOE, APR 1972 (UNPUBL)

32 WORTHINGTON, W.H.
EVALUATION OF FACTORS AFFECTING THE OPERATING STABILITY OF WHEELED TRACTORS.
AGRICULTURAL ENGINEERING VOL 30, NO 3 MAR 1949

33 SACK, H.W.
LONGITUDUAL STABILITIES OF TRACTORS
AGRIC. ENGNG. VOL 37, NO 5. 328-333 MAY 1956

34 KOCH, J.A.; BUCHELE, W.F.; MARLEY, S.F.
VERIFICATION OF A MATHEMATICAL MODEL TO PREDICT TRACTOR TIPPING BEHAVIOUR
ASAE PAPER NO. 68-107, 1968

35 SMITH, D.W.; LILJEDAHL, J.B.
SIMULATION OF REARWARD OVERTURNING OF FARM TRACTORS.
ASAE PAPER NO 70-150 JULY 1970

36 MITCHELL, B.W.; ZACHARIAH, G.L.; LILJEDAHL, J.B.
PREDICTION AND CONTROL OF TRACTOR STABILITY TO
PREVENT REARWARD OVERTURNING
ASAE PAPER NO 70-535 1970

37 PONZIO, L.
BACKWARD OVERTURNING OF AN AGRICULTURAL TRACTOR.
A.T.A., 1972, 25 (3) 151-163 (I).

38 BAIRD, D.R.
AN INTRODUCTION TO ARTICULATED WHEELED
SKIDDER STABILITY ON STEEP SLOPES.
ECONOMIC COMMISION FOR EUROPE FOOD AND
AGRICULTURE ORGANIZATION INTERNATIONAL
LABOUR ORGANIZATION OCT 1971

39 GIBSON, H.G.; ELLOITT, K.C.; PERSON, S.P.E.
SIDE SLOPE STABILITY OF ARTICULATED FRAME
LOGGING TRACTORS
J. OF TERRAMECHANICS VOL 8 NO 2,65-79(1971)

40 DASKALOV, A.
DYNAMIC STABILITY OF TRACTORS AGAINST
OVERTURNING.
SELSKOSTOP. TEKH.,2971,8(5) 3-15

41 VASILENKO, P.M.; KUZMINSKII, V.G.
DYNAMICS OF OVERTURNING OF SELF-PROPELLED
FARM MACHINERY
ZEMLED. MEKH. 12, AKAD. SELKHOZ. NAUK,
MOSCOW, 1969, 52-61

42 KARAGECHEV, G.; STOYANOV, KH.
ON THE QUESTION OF LATERAL STABILITY OF TRACTORS
SELSKOSTOP. TEKH., 1970, 7 (2) 51-59

43 PARTINOV, P.
STABILITY OF LINEAR REGULAR MOTION OF
A MACHINE-TRACTOR UNIT ACROSS THE SLOPE
NAUCH. TRUD. INST. MASHINOSTROENE MEKH. ELEKTR.
SELSK. STOP., RUSE,1971,13,PT 1:SELSKOSTOP.
MASHINOSTROENE MEKH. SALSK. STOP.,123-130

44 STOICHEV, S.
STUDY OF THE STABILITY OF A WHEEL TRACTOR
OF THE 0.2 T CLASS
SELSKOSTOP. TEKH., 1972, 9 (3) 15-28.

45 SMITH, D.W.; PERUMPRAL, J.V.; LILJEDAHL, J.B.
A MATHEMATICAL MODEL TO PREDICT THE SIDEWAYS
OVERTURNING BEHAVIOUR OF FARM TRACTORS
ASAE PAPER NO 71-604 1971

46 LARSON, D.L.; SMITH, D.W.; LILJEDAHL, J.B.
THE DYNAMICS OF THREE-DIMENSIONAL TRACTOR MOTION.
TRANS. ASAE, 1976, 19( ) 195-200.
ALSO ASAE PAPER NO 73-5546.

47 LARSON, D.; LILJEDAHL, J.R.
SIMULATION OF SIDEWAYS OVERTURNING OF WHEEL TRACTORS ON SIDE SLOPES
S.A.E. PAPER NO. 710709, FARM CONSTRUCTION AND INDUSTRIAL MACHINERY MEETING, SEPT 13-16 1971

48 DAVIS, D.C.; REHKUGLER, G.E.
AGRICULTURAL WHEEL-TRACTOR OVERTURNS
PART 1: MATHEMATICAL MODEL
PART 2: MATHEMATICAL MODEL VERIFICICATION BY SCALE-MODEL STUDY.
TRANS. ASAE VOL 17, NO 3, MAY-JUNE 1974

49 REHKUGLER, G.E.; KUMAR, V.; DAVIS, D.C.
SIMULATION OF TRACTOR ACCIDENTS AND OVERTURNS.
TRANS. ASAE, 1976, 19(4) 602-609,613.
ALSO ASAE PAPER NO 75-1047.

50 MCHENRY, R.R.
RESEARCH IN AUTOMOBILE DYNAMICS- A COMPUTER SIMULATION OF GENERAL THREE-DIMENSIONAL MOTIONS.
SAE PAPER NO. 710361

51 ZAKHARYAN, E.B.
EVALUATION OF THE DYNAMIC OVERTURNING STABILITY OF A TRACTOR AND TRACTOR OUTFIT FROM THE ENRGY POINT OF VIEW.
TRAKT. SELKHOZMASH., 1972 (7) 2-4
(NIAE TRANSL. 362)

52 SPENCER, H.B.; GILFILLAN, G.
AN APPROACH TO THE ASSESSMENT OF TRACTOR STABILITY ON ROUGH SLOPING GROUND.
J. AGRIC. ENGNG RES., 1976, 21,(2),169-176.

53 SCHWANGHART, H.
METHOD FOR CALCULATING THE OVERTURNING BEHAVIOUR OF TRACTORS ON SLOPES.
GRUNDL. LANDTECH., 1973, 23 (6) 170-176.

54 SCHWANGHART, H.
EXPERIMENTAL INVESTIGATIONS ABOUT IMPACTS ON THE SOIL AND APPLICATION IN CALCULATING THE OVERROLL BEHAVIOR OF A VEHICLE.
PROC. 5TH INT. CONF. SOC. TERRAIN VEHICLE SYSTEMS, DETROIT, 2-6 JUNE 1975.

55 BOYER, F.
SIMULATION D'UN ESSAI DE RENVERSEMENT LATERAL D'UN TRACTEUR AGRICOLE SUR UNE PENTE UNIFORME.
REP. NTI-DTE 75/026,1975, C.E.T.I.M., SENLIS, FRANCE

56 SCHWANGHART, H.
PRIVATE COMMUNICATION.

57 COBB, L.J.
ROPS FORCE AND ENERGY ABSORPTION FROM SIMULATED OVERTURN ANALYSIS.
SAE PAPER NO. 760691, 1976.

58 EMMERSON, W.C.; FOWLER, J.E.
SIMULATION OF FRONTAL VEHICLE IMPACTS.
CONF. ON VEHICLE SAFETY LEGISLATION, CRANFIELD,
JULY 1973, INSTN. MECH. ENGRS. CONF. PUBL. 16

59 IBM
SYSTEM/360 CONTINUOUS SYSTEM MODELING PROGRAM
(360A-CX-16X) USER'S MANUAL.
IBM H20-0367-2

60 LAMBERT, J.R.
THE USE OF CSMP FOR AGRICULTURAL
ENGINEERING PROBLEMS.
ASAE PAPER 71-529, 1971

61 CHISHOLM, C.J.
COMPUTER SIMULATION OF TRACTOR SIDEWAYS OVERTURNING.
DEP. NOTE DN/E/465/1425, NAT. INST. AGRIC. ENGNG.
SILSOE, 1978 (UNPUBL)

62 CHISHOLM, C.J.
EQUIPMENT FOR TRACTOR OVERTURNING EXPERIMENTS.
DEP. NOTE DN/E/530/1425, NAT. INST. AGRIC. ENGNG.
SILSOE, 1976 (UNPUBL).

63 MANBY, T.C.D.
REPORT OF O.E.C.D. STUDY GROUP ON "TESTING OF
SAFETY CABS INCLUDING SUSPENDED AND BREAK-AWAY
MODELS" HELD AT STATENS MASKINPROVNINGAR,
UPPSALA, SWEDEN.
DEP NOTE DN/TMD/124/4500.

64 ASHBURNER, J.E.
ASPECTS OF THE DESIGN AND TESTING OF TRACTOR SAFETY
FRAMES.
CONF. ON OFF-HIGHWAY VEHICLES, TRACTORS AND
EQUIPMENT, INST. MECH. ENGRS., LONDON, OCT 1975.

65 BILLINGTON, W.P.
THE NIAE MARK II SINGLE WHEEL TESTER.
J. AGR. ENGNG. RES., 1973, 18, P67.

66 ELLIS, J.R.
VEHICLE DYNAMICS.
BUSINESS BOOKS, LONDON, 1969

67 VAN WIJK, M.C.; PINKNEY, H.F.L.
A SINGLE CAMERA METHOD FOR THE 6-DEGREE OF FREEDOM
SPRUNG MASS RESPONSE OF VEHICLES REDIRECTED BY
CABLE BARRIERS.
PROC. SOC. PHOTO-OPT. INSTR. ENGRS, 1972.

68 ROBBINS, D.H.; BOWMAN, B.M.; ALEM, N.M.
MOTION MEASUREMENT OF A RIGID BODY IN
THREE DIMENSIONS.
PROC. SOC. PHOTO OPTICAL INSTR. ENGRS.,
DEARBORN, MICHIGAN, 1972

69 SIEGAL, S.
NON-PARAMETRIC STATISTICS FOR THE BEHAVIOURAL
SCIENCES.
MCGRAW-HILL KOGAKUSHA, TOKYO, 1976.

70 CHISHOLM, C.J.
SMOOTHING OF DIGITAL SIGNALS.
DEP. NOTE DN/E/752/1425, NAT. INST. AGRIC. ENGNG.
SILSOE, 1976 (UNPUBL).

71 CHISHOLM, C.J.
TRACTOR OVERTURNING TESTS: 1973-75.
DEP. NOTE DN/E/693/1425, NAT. INST. AGRIC. ENGNG.
SILSOE, 1977 (UNPUBL)

72 RAWLINGS, B.
THE PRESENT STATE OF KNOWLEDGE OF THE
BEHAVIOUR OF STEEL STRUCTURES UNDER THE
ACTION OF IMPULSIVE LOADS.
TRANS. (AUSTRALIA) INST. CIVIL ENG.
VOL CE5, NO. 2, PAPER NO 1693

73 ASHBURNER, J.E.
AN INVESTIGATION INTO ASPECTS OF THE DESIGN AND
TESTING OF TRACTOR SAFETY CABS AND FRAMES.
PH.D. THESIS, UNIVERSITY OF READING, 1972

74 MANJOINE, M.J.
INFLUENCE OF RATE OF STRAIN AND TEMPERATURE ON
YIELD STRESSES OF MILD STEEL.
TRANS. ASME J. APPL. MECH. VOL 66, DEC 1944.

75 PARKES, E.W.
THE PERMAMENT DEFORMATION OF A CANTILEVER
STRUCK TRANSVERSELY AT ITS TIP.
PROC OF ROYAL SOC. (A)
VOL 228, 462-476 MAR 1955.

76 RAWLINGS, B.
DYNAMIC BEHAVIOUR OF A RIGID PLASTIC STEEL BEAM.
J. OF (AUSTRAL.) MECH. ENG. SCIENCE.
VOL 4. NO 1., 1962

77 RAWLINGS, B.
THE DYNAMIC BEHAVIOUR OF MILD STEEL IN PURE FLEXURE.
PROC OF ROYAL SOC. (A) VOL 275, MARCH 1963.

78 GOLDSMITH, W.
IMPACT.
EDWARD ARNOLD, LONDON, 1960.

79 CHISHOLM, C.J.; PARKER, J.F.
THE PREDICTION OF TRACTOR SAFETY CAB DEFORMATION:
PART I - A PRELIMINARY STUDY.
DEP. NOTE DN/E/435/1425, NAT. INST. AGRIC. ENGNG.
SILSOE, 1974 (UNPUBL).

80 CHISHOLM, C.J.
THE PREDICTION OF TRACTOR SAFETY CAB DEFORMATION:
PART II - THE NIAE MKII EXPERIMENTAL FRAME.
DEP. NOTE DN/E/711/1425, NAT. INST. AGRIC. ENGNG.
SILSOE, 1977 (UNPUBL)

81 STAFFORD, J.V.; TANNER, D.W.
THE FRICTIONAL CHARACTERISTICS OF STEEL SLIDING ON SOIL.
DEP NOTE DN/T/728/1162, NAT. INST. AGRIC. ENGNG., SILSOE, 1976 (UNPUBL)

82 BOYER, F.; CHISHOLM, C.J.; SCHWANGHART, H.
ROLL-OVER PROTECTIVE STRUCTURES FOR WHEELED AGRICULTURAL OR FORESTRY TRACTORS.
FINAL REPORT OF THE ROPS STUDY GROUP TO THE COMMISSION OF THE EUROPEAN COMMUNITIES, BRUSSELS, OCTOBER 1976.

83 STAYNER, R.M.; BOLDERO, A.G.
THE DYNAMIC STIFFNESS OF TRACTOR TYRES: MEASUREMENTS IN THE HORIZONTAL PLANE.
NAT. INST. AGRIC. ENGNG., DEP NOTE DN/TC/386/1445, SILSOE, 1973 (UNPUBL)

84 SCHWANGHART, H.
VIEWS ON THE STRENGTH OF TRACTOR SAFETY FRAMES, PARTICULARLY WHERE OLDER TRACTORS ARE TO BE FITTED.
LANDTECHNIK, 1975, 30(10), 441-445

85 O'DOGHERTY, M.J.
A DYNAMOMETER TO MEASURE FORCES ON A SUGAR BEET TOPPING KNIFE.
J. AGRIC. ENGNG. RES. (1975) 20, 339-345.

86 GERALD, C.F.
APPLIED NUMERICAL ANALYSIS.
ADDISON WESLEY, 1970.

87 WOLOWICZ, C.H.; YANCEY, R.B.
EXPERIMENTAL DETERMINATION OF AIRPLANE MASS AND INERTIAL CHARACTERISTICS.
NASA TECH. REP. TR R-433, WASHINGTON D.C., 1974.

88 GORAN, M.B.; HURLONG, G.W.
DETERMINING VEHICLE INERTIAL PROPERTIES FOR SIMULATION STUDIES.
BENDIX TECH. J. VOL 6 NO 1, SPRING 1973.

89 BARTOS, J.
DETERMINATION OF THE MOMENT OF INERTIA OF MOTOR VEHICLES.
AUTOMOBIL, JAN 75. P 3.

90 WINKLER, C.B.
MEASUREMENT OF INERTIAL PROPERTIES AND SUSPENSION PARAMETERS OF HEAVY HIGHWAY VEHICLES.
SAE PAPER NO 730182

91 MATTHEWS, J.; TALAMO, J.D.C.
RIDE COMFORT FOR TRACTOR OPERATORS: III INVESTIGATION OF TRACTOR DYNAMICS BY ANALOGUE COMPUTER SIMULATION.
J. AGRIC. ENGNG. RES. VOL 10, NO 2, 1965.

92 GOERING,C.E.; MARLEY,S.J.; KOCH,J.A.; PARISH,R.L.
DETERMINING THE MASS MOMENT OF INERTIA OF A TRACTOR USING FLOOR SUSPENSION.
SAE TRANSACTION 11 (3) 416-418, 1968

93 CHISHOLM, C.J.
THE MEASUREMENT OF TRACTOR MOMENT OF INERTIA AND CENTRE OF MASS POSITION.
DEP. NOTE DN/E/712/1425, NAT. INST. AGRIC. ENGNG. SILSOE, 1977 (UNPUBL).

94 BERGMAN, W.; CLEMETT, H.R.
TIRE CORNERING PROPERTIES.
TIRE SCIENCE AND TECHNOLOGY, 3(3),AUG 1975,135-163

95 HOLMES, K.E.; STONE, R.D.
TYRE FORCES AS FUNCTIONS OF CORNERING AND BRAKING SLIP ON WET ROAD SURFACES.
TRANSPORT & ROAD RES. LAB. REP. LR 254, 1969.

96 SMILEY, R.F.; HORNE, W.B.
MECHANICAL PROPERTIES OF PNEUMATIC TIRES WITH SPECIAL REFERENCE TO MDERN AIRCRAFT TIRES.
NASA TECH.REP. TR R-64, 1960.

97 SCHURING, D.J.; ROLAND, R.D.
RADIAL PLY TIRES - HOW DIFFERNT ARE THEY IN THE LOW LATERAL ACCELERATION REGIME.
SAE PAPER NO 750404, 1975.

98 TRANSPORT AND ROAD RESEARCH LABORATORY.
INSTRUCTIONS FOR USING THE PORTABLE SKID RESISTANCE TESTER.
ROAD NOTE NO.27, HMSO.

99 RADT, H.S.; MILLIKEN, W.F.
MOTIONS OF SKIDDING AUTOMOBILES.
SAE PAPER NO 205A, 1960

100 BERGMAN, W.; BEAUREGARD, C.
TRANSIENT TIRE PROPERTIES.
SAE PAPER NO 740068, 1974.

101 MULQUEEN, J.; STAFFORD, J.V.; TANNER, D.W.
EVALUATION OF PENETROMETERS FOR MEASURING SOIL STRENGTH.
DEP NOTE DN/T/738/1162, NAT. INST. AGRIC. ENGNG., SILSOE, 1976 (UNPUBL)

102 CHISHOLM, C.J.
DESIGN AND TEST CRITERIA FOR SAFETY CABS.
TRACTOR ERGONOMICS SUBJECT DAY, PAPER NO. 7.
NAT. INST. AGRIC. ENGNG. REPORT NO.10,SILSOE,1973.

APPENDIX 2.1

Classification of fatal sideways overturning accidents in England and Wales, 1969-1971

The classification of each of the 76 accidents are tabulated, together with the heights and slopes of banks in those 'C'-type accidents for which these data were recorded.

The classification system, described in section 2.1, is summarised below:-

(i) Terrain profile: A = Overturning of flat ground, either level or with a uniform slope (Fig. 2.2a).

B = Overturning initiated by the tractor mounting a bank or large obstacle from flat ground (Fig. 2.2b).

C = Overturning initiated by the tractor wheels falling over the edge of a bank, or into a ditch (Fig. 2.2c).

(ii) Ground hardness: H = Hard ground.

S = Soft ground.

(iii) Vehicle control: L = Loss of control of the speed of the tractor before overturning.

N = Normal operation (No loss of control).

(iv) Implements and trailers: S = Solo tractor.

M = Mounted implement or equipment supported entirely or principally by the tractor.

T = Trailer or implement trailed from the drawbar.

(v) Additional contributory factors: 1 = Side slope

2 = Sudden change of direction (Steering).

3 = Surface with bumps or hollows.

4 = Implement effect.

5 = Other.

Where a classification is uncertain, either because of insufficient information or in a borderline case, the most likely class is given in parentheses.

Classification of fatal sideways overturning accidents, 1969-1971

M.A.F.F. Fatal Accident Reference Number	Class (i)	(ii)	(iii)	(iv)	(v)	Bank in 'C' type accident: Height, ft	Slope
2/69	B	H	(N)	S	(1), (2)		
10/69	C	(H)	N	(S)		3	
11/69	A	(S)	N	(S)	1, 2		
17/69	(B)	H	(N)	M	(2), (4)		
18/69	C	S	N	M	(3), (4)	2.5	
19/69	C	(S)	N	(T)		5	Vertical
20/69	A	S	N	(S)	2		
22/69	C	H	N	M	(4)	10	Steep
25/69 & 26/69	A	S	(N)	M	1, 2, 4		
42/69	B	H	(N)	(S)			
43/69	A	S	L	T	1, (2), 3, 4		
45/69	A	(H)	L	(T)	1, 2		
46/69	C	(S)	N	(M)		10	
47/69	B	H	L	T	(2) (4)		
58/69	(A)	S	N	M	(2)		
59/69	A	S	(L)	(M)	1, (2)		
62/69	C	S	N	T		3 to 6	Steep
69/69	A	S	(L)	T	1, 2, 4		
71/69	A	H	L	T	(1) (2) 4		
73/69	B	H	L	S	(1), 2		
74/69	A	S	N	(M)	1, (2)		
81/69	A	S	N	(M)	(1), (4)		
82/69	C	S	N	M	(1)	20	45°
89/69	C	(S)	N	M		12.5	Near Vertical
94/69	B	(S)	L	M	(1), (2), (4)		
96/69	(C)	(S)	(L)	(M)	5		
105/69	C	(S)	(N)	(T)		3	

Classification of fatal sideways overturning accidents, 1969-1971 (Cont.)

M.A.F.F. Fatal Accident Reference Number	Class (i) (ii) (iii) (iv) (v)	Bank in 'C' type accident	
		Height, ft	Slope
113/69	C - (S) - N - (M) - 4	3	1 in 3
114/69	B - H - N - M - 1, (2) 3 (4)		
1/70	A - S - L - S - 1, 2		
6/70	A - S - L - T - 1, 2, 4		
19/70	(A) - S - L - S - 1, 2, 5		
21/70	A - S - N - T - 1, 2, (4)		
26/70	A - S - L - M - 1, 2, (3), (4)		
27/70	A - (H) - L - T - (1),(2),(4)		
28/70	B - H - N - (S) - (2)		
32/70	C - (S) - N - M - (4)	10	45°
33/70	C - S - L - T - (1),(2)	15	
34/70	C - S - N - T - 4	10	Vertical
35/70	A - S - L - T - 1, 2, 3,(4)		
36/70	B - H - L - (S) - (1) (2)		
42/70	C - H - N - T	15	Near Vertical
43/70	C - S - N - M	6.5	
48/70	C - S - N - (T)	12	
51/70	B - H - L - (S) - 2		
55/70	A - S - L - M - 1, 2, 4		
61/70	B - S - L - M - (1),(2) (4)		
68/70	C - S - N - T - (2) (4)		
72/70	C - H - N - T - 5	8	Vertical
87/70	B - H - L - S - 2, (5)		
90/70	C - S - N - S - 1, (3)		1 in 2 to 1 in 3
96/70	A - S - N - T - 1, 3, 4		
100/70	(C) - H - N - M - 1, 2, (4)	5	

Classification of fatal sideways overturning accidents, 1969-1971 (Cont.)

M.A.F.F. Fatal Accident Reference Number	Class (i) (ii) (iii) (iv) (v)	Bank in 'C' type accident	
		Height, ft	Slope
4/71	C - S - N - T - (1)	5	
6/71	B - H - N - M - 2		
7/71	(A) - S - N - S - 1, 2, 3		
9/71	A - (S) - L - S - 1, 2		
13/71	B - H - L - S - 1, 2		
18/71	(C) - S - (L) - M		
32/71	A - S - L - T - 1, 2, 4		
38/71	A - H - (L) - T - 1, (2) 4		
43/71	A - S - N - M - (1),(2),(4)		
45/71	A - S - N - T - 1, (2),(4)		
50/71	C - S - (N) - M	30	
51/71	B - H - L - T - 1, (2),(3),(4)		
57/71	C - S - L - T - 1, (4)	8-10	Near Vertical
63/71	B - H - N - S		
74/71	B - H - N - T		
82/71	A - S - L - M - 1, 2		
90/71	C - S - L - S - 1	2	
94/71	C - S - N - S - 2	4	45°
98/71	(C) - S - (N) - M - 3		
102/71	B - S - (L) - S - 1		
108/71	(C) - S - L - T - 1, 2, 4		
110/71	B - H - (L) - S		
115/71	C - S - N - M - (2)		

Classification of 38 sideways overturning accidents involving tractors with safety cabs

The table includes classifications, defined in Appendix 2.1, and the heights and slopes of banks in those 'C'-type accidents for which these data were recorded.

Also given are tractor speeds before overturning, angles of tractor rotation and details of driver behaviour using the following notation:-

1. Position during overturning:
   - R = Remained in cab throughout.
   - E = Ejected.
   - J = Jumped out intentionally.
   - ? = Unspecified
   - N = Tractors that ran away driverless

2. Driver retained hold of steering wheel throughout overturning.
3. Driver stayed in seat throughout overturning.

   - Y = Yes, N = No (in parentheses if not certain)
   - ? = Not known

Classification of overturning accidents involving tractors with safety cabs

M.A.F.F. Serial No.	Class	Bank in C-type accidents Height, ft.	Bank in C-type accidents Slope	Tractor speed mile/h	Tractor rotation	Occupant behaviour during overturni[illegible] Position[1]	Held onto[2] steering wheel	Stayed[3] in seat
25	A - S - N - M - 1, 4			1	90°	R	Y	N
26	(C) - S - L - S - 1, (2)	2.5	Vertical	"high"	180°	J	N	N
27	C - S - N - T - 1, 4	6-8		0-1	180°	R	Y	N
28	C - S - L - S - 1, 2	30	3 in 1	15	2 + rev	R	N	N
29	A - H - N - T - 1, 2 (4)			10-12	270°	R	N	N
30	C - S - N - M - 3, (4)	3		5-10	90°	R	(N)	N
31	C - S - N - (T) - 5	5		2	90°	R	(N)	N
32	(C) - S - N - T			0-1	2.5 rev	J	N	N
33	A - S - N - T - 1, 3, 4			3.5	90°	E	N	N
34	A - S - L - T - 1, 2, 4			10-15	135°	R	Y	Y
35	(A) - (S) - (L) - T - (1), (4)				90°	N	-	-
36	A - S - N - T - 1, 3, 4			5	180°	R	Y	(Y)
37	(C) - S - N - T - (1), 4	4		3+	180°	R	Y	Y
38	C - S - N - T - 1, 2, 4		1 in 1 to 1 in 2		2.5 rev	R	Y	N
39	C - S - (N) - M - 5	30	1 in 2	20	2 rev	R	Y	N
40	B - H - N - S			10	90°	R	Y	Y
41	(Rearward overturning)							
42	(C) - S - N - M - 1, 4, 5	1		5	1.25 rev	?	?	?
43	A - S - N - T - 1, 3			1	8 rev	E	N	N
44	A - H - N - T - 4, 5			10	90°	R	N	N
45	(B) - H - L - S				90°	N	-	-
46	(A) - S - N - T - 4, (5)			0-1	90°	R	N	N

Classification of overturning accidents involving tractors with safety cabs (Cont.)

M.A.F.F. Serial No.	Class	Bank in C-type accidents		Tractor speed mile/h	Tractor rotation	Occupant behaviour during overturning		
		Height, ft.	Slope			Position[1]	Held onto[2] steering wheel	Stayed[2] in seat
47	B - H - N - S			10-15	180°	R	?	?
48	C - (S) - N - M	10		1	180°	R	N	N
49	(B) - S - L - (T) - 1, 2			5	2 rev	E	N	N
50	A - S - N - (M) - 1, 2			3	90°	R	(N)	(N)
51	(A) - S - L - T - 1, (2), (3) (4)			6-8	8 or 9 rev	N	-	-
52	(A) - S - N - T - 1, 3, 4			4	360°	R	(Y)	?
53	C - (H) - N - S - 1, 5	9		0	90°	R	(Y)	?
54	C - S - N - M	10	75°	10	80°	R	Y	Y
55	(Rearward overturning)							
56	B - (S) - N - (T) - 1, 3			4-5	135°	R	?	?
57	A - S - N - M - 1			2	90°	R	Y	Y
58	A - S - N - T - 1, 4				180°	R	(Y)	(N)
59	C - (S) - N - S	15		15	180°	R	(Y)	?
60	A - S - N - T - 1			5	90°	R	N	N
61	A - S - N - M - 1, 4			5	90°	R	N	N
62	B - S - L - M - 1, 3			25-30	3 or 4 rev	N	-	-
63	A - H - N - M - 2, 4, 5			10	90°	R	(Y)	(Y)
64	A - S - N - T - 1, 4			5	90°	R	?	(Y)

APPENDIX 2.3

Total Numbers of Fatal Sideways Overturning Accidents

The numbers of fatal sideways overturning accidents in 1969-71 published by M.A.F.F are 27, 23, and 22 respectively, compared with 29, 24 and 23 quoted in this thesis. The main reason for this lies in a slightly different definition of the term "sideways".

1. M.A.F.F. definitions: Overturning accidents are assigned a class number ending in 00 if the principal direction of overturning is sideways, and 01 if it is endways (forwards or rearwards) regardless of the cause of the accident.

2. Definitions used in this thesis Because the main object of this survey was to provide information for research in the dynamics of overturning the most useful distinction was thought to be between accidents where the tractor rears up while trying to two out a bogged vehicle, for example, and those caused by the tractor's gravitational and inertial forces. Since the latter include most "sideways" overturns, the following defintions were chosen:-

   Rearwards: Accidents initiated solely or principally by torque in the tractor rear axle.

   Sideways: All other overturning accidents.

3. Comparison: As a result of the different definitions, one accident in which the principal direction was sideways (M.A.F.F. class 00) was initiated by torque in the rear axle, and six endways accidents were not so caused - in most of these cases the direction of overturning was forwards. In addition one accident claimed two lives.

Total Numbers of Fatal Sideways Overturning Accidents

	1969	1970	1971
Total M.A.F.F. class 00 - Number of fatalities	27	23	22
- Number of accidents*	26	23	22
Subtract class 00 accidents considered as rearward by the definition in this note:-			(81/71)
	26	23	21
Add class 01 accidents considered as sideways by the definition in this note:-	(89/69) (96/69) (105/69)	(42/70)	(9/71) (18/71)
	29	24	23

*One accident claimed two lives - 25/69 and 26/69

APPENDIX 3.1

Simulation Program Details

(a) The test for surface contact is carried out before the deflections in the current step are available. Instantaneous loss of contact must therefore be prevented at this stage, and is only allowed if the subsequently calculated ground reaction F_v is $<$ zero. No contact oscillation instability occurred with the program in this form.

(b) The slip angle ψ is calculated from the nominal forward velocity and lateral velocity along the surface of the point in the wheel plane corresponding to zero tyre spring force. The true velocity of the tyre contact point in the previous step may be used instead, but this was found to give rise to oscillation that was probably spurious. It is in any case the wheel plane that is normally used to define ψ.

(c) An effective "slip angle" for ROPS/soil is calculated using a very large value of $\left(\frac{d\mu}{d\psi}\right)_{\psi=0}$. The purpose is to avoid instability arising from an instantaneous change in side force from $+\mu_{max} . F_v$ to $-\mu_{max} . F_v$ at changes of sign $\dot{u}$. The effect is probably a fair representation of reality and has no significance in the dynamic behaviour.

(d) The structural line changes are determined on the basis of deflection from the initial position. To avoid the need to consider both positive and negative deflections in each direction at each point, a sign of the direction of non-linear behaviour is associated with each. Thus, for example, the deflection limits XL in Fig.3.7 are applied to positive x_1 deflections for odd-numbered vehicle points, and to negative x_1 deflections for even numbered points. Any deflections that occur in the opposite directions are assumed to be linear elastic. These are likely to be small except in the case of the tyres, which are entirely linear.

(e) Deflection is tested rather than force to avoid the need to subtract damping forces, and because some limits apply strictly to deflection. In the normal case, the limiting force, and hence deflection, is affected by yield enhancement, but for points 3 and 4 at the tops of the rims, the lateral deflection in the plastic phase is limited by contact with the tractor base frame.

(f) Each structural line is assigned a value 'elastic' or 'plastic'. If the line is elastic it is retained during unloading; otherwise the recovery line is selected (shown dotted in Fig.3.7). If the force subsequently increases, on renewed ground contact, for example, the recovery line (or appropriate elastic line) is used until the previous maximum deflection is reached, when the original loading line is resumed.

The first line of each characteristic is always elastic; subsequent lines may be either elastic or plastic. The present model is limited to a single recovery line, but multiple lines with elastic/plastic options would improve the simulation of anti-vibration mount behaviour, for example. In this case the change tests during recovery would become rather complex.

All the k_x etc values and the x_{1fo} etc values for the loading lines are fixed parameters. The x_{1fo} etc for the unloading lines are determined from the previous maximum force and deflection, which are updated whenever a 'plastic' line is in use.

The requirement for positive finite k_x precludes the use of a zero plastic stiffness. A very large k_x, however, achieves substantially the same effect. This results in high sensitivity of deflection to force variation, and forms an additional requirement for double precision variables.

(g) When a particular structural line change is encountered for the first time, the contact point equations are recalculated with the new line, as shown in Fig.3.5 & 3.7. The line is then rechecked according to Fig.3.7. The tolerance on deflection change between calculations from the two lines is necessary to avoid oscillation. The tolerance is automatically exceeded at the first change by setting the previous deflection to a large nominal value outside the loop. If the tolerance is not met after ten iterations the simulation is aborted. One iteration is normally sufficient except when two coordinates, such as x_1 and v change lines at the same time step.

(h) The increment in work done by the forces is calculated as the mean of the forces in the current and previous steps multiplied by the increment in displacement. At surface changes, the ground coordinates u and v may undergo large step changes because they are defined from the surface slope. To avoid spurious work calculation in these cases, the effective values of u and v in the previous step are calculated from the previous x_1, y_1, x_g, y_g and θ, using the <u>current</u> surface slope in equations (3.3a) and (3.4a).

(i) Several shortcuts are taken to reduce execution time:

In the bank overturn version of the program, the vehicle points 1, 3, 5 and 7 are omitted. The structural line test is omitted before impact, when the only points in contact are the elastic tyres. At the first impact with the ground, surface 4, the program reverts to the end of the previous step with the new, smaller value of step length.

In the multiple roll version, the test for regions (1)-(4) in Fig.3.6 is omitted, and the surface test reduces to a check for contact with surface 4. The nominal initial conditions are the unstable equilibium with the centre of mass vertically above point 10 (outside of tyre) which is in contact with the surface, and an initial angular velocity about this contact point. To avoid the slow initial movement when this velocity is small, the actual initial conditions for the program refer to the time when θ reaches -90° under rotation about the contact point 10. The velocities are determined from those in the nominal conditions assuming equivalence between potential and kinetic energy changes between the two positions.

APPENDIX 4.1

OVERCONSTRAINT OF THE TOP FRAME

The effect of constraint can be considered by treating the eight plastic hinges at the ends of the vertical bars as ball joints. Relative movement of the top frame in pure translation, as any combination of longitudinal and lateral motions, results in equal angular deflections of all the ball joints. For significant angular deflections Θ_i there will be a small vertical deflections S_{y_i} of the top of each bar

$$\delta_{y_i} = h^1 (1 - \cos \Theta_i) \qquad -(4.1)$$

(where h^1 is the effective height between hinges)
but in this case these four vertical deflections will be equal and the top frame will ramain parallel to the base frame. The same holds for relative movement in pure rotation about the centre of the top frame. If rotation and translation are combined, however, the four angular deflections, and hence the vertical deflections will be different. Furthermore, the vertical deflection will not in general be proportional to the horizontal distance to the effective centre of rotation and this gives rise to overconstraint. The kinematics of this type of movement are quite complicated but as the vertical deflections will always be small compared with the horizontal, a simple estimate of the degree of overconstraint can be made.

Three uprights are just sufficient to provide constraint; the lack of fit e_Δ in any deflected position can be defined as the vertical difference between the position of the top of the fourth upright predicted from the other three and its position derived from rotation about its own bottom hinge. The lack of fit increases with increasing slope of the top frame to the horizontal, although the relationship is not linear. For a given horizontal deflection at one upright this slope will be greatest when the deflection of an adjacent upright is zero. Thus the case giving maximum e_Δ is rotation of the top frame about one upright, i.e. one corner.

As an example (Fig. 4.9) consider a horizontal deflection of $0.2h^1$ at the two uprights (2 and 4) adjacent to the fixed one (1), giving approximately $0.2\sqrt{2}h^1$ at the fourth (3), diagonally opposite the fixed one. This is as large a deflection in this mode as is likely in practice.

Then the vertical deflection δ_{y_i} are

$$\delta_{y_1} = 0$$

$$\delta_{y_2} = \delta_{y_4} = h^1\,(1 - \cos\,(\text{Sin}^{-1}0.2)\,) = 0.0202\ h^1$$

$$\delta_{y_3} = h^1\,(1 - \cos\,(\text{Sin}^{-1}0.2\sqrt{2})\,) = 0.0408\ h^1$$

But in this case the deflection δ_{y_3} predicted from the other three deflections is approximately

$$(\delta_{y_3})_p = \sqrt{2}\ \delta_{y_2} = 0.0286\ h^1$$

$$\therefore\ e_\Delta = \delta_{y_3} - (\delta_{y_3})_p = (0.0408 - 0.0286)\ h^1 = \underline{\underline{0.0122\ h^1}}$$

The lack of fit is therefore only about 1% of the effective distance between hinges.

The lack of fit is compensated by change in the effective distance between hinges, together with a relatively small contribution from twisting of the stiff, top frame. In the case above, the adjustment would take place by the two hinges in each of uprights 2 and 4 moving closer together by about 1%, since the hinges in uprights 3 cannot move further apart.

In a real frame the hinges are not at the ends of the bars but displaced a distance depending on the bar diameter. This distance is not known very accurately, and the likely maximum error of about 1% due to overconstraint is therefore not important.

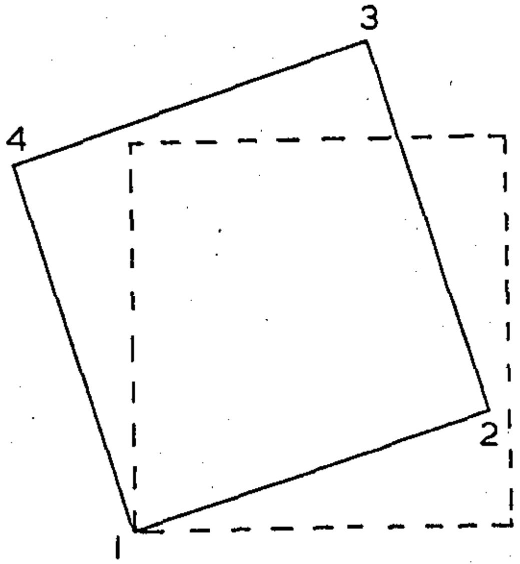

Fig. 4.9
Rotation of top frame about an upright

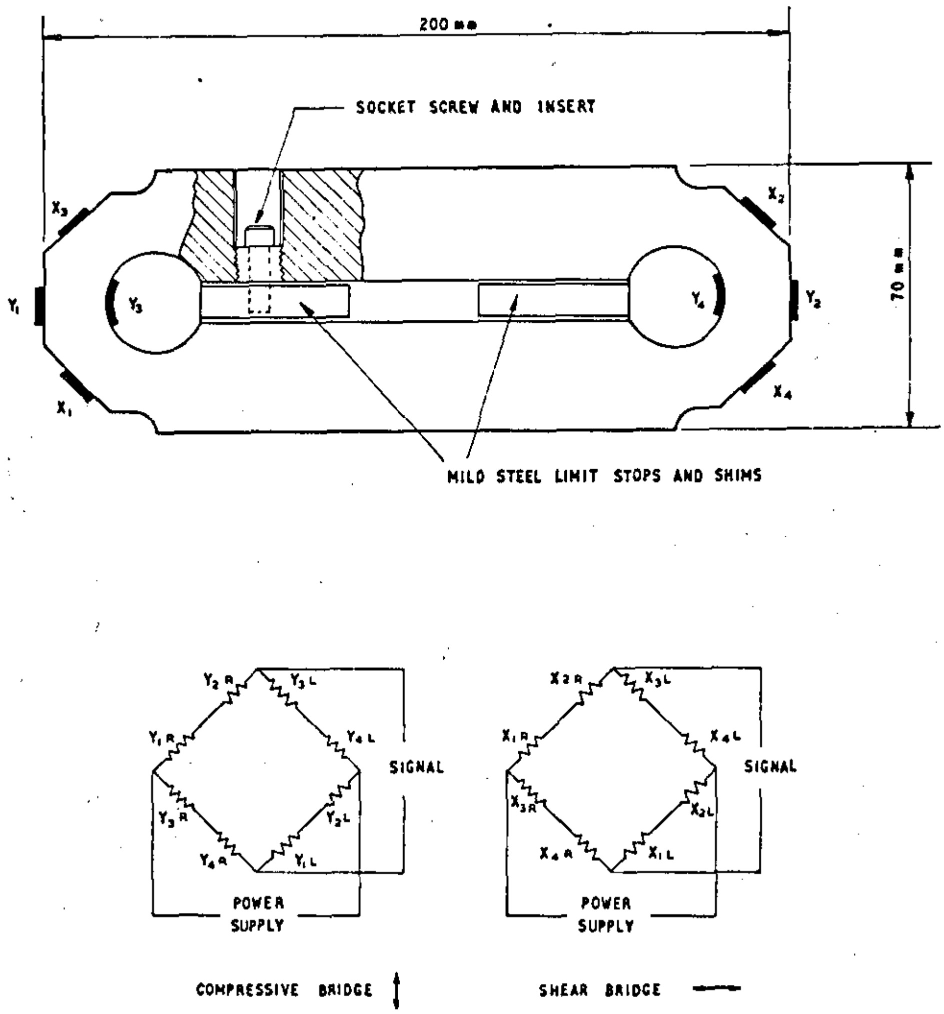

Fig.4.10 Load cell showing positions of strain gauges X and Y and bridge wiring diagrams

APPENDIX 4.2

TRANSDUCERS AND INSTRUMENTATION SYSTEM

Load cells

The form of the cells is the widely used flattened octagonal proving ring with strain gauges positioned to give greatest independence of force measurement in the two directions (85) (Fig. 4.10).

The design is a compromise between performance and size. In other situations where the maximum loads are small in relation to the space available, performance is optimised by making the mounting faces much thicker than the gauged sections. Applied to this case, however, optimisation would have resulted in an unmanageable overall size. The relative thickness and small radius of the gauged parts give rise to some non linearity, hysteresis and cross sensitivity in the compressive direction (Fig. 4.11), although behaviour in shear is good.

Each cell is effectively two octagonal rings placed side by side and connected by the mounting faces. The sideways separation and added mounting face width (125 mm) give force measurement independent of point of application, i.e. moment insensitivty, and help to offset the effect of the other dimensional compromises.

Limit stops

The stops are four 40 mm square pads fitted into the central cell gap (Fig. 4.10). The effective thickness is controlled by shims to give contact at the required load. Each assembly is fixed to one face of the cell by a grub screw passing through an insert in one of the main cell mounting holes. The surface of the inside gap faces had not been finished with this application in mind but it was hoped that mating would be improved by plastic surface deformation of the mild steel stops under overloading after assembly.

Preliminary tests established the gap width variations in the region of the stops, and the likely thickness required. The deflection of each cell at the rated load of 225 kN was about 0.3 mm. The predicted

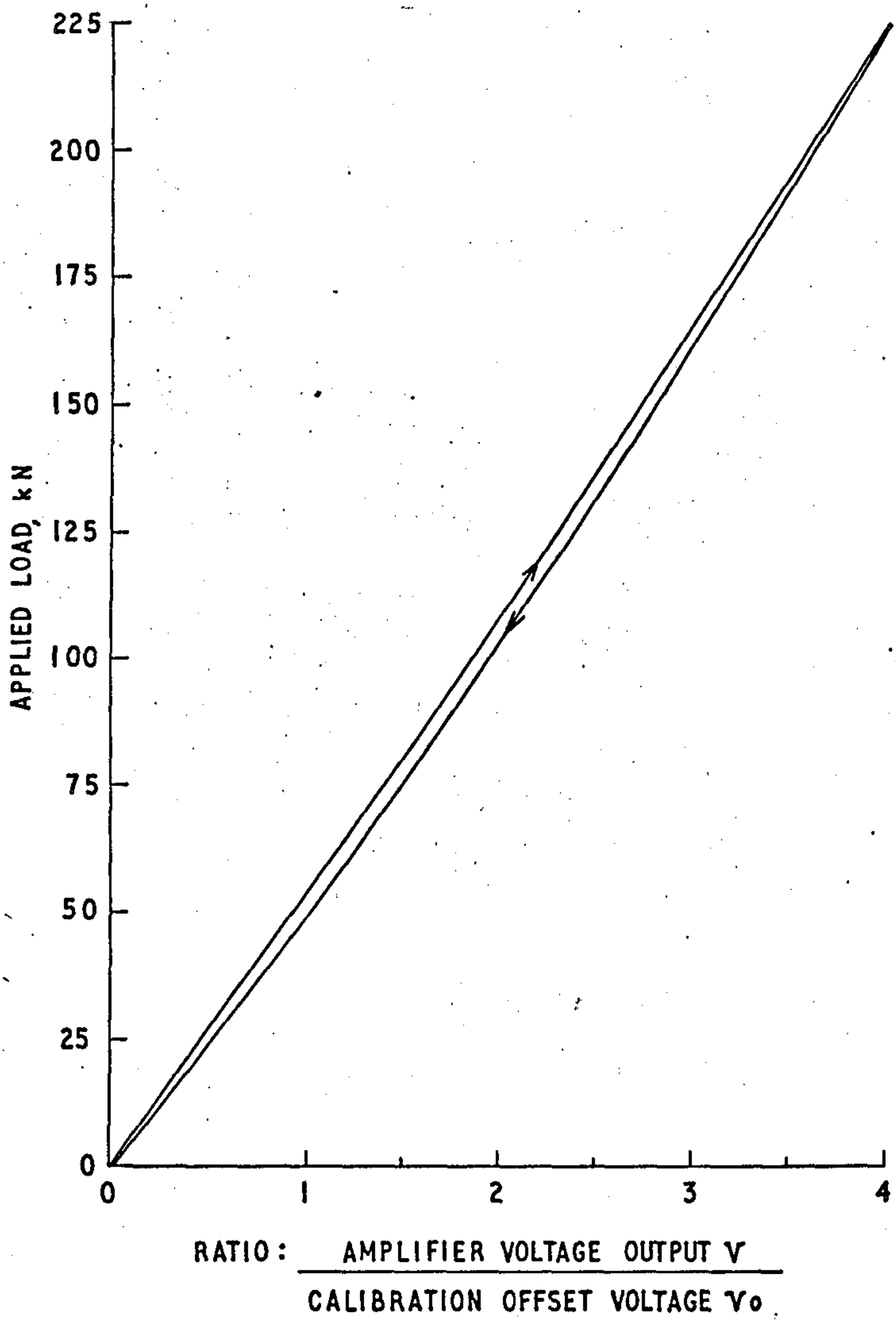

Fig.4.11 Compressive load-cell response for increasing and decreasing load (typical)

shim combinations were then fitted and modified so that each of the four stops began to make contact at approximately the same load. Further uniform shim changes were made to all stops to optimise the total load-deflection behaviour. Ideally this would have resulted in unchanged deflection up to rated load followed by no further increase under overload (Fig. 4.12). In practice the effect of the stops increased gradually and compromised criteria had to be adopted.

Accidental overload in previous impact tests had shown no physical damage under forces estimated to be several times the rated load. Permanent set was recorded, as a change in output at zero load, but sensitivity remained unaltered. An overload of $1\frac{1}{2}$ times rated load was judged to be the greatest that could be accepted without significant permanent set.

The criteria used in finalising shims were therefore set:

(i) no significant change in behaviour up to 75 kN and

(ii) a force of 1000 kN to be withstood without gauge output (corresponding to deflection) exceeding $1\frac{1}{2}$ x that of the cell without stops at rated load, and without significant permanent set.

These criteria were met by all four cells, a typical response being given in Fig. 4.12.

In their modified form the cells are suitable for measurement of forces up to 75 kN. At higher compressive loads the action of the stops interferes with shear measurement, although the extent of this could not be determined in the absence of equipment to apply forces simultaneously in the two directions. The accuracy of measurement of high compressive forces themselves is degraded but calibrations including the effect of the stops showed that the high-force behaviour is moderately repeatable, allowing estimates of impact peaks to be obtained.

<u>Displacement transducers</u>

Rotation measurement is effected by strain-gauged spring leaves

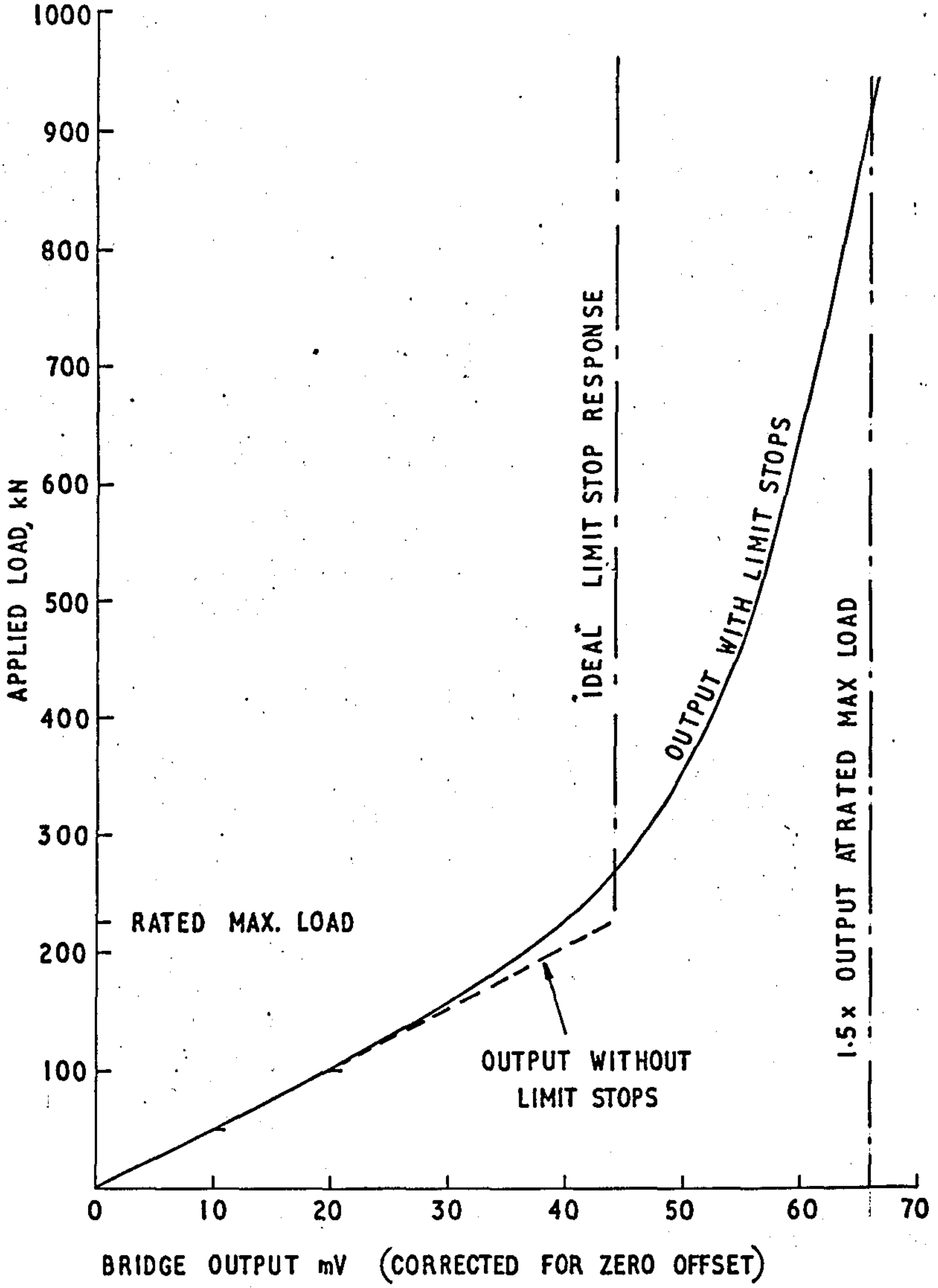

Fig.4.12 Ideal and achieved load-cell limit stop behaviour (typical)

riding on cams that form the cross of the bottom hooke-joint (Fig. 4.13). The fixed end of each leaf is mounted on a block which can be moved nearer or farther from the cam to alter the range of angles that can be measured. The total range is about 40°; with the block at one end it extends from -40° to 0° (vertical), and at the other end, from 0° to +40°. Intermediate positions may be chosen.

The leaves are made from beryllium-copper strip for high sensitivity and freedom from corrosion. They are tapered to ensure more uniform bending stress.

Instrumentation system

The two 50m umbilicals are each 25-way cables, one carrying the bridge power supplies and the other the signals. The greatest hazard would be for the cables to get caught round a rear wheel or on part of the platform. To help avoid this they hang behind the tractor from a support arm reaching nearly to the height of the top frame, are dragged along the platform and pass over a 4.2m high guide. The junction box receiving the cables is fixed to the tractor by shear-bolts to minimise damage if the cables did become fouled. Cable drag and inertia forces are transmitted to the tractor by a spring.

At the tractor end of the umbilicals they are connected through further distribution boxes and light, four-way leads to the individual transducers. At the van end they pass directly to a twelve-channel power supply and signal conditioning unit designed and built by Instrumentation Services Department. (Fig. 4.14)

Potentiometers at the amplifier inputs are used to balance the transducer bridges and alter the overall gain. Output is monitored on a digital voltmeter (DVM); on each channel the required gain setting is indicated by the offset produced when a calibration resistor is switched across a bridge arm. In the replay mode the tape recorder replaces the transducer connections as input to the amplifiers.

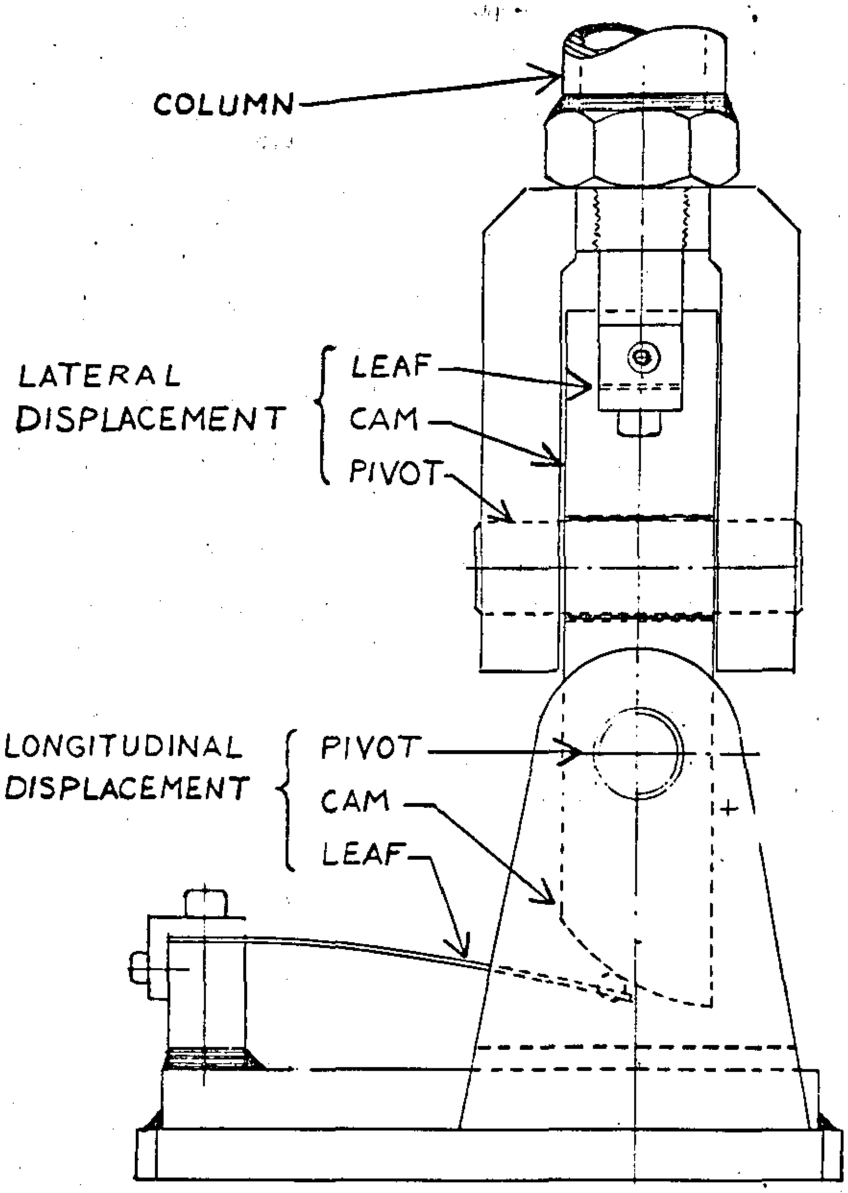

Fig.4.13 Displacement transducer

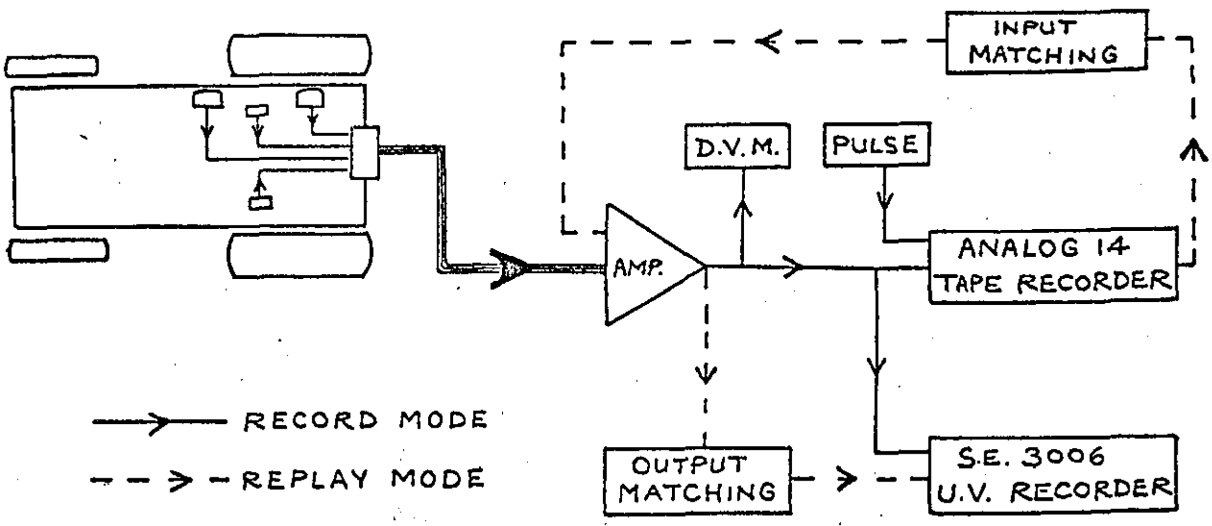

Fig.4.14 Block diagram of instrumentation

A remote control unit allows the operator to start and stop the tape recorder from a position outside the van. A switch is included to simultaneously put a one-volt pulse on the thirteenth channel, fire the flash units and start the oscillograph.

Cine film equipment:

Cameras:	Bolex H 16, 16 mm
	Nominal speed: 64 frames/s
Lenses:	16–100 mm zoom on 100 mm (rear camera)
	17–68 mm zoom on 17 mm (side camera)
Film:	Ilford Mk V or FP4 (monochrome)
	Kodak Ektachrome Commercial (colour)

Tractor speed measurement:

Synatel SSP.1 photoelectric system

Magnetic tape recorder

Philips Analog 14 Instrumentation recorder/reproducer.

14 channels + edge track on 1 inch wide tape.

Tape speed used for tests: 30 inch/s.

Tape: Pye TVT 8990/211/28020 Instrumentation tape.

UV Oscillograph:

SE Laboratories Type 3000/B/L.T

Chart speed used for tests: 250 mm/s

Galvanometers: Type M1000

Paper: Agfa Gevaert Oscilloscript D, width 152.4 mm.

APPENDIX 4.3

CALIBRATION

For final analysis the recorded signals may appear in several forms, such as lines on paper charts or sequences of numbers produced by analogue-digital (A-D) conversion. The technique of recording calibration voltage offsets before each test makes the reconversion of the final data into mechanical units very straightforward. It is assumed that all operations on the original transducer signal are linear, including those both before and after recording. The validity of this assumption was tested by calibration of the individual instrumentation units. There is no requirement for the mechanical-input/signal-output relationship of the transducer to be linear but it must be capable of definition by a mathematical function, such as a polynominal.

The overall procedure is as follows:

(i) The relation between mechanical units u' (force, displacement, etc.) and electrical amplifier output v' is obtained using suitable testing equipment. The transducer is connected to the instrumentation system and the voltage that would normally be recorded on tape is read from the DVM. The normal zero and gain setting-up procedure is followed and the voltage offset v_o produced by the calibration resistor is noted.

(ii) A mathematical function is fitted to this relationship in the form:

$$u' = f\left(\frac{v'}{v'_o}\right) \qquad -(4.2)$$

The function most appropriate for the present data is a cubic:

$$u' = U_1\left(\frac{v'}{v'_o}\right) + U_2\left(\frac{v'}{v'_o}\right)^2 + U_3\left(\frac{v'}{v'_o}\right)^3 \qquad -(4.3)$$

where the fitted constants U_1, U_2 and U_3 have the same units as the mechanical variable u'.

The curve must pass through the origin by definition from the zeroing procedure.

(iii) On analysis the new variable w (e.g. digitised values) with its associated offset w_o is converted back to mechanical units by the same function.

$$u' = U_1\left(\frac{w}{w_o}\right) + U_2\left(\frac{w}{w_o}\right)^2 + U_3\left(\frac{w}{w_o}\right)^3 \qquad -(4.4)$$

In this way the individual gains of the recording and analysis processes need not be known, providing they are applied identically to the data and the calibration offset. The same function and fitted constants may be used regardless of the form of the analysed variable.

Load cells

A Mayes servo-hydraulic universal testing machine applies compressive forces to the cells. To provide mounting arrangements equivalent to those of the top frame and domed plates, and to allow testing in the shear directions, the cells are fitted into a special jig. The two parts each comprise three mutually perpendicular welded faces, one of which is bolted to the cell. The complete assembly resembles a cube and compressive loading across each of the three pairs of faces correspond respectively to the compression and two shear directions.

Force was normally incremented in 25 kN steps up to 225 kN on the 250 kN range of the Mayes machine. In some cases additional tests were carried out in smaller steps and on lower ranges. The agreement between tests on different ranges was better than 1%.

Although the width of the 0-225 kN-0 compressive hysteresis loop is significant (typically 4 to 7% of indicated load in the 0-75 kN range), this is rather artificial. When loaded to a lower maximum more comparable to overturning test forces the absolute hysteresis is greatly reduced (e.g. 1.5% at 10 kN after loading to 25 kN). For this reason, load-increasing values only are used in calculating calibration coefficients.

A polynominal-fitting FORTRAN program based on the least-squares method (86) was made available by A.K. Dale. Ergonomics Department. This was modified by an iteration that adjusted the data to correct any zero error so that the curve was forced through the origin.

Cross-axis sensitivity

For each pair of cells, the calibration included measurements of the output of each channel in response to forces in the other two directions.

The sensitivity of the shear channels to forces in compressive and transverse directions was negligible.

The sensitivity of the compressive channels to force in the shear direction was up to 10% of the compressive sensitivity, and to force in the transverse direction up to 6% at loads up to 50 kN. For full scale loads the cross sensitivities increase to up to 18% in the worst case. Because of the relative unimportance of high shear and transverse loads a simple linear approximation to the cross sensitivity of the compressive channels is derived for the range 0-50 kN.

Assuming the linearity is sufficiently good to allow the principal of superposition to hold, the voltage output from a compressive channel due to a known shear force may be estimated and subtracted from the measured compressive voltage. The nett compressive force is then obtained from the compressive calibration function. This method is only possible because of the lack of cross sensitivity of the shear channels.

Consider one pair of cells subjected to a combined loading:

Compressive component : F_C

Vertical component : F_V

Horizontal component : F_H

Then the voltages v'_{XV} and v'_{XH} in the compressive channel due to F_V and F_H will be given by:

$$F_V = U_{XV} \frac{(v'_{XV})}{(v'_{OC})} \qquad -(4.5)$$

and $F_H = U_{XH} \left(\frac{v'_{XH}}{v'_{OC}}\right)$ -(4.6)

where U_{XV} and U_{XH} define the linear cross sensitivities from the cross-axis calibration and v'_{OC} is the calibration offset of the compressive channel.

The voltage v'_{CM} measured at the compressive channel is then the sum of v'_{XV}, v'_{XH} and the output v'_C due to the compressive component F_C,

$$\text{or} \quad \frac{v'_C}{v'_{OC}} = \frac{v'_{CM}}{v'_{OC}} - \frac{v'_{XV}}{v'_{OC}} - \frac{v'_{XH}}{v'_{OC}} \qquad \text{-(4.7)}$$

$$= \frac{v'_{CM}}{v'_{OC}} - \frac{F_V}{U_{XV}} - \frac{F_H}{U_{XH}} \qquad \text{-(4.8)}$$

F_V and F_H are calculated from the measured relative shear voltages

$$\frac{v'_V}{v'_{OV}} \quad \text{and} \quad \frac{v'_H}{v'_{OH}}$$

and the shear coefficients. The value of V'_C/V'_{OC} may then be used with the compressive coefficients to determine F_C.

Since the shear relationships are linear, the calculation may be further simplified to allow F_C to be obtained directly from the voltages and coefficients without intermediate determination of F_V and F_H:

$$F_V = U_V \left(\frac{V'_V}{V'_{OV}}\right) \qquad \text{-(4.9)}$$

$$F_H = U_H \left(\frac{V'_H}{V'_{OH}}\right) \qquad \text{-(4.9)}$$

where U_V and U_H are the relevant U_1 coefficients

$$\text{then } \frac{V'_C}{V'_{OC}} = \frac{V'_{CM}}{V'_{OC}} - \frac{U_V}{U_{XV}} \left(\frac{V'_V}{V'_{OV}}\right) - \frac{U_H}{U_{XH}} \left(\frac{V'_H}{V'_{OH}}\right) \qquad \text{-(4.11)}$$

Displacement transducers

A simple calibration jig is used to allow linear movement of the top of the transducers. The top frame mounting bracket is removed and a long bar, marked in 10 mm steps, is fitted through the top pivot pin hole in the cross piece. The bar is anchored to the timber frame and the calibration is performed by recording electrical output as the top joint is moved progressively along the bar.

Although the linear movement during calibration is similar to the movement of the top frame it is not identical due to the height changes constrained by the deformation of the bars. To allow this to be taken into account the linear movements are converted to angular displacements of the pivots in degrees, and the calibration coefficients are expressed in these units.

The horizontal deformation δ of the top frame in a test are derived from the calibrated angular displacements θ_t of the transducers by:

$$\delta = h_o \sin \theta_t$$

This is an approximate relationship depending on the assumption that the effective distance h' between plastic hinges is the same as that between the transducer pivots. The error introduced by this assumption is less than 1%.

Calibration results

Details of individual calibrations and tables of coefficient values obtained are given in reference 62.

APPENDIX 5.1

ESTIMATION OF UNOBTAINABLE PENETROMETER READINGS

At the first depth (0, 3, 6, 9 in) for which the reading could not be obtained a value of 300 (corresponding to a cone resistance of 2730 kN/m^2) was assigned. This is slightly greater than the maximum that could be reached manually. Means were than calculated at each depth, in some cases of less than the ten values where the obtained readings stopped before the previous depth. These new means were corrected as appropriate by multiplying by the ratio of the new/old mean for the previous depth to take some account of the missing values. This was particularly important where the mean value reduced with depth, as occurred in some cases from 6 in to 9 in due to the hard crust formed over softer ground.

The procedure is illustrated in Table 5.19 by an example.

Table 5.19. Penetrometer readings for Test No. 25

(To obtain cone resistance in kN/m^2, multiply reading by 9.0897)

Depth, in	Individual readings at ten stations (*Estimated)										Of actual readings		Of actual + estimated readings		Correction factor	Corrected mean
											Mean	No.	Mean	No.		
0	150	90	90	25	40	90	20	40	50	70	67	10			1	67
3	225	220	170	90	140	300*	100	130	130	180	154	9	169	10	1	169
6	215	300*	240	220	190		230	190	170	160	202	8	213	9	$\frac{169}{154}$	233
9	200		300*	140	90		230	260	50	180	164	7	181	8	$\frac{233}{202}$	209

Calculating back from the corrected means, the missing value at 6 in is found to be estimated as 413, and the two missing values at 9 in each to be 321.

APPENDIX 5.2

Method of analysis of film measurements

(i) Derivation of rotation equations

Starting from the fixed co-ordinates x_o y_o z_o, the body co-ordinates are obtained by the three successive rotations shown fig. 5.2.

For the first rotation through θ_z about Oz_o to x_1 y_1 z_1:

$$\begin{vmatrix} x_1 \\ y_1 \\ z_1 \end{vmatrix} = \begin{vmatrix} \cos\theta_z & \sin\theta_z & 0 \\ -\sin\theta_z & \cos\theta_z & 0 \\ 0 & 0 & 1 \end{vmatrix} \begin{vmatrix} x_o \\ y_o \\ z_o \end{vmatrix} \qquad -(5.1)$$

For the second rotation θ_y about Oy_1 to x_2 y_2 z_2:

$$\begin{vmatrix} x_2 \\ y_2 \\ z_2 \end{vmatrix} = \begin{vmatrix} \cos\theta_y & 0 & -\sin\theta_y \\ 0 & 1 & 0 \\ \sin\theta_y & 0 & \cos\theta_y \end{vmatrix} \begin{vmatrix} x_1 \\ y_1 \\ z_1 \end{vmatrix} \qquad -(5.2)$$

For the third rotation θ_x about ox_2 to x_3 y_3 z_3:

$$\begin{vmatrix} x_3 \\ y_3 \\ z_3 \end{vmatrix} = \begin{vmatrix} 1 & 0 & 0 \\ 0 & \cos\theta_x & \sin\theta_x \\ 0 & -\sin\theta_x & \cos\theta_x \end{vmatrix} \begin{vmatrix} x_2 \\ y_2 \\ z_2 \end{vmatrix} \qquad -(5.3)$$

(5.1) x (5.2) gives:

$$\begin{vmatrix} x_2 \\ y_2 \\ z_2 \end{vmatrix} = \begin{vmatrix} \cos\theta_y\cos\theta_z & \cos\theta_y\sin\theta_z & -\sin\theta_y \\ -\sin\theta_z & \cos\theta_z & 0 \\ \sin\theta_y\cos\theta_z & \sin\theta_y\sin\theta_z & \cos\theta_y \end{vmatrix} \begin{vmatrix} x_o \\ y_o \\ z_o \end{vmatrix} \qquad -(5.4)$$

(5.3) x (5.4) gives:

$$\begin{vmatrix} x_3 \\ y_3 \\ z_3 \end{vmatrix} = \begin{vmatrix} \cos\theta_y\cos\theta_z & \cos\theta_y\sin\theta_z & -\sin\theta_y \\ -\sin\theta_z\cos\theta_x + \sin\theta_x\sin\theta_y\cos\theta_z & \cos\theta_x\cos\theta_z + \sin\theta_x\sin\theta_y\sin\theta_z & \cos\theta_y\sin\theta_x \\ \sin\theta_x\sin\theta_z + \cos\theta_x\sin\theta_y\cos\theta_z & -\sin\theta_x\cos\theta_z + \cos\theta_x\sin\theta_y\sin\theta_z & \cos\theta_x\cos\theta_y \end{vmatrix} \begin{vmatrix} x_o \\ y_o \\ z_o \end{vmatrix} \qquad -(5.5)$$

Equation (5.5) is the rotation transform from fixed to body co-ordinates and may be expressed in the form

$$\bar{x}_3 = \bar{T}_\theta \times \bar{x}_o \qquad -(5.6)$$

The transformation of the roll angle θ_z may be followed by considering the behaviour of a line parallel to the axis Ox_o. The film plane is parallel to the $x_o\, y_o$ plane so that a line will map to its projection on this plane. The first rotation about Oz_o is in this plane so the projected angle remains the true angle. The second rotation is about Ox_1 which is still in the $x_o\, y_o$ plane, so that the projection of Ox_2 onto the plane is identical to Ox_1. The final rotation leaves Ox_3 coincident with Ox_2 and hence the projection of Ox_3 onto the $x_o y_o$ plane provides the true angle θ_z. Measurement of the rotation of any line parallel to Ox_3, may be used. The other variables measured from film are the x_o and y_o co-ordinates of marked points on the tractor. A complete description of the tractor's position may be obtained from two such points, P and Q, assuming that the z_o co-ordinate is determined separately, and the differences between the x_o and y_o co-ordinates of P and Q may be used to determine the pitch and yaw angles θ_x and θ_y from the transformation equation (5.5). The derivation is most simple if P and Q are chosen to lie on the tractor centreline giving $x_{3P} = x_{3Q} = 0$. The matrix is most easily handled as its transpose to exclude z_o co-ordinates from the equations.

Put $S = \sin\theta_z$ and $C = \cos\theta_z$ $\qquad$ -(5.7)

and define the differences in the co-ordinates of P and Q by the suffix B:

$$x_{3B} = \left(x_3\right)_P - \left(x_3\right)_Q$$
$$x_{oB} = \left(x_o\right)_P - \left(x_o\right)_Q \quad \text{and similarly for } y_{3B} \text{ and } y_{oB} \qquad -(5.8)$$

Expanding the inverse of (5.5) using (5.7) and (5.8) gives:

$$x_{oB} = (y_{3B}\sin\theta_x + z_{3B}\cos\theta_x).C\,\sin\theta_y + (-y_{3B}\cos\theta_x + z_{3B}\sin\theta_x).S$$
$$\text{and}\quad y_{oB} = (y_{3B}\sin\theta_x + z_{3B}\cos\theta_x).S\,\sin\theta_y - (-y_{3B}\cos\theta_x + z_{3B}\sin\theta_x).C \qquad -(5.5a)$$

$$\text{i.e.}\quad x_{oB}S - y_{oB}C = (-y_{3B}\cos\theta_x + z_{3B}\sin\theta_x)$$

$$\text{put}\quad t_x = \tan\tfrac{1}{2}\,\theta_x \qquad -(5.9)$$

then $(x_{oB}S - y_{oB}C) \quad (1 + t_x^{\,2}) = - y_{3B}(1 - t_x^{\,2}) + 2\, t_x z_{3B}$

solving for the quadratic in t_x gives

$$t_x = \frac{z_{3B} \pm \sqrt{z_{3B}^{\,2} + y_{3B}^{\,2} - (x_{oB}S - y_{oB}C)^2}}{x_{oB}S - y_{oB}C - y_{3B}} \qquad -(5.10)$$

For the case where point Q is forward of point P, giving $z_{3B} < 0$, the positive root gives the required solution.

In the case where

$x_{oB}S - y_{oB}C - y_{3B} = 0$

the solution is obtained from

$$t_x = y_{3B}/z_{3B} \qquad -(5.10a)$$

in place of (5.10).

Equations (5.10) contain known values and may be used directly with (5.9) to determine the pitch rotation θ_x.

The yaw θ_y may be then obtained from (5.5a)

$$\sin\theta_y = \frac{x_{oB} + (y_{3B}\cos\theta_x - z_{3B}\sin\theta_x)S}{(y_{3B}\sin\theta_x + z_{3B}\cos\theta_x) \quad C} \qquad -(5.11)$$

or if $\theta_z = 90^o$ and $C = 0$

$$\sin\theta_y = \frac{y_{oB} - (y_{3B}\cos\theta_x - z_{3B}\sin\theta_x)C}{(y_{3B}\sin\theta_x + z_{3B}\cos\theta_x) \quad S} \qquad -(5.11a)$$

The value of $(y_{3B}\sin\theta_x + z_{3B}\cos\theta_x)$ becomes zero only if the pitch rotation brings Q and P into the same $x_o\, y_o$ plane, i.e. $z_{oB} = z_o$. This is unlikely for a reasonable choice of P and Q.

Angular velocities in the body co-ordinates

Consider two successive positions of the tractor defined by the rotation angles $[\theta]_i$ and $[\theta + \delta\theta]_i$, where i is used to denote the sequence x, y, z. The incremental angles in the body co-ordinates may then be defined in terms of a rotation transform matrix $\Delta\bar{T}$, where:

$$[\bar{x}_3]_{\theta + \delta\theta} = \Delta\bar{T} \times [\bar{x}_3]_{\theta} \qquad -(5.12)$$

and $\bar{x}_3$ are the co-ordinates in the body system of a stationary point in the fixed system.

$[\delta\theta_3]_i$ If $\overline{\Delta T}$ can be found from known values, the required incremental angles are given by manipulation of its elements. By analogy with the equivalent rotation transform $\overline{T}_\theta$ (equation 5.5).

$$\left.\begin{aligned} \tan \delta\theta_{3x} &= \overline{\Delta T}\ (2,3) / \overline{\Delta T}\ (3,3) \\ \sin \delta\theta_{3y} &= -\overline{\Delta T}\ (1,3) \\ \tan \delta\theta_{3z} &= \overline{\Delta T}\ (1,2) / \overline{\Delta T}\ (1,1) \end{aligned}\right\} \quad -(5.13)$$

$$\left.\begin{aligned} \text{now}\ \left[\bar{x}_3\right]_\theta &= \overline{T}_\theta \times \bar{x}_o \\ \text{and}\ \left[\bar{x}_3\right]_{\theta+\delta\theta} &= \overline{T}_{\theta+\delta\theta} \times \bar{x}_o \end{aligned}\right\} \quad -(5.14)$$

where $\bar{x}_o$ are the co-ordinates of the point in the fixed system.

From (5.12) and (5.14):

$$\overline{T}_{\theta+\delta\theta} \times \bar{x}_o = \overline{\Delta T} \times \left[x_3\right]_\theta$$

$$= \overline{\Delta T} \times \overline{T}_\theta \times \bar{x}_o$$

multiplying by $\overline{T}_\theta^{-1}$, the inverse of $\overline{T}_\theta$:

$$\overline{T}_{\theta+\delta\theta} \times \overline{T}_\theta^{-1} \times \bar{x}_o = \overline{\Delta T} \times \overline{T}_\theta \times \overline{T}_\theta^{-1} \times \bar{x}_o$$

$$\text{or } \underline{\overline{\Delta T} = \overline{T}_{\theta+\delta\theta} \times \overline{T}_\theta^{-1}} \quad -(5.15)$$

Scaling

Scaling is based on the mean length of one metre on the fixed vertical pole as measured during analysis in the same units as the tractor co-ordinates. This is then corrected for the estimated z_o position of the tractor (Fig. 5.11).

$$z_o = \left[z_o\right]\text{impact} + DZ\,(t_{\text{impact}} - t) \quad -(5.16)$$

Thus the apparent x_o co-ordinate of P, the tractor point is given by

$$x'_{oP} = \frac{-D_oP'}{SCALE}$$

where SCALE = mean length on analysis of 1 metre at pole.

Then true x_o co-ordinate of P is

$$x_{oP} = \frac{(-D_oP')}{SCALE} \times \frac{-z_oP}{-z_oD}$$

but $D_oP' = DP' - DD_O = x_{Pf} - x_{Ef}$

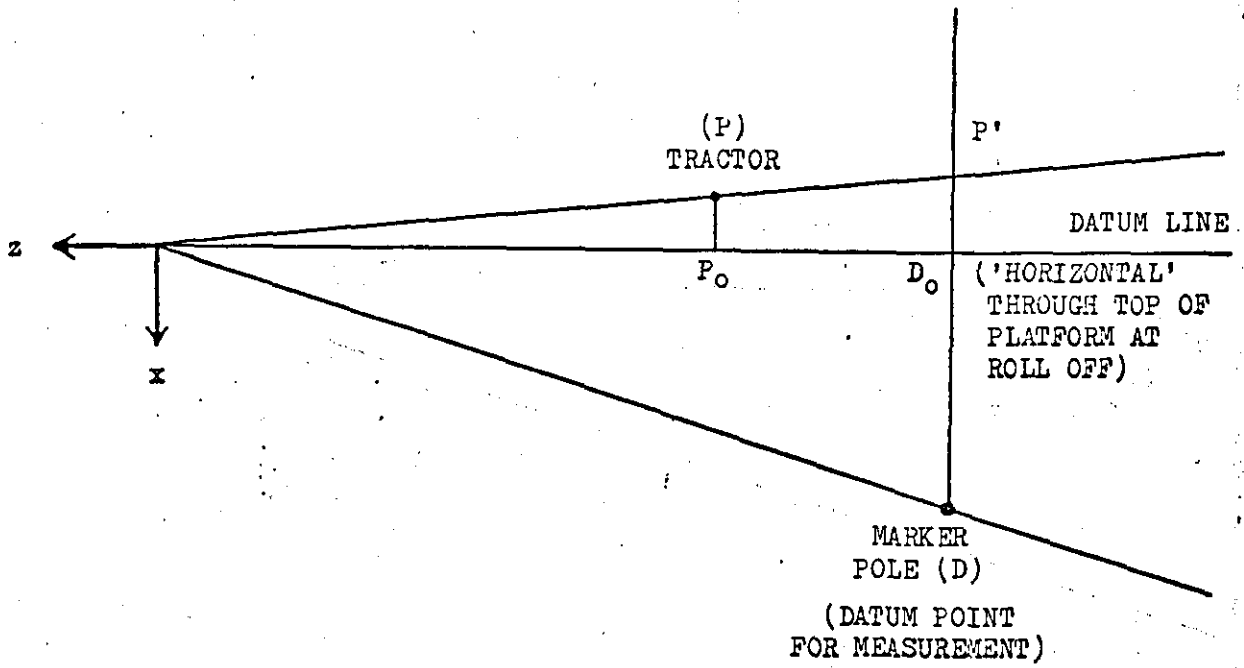

Fig.5.11 Scaling diagram (plan view)

where x_{Pf} and x_{Ef} are the measured x co-ordinates of P and the edge of the bank respectively on analysis

(Note: for convenience, the x co-ordinates on analysis were measured in the - ve x direction)

Then $$x_{oP} = \frac{(x_{Ef} - x_{Pf})\, z_{oP}}{\text{SCALE} \times z_{oD}} \qquad -(5.17)$$

similarly $$y_{oP} = \frac{(y_{Pf} - y_{Ef})\, z_{oP}}{\text{SCALE} \times z_{oD}} \qquad -(5.18)$$

The measured co-ordinates of Q are obtained in the same way.

APPENDIX 5.3

Transformation of impact forces and deflections

The transformations from the top frame co-ordinates x_4, z_4, to the tractor co-ordinates x_3, z_3 (fig.5.12) are:

$$x_3 = x_{3o} + x_4 \cos\theta_{3y} + z_4 \sin\theta_{3y} \qquad -(5.19)$$

$$z_3 = z_{3o} - x_4 \sin\theta_{3y} + z_4 \cos\theta_{3y} \qquad -(5.20)$$

The value of x_3 is given by the calibrated lateral displacement of transducer D1 (CH7):

$$x_{3D1} = CH7 + b_1 \qquad -(5.21)$$

and z_3 by the calibrated longitudinal displacements of D1 (CH9) and D2 (CH8):

$$\left.\begin{aligned} z_{3D1} &= CH9 + b_4 \\ z_{3D2} &= CH8 + b_4 \end{aligned}\right\} \qquad -(5.22)$$

Then the deflections δx_{3o} and δz_{3o} are:

from (5.19): $\delta x_{3o} = CH7 + b_1 - b_1 \cos\theta_{3y} - b_4 \sin\theta_{3y}$ $\qquad -(5.23)$

from (5.20): $\delta z_{3o} = CH9 + b_4 + b_1 \sin\theta_{3y} - b_4 \cos\theta_{3y}$ $\qquad -(5.24)$

& $\delta z_{3o} = CH8 + b_4 - b_1 \sin\theta_{3y} - b_4 \cos\theta_{3y}$

from (5.23) and (5.24):

$$z_{3o} = \tfrac{1}{2}(CH9 + CH8) + b_4\,(1-\cos\theta_{3y}) \qquad -(5.25)$$

$$\text{and} \quad \sin\theta_{3y} = \frac{1}{2b_1}\,(CH8 - CH9) \qquad -(5.26)$$

The deflections at the load cells L1 and L2 are then:

$$\delta x_{3L1} = \delta x_{3o} + b_5 \cos\theta_{3y} + b_6 \sin\theta_{3y} - b_5 \qquad -(5.27)$$

$$\delta x_{3L2} = \delta x_{3o} + b_5 \cos\theta_{3y} - b_6 \sin\theta_{3y} - b_5 \qquad -(5.28)$$

$$\delta z_{3L2} = \delta z_{3o} - b_5 \sin\theta_{3y} - b_6 \cos\theta_{3y} + b_6 \qquad -(5.29)$$

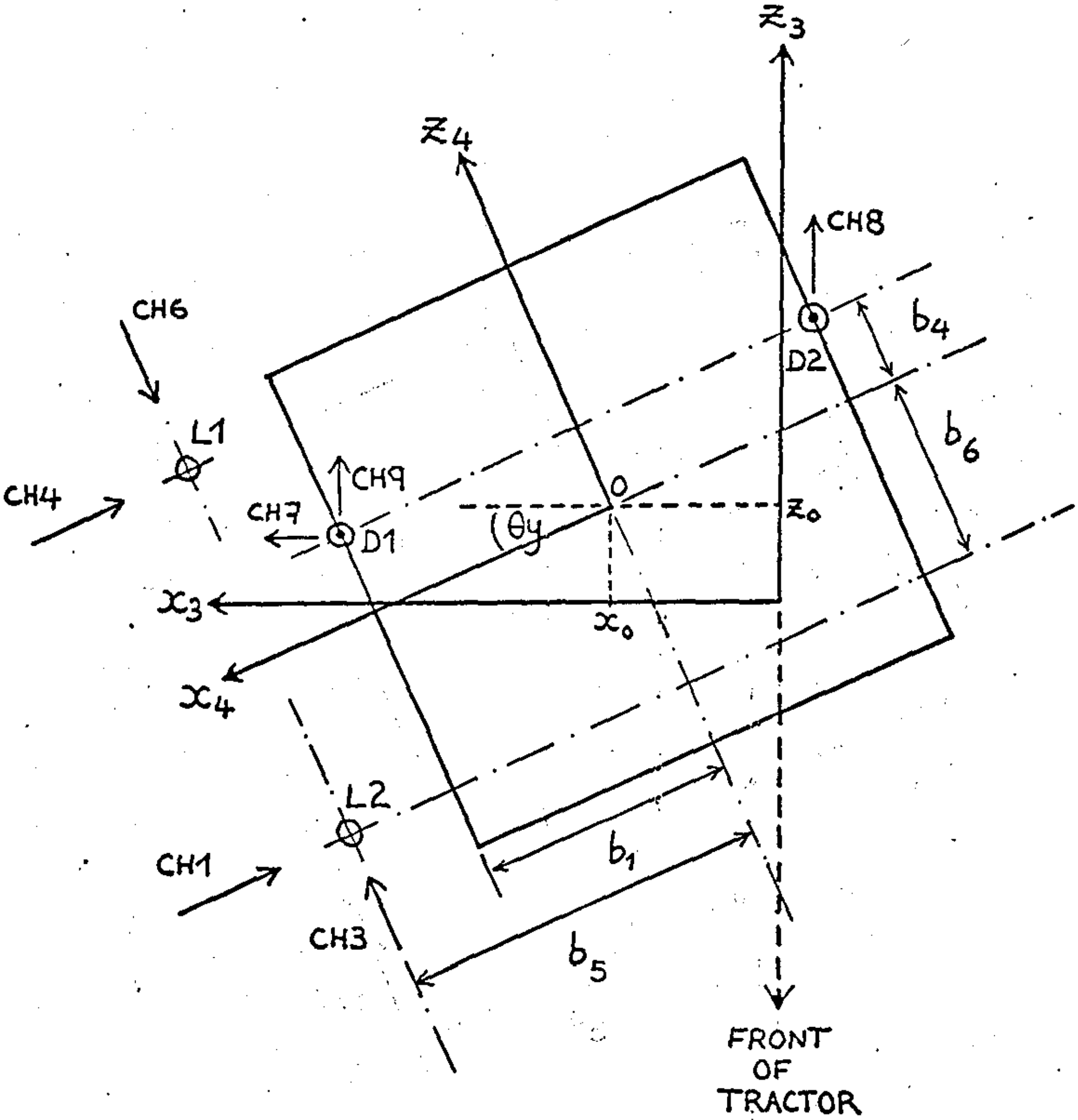

Fig. 5.12 Impact force and deflection diagram, as a plan view of the top frame

Note: Relationships defining load cell co-ordinates b_5 and b_6 in Fig. 5.12, and b_2 and b_3 in Fig. 6.6, are:

$$b_1 = b/2$$

$$b_5 = b_1 + b_3$$

$$b_6 = b_1 + b_2$$

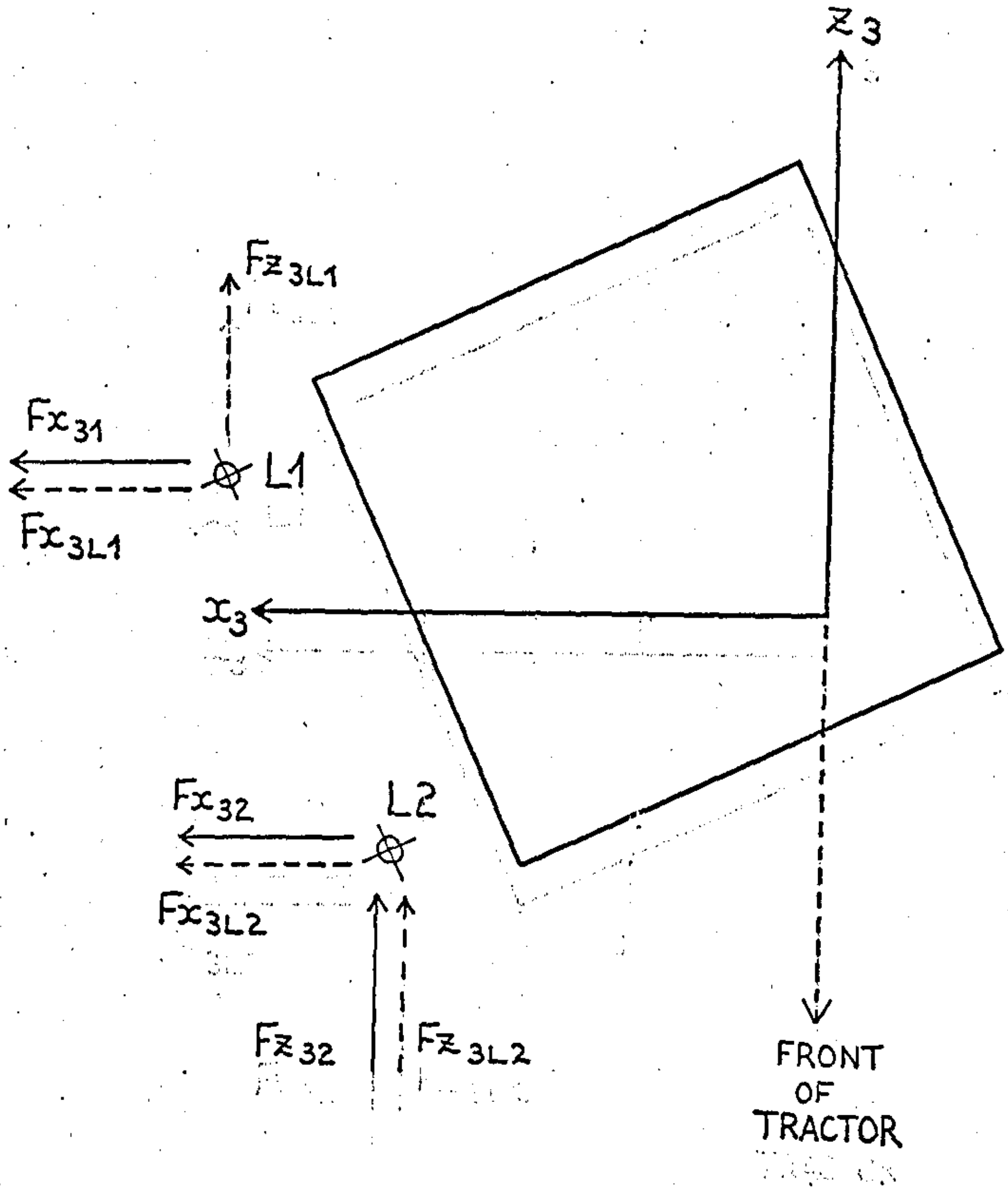

Fig.5.13 Two equivalent sets of impact forces

The measured forces are in the x_4 and z_4 directions. Taking account of the signs of the transducer signals (fig. 4. 8) the forces on the frame in the x_3 and z_3 directions are:

$$F_{x_{3L1}} = -CH3 \cos \theta_{3y} - CH6 \sin \theta_{3y} \qquad -(5.30)$$

$$F_{z_{3L1}} = CH4 \sin \theta_{3y} - CH6 \cos \theta_{3y} \qquad -(5.31)$$

$$F_{x_{3L2}} = -CH1 \cos \theta_{3y} + CH3 \sin \theta_{3y} \qquad -(5.32)$$

$$F_{z_{3L2}} = CH1 \sin \theta_{3y} + CH3 \cos \theta_{3y} \qquad -(5.33)$$

This system of four forces is then replaced by an equivalent system of three forces corresponding to the three chosen characteristic deflections (fig. 5.13).

$$F_{x_{32}} + F_{x_{31}} = F_{x_{3L2}} + F_{x_{3L1}} \qquad -(5.34)$$

$$F_{z_{32}} = F_{z_{3L2}} + F_{z_{3L1}} \qquad -(5.35)$$

$$F_{x_{31}} . 2b_6 \cos \theta_{3y} = F_{x_{3L1}} . 2b_6 \cos \theta_{3y} - F_{z_{3L1}} . 2b_6 \sin \theta_{3y}$$

$$\text{or } F_{x_{31}} = F_{x_{3L1}} - F_{z_{3L1}} \tan \theta_{3y} \qquad -(5.36)$$

(5.34) in (5.36) gives:

$$F_{x_{32}} = F_{x_{3L2}} + F_{z_{3L1}} \tan \theta_{3y} \qquad -(5.37)$$

Hence the three deflections are found from equations (5.27)-(5.29), using (5.26) to determine θ_y and (5.23) and (5.25) for δx_{3_0} and δz_{3_0}. The three forces are found from (5.35)-(5.37), using θ_y in (5.30)-(5.33) to find the intermediate forces.

APPENDIX 6.1

THE COMPUTER PROGRAM STAF6

The program is written in FORTRAN for use on the ICL 4-70 at Rothamsted Experimental Station.

For a set of input deflections the resultant external forces are calculated from equations (6.31)-(6.41). It had been found that y_D varied between about -1 and +1 for unit deflection at B; also the force F_{yD} or F_{yD1} increased monotonically with increasing y_D for a particular value of β_B, as shown in Fig. 6.22. This curve is not well conditioned for a Newton-Raphson iteration, however, because of the large changes in slope in the range of possible solutions. In addition the differential coefficient of F_{yD1} would be fairly complicated. To overcome these problems a search based on a modified Newton technique was used following a simple search from below the solution.

From an initial value of say, -2, y_D was increased in small steps until F_{yD1} changed sign. At this point the modified Newton technique took over, the steps of y_D being determined by finite differences using previous values instead of the differential coefficient.

Thus in Newton $x_{n+1} = x_n - \dfrac{f(x_n)}{f'(x_n)}$ -(6.56)

replacing $f'(x_n)$ by $\dfrac{f(x_n) - f(x_{n-1})}{x_n - x_{n-1}}$ gives:

$$x_{n+1} = x_n - \frac{x_n - x_{n-1}}{1 - f(x_{n-1})/f(x_n)} \qquad -(6.57)$$

or in terms of the present variables

$$(y_D)_{n+1} = (y_D)_n + (\delta y_D)_n \qquad -(6.58)$$

where $(\delta y_D)_n = -\dfrac{(y_D)_n - (y_D)_{n-1}}{1 - (F_{yD1})_{n-1}/(F_{yd1})_n}$ -(6.59)

To avoid the instability resulting from the highly non-linear parts of the curve the value of y_D is constrained to lie between the

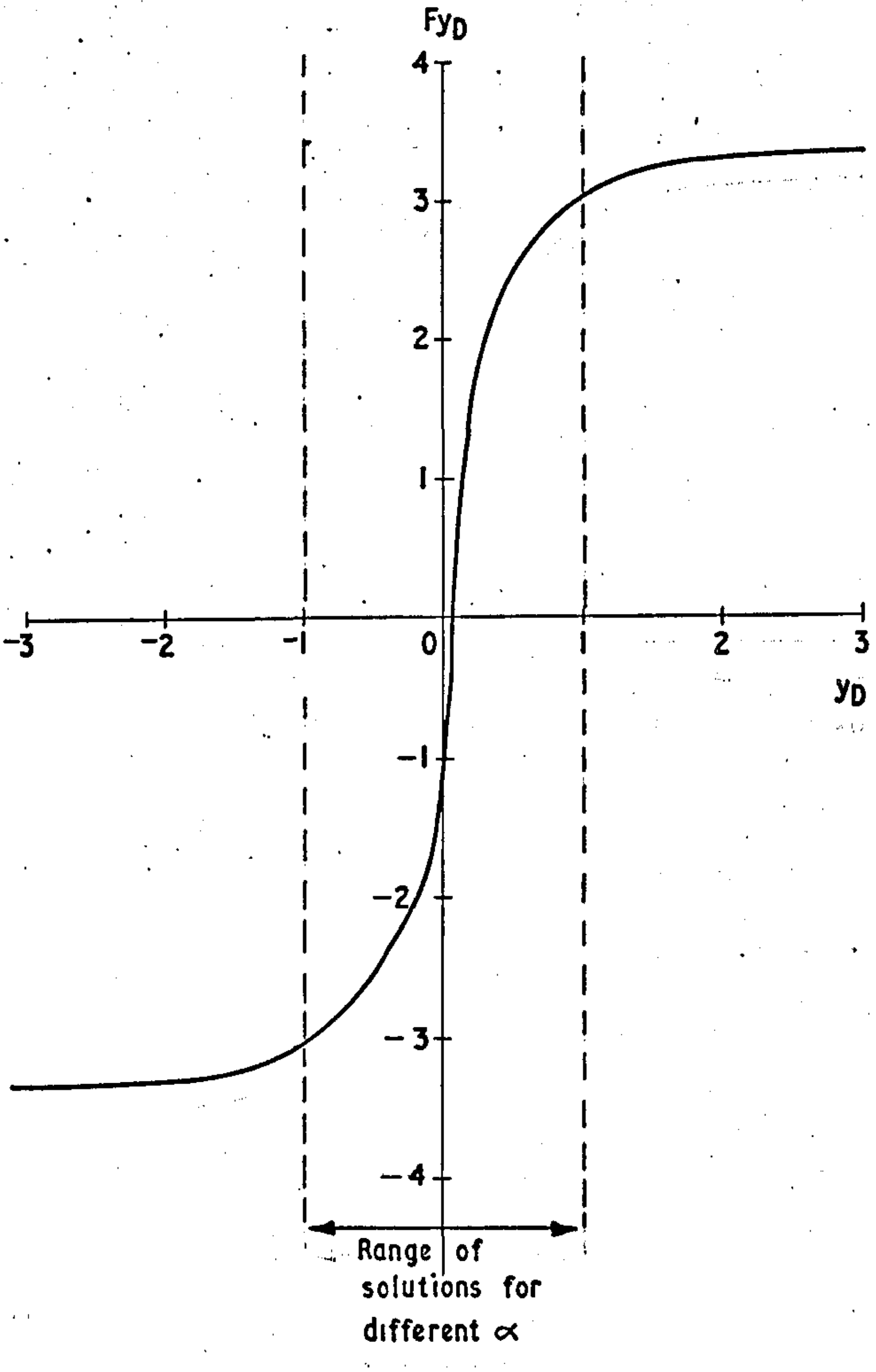

Fig.6.22 Variation of force and deflection at D for constant deflection at B (β_B = 320°, $b_2 = b_3 = 0$)

the two previously found values that are closest to the solution. At each step the maximum value of y_D is the lowest previous value for which F_{yD1} was positive, and the minimum is the highest value for which F_{yD1} was negative. This results in use of the efficient Newton technique wherever possible. The method works well and gives a fast iteration for this type of function.

APPENDIX 6.2

DETERMINATION OF YIELD STRESS

Hounsfield No.14 tensile test specimens were cut from four positions in each of six of the 42 mm bars used in the tests. The specimens have a diameter of 6.44 mm and a gauge length of 22.7 mm. One specimen from each bar was taken papallel to the axis on the tensile side at the position of the plastic hinge (No. 1 - Fig. 6.23). The other three were taken from parts of the bar that had not been deformed plastically, approximately 250 mm from the hinge, No. 2 being parallel to the axis and 3 and 4 transverse to form an orthogonal triad.

The specimens were tested to failure in a Mayes servo-hydraulic universal testing machine at a constant deflection rate of 5 mm/minute. Taking account of deflections in mounting fixtures and load cell this gave a strain rate in the elastic range of about 2×10^{-4} per second. Load deflection curves were produced automatically on an X-Y plotter from a 25 kN load cell and a displacement transducer in the machine. A typical set of stress strain curves calculated from these values is given in Fig.6.23. The strain was estimated by subtracting the machine deflection from the overall measured deflection. As the machine deflection was a large proportion of the total in the elastic range of the specimen, the estimated strains in this region are only approximate.

Stress-strain curves for specimens from the same part and orientation in different bars almost identical. The specimens that had not been plastically deformed (Nos. 2, 3 and 4) showed a gradual transition from elastic to plastic behaviour. The axial specimens (No. 2) had a higher elastic limit and strain hardening rate than the transverse specimens (3 and 4). This difference is due to the cold drawing process used to form the bar, in which grain structure and inclusions are elongated along the axis. Values of reduction in area at fracture show that the ductility is also higher in the axial direction.

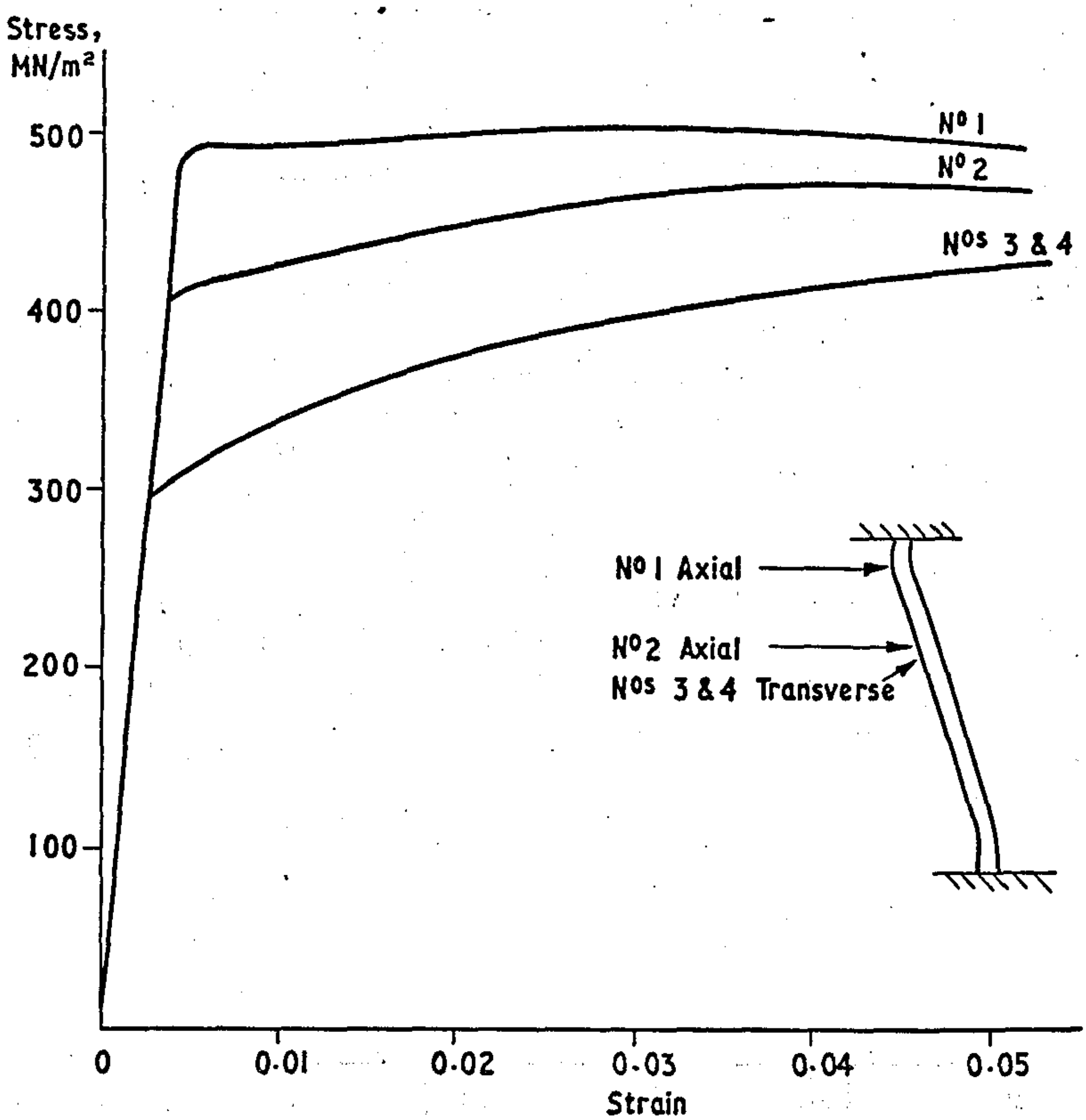

Fig. 6.23 Stress-strain curves and (inset) position of specimens. Tests on bar L4-B

The specimens from the plastically deformed part (No. 1) had the highest elastic limits and showed yield point phenomena, a just-distinguishable upper and lower yield stress. The strain hardening rate after the yield point was lower than for the other specimens.

Throughout this thesis the term yield stress has been used to denote the constant stress in the plastic region of elastic-ideally plastic behaviour. This is the value most relevant to the present study but it may not be quite the same as the stress that metallurgists would term yield stress in a real material. For curves of the type shown by No. 2, 3 and 4 there is, strictly speaking, no yield point. For practical purposes the stress at which the original tensile load/deflection curves depart significantly from linearity has been called the yield stress. This is more nearly equivalent to a 0.1% proof stress than a true elastic limit because of the relatively insignificant specimen elastic deflections described above.

The results are summarised in Table 6.9. The yield stress used for the calculations of collapse force is the mean value for the No.2 specimens. The stress-strain curve is very nearly elastic-ideally plastic up to the small strains occurring in the impact tests.

TABLE 6.9

Means and Standard Deviations (S.D.) for tests on six bars

Specimen position	Yield stress, MN/m^2		Max stress,* MN/m^2		Elongation at break, %		Reduction in area %	
	Mean	S.D.	Mean	S.D.	Mean	S.D.	Mean	S.D.
No. 1	513	27	519	21	19.8	2.8	62.5	1.8
No. 2	410	5	481	8	24.7	1.8	64.8	0.8
No. 3 and 4	302	10	440	12	22.1	1.2	54.7	2.2

*Engineer's stress i.e. maximum load/original area

APPENDIX 6.3

Collapse mode in pure rotation about one upright

The case for rotation about J is covered in section 6.3.2.

$$F_L \cos\alpha (b + b_2) - F_L \sin\alpha \, (b + b_3) = P\,(b + b + b\sqrt{2}) \quad -(6.43a)$$

where the LHS is the moment of F_L and the RHS is the moment of the individual upright collapse forces.

This gives:

$$Q_s = \frac{F_L}{4P} = \frac{\frac{b}{4}\,(2 + \sqrt{2})}{(b + b_2)\cos\alpha - (b + b_3)\sin\alpha} \quad -(6.43b)$$

For the rotation about other uprights, the moment of the upright collapse forces remains the same and the RHS of (6.43a) and the numerator of (6.43b) are changed. The denominator of (6.43b), the moment arm of F_L, becomes:-

	$b_2 \cos\alpha - (b + b_3)\sin\alpha$	*for rotation about D*
or	$(b + b_2)\cos\alpha - b_3 \sin\alpha$	*for rotation about G*
or	$b_2 \cos\alpha - b_3 \sin\alpha$	*for rotation about B*

APPENDIX 7.1

MEASUREMENT OF INERTIAL PARAMETERS

The inertial characteristics of a rigid body are completly described by the following parameters:

(i) Mass.

(ii) Three independent coordinates of centre of mass in relation to three, normally orthogonal datum axes in the body.

(iii) The directions of the three principal axes of inertia in relation to the datum axes.

(iv) The three principal moments of inertia.

While (i) and (ii) may be found using simple, static methods, a complete determination of (iii) and (iv) requires more complex, dynamic measurement using special jigs. In the dynamic methods, the vehicle or element is made the inertial part of an oscillating system, the stiffness being provided by a pendulum suspension, a mechanical spring system or a combination of both. The techniques generally provide one moment or product of inertia from each oscillating system, a number of measurements in different configurations being required for a complete determination of parameters.

The most sophisticated method is probably that developed by NASA for aircraft (87), based on combinations of pendulum and coil-spring suspensions. Great care was taken in the design and conduct of these experiments to ensure accuracy; for example, rig suspensions were designed to compensate for non-linearity at large amplitudes and to minimise unwanted modes in single point suspensions. As a result of this and the complete determination of parameters, the equipment, procedure and analysis of results are complex. The report contains a bibliography of methods used in aeronautics.

Inertia measurements of automotive vehicles include those of Goran and Hurlong (88), (pendulum), Bartos (89), using a spring suspension; and Winkler (90), who used a pendulum suspension for pitch and roll and a combined spring and pendulum method for yaw. In some of these and other cases, the principal axes of inertia are assumed to coincide with the chosen datum axes of symmetry of near-symmetry. Goran and Hurlong include a determination of the roll-yaw product of inertia by suspending the vehicle in a tilted position.

The only published descriptions of methods used for agricultural tractors appear to relate only to pitch inertia. Matthews and Talamo reported on the NIAE suspended platform (91) and Goering et al (92) used a beam spring method with a relatively high natural frequency ($\simeq$ 10 Hz) and a simple technique to separate pitch and bounce modes.

Measurements required

The inertial parameters of the tractor fitted with the experimental frame were needed for simulation and analysis of experimental results. Values for several other tractors were also required for comparison. The centre of mass position and pitch inertia were found using the suspended platform, essentially as described (91). The most important moment of inertia for sideways overturning studies, however, is that in roll. Although it is possible to adapt the suspension system for roll measurement using brackets fixed to the tractor, the method is cumbersome, and accuracy is difficult to achieve if the rig is frequently changed. The prime requirement was therefore the development of a simple technique for roll inertia measurement.

It would have been of some benefit to develop also methods of yaw and product measurement. The effort was not considered justifiable, however, because the shape of the tractor supports the assumptions:

(i) that the principal axes coincide with the coordinate axes (i.e. the measured pitch and roll values are close to the principal inertias) and

(ii) that the yaw inertia may be estimated from the pitch inertia, since it is required only to a low accuracy.

A spring method for roll inertia

The main theoretical attraction of pendulum suspension methods is that the stiffness, provided by gravity, may be accurately determined and remains constant. This applies to practical measurement only if the support and suspension are extremely rigid, however, and this requirement imposes the main limitation on real systems. A secondary practical problem is the need to provide means of attaching the suspension to the vehicle, especially if complicated brackets have to be made for each test. This is overcome in pitch measurement using a suspended platform but the inertia of the platform itself reduces overall accuracy and the method is difficult to apply in roll.

To overcome these limitations, in view of the lack of a ready-made rigid suspension support at the NIAE, an alternative method was developed for roll inertia measurement (93). In this technique, the tractor is supported from below on a longitudinal knife edge, the stiffness being provided by vertical coil-springs attached to extensions of the rear hubs (Fig. 7.23). This has the added advantage that the oscillation axis is closer to the centre of mass, increasing the relative contribution of moment of inertia about the point, and hence accuracy.

The overall roll stiffness has two components:

(i) the spring couple which tends to restore the system from a deflected position back to equilibrium and

(ii) the inverted pendulum effect of the tractor mass, directed away from equilibrium.

The derivation of the system equations is given in reference (93), together with details of experimental equipment and accuracy; it is shown that the stiffness is uniform, under the stated assumptions, and the resulting motion is simple harmonic.

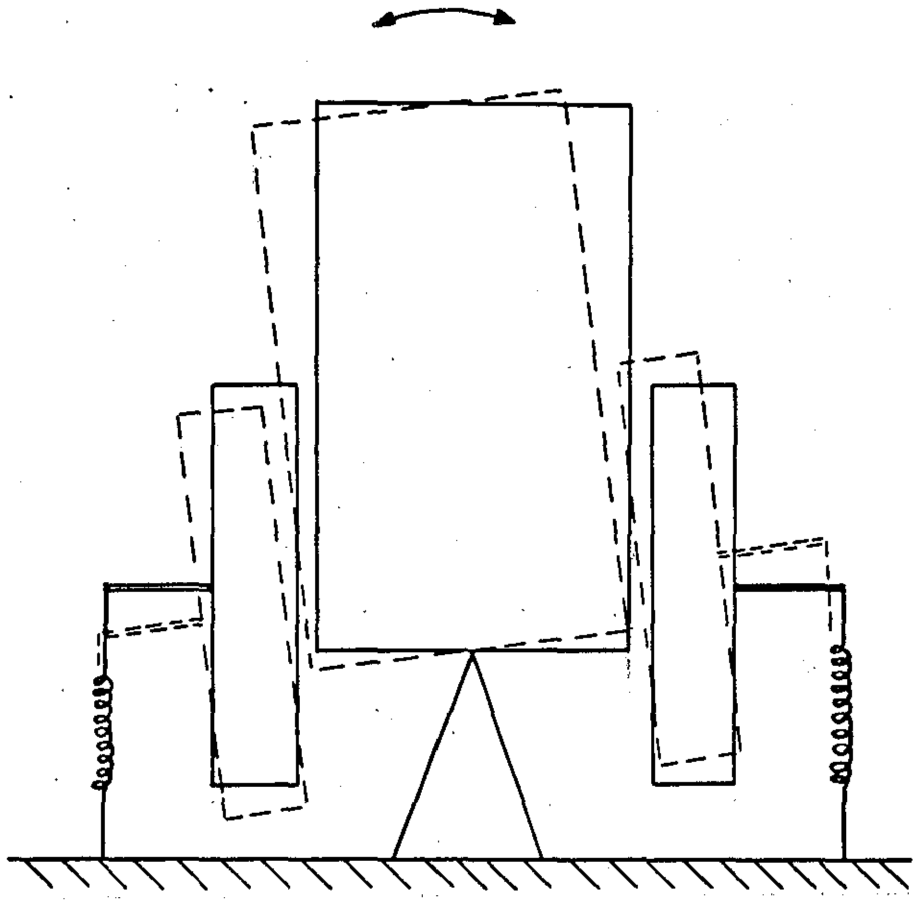

Fig. 7.23. Roll inertia measurement method

In the most general application of the method, the force-deflection characteristics of the springs must be found. This allows the height of the centre of mass and its lateral offset from the pivot axis to be dertimined by measuring the overall roll stiffness of the assembly. If, however, the height of the centre of mass is know in advance and the tractor is balanced on the knife edge sufficiently accurately to allow the lateral offset to be ignored, the inertia may be obtained either from the spring characteristics or from the roll stiffness, but both are not required.

Results

The results of measurements are given in Table 7.2 for the Fordson tractor with experimental frame used in the overturning studies and for several other tractors with and without cabs.

Two different pairs of springs were used for the measurements on the overturning tractor, one pair being about twice the stiffness of the other. The two sets of results agree closely.

Table 7.2 Results of measurements on roll rig and suspended platform

	Roll Measurement Spring Stiffness		Pitch measurement Suspended platform pivot height, m			
	Low	High	1.435	1.588	1.740	1.892
(1) FORDSON MAJOR WITH NIAE EXPERIMENTAL FRAME (Mk II TOP)(mass = 3065 kg)						
Centre of mass ht(y_G),m	0.882	0.891		0.895		0.893
Radius of gyration, m	0.618	0.624		0.960		0.950
(2) FORDSON MAJOR WITHOUT FRAME (mass = 2330 kg)						
Centre of mass ht(y_G),m	0.759					0.723
Radius of gyration,m	0.409		0.953	0.936	0.898	0.903
(3) FORDSON MAJOR WITH DUNCAN CAB (mass = 2488 kg)						
Centre of mass ht(y_G),m	0.764					0.745
Radius of gyration,m	0.500		0.960	0.926	0.930	0.908
(4) MASSEY FERGUSON 178 WITHOUT CAB (mass = 2396 kg)						
Centre of mass ht(y_G),m	0.778				0.780	0.776
Radius of gyration,m	0.505				0.935	0.949
(5) MASSEY FERGUSON 178 WITH STA-DRI CAB (mass = 2574 kg)						
Centre of mass ht(y_G),m	0.842		0.831	0.776	0.835	0.865
Radius of gyration,m	0.585		0.941	1.025	0.975	0.998
(6) DAVID BROWN 995 WITHOUT CAB (mass = 2218 kg)						
Centre of mass ht(y_G),m	0.791					
Radius of gyration,m	0.491					
(7) DAVID BROWN 995 WITHOUT CAB BALLASTED (227 kg each rear wheel, 31 kg each front wheel - total mass = 2733 kg)						
Centre of mass ht(y_G),m	0.741			0.742		0.748
Radius of gyration,m	0.704			0.863		0.869

For the suspended platform tests, inertias were generally calculated for each of several pivot heights, rather than plotting a curve of periodic time against height as previously (91). In most cases, agreement of the centre of mass heights is good between the two methods, and for different pivot height of the suspended platform. The most serious error is for the Massey-Ferguson 178 with cab at a pivot height of 1.588 m; no explanation can be found for this discrepancy. The agreement of pitch radius of gyration at different pivot heights is only fair.

APPENDIX 7.2

TYRE CHARACTERISTICS

Side force

The steady-state side force generated by a rolling tyre depends in a complex way on a large number of parameters: tyre size and type; tread and sidewall construction; tread pattern and state of wear; material and texture of ground surface; inflation pressure; normal load; tangential load; slip angle; camber angle; speed. When some parameters, such as slip angle, are continually varying, the side force does not directly assume its corresponding steady-state value at each change but develops the new force gradually as it rolls.

In a number of analytical studies the tyre and contact patch have been treated as various combinations of spring elements in order to gain an understanding of the mechanism of force generation[66, 94]. Most investigations of tyre behaviour have been empirical, however, and many relationships between side force and kinematic variables have been published for particular types of tyre (see, for example, refs.95-97., and the review given in 94). There is unfortunately little useful data available on tractor tyres, where the large diameter and lug pattern influence behaviour. Most measurements relate to car tyres at small slip and camber angles for use in handling studies. A further problem is the wide diversity of measurement techniques and methods of presenting results. No definitive reference or review paper giving quantitative data in an adequate range of conditions could be found in the literature.

It was not possible to measure side force directly in the conditions of the overturning experiments. Some measurements of front tyre side force in various combinations of normal load and slip angle were made using the NIAE Rolling Resistance Rig and a concrete surface adjacent to the over-turning platform. These added to the information gained from the literature, but the rig would not accept large rear tyres and could not be operated on the platform itself.

Discussion with experts and a review of the literature resulted in the following compromise solution:

(i) The limiting coefficient of sideways resistance (corresponding to μ_s) at large slip angles for rubber tyres on the concrete and steel plates of the platform, in wet and dry conditions, was estimated from tests using a Portable Skid Resistance Tester(98)

(ii) The cornering stiffness, the slope of the side force/slip angle curve at low slip angle, was kindly measured by Michelin Ltd on a tyre of similar size, construction and lug pattern, at a number of normal loads for the inflation pressures used in the overturning experiments.

(iii) The shape of the side force/slip angle curve was assumed to be a limited cubic. Ellis(66) and NASA(96) recommend a function with ψ and ψ^3 terms only, in which case the two coefficients are defined uniquely from the cornering stiffness and limiting side force coefficient. In non-dimensional form this relationship may be expressed as

$$\frac{\mu}{\mu_{max}} = \psi_n - \frac{4}{27} \psi_n^3 \qquad -(7.1)$$

(for $-1.5 \leqslant \psi_n \leqslant 1.5$)

and $$\frac{\mu}{\mu_{max}} = 1 \quad (\text{for } |\psi_n| > 1.5) \qquad -(7.2)$$

where μ_{max} is the limiting value of μ at large slip angles and ψ_n is a normalised slip angle defined in relation to the actual slip angle ψ and the cornering stiffness $\left\{\frac{d\mu}{d\psi}\right\}_{\psi=0}$ by:

$$\psi_n = \frac{\psi}{\mu_{max}} \left\{\frac{d\mu}{d\psi}\right\}_{\psi=0} \qquad -(7.3)$$

A theoretical justification for excluding the ψ^2 term from (7.1) is the symmetry of the curve about the origin. Radt and Milliken[99], however, found that adding a term in $\psi_n \cdot |\psi_n|$ improved the fit of the curve; this preserves symmetry, although it creates a discontinuity in $\frac{d^2\mu}{d\psi^2}$ at the origin. Their equation, which was later used by McHenry[50] is:

$$\frac{\mu}{\mu_{max}} = \psi_n - \frac{1}{3}\psi_n \cdot |\psi_n| + \frac{1}{27}\psi_n^3 \qquad -(7.4)$$

In this case the bounds for the cubic form are $-3 \leqslant \psi_n \leqslant 3$.

(iv) The build up of side force under a step change of slip angle was assumed to follow an exponential relationship with the distance rolled[66]. The distance at which 1/e of the steady state force is developed, the relaxation length, is generally considered to be approximately equal to the rolling radius, although little support for this appears in the literature.

Bergman measured side force under conditions in which the slip angle oscillated as a truncated triangular function[100]. An attempt by Chisholm to verify the relaxation length hypothesis using Bergman's data was only partially successful. The shape of the experimental loop was matched better if the input was assumed to be sinusoidal rather than triangular, but prediction of the loop width was only fair. The tyre data given in the paper were incomplete, however, and incorrect assumed values may explain the difference.

(v) All other parameters were assumed to have second-order effects and were ignored.

Tyre side force/slip angle measurements

Details of the rear tyres fitted to the overturning tractor, and of the tyre tested by Michelin Tyres Limited, are given in Table 7.3.

TABLE 7.3

Tyre details

	Overturning tests	Slip angle tests
Make	Firestone	Michelin
Type	Cross ply	Cross ply
Ply rating	4-ply	4-ply
Size	11-36	12.4-36(11-36)
Number of lugs	46	46
Lug angle	45^{o}	45^{o}
Lug length, mm	230	225
Lug width, mm - inside	27	27
- outside	32	27
Wear	Part worn	New

The normal inflation pressure in the overturning tests was 103 kPa and the static load 9.61 kN. In the test in which the tractor was ballasted, the pressure was 152 kPa and the static load 12.30 kN. The dynamic load during overturning probably varied between zero and about twice the static load. Three combinations of pressure and load were used in the slip angle tests to take some account of this variation (Table 7.4).

The rolling speed in the slip angle tests was 3 km/h (0.889 m/s) compared with typical overturning test speeds of about 5.4 km/h (1.5 m/s). The test surfaces were similar but no measurement of limiting friction on the slip angle test surface was available.

Normalised cornering stiffness in each condition given in Table 7.4 were calculated according to:

$$\text{Normalised cornering stiffness, rad}^{-1} = \frac{\text{mean}\left(\dfrac{\text{side force, kN}}{\text{slip angle, rad}}\right)}{\text{normal force, kN}}$$

Forces were measured at low slip angle only, because of limitations of the equipment. In this range, the behaviour is nearly linear.

TABLE 7.4

Results of side force/slip angle measurements

Pressure kPa.	Normal force, kN	Side force, kN, at slip angle:			Normalised cornering stiffness, rad^{-1}
		2^o	3^o	4^o	
170	17.65	2.80	4.02	5.12	4.36
170	21.60	3.24	4.51	5.80	4.07
220	21.60	3.43	4.85	6.10	4.29

Measurement of limiting coefficient of friction

The County Surveyor's Department of Bedfordshire County Council carried out the measurements with the Portable Skid Resistance Tester. The apparatus is normally used to assess the skid resistance of road pavements prior to a decision to resurface. It consists of a small pendulum mounted in a frame that stands on the surface, and functions in the manner of an Izod impact testing machine. The pendulum is fitted with a rubber foot that makes passing contact with the surface as the pendulum swings; the height reached by the pendulum after contact is a measure of the energy absorbed, and is recorded on a calibrated scale. Measurments at TRRL of the sideways resistance of a rolling wheel using a vehicle based machine (SCRIM) have allowed correlation of the pendulum scale with a coefficient of sideways resistance, which may be interpretted in this case as coefficient of friction.

Tests were made on the dry concrete surface near the overturning part, on the wetted plastic flooring material, and on a small sample of painted metal sheet representing the plates, both dry and wet. Repeat tests on the plastic flooring and metal plates gave identical values to within the reading accuracy; tests on the concrete at different points and in different directions showed changes due to variation in the micro-surface. Results are summarised in Table 7.5.

TABLE 7.5

Coefficients of friction

Test condition	Surface (and direction)	Coefficient of sideways resistance	
		Individual means*	Overall mean
Dry	Concrete (-along platform)	0.895 0.78 0.715	080
	Concrete (-across platform)	0.79 0.77 0.83	0.80
	Metal plate	1.00	1.00
Wetted with 1:500 detergent in water	Plastic floor covering	0.095 0.105	0.10
	Metal plate	0.14	0.14

*Each individual mean is the mean of five repeat readings of the instrument at one point on the surface. The three indiviual means for each direction on the concrete represent readings at three different point in the overturning area.

- 341

Stiffness and damping

Values of dynamic tyre stiffness and damping in vertical, lateral and longitudinal directions for a variety of tractor tyres under different conditions of load, pressure and wear were reported by Stayner and Boldero[83]. The parameters were estimated from measurements of transient response in a laboratory rig, assuming a linear, second-order system. Some of the response curves showed evidence of non-linear behaviour but no attempt was made to fit higher order models. Although all response curves were found to be closely repeatable, some inconsistent variations of stiffness with load were reported and the effect of wear was significant. In addition, temperature variation is thought to cause unpredictable parameter changes.

In view of all these uncertainities and the lack of other data, there seemed to be no justification for including non-linear tyre charateristics in the overturning model, and values appropriate to inflation pressure, nominal load and estimated wear taken directly from reference (83).

APPENDIX 7.3

Structural characteristics of wheel discs

Forces were applied slowly to the wheel rim by hydraulic ram, while the tractor was supported with the rear tyres raised above the ground. Tests were carried out on the disc centres fitted as standard to the 11.36 rear wheels of the Fordson Major tractor, and on the N.I.A.E. "strap" centre used in the overturning tests.

The results (Fig.7.24) show typical elasto-plastic bending behaviour that is described quite well by a model with only two piece-wise linear loading portions. The shape of the plastic part for the strap centre is due to geometric effects. The test repeatability was good overall but some variation was shown in the local curve shapes because of the complex failure modes and the effects of slip at the fixing bolts.

The present model has some shortcomings in describing the rim characteristics: (i) the top and bottom of the rim are not entirely independent, though coupling is less than might be imagined; (ii) a significant amount of colomb friction is probably present, particularly in the case of the experimental spoke centre; and (iii) the experimental unloading curve is significantly non-linear. To minimise the effects of these limitations, the model damping and unloading stiffness were adjusted empirically.

Yield enhancement for the ROPS and rims were determined from the relative x_1 velocity at impact. This had been found satisfactory in the prediction of the ROPS laboratory test results.

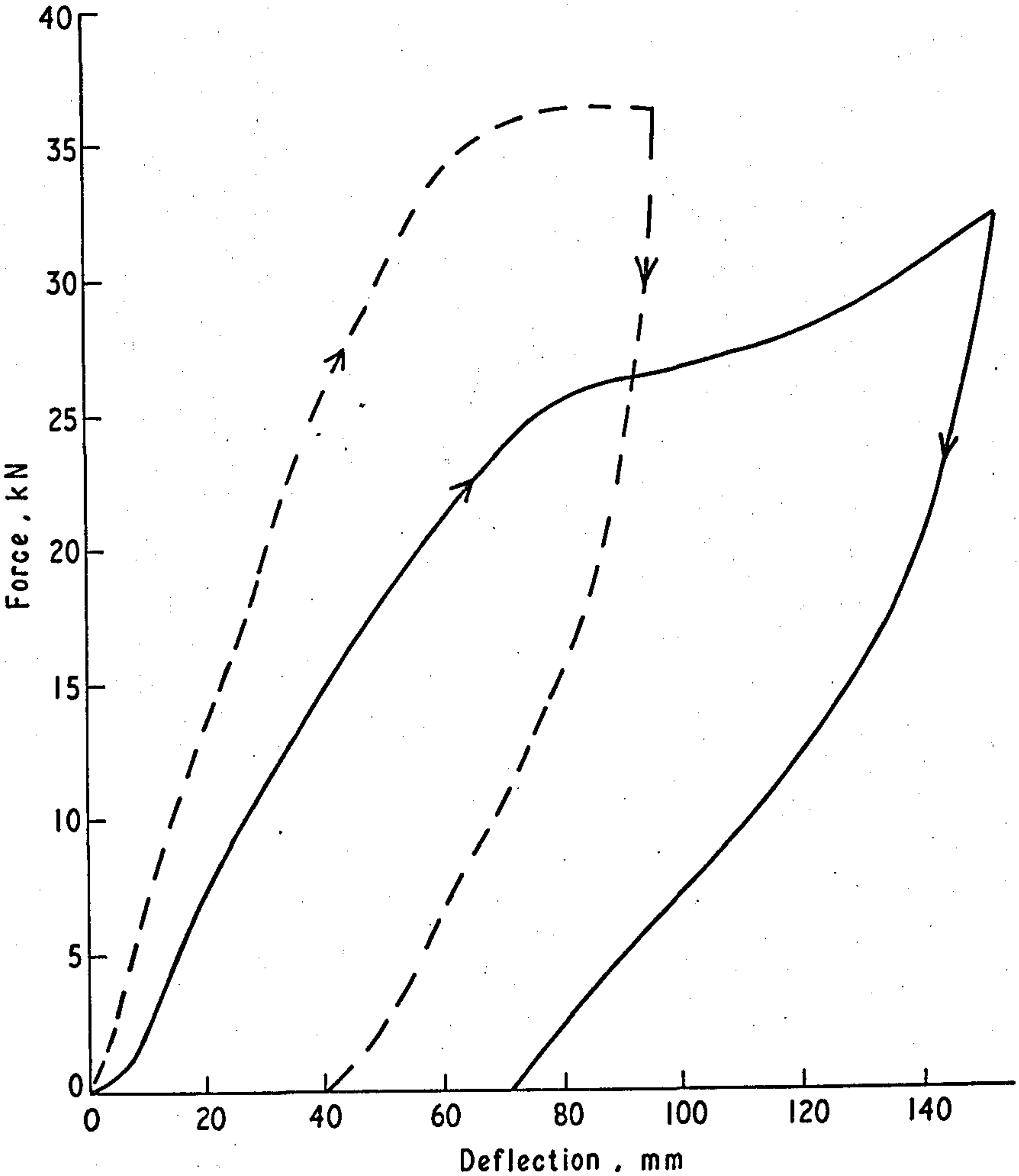

Fig. 7.24 Force-deflection curves for sideways loading at wheel rim.

– – – – – Standard Ford disc centre

———— NIAE strap centre

APPENDIX 7.4

SOIL CHARACTERISTICS

Plate sinkage measurements depend mainly on compressive strength, whereas cone penetrometer readings are additionally influenced by shear strength, and this becomes the predominant factor as water content increases[101]. For cone penetrometer measurements to be a reliable indicator of the relevant strength it would have been necessary to record also the water content and bulk density of the soil. More confidence may be placed in the measurements for those tests when the soil had been very dry for some time.

The best attempt that may be made to model the soil behaviour in the overturning experiments is to take the penetrometer measurements, perhaps modified subjectively according to the perceived wetness of the soil. In view of the limitations described above and the relatively large standard deviations of simultaneous penetrometer measurements at different positions in the impact area, the agreement between simulation and experiment at impact cannot be expected to be good. The comparison may, however, be interpreted to add information about the soil behaviour.

From limited relevant studies on impact[9, 54] it was concluded that the soil behaviour may be represented adequately by an idealised elasto-plastic characteristic, assuming the strength is known. Rate effects appear to be small and so badly defined that they are better omitted.

The area of the load cells, taken together, in a plane perpendicular to the x_1 axis is $0.1\ m^2$. The direction of impact is at an angle to this axis, when the shape becomes more like a wedge than a flat plate and the effective area depends on the sinkage. The impressions left in the soil, however, generally had reasonably horizontal, square bases, and support the assumption of an constant area of $0.1\ m^2$ as a first approximation.

When the tractor is upright the tyre contact area depends on the normal load and tyre pressure. During impact, θ is around -90°, and the tyre sidewalls transmit a considerable proportion of the normal load directly to the rim. When the wheel lies flat on the ground with a normal force high enough to cause significant penetration, the area is probably close to the projected area of the tyre sidewall annulus, in this case 0.89 m^2. The effective area of the rim itself is negligible, and sidewall deflection allows this to sink slightly further than the tyre. In the present model, the area of a tyre is shared between upper and lower halves, and each half between tyre point and rim point. To take account of the sidewall flexibility and if the reduction in effective area as θ varies from -90°, the nominal areas for each point were adjusted empirically with the range 0.1 and 0.2 m^2.

The surface frictional force resisting sliding motion is also poorly defined. Forces generated by pure sliding movement have been shown to approximate closely to a coulomb-type relationship with normal force(81), although the coefficient of friction is influenced by density and moisture content. The effect of penetration on sliding resistance is not clearly understood, however, and probably contibutes more to the total force than pure sliding friction in the present conditions. Resistance due to penetration rises with increasing sinkage, and hence also with normal force, but the effective area also increases. In the absence of quantitative evidence it seems reasonable to assume that the total side force is proportional to the normal force, giving a constant of friction for any particular condition.

This description of soil behaviour has emphasised the uncertainties. The lack of reliable quantitative data does make the comparison of simulated and experimental results more difficult. But since the behaviour is fairly well defined qualitatively, the power of the model to predict the effect of parameter variation is not diminished.